Structural Studies of the Adsorption of Molecules on Cu(110)

Report submitted in accordance with the requirements of the University of Liverpool for the degree of Doctor in Philosophy

By

Geoffrey Thomas

Department of Surface Science

University of Liverpool

22 January 2013

Table of Contents

Abstract

The adsorption of thymine and melamine on Cu(110) has been investigated using a combination of experimental and theoretical techniques. These techniques have allowed the development of an extensive picture of how these molecules may orient on this surface. Many Density Functional Theory (DFT) calculations using the latest version of the Vienna Ab-Initio Simulation Package (VASP) have allowed the production of a series of models which have, in general, corroborated the experimental data. The additional utilisation of semi-empirical techniques (like those used by Grimme), which seek to simulate long-range inter-molecular vdW interactions, have allowed the creation of a firm foundation of, not only how the individual molecules bond to the Cu(110) surface, but of how they arrange themselves into long-range structures.

With thymine, two long-range phases were observed; a room temperature structure, which aligned along the [001] direction in 1-D chains, one molecule thick and with the cyclic plane roughly parallel to the [110] direction. The higher temperature phase occurred after annealing between 350-400K and consisted of two distinct 1-D chains, two molecules thick and angled at $\sim\pm 20^{o}$ to the [001] direction. In both cases the thymine was deprotonated at the N(1) atom. With melamine, only the room temperature phase is discussed and this consisted of a 2-D "hexagonal" structure arranged on a (6x2) unit cell.

Although structural relaxation techniques give good indications of the stability of the models, the technique of Scanning Tunneling Microscopy (STM) simulation has been used extensively with both thymine and melamine systems in order to verify their validity. Although it is not yet possible to directly observe individual atoms in such small molecules it is possible (with STM) to observe their electronic "footprint" and to then re-create this observed image. The similarity of this "simulated STM" to the "experimental STM" combined with a relaxed stable model is a strong indication that the model is in good accordance with the observed (static) system. Combining this analysis technique with experimental data, models are proposed for both the room temperature thymine and melamine phases as well as the annealed thymine phase.

Acknowledgements

I would like to express my gratitude to a number of people who have helped me during my PhD studies. Obviously my supervisors Prof. Rasmita Raval and Dr. George Darling who have successfully managed to steer me through the past four (occasionally rocky) years journey.

Dr. Sam Haq and Dr. Matt Dyer have also offered me a great deal of assistance with both the experimental and theoretical aspects of this thesis.

Dr. Matt Forster, Dr. Andrew Mark and Dr. Israel Temprano have also offered me great deal of help and I feel deserve a special mention as well as several other people (they know who they are).

I have never been shy in asking for help from a variety of sources and have taken snippets of information and experience from far too many people to mention here. However, this is my way (I guess) of paying them back. It's been a struggle for me to produce a piece of work on this level and, although far from being a masterpiece, I'm (reasonably) proud of it.

I'd also like to thank my father for all the little (and big) things he has done to help as well as his constant faith and all the rest and I'd like to dedicate this thesis to him.

Abbreviations

CCSD(T)	-	Coupled-Cluster with Single and Double and Perturbative Triple excitations
DFT	-	Density Functional Theory
DNA	-	Deoxyribonucleic acid
ES	-	Electrostatic
ER	-	Exchange-Repulsion
HOMO	-	Highest Occupied Molecular Orbital
LUMO	-	Lowest Unoccupied Molecular Orbital
Melamine	-	Mel/M
NASA	-	National Aeronautics and Space Administration
RAIRS	-	Reflection Absorption Infra-Red Spectroscopy
RNA	-	Ribonucleic acid
SPM	-	Scanning Probe Microscopy
STM	-	Scanning Tunneling Microscopy
Tantalum	-	Ta
Thymine	-	Thy/T
TPD	-	Temperature Programmed Desorption
vdW	-	van der Waal
VASP	-	Vienna Ab-Initio Simulation Package
XPS	-	X-Ray Photoelectron Spectroscopy

1. Chapter One – Introduction

1.1. Thesis Aims

Electronic devices based on inorganic semiconductors have been part of our daily lives for over 60 years. However, now, in the beginning of the new millennium the increased development and knowledge of organic semiconductors has led to a tendency to explore alternative avenues than inorganic semiconductors and focus on the creation of electronic devices based on organic molecules. In order to construct such hybrid molecular based nanoscale devices, methods for the controlled fabrication of well-defined organic nanostructures need to be developed. One of the most promising methods to date is the "bottom-up" approach, wherein ordered structures with nanometre precision over an extended large scale can be constructed. The concept of this approach is to exploit multiple non-covalent interactions between pre-engineered molecules, which through their selective recognition are able to form convergent assemblies. Due to the intermolecular interactions, a dynamic equilibrium exists between the individual molecular components and the assembly as a whole thus leading to thermodynamically controlled multi-stable systems, the reversibility of which allows for the self-rearrangement and self-correction of the components within the assembled structure. This so-called 'self-healing' contributes to the formation of long-range ordered and defect-free systems, unachievable through conventional covalent synthesis.

It is possible for organic molecules, such as DNA, to form highly-ordered ''self-assembled'' structures. Various factors are responsible for this but it is mainly their ability to form relatively weak intermolecular bonds that are stable enough to hold them in place at room temperature. Some research groups have predicted that understanding such a self-assembly system opens a new avenue of research into the emergence of life. On top of this the interaction of biologically-related molecules with surfaces is attracting increasing interest due to its potential relevance to areas such as biocompatibility, biosensors and the fabrication of novel biomaterials. However, typical biological molecules such as DNA and proteins are far too complex to be investigated on surfaces at an atomic scale, although remarkably detailed STM images have been obtained in the last few years of single, isolated, small organic

molecules on various different surfaces.

Thus, the investigations carried out in this thesis aims to add to this increasingly burgeoning wealth of knowledge. The molecules investigated in this thesis were, unfortunately, too small to be imaged as anything other than bright spots with scanning tunnelling microscopy (STM) and therefore only their long-range structures could be elucidated with this technique and not their bonding orientations to either the surface or to one another. However, combining this technique with the recently developed density functional theory (DFT) as well as the various other experimental techniques available have resulted in the production of a cohesive picture of how thymine forms both a room temperature 1-dimensional (1D) structure as well as a separate and distinct high temperature 1D structure upon dosing on a copper (Cu) crystal surface, both of which are described in chapter 3. Chapter 4 then continues by utilising these same techniques to produce a description of a further system in which melamine forms a stable 2-dimensional (2D) room temperature upon dosing on the same copper (Cu) crystal surface.

The experiments presented in this thesis were carried out in order to gain a better understanding of the organisation and bonding of thymine and melamine on a Cu surface at the single molecule level. This level of characterisation requires a detailed knowledge of the chemical form, geometry, bonding points to the surface for each molecule in addition to the intermolecular forces that stabilise the organisation. In order to obtain as detailed and reliable an analysis as possible various techniques, both experimental as well as theoretical were employed in tandem. The experimental techniques utilised the very latest developments in ultra-high vacuum (UHV) in order to create an environment where both the metal surface as well as the molecule under investigation could be scrutinised unimpeded by contamination. This approach enabled the use of a powerful range of surface science techniques which provide complimentary information in order to construct a detailed understanding of each of the systems. STM, low energy electron diffraction (LEED), reflection absorption infra-red spectroscopy (RAIRS), temperature programmed desorption (TPD) and X-ray photoelectron spectroscopy (XPS) experiments as well as various DFT calculations were all utilised in this thesis in combination in order to provide a detailed understanding of each of the systems.

1.2. Surfaces and the Origins of Life

The exciting and challenging field of surface science has sprung up, relatively recently, in response to an increased demand, not only for greater efficiency in industrial processes, but also for a greater understanding of biological processes. This has necessitated a much more detailed understanding of how molecules interact with surfaces. Indeed, it is quite likely that surfaces played an integral part in the evolution of life itself! Nucleic acids, the constituent molecules that reside within both DNA and RNA, are categorised as both the information carriers and storers of the necessary proteins required to construct all living things (both plant and animal) on planet Earth.

The presiding theory in science today purports that the Earth's early atmosphere contained such molecules as methane, ammonia, carbon dioxide and water and, triggered by UV radiation from the sun and lightning produced biomolecular monomers such as hydrogen cyanide, amino acids, aldehydes and both 5 and 6-membered ring molecules. It has been suggested [1] that certain clays may have provided catalytic surfaces for polymerisation of these monomers into cyclic bases. Thus, it is quite possible that surface processes played an essential part in the initial formation of DNA and RNA.

However, in order to discuss the origins of life, one must first decide on a definition and many scientists have adopted NASA's [2]. This states that:-

An organism is considered to be alive if it is a "self-sustained chemical system capable of undergoing Darwinian evolution," implying that it must have what we will call genetic material and it must be possible for the genetic material to replicate and mutate [3].

Currently, most scientists believe that RNA molecules were capable of performing both enzymatic activity and self-replication. This is known as the "RNA world" scenario. Once proteins are built they are then able to act as enzymes and catalyse various chemical reactions. However, protein enzymes require that RNA strands first be present in order to form them, this is known as "the chicken and the egg problem". Therefore, the phosphate, sugar and base groups must have bonded through abiotic (non-biological) means. Thus far, scientists have been unable to bind the phosphate to the sugar and base group using conditions that were thought to have been present on the early Earth; this is a very active, current field of research [4]. However, once a full nucleotide unit has been formed, scientists

have been able to make extended chains of RNA, of up to 50 units (mers) in length, which could then fold to perform catalytic activity, accelerating the ease of synthesis for future molecules and initiating the RNA world [5].

When free nucleotides are combined in solution they do not react at all, so many scientists have been searching for different types of activating groups and inorganic catalysts that may have been involved in the first polymer bonding processes. Montmorillonite clay is one material which facilitates this reaction and provides a medium in which the individual activated RNA units combine to form larger chains [6]. In the case of montmorillonite clay, the aluminium (Al^{+3}) and silicon (Si^{+4}) which have dissolved out of volcanic rock along with oxygen and hydrogen form a three layer crystal structure. Composed of a silica layer, an alumina layer, and another silica layer, these three-layer crystals have a negative charge on their faces. While the individual three layer crystals are very rigid, the whole multi-layer structure can be quite flexible. The surface between the layers is negatively charged, so it attracts a large concentration of calcium (Ca^{2+}), sodium (Na^{+}), magnesium (Mg^{2+}), copper (Cu^{2+}), iron (Fe^{2+}) and other positively charged ions. The phosphate groups of individual nucleotides, the polymers of which make up long strands of RNA, are negatively charged. Theoretically, they are attracted to the positive pool in the fluid layer of the montmorillonite clay. Entering into the layer, they repel the negative charges on the surfaces of the aluminate layers, naturally positioning themselves in the middle of the positive layer and splitting the distance between the two negative surfaces.

The reactions which can then occur between the nucleotides allow them to be held strongly in position. This gives them the opportunity to form bonds between the monomers which are attracted to the positive layer. This is about twice as strong as the attachment strength of just one unit alone and as more and more nucleotides bond together, this linear relationship continues. Therefore, because the longer strands are held to the clay more firmly than are the individual nucleotides or shorter strands, it is possible that two longer strands would have a higher probability of bonding with each other because of increased contact. Adding strength to this theory is the fact that the dry ground-up clay swells to fifteen times its volume when exposed to water [7].

1.3. Recent Developments in Surface Science

Heterogeneous catalysis, pioneered by Paul Sabatier on hydrogenation and Fritz Haber on the Haber process could be called the start of surface science [8]. Irving Langmuir was also one of the founders of this field and the Langmuir adsorption equation is used to model monolayer adsorption. Also, Gerhard Ertl in 1974 described for the first time the adsorption of hydrogen on various metallic surfaces [9-13]. More recent developments include Gerhard Ertl's (2007 Nobel Prize in Chemistry winner) for his investigation of the interaction between carbon monoxide molecules and platinum surfaces.

However, interest in studying chemical reactions at surfaces dates back to the nineteenth century when scientists like Davy, Henry and Faraday began noticing catalytic effects on platinum surfaces [14]. Dobereiner then introduced his tinderbox which enabled hydrogen and oxygen to combine to yield a small flame. Thus, catalysis has been a mainstay of the development of surface science ever since. However, more recently, advances in solid state semiconductor electronics combined with the development of Ultra High Vacuum (UHV) systems has further driven interest in the field. A vast array of spectroscopic techniques have now been developed and combined with powerful ab-initio modelling algorithms and computers and it is now possible to carefully scrutinise how molecules bond and arrange onto virtually any type of surface imaginable.

Not only is it possible to quantify different arrangements of chemisorbed molecules to a high degree of accuracy but also physisorbed molecules as well. However, it is not just bonding between the molecule and the surface that co-ordinate how molecules arrange, but also inter-molecular bonding. This can manifest itself in various forms. Hydrogen bonding, van der Waals (vdW) forces and surface reconstruction also have a part to play. Indeed, the problem of how to accurately model vdW forces has become increasingly important in the field of surface science and, although various techniques now exist, these are not without issues [15,16].

1.4. Biological Molecules

Biological molecules, or biomolecules, are organic molecules which consist primarily of carbon, hydrogen, nitrogen, and oxygen, and, to a lesser extent, phosphorus and sulphur. These are found in all living organisms and include large polymeric molecules (i.e. proteins), polysaccharides and nucleic acids. It is possible for biomolecules to have complex structures dictated by the functions for which they must perform. However, biomolecules (in living organisms) are self-organized, typically built from simple building blocks such as amino acids, nucleic acids, lipids and sugars, and often function in a crowded intracellular environment to initiate crucial biological functions. Therefore, understanding the molecules, their assembly, and their interactions, is of paramount importance nowadays. There is also much interest in new materials that can be derived by combining the biological molecules in unusual ways, or by combining biological molecules with synthetic species, including nanoparticles and inorganic surfaces.

These molecules are far too large for their surface interaction to be probed at an atomic scale with any available methods. However, these molecules interact with surfaces through key molecular components but even these 'small' molecules present a major challenge for surface structure determination. Most surface science experiments have been performed on metal and semiconductor surfaces; however, most methods to probe surface properties, that have been developed, work only in very good ('ultra-high') vacuum conditions (UHV). This is because lowering the pressure of the gas (air) surrounding a surface lowers the rate at which molecules arrive from the air and contaminate the surface, and therefore, ensuring this process is slow enough to keep a sample clean for an hour or so, one needs to work in a pressure of about one million-billionth of an atmosphere (comparable to, but somewhat higher than, the pressure in outer space).

The interaction with surfaces of biological molecules is important in medical screening for disease, and in ensuring the body does not reject medical implants (e.g. artificial hip joints). Therefore, the properties and processes of biomolecules at surfaces are of particular relevance in such areas as medical implants [17,18]. Therefore, the challenge is to map out structures, bonding mechanisms and dynamics of biomolecules at surfaces in the same way as has been done for simpler molecules. These biomolecules are the building blocks of DNA and proteins, so understanding how the mechanisms of these subunits interact with surfaces will

yield greater understanding of how larger conglomerates also interact and bind to different surfaces. Therefore, biomolecular interactions at surfaces are relevant in medical diagnosis, however, to date, very few adsorption studies have been done [19-23].

1.5. Metallic Surfaces

At the microscopic level, most solid materials, with the exception of a few truly amorphous specimens, can be considered to be a collection of single crystal crystallites. The surface chemistry of the material as a whole depends upon the nature of the exposed surface of the crystallites. Therefore, in principle, it is possible to understand the surface properties of any material if the amount of surface exposed is known and have knowledge of the properties of each surface plane (neglecting crystal defects). By studying well-defined surfaces it is therefore possible to understand the properties of a material. The commonly used technique is to prepare macroscopic single crystals (1-5cm) of metals and then cut them in a way as to expose a specific area of interest.

A crystal structure is composed of a set of atoms arranged in a particular way and a lattice exhibiting long-range order and symmetry [28]. Patterns are located upon the points of a lattice, which is an array of points repeating periodically in three dimensions. The points can be thought of as forming identical tiny boxes, called unit cells, that fill the space of the lattice. The unit cell is given by its lattice parameters, which are the length of the cell edges and the angles between them, while the positions of the atoms inside the unit cell are described by the set of atomic positions (x_i, y_i, z_i) measured from a lattice point. The lengths of the edges of a unit cell and the angles between them are called the lattice parameters. The symmetry properties of the crystal are embodied in its space group and represent a description of the symmetry of the crystal [29]. A crystal's structure and symmetry play a role in determining many of its physical properties, such as cleavage, electronic band structure, and optical transparency.

A system of nomenclature is used to categorize the structural forms of the crystal structures of crystalline materials (see figure 1.1). Miller indices form a notation system in crystallography for planes in crystal (Bravais) lattices. In particular, a family of lattice planes is determined by three integers h, k, and ℓ, the Miller indices. They are written (hkℓ), and

each index denotes a plane orthogonal to a direction (h, k, ℓ) in the basis of the reciprocal lattice vectors. By convention, negative integers are written with a bar, as in 3 for −3. The integers are usually written in lowest terms, i.e. their greatest common divisor should be 1. Miller index 100 represents a plane orthogonal to direction h; index 010 represents a plane orthogonal to direction k, and index 001 represents a plane orthogonal to ℓ [27].

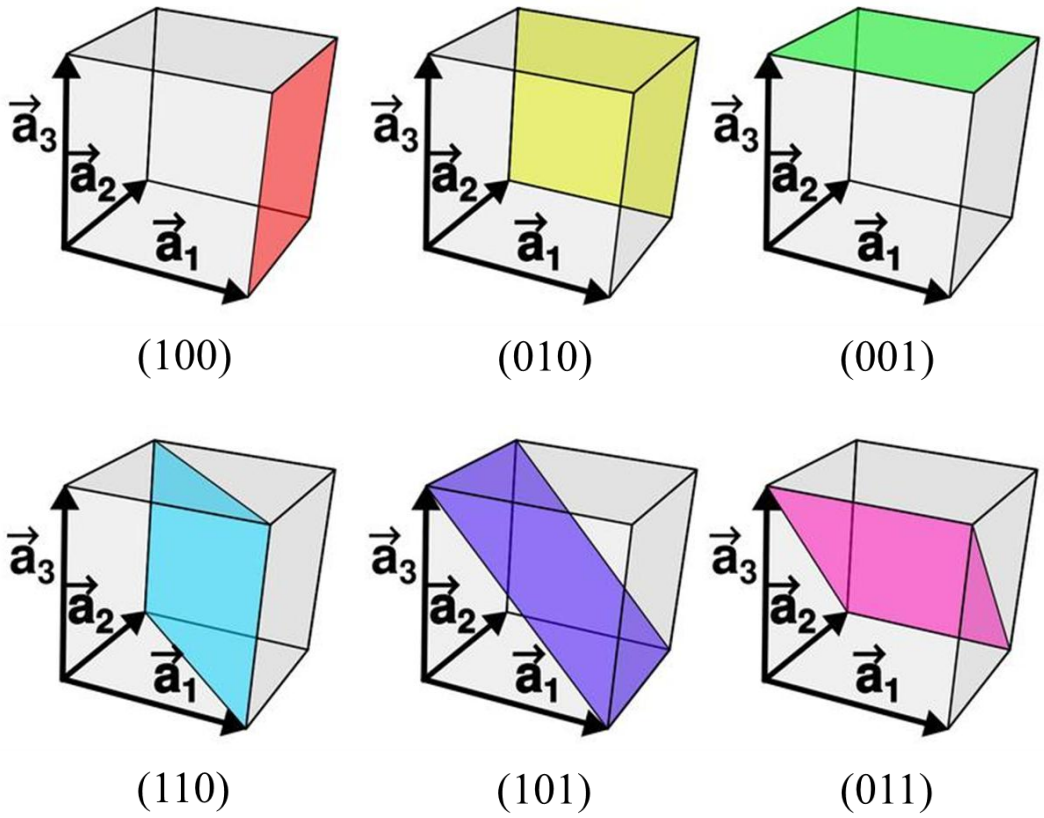

Figure 1.1 - Planes with different Miller indices in cubic crystals.

Most metals exist in only one bulk structural form, the most common ones being body-centred cubic (bcc), face-centred cubic (fcc) and hexagonal close-packed (hcp). For each of these there are, in principle, an infinite number of possible surfaces which can be exposed. However, in practice, only a limited number (so-called “low-index”) planes are found to exist in significant quantities. Most of the technologically most important metals possess the fcc structure (i.e. Pt, Rh, Pd, Ag, Au and Cu) and the low-index faces are what are most commonly studied.

1.5.1. The fcc (100) Surface

The (100) surface is obtained by cutting the fcc metal parallel to the front surface of the fcc cubic unit cell (see Figure 1.1a) this exposes a surface (the atoms in blue) with an atomic arrangement of 4-fold symmetry. The conventional birds-eye view of the (100) surface (see Figure 1.1b) is obtained by rotating the preceding diagram through 45° to give a view which emphasises the 4-fold (rotational) symmetry of the surface layer atoms. The second layer atoms are visible through the holes in the first layer but would not be accessible to molecules arriving from the gas phase.

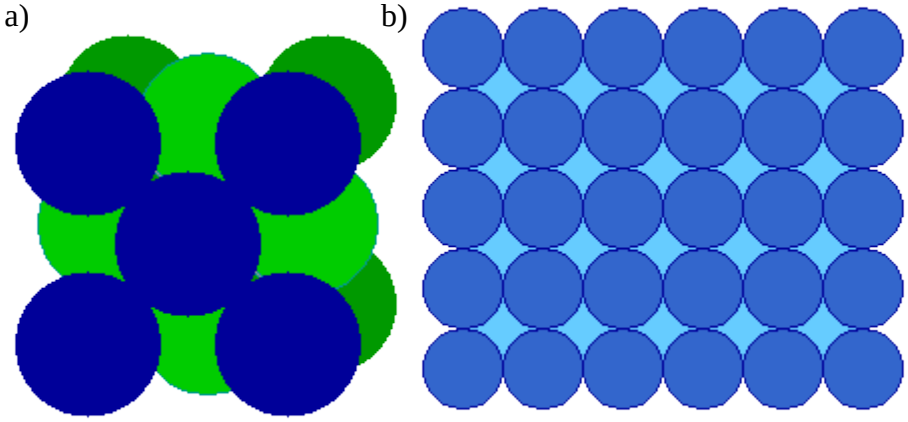

Figure 1.2: Diagram of a (100) surface:- a) shows the slice (in blue) of the crystal and b) shows the surface generated.

1.5.2. The fcc(110) Surface

The (110) surface is obtained by cutting the fcc unit cell that intersects the x and y axes but not the z-axis (see Figure 1.2). This exposes a surface with an atomic arrangement of 2-fold symmetry. The topmost layer is much less closely packed than on the (100) surface, i.e. the distance between atoms is equal to twice the metallic (atomic) radius, but in the orthogonal direction there is a substantial gap between the rows. This means that the atoms in the underlying second layer are also, to some extent, exposed at the surface.

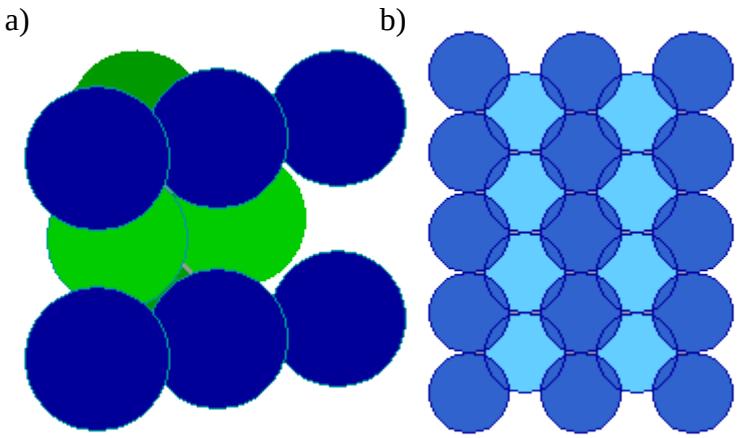

Figure 1.3: Diagram of a (110) surface, a) – shows the slice (in blue) of the crystal and b) shows the surface generated.

1.5.3. The fcc (111) Surface

The (111) surface is obtained by cutting the fcc metal in such a way that the surface plane intersects the x-, y- and z- axes at the same value (see Figure 1.3). This exposes a surface with an atomic arrangement of 3-fold (apparently 6-fold, hexagonal) symmetry. This layer of surface atoms actually corresponds to one of the close-packed layers on which the fcc structure is based. Since this is the most efficient way of packing atoms within a single layer, they are said to be "close-packed".

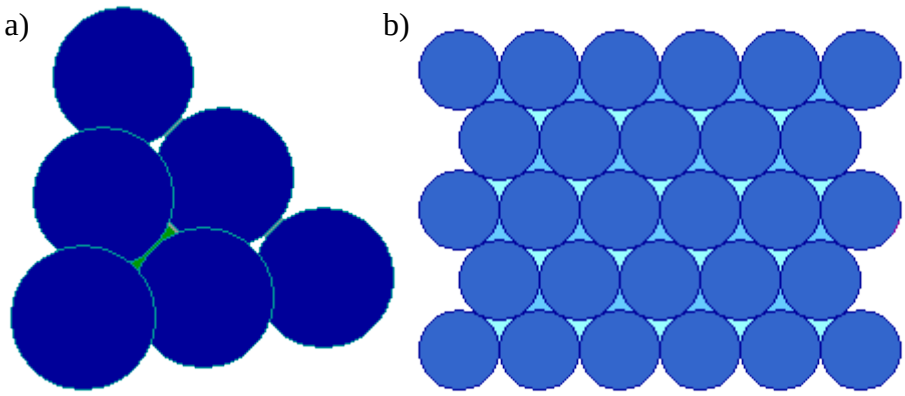

Figure 1.4: Diagram of a (111) surface:- a) shows the slice (in blue) of the crystal and b) shows the surface generated.

1.6. Adsorption of Molecules on Metal Surfaces

Adsorption of molecules at surfaces can be described, in general, by two classifications, namely physisorption and chemisorption. A physisorbed molecule retains most of its electronic structure upon adsorption and is only weakly bound to the surface. However, a chemisorbed substance is much more strongly bound and the adsorbate's electronic structure is modified by the adsorption process [29]. Physisorbed molecules bond via dipole forces (such as van der Waals forces) [30]. Chemisorbed molecules can bond via ionic or covalent bonds [31,32]; ionic bonding results from broadened molecular orbitals (HOMO or LUMO) crossing the Fermi level whereas covalent bonding occurs due to unoccupied molecular orbitals overlapping (or hybridising) with partially filled d-bands of transition metals. Chemisorbed molecules bond, on average, an order of magnitude stronger than physisorbed molecules and can significantly alter the electronic structure of the surface.

Adsorbed molecules must be sufficiently mobile in order to attain the lowest stabilisation energy. Therefore, molecules must be able to diffuse across the surface and this process depends upon a range of factors. These can be quantified by a diffusion co-efficient, D(θ,T) which represents the energy barrier the molecule must overcome in order to reach its final state. This can be represented by the equation:-

$$D(T) = D_0 \exp(-\frac{E_A}{RT}) \qquad (1.1)$$

Where D(T) is called the diffusion coefficient (cm^2s^{-1}), E_A is the activation energy ($KJmol^{-1}$), T is the temperature (K) and D_0 is the diffusivity (cm^2s^{-1}), R is the gas constant ($KJmol^{-1}T^{-1}$). Physisorbed molecules have lower diffusion activation energies and higher mobility, whereas, chemisorbed molecules have higher diffusion activation energies and lower mobility. However, variations across systems exist and this is only a general tendency.

1.7. Inter-Atomic and Inter-Molecular Bonding

Inter-molecular interactions play a crucial part in many surface chemical systems. Although hydrogen bonding falls into this category, it is becoming increasingly apparent that an understanding of dispersive forces is also necessary. The van der Waals force (or van der Waals interaction) is the sum of the attractive and repulsive forces between molecules (or between parts of the same molecule) other than those due to covalent bonds or to the electrostatic interaction of ions with one another or with neutral molecules [24]. The term includes:-

- The force between two permanent dipoles (Keesom force).
- The force between a permanent dipole and a corresponding induced dipole (Debye force).
- The force between two instantaneously induced dipoles (London force).

However, nowadays it is usually used to describe the totality of intermolecular forces (excluding hydrogen bonds). Van der Waals forces are relatively weak compared to other chemical bonds, but because they play a fundamental role in surface science systems it is crucial to be able to accurately describe them. Van der Waals forces include attractions between atoms, molecules, and surfaces. They differ from covalent and ionic bonding in that they are caused by correlations in the fluctuating polarizations of nearby particles (a consequence of quantum dynamics [25]). They are in detailed balance with electrostatic (ES) and exchange-repulsion (ER) interactions and, together, they control the structures of DNA and proteins, the packing of crystals, the formation of aggregates, host-guest systems and the orientation of molecules on surfaces or in molecular films. Intermolecular forces have four major contributions:-

1) A repulsive component resulting from the Pauli Exclusion Principle that prevents the collapse of molecules.
2) Attractive or repulsive electrostatic interactions between permanent charges (in the case of molecular ions), dipoles (in the case of molecules without an inversion centre), quadrupoles (all molecules with symmetry lower than cubic), and in general between permanent multipoles. The electrostatic interaction is sometimes called the Keesom interaction or Keesom force after Willem Hendrik Keesom.

3) Induction (also known as polarization), which is the attractive interaction between a permanent multipole on one molecule with an induced multipole on another. This interaction is sometimes called the Debye force after Peter J.W. Debye.
4) Dispersion (or London force, named after Fritz London), which is the attractive interaction between any pair of molecules, including non-polar atoms, arising from the interactions of instantaneous multipoles.

Returning to nomenclature, different texts refer to different things using the term "van der Waals force". Some texts mean by the van der Waals force the totality of forces (including repulsion); others mean all the attractive forces (and then sometimes distinguish van der Waals-Keesom, van der Waals-Debye, and van der Waals-London); finally, some use the term "van der Waals force" solely as a synonym for the London/dispersion force. However, nowadays, the common trend is that biochemistry and biology books, more frequently than chemistry books, use "van der Waals forces" as a synonym for London forces only.
All intermolecular/van der Waals forces are anisotropic (except those between two noble gas atoms), which means that they depend on the relative orientation of the molecules. That is, the electrostatic force can be attractive or repulsive, depending on the mutual orientation of the molecules. When molecules are in thermal motion, as they are in the gas and liquid phase, the electrostatic force is averaged out to a large extent, because the molecules thermally rotate and thus probe both repulsive and attractive parts of the electrostatic force. Sometimes this effect is expressed by the statement that "random thermal motion around room temperature can usually overcome or disrupt them" (which refers to the electrostatic component of the van der Waals force). Clearly, the thermal averaging effect is much less pronounced for the attractive induction and dispersion forces.

The Lennard-Jones potential is often used as an approximate model for the isotropic part of a total (repulsion plus attraction) van der Waals force as a function of distance. Van der Waals forces are responsible for certain cases of pressure broadening (van der Waals broadening) of spectral lines and the formation of van der Waals molecules. The London van der Waals forces are related to the Casimir effect for dielectric media, the former being the microscopic description of the latter bulk property. The first detailed calculations of this were done in 1955 by E. M. Lifshitz [3,4].

Theoretically, the ER and ES effects can already be described relatively accurately at a mean-field (i.e. Hartree-Fock, HF) level while the dispersive part is a pure electron correlation effect [25,16]. In the framework of standard *ab initio* wave function theory [26] it can be described by double excitations between occupied and virtual orbitals of the supermolecule (coupled monomer single excitations). Accurate computations based on, for example, coupled-cluster methods like CCSD(T) [56], however, suffer from unacceptable computation times even for medium-sized systems, and can thus routinely be applied only to benchmark studies of small complexes. Cheaper alternatives like second-order Møller-Plesset perturbation theory (MP2) [28] on the other hand, are computationally simpler and thus more widely used. However, especially for dispersive interactions, standard MP2 systematically overestimates the binding energies and underestimates intermolecular equilibrium distances [4,5].

Although today the most widely used theoretical approach to molecular structure, the density functional theory (DFT) [6,7] includes electron correlation effects in an approximate manner, it is now clear that almost all gradient-corrected density functionals are unable to describe dispersive interactions [8–10]. Although this problem now has become a very active field of research [11,12], it seems to be very difficult to account for dispersion within the standard Kohn–Sham picture of DFT. These nonlocal, long-range electron correlations already appear for the vanishing overlap of the electron densities of the fragments. Accordingly, they have only a tiny effect on the electron density of the fragments that is furthermore buried by the influences of the chemical environment.

All non-empirical attempts to introduce van der Waals interactions in DFT inevitably end up with methods that are at least as complex as the simplest wave function (i.e., MP2) methods. Another empirical strategy to solve the problem is to modify [13] or to combine [14] existing density functionals to reproduce, for example, the interaction potentials of rare gas dimers. These approaches cannot be considered as successful in a sense that the modified functionals are not applicable (transferable) for different systems (i.e., Ne_2 vs. Kr_2 vs. cytosine) [13]. The recently proposed XLYP functional [14] has solely been tested on He_2, Ne_2, and H_2O and thus, its "real" performance cannot be judged. Therefore, the modelling of van der Waals interactions using DFT is still a highly contentious one and is currently in a state of flux. However, it is currently believed that the empirically (or so-called Grimme) corrected is the best (or perhaps only) way forward with dealing with these inherent weaknesses of the DFT

method [15,16]. Reasonably accurate results that are in good accordance with experimental data have been obtained and this thesis utilises this method in accounting for all inter-molecular interactions.

1.8. Molecular Self-Assembly

Once adsorbed on the surface molecules may self-assemble to produce patterned surfaces with periodic nanoscale structures [33-34]. Due to the molecular resolution of Scanning Probe Microscopy (SPM) it has been possible to demonstrate that many molecules have the ability to form complex super-structures on crystal surfaces. When these molecules are thought of as ‘‘LEGO pieces’’ that can be attached to each other following certain rules it is possible to generate many different structures [1]. This organisational behaviour is dependent upon a fine balance between molecule-surface as well as molecule-molecule interactions. This variability often results in a multitude of organised structures for a single molecular species which can include one-dimensional (1D) chains and two-dimensional (2D) clusters [33,34]. This variety has led to the creation of the field of supramolecular surface chemistry and seeks to utilise chemical principles to create specific molecular architectures on various (usually, but not exclusively) metallic surfaces. These principles involve:-

1) Electrostatics (ion-ion, dipole-ion and dipole-dipole interactions).
2) Hydrogen bonding.
3) Π-Π stacking.
4) Dispersion/induction forces (i.e. van der Waals).
5) Hydrophobic and solvatophobic effects.

With the use of organic molecules, nucleic acids etc., which contain cyclic ring structures with peripheral functional groups and atoms that can hydrogen bond (i.e. nitrogen, oxygen, fluorine etc.) it is possible to produce 2D molecular structures that are bonded together by hydrogen and/or Π bonds. By utilising relatively unreactive metals (e.g. Au, Ag, Cu etc.), which hold the molecules in place, it is possible for them to form inter-molecular bonds [35-43]. Then (in order to produce different structures) different functional groups and metals of various indexes can be tried in order to “fine-tune” various surface structures [44-47]

although research is continuing to develop more advanced techniques [48-54]. These involve using Π-Π stacking to direct large scale structures [48], using metal ions to act as electron acceptors and thus bind as ligands [50,52] or metal-organic frameworks [53]. This has led to speculation that such 2D structures will find applications in molecular storage [49,51] as well as novel new magnetic materials [54,55].

Although inter-molecular interactions are utilised to direct the self-assembly of surface structures it is important not to forget that these structures must be held in place somehow. Therefore, the role of the molecule-substrate interaction must always be considered. The desired strength of this is permanently set when choosing the type of metal and the crystal cleave plane to be used. So, if you want the molecule to be weakly bound then Au is the obvious choice. However, in order to fix molecules in place more firmly requires a more reactive metal like Ni. However, an in-depth understanding of a quantitative nature of this so-called "adsorption footprint" is, at present, sadly lacking. It is for this reason that Cu, of intermediate reactivity, is often used in investigations of this type. Thus, Cu is able to securely hold most molecular structures firmly in place at room temperature but yet is still able to allow individual molecules a high degree of mobility. On top of this, if the surface is subjected to higher temperatures, then these said structures are then able to re-arrange themselves into further structures as well as to react with the surface.

1.9. Bibliography

[1] S. Radel, M. Navidi. *"Chemistry 2nd Edition."* West Publishing Company, 1994, 1158.

[2] L. Vrolyk. "*Clay and the Origins of Life*." New York Centre for Studies on the Origins of Life (July, 2000).

[3] G. Zubay. "*Origins of Life on the Earth and in the Cosmos."* San Francisco, Academic Press, 2000, 168.

[4] W. J. Hagan. *"Priming the Pre-RNA World."* Presentation July 27, 2000 at the New York Centre for Studies on the Origins of Life.

[5] Dr. J. P. Ferris. "*Montmorillonite Catalysis of RNA Oligomer Formation in Aqueous Solution. A Model for the Prebiotic Formation of RNA."* Journal of the American Chemical Society 1993, **155**, 12270-12275.

[6] K. Rybij. "*The 'RNA World' and the Polymerization of RNA Using Clay and Mineral Catalysis."* Presentation July 13, 2000.

[7] Dr. I. E. Odom. *"Sodium Montmorillonite and Calcium Montmorillonite: Properties and Uses."* Technical Data Sheet IC-1001 28 Nov.90W. American Colloid Company Industrial Chemical Division.

[8] H. Wennerström, S. Lidin. "*Scientific Background on the Nobel Prize in Chemistry 2007 Chemical Processes on Solid Surfaces*."

[9] H. Conrad, G. Ertl, E. E. Latta, (February 1974). *"Adsorption of hydrogen on palladium single crystal surfaces."* Surface Science **41** (2), 435–446.

[10] K. Christmann, G. Ertl, T. Pignet, (February 1976). *"Adsorption of hydrogen on a Pt(111) surface"*. Surface Science **54** (2), 365–392.

[11] K. Christmann, O. Schober, G. Ertl, M. Neumann (June 1, 1974). *"Adsorption of hydrogen on nickel single crystal surfaces"*. The Journal of Chemical Physics **60** (11), 4528–4540.

[12] K. Christmann, R. J. Behm, G. Ertl, M. A. Van Hove, W. H. Weinberg. *"Chemisorption geometry of hydrogen on Ni(111): Order and disorder"*. The Journal of Chemical Physics (May 1, 1979), **70** (9), 4168–4184.

[13] R. Imbihl, R. J. Behm, K. Christmann, G. Ertl, T. Matsushima. *"Phase transitions of a two-dimensional chemisorbed system: H on Fe(110)."* Surface Science, (May 2, 1982), **117**, 257–266.

[14] J. M. Thomas and W. J. Thomas. *"Principles and Practice of Heterogeneous Catalysis."* VCH, (Oct 15, 1996).

[15] S. Grimme, J. Antony. *"Density functional theory including dispersion corrections for intermolecular interactions in a large benchmark set of biologically relevant molecules*". Phys. Chem. Chem. Phys. (August 31, 2006), **8**, 5287-5293.

[16] S. Grimme. *"Accurate description of van der Waals complexes by density functional theory including empirical corrections".* J Comp. Chem. (April 29, 2004), **25**, 1463-1473.

[17] P. Chang, N. P. Lang, W. P. Giannobile. *"Evaluation of Functional Dynamics during Osseointegration and Regeneration Associated with Oral Implants: A Review".* Clin. Oral Implants Res. (Jan, 2010), **21**(1), 1–12.

[18] N. Ferraz, J. Hong, M. Santin, M. Karlsson. *"Nanoporosity of Alumina Surfaces Induces Different Patterns of Activation in Adhering Monocytes/Macrophages"*. Int. Journal of Biomaterials (2010), Article ID 402715, 8 pages.

[19] W. Gopel. *"Biosensors and bioelectronics."* (1998), **13**, 723.

[20] F. Allegretti, M. Polcik and D.P. Woodruff. *"Quantitative Determination of the Local Structure of Thymine on Cu(110) Using Scanned-Energy Mode Photoelectron Diffraction."* Surface Science (2007), **601**(17), 3611-3622.

[21] R. E. A. Kelly, L. N. Kantorovich. *"Homopairing Possibilities of the DNA Base Thymine and the RNA Base Uracil: An Ab Initio Density Functional Theory Study."* J. Phys. Chem. B (2006), **110**(5), 2249-2255.

[22] W. Xu, R. Kelly, R. Otero, M. Schock. *"Probing the Hierarchy of Thymine-Thymine Interactions in Self-Assembled Structures by Manipulation with Scanning Tunnelling Microscopy."* Small (2007), **3**(12), 2011-2014.

[23] A. McNutt, PhD thesis, University of Liverpool, 2002.

[24] IUPAC, Compendium of Chemical Terminology, 2nd ed. (the "Gold Book") (1997). Online corrected version: (1994) "Van der Waals forces".

[25] A. A. Abrikosov, L.P. Gorkov, I.E. Dzyaloshinsky. "*Methods of Quantum Field Theory in Statistical Physics*." Dover Publications (1963–1975). ISBN 0-486-63228-8. Chapter 6 - Electromagnetic Radiation in an Absorbing Medium.

[26] W. Kutzelnigg, W. Einfűhrung in die Theoretische Chemie: Band 2, Di chemische Bindung; Varlag Chemie: Weinheim, 1978.

[27] T. Helgaker, P. Jørgensen, J. Olsen. *"Molecular Electronic-Structure Theory."* J. Wiley: New York, 2000.

[28] D. Cremer, P. von Rague–Schleyer. *"Encyclopaedia of Computational Chemistry."* J. Wiley: New York, 1998, **3**, 1706.

[29] A. Zangwill. *"Physics at Surfaces."* Cambridge University Press, Cambridge, 1988.

[30] G. Attard, C. Barnes. *"Surfaces."* Oxford University Press, 1988.

[31] N. D. Lang, A. R. Williams. *"Theory of Atomic Chemisorption on Simple Metals."* Phys. Rev. B., 1978, **18**(2), 616-636.

[32] R. Hoffman. *"Reviews of Modern Physics."* 1988, p. 601, vol. 60.

[33] J. V. Barth, G. Costantini, K. Kern. *"Engineering Atomic and Molecular Nanostructures at Surfaces."* Nature 2005, **437**(7059), 671-679

[34] J. V. Barth. *"Molecular architectonic on metal surfaces."* Annu. Rev. Phys. Chem. 2007, **58**, 375-407.

[35] P. D. Beer, P. A. Gale, D. K. Smith. *"Supramolecular Chemistry."* Oxford University Press 1999.

[36] S. Weigelt, C. Busse, L. Petersen. *"Chiral switching by spontaneous conformational change in adsorbed organic molecules."* Nature Materials 2006, **5**, 112-117.

[37] C. Bombis, S. Weigelt, M. M. Knudsen. *"Steering organizational and conformational surface chirality by controlling molecular chemical functionality."* ACS Nano 2010, **4**(1), 297-311.

[38] M. Matena, A. Llanes-Pallas, M. Enache. *"Conformation-Controlled Networking of H-Bonded Assemblies on Surfaces."* Chem. Comm. 2009, **24**, 3525-3527.

[39] N. Wintjes, J. Hornung, J. Lobo-Checa. *"Supramolecular Synthons on Surfaces: Controlling Dimensionality and Periodicity of Tetraarylporphyrin Assemblies by the Interplay of Cyano and Alkoxy Substituents."* Chem. Eur. J. 2008, **14**(19), 5794-5802.

[40] F. Klappenberger, M. Canas-Ventura, S. Clair. *"Conformational adaptation in supramolecular assembly on surfaces."* ChemPhysChem, 2007, **8**(12), 1782-1786.

[41] L.A. Fendt, M. Stohr, N. Wintjes. *"Modification of Supramolecular Binding Motifs Induced by Substrate Registry: Formation of Self-Assembled Macrocycles and Chain-like Patterns."* Chem. Eur. J. 2009, **15**(42), 11139-11150.

[42] A. Llanes-Pallas, C. A. Palma, L. Piot. *"Engineering of Supramolecular H-Bonded Nanopolygons via Self-Assembly of Programmed Molecular Molecular Modules."* J. Am. Chem. Soc. 2009, **131**(2), 509-520.

[43] A. Llanes-Pallas, M. Matena, T. Jung. *"Trimodular Engineering of Linear Supramolecular Miniatures on Ag(111) Surfaces Controlled by Complementary Triple Hydrogen Bonds."* Angew. Chem. Int. Ed. 2008, **47**(40), 7726-7730.

[44] M. Abel, V. Oison, M. Koudia. *"Designing a New Two-Dimensional Molecular Layout by Hydrogen Bonding."* Chemphyschem. 2006, **7**(1), 82-85.

[45] K. W. Hipps, L. Scudiero, D. E. Barlow. *"A self-organized 2-dimensional bifunctional structure formed by supramolecular design."* J. Am. Chem. Soc. 2002, **124**(10), 2126-2127.

[46] W. Auwarter, A. Weber-Bargioni, A. Schriffrin. *"Self-Assembly and Conformation of Tetrapyridyl-Porphyrin Molecules on Ag(111)."* J. Chem. Phys. 2006, **124**(19), 194708.

[47] L. Gross, F. Moresco, P. Raffieux. *"Tailoring Molecular Self-Organization by Chemical Synthesis: Hexaphenylbenzene, Hexa-peri-hexabenzocoronene, and Derivatives on Cu(111)."* Phys. Rev. B. 2005, **71**(16), 165428.

[48] P. J. Donovan, PhD Thesis, University of Liverpool, 2009.

[49] M. E. Kosal, J. Chou, S. R. Wilson. *"A Functional Zeolite Analogue Assembled from Metalloporphyrins."* Nat. Mater. 2002, **1**(2), 118-121.

[50] S. L. Tait, Y. Wang, G. Costantini. *"Metal-Organic Coordination Interactions in Fe-Terephthalic Acid Networks on Cu(100)."* J. Am. Chem. Soc. 2008, **130**(6), 2108-2113.

[51] M. Eddaoudi, J. Kim, N. Rosi. *"Hydrogen Storage in Microporous Metal-Organic Frameworks."* Science 2003, **300**(5622), 1127-1129.

[52] M. A. Lingenfelder, H. Spillmann, A. Dmitriev. "*Towards Surface-Supported Supramolecular Architectures: Tailored Coordination Assembly of 1,4-Benzenedicarboxylate and Fe on Cu(100)."* Chem. Eur. J. 2004, **10**(8), 1913-1919.

[53] M. J. Ingleson, J. Bacsa, M. J. Rosseinsky. *"Homochiral H-Bonded Proline Based Metal Organic Frameworks."* Chem. Comm. 2007, **29**, 3036-3038.

[54] S. Chui, S. Lo, J. Charmant. *"A Chemically Functionalizable Nanoporous Material [Cu3(TMA)2 (H2O)3](n)."* Science 1999, **283**(5405), 1148-1150.

[55] P. Gambardella, S. Stepanow, A. Demitriev. *"Supramolecular Control of the Magnetic Anisotropy in Two-Dimensional High-Spin Fe Arrays at a Metal Interface."* Nat. Mater. 2009, **8**(3), 189-193.

[56] S. Wilson, *"A critical analysis of the 'CCSD(T)' model for the study of electron correlation effects in atoms and molecules."* Rutherford Appleton Laboratory, http://epubs.cclrc.ac.uk/bitstream/317/raltr-2003035.pdf

2. Chapter Two - Theoretical Techniques

2.1. Density Functional Theory (DFT) – A General Overview

2.1.1. Introduction – What Is Density Functional Theory?

Density functional theory is a phenomenally successful approach to finding solutions to the fundamental equation that describes the quantum behaviour of atoms and molecules, the Schrödinger equation, in settings of practical value. Although DFT has been used since the 1970s it was only in the 1990s when better approximations for the exchange and correlation interactions were implemented that it became more widely used. Because it is much less computationally costly than methods based on complex many electron wavefunction theories (like Hartree-Fock) it has become the main method used now in quantum chemistry. For a good introduction to DFT see "The ABC of DFT" [12].

2.1.2. The Schrödinger Equation

Let us imagine a situation where we would like to describe the properties of some well-defined collection of atoms – you could think of an isolated molecule or the atoms defining the crystal of an interesting mineral. One of the fundamental things we would like to know about these atoms is their energy and, more importantly, how their energy changes if we move the atoms around. To define where an atom is, we need to define both where its nucleus is and where the atom's electrons are. In order to obtain a microscopic description of the interactions taking place between molecules it is necessary to solve the many-body Schrödinger equation:-

$$\left[-\frac{1}{2}\sum_{i=1}^{N}\nabla_{\mathrm{i}}^{2} + \sum_{\mathrm{i}=1}^{N}\mathrm{V}(\mathbf{r}_{\mathrm{i}}) + \sum_{i=1}^{N}\sum_{j<i}U(\mathbf{r}_i,\mathbf{r}_j)\right]\psi = E\psi \qquad (2.1)$$

The three terms on the left side of this equation represent, in order, the kinetic energy of each electron (with ∇^2 as the 'Laplacian'), the interaction energy between each electron and the collection of atomic nuclei and the interaction energy between different electrons (with V and U representing the potential energy, r representing the distance between electrons as a vector and i and j representing individual electrons). This combination of terms represents what is known as the 'Hamiltonian' operator and ψ represents a set of solutions, or eigenstates, of the Hamiltonian. It is called the electronic wave function, which is a function of each of the spatial co-ordinates of each of the N electrons, so $\psi = \psi(r_1, \ldots . r_N)$. Each of these solutions, ψ_n (which is a complex number), has an associated eigenvalue, E_n (which is a real number), that satisfies the eigenvalue equation. The detailed definition of the Hamiltonian depends on the physical system being described by the Schrödinger equation. Also, as the ground-state energy is independent of time, this is what is known as the 'time-independent Schrödinger equation'.

Although this gives a complete description of any system the problem is that the dimension of the wave function grows very rapidly with the number of electrons. Therefore, a method of simplifying the mathematics is required. DFT provides this simplification and the problem of many-electrons interacting is replaced with an effective potential. The many-electron wave function is replaced by the electron density thus reducing the problem from 3N dimensions to one of just N electrons.

2.1.3. DFT – From Wave Functions To Electron Density

Density functional theory rests on just two fundamental mathematical theorems proved by Kohn and Hohenberg and the derivation of a set of equations by Kohn and Sham in the mid-1960s. The Kohn-Sham equations provide the framework for finding the exact density and energy of the ground state of a many-body electron system using standard independent particle methods. The first theorem, proved by Hohenberg and Kohn, is: *The ground-state energy from Schrödinger's equation is a unique functional of the electron density*. The theorem states that there exists a one-to-one mapping between the ground-state wave function and the ground-state electron density. However, this theorem says nothing about what the functional actually is. The second Hohenberg-Kohn theorem defines an important property of the functional:-

The electron density that minimizes the energy of the overall functional is the true electron density corresponding to the full solution of the Schrödinger equation.

We can write down the functional described by the Hohenberg-Kohn theorem in terms of the single-electron wave functions, $\psi_i(\mathbf{r})$ which defines the electron density $n(\mathbf{r})$. The energy functional can be written as:-

$$E[\{\psi_i\}] = E_{known}[\{\psi_i\}] + E_{XC}[\{\psi_i\}] \tag{2.2}$$

The "known" terms can be written as:-

$$E_{known}[\{\psi_i\}] = -\sum_i \int \psi_i^* \nabla^2 \psi_i \, d^3r + \int V(\boldsymbol{r}) n(\boldsymbol{r}) \, d^3r + \frac{e^2}{2} \int \int \frac{n(r) n(r')}{|r-r'|} d^3r d^3r' + E_{ion} \tag{2.3}$$

The equation represents, in order, the electron kinetic energies, the Coulomb interactions between the electrons and the nuclei, the Coulomb interactions between pairs of electrons, and the Coulomb interactions between pairs of nuclei. The unknown term, $E_{XC}[\{\psi_i\}]$ is called the exchange-correlation functional.

Kohn and Sham showed that the right electron density can be expressed in a way that involves solving a set of equations in which each equation only involves a single electron. These have the form:-

$$\left[-\frac{1}{2}\nabla^2 + V(\boldsymbol{r}) + V_H(\boldsymbol{r}) + V_{XC}(\boldsymbol{r}) \right] \psi_i(\boldsymbol{r}) = \varepsilon_i \psi_i(\boldsymbol{r}) \tag{2.4}$$

The first two terms are known. The third term is called the Hartree potential and is defined as:-

$$V_H(\mathbf{r}) = e^2 \int \frac{n(r')}{|r-r'|} d^3r' \tag{2.5}$$

This describes the Coulomb repulsion between the electron being considered in one of the Kohn-Sham equations and the total electron energy density. The fourth term is defined as the

"functional derivative" of the exchange-correlation energy:-

$$V_{XC}(\mathbf{r}) = \frac{\delta E_{XC}(\boldsymbol{r})}{\delta n(\boldsymbol{r})} \tag{2.6}$$

All this ultimately leads to a circular problem. In order to solve the Kohn-Sham equations we need to define the Hartree potential and to define the Hartree potential we need to know the electron density. However, to find the electron density we must know the single-electron wave functions and to know these we must solve the Kohn-Sham equations. Thus, we are led to an iterative approach:-

1. Define an initial, trial electron density, $n(\mathbf{r})$.
2. Solve the Kohn-Sham equations to find the single-particle wave functions, $\psi_i(\mathbf{r})$.
3. Calculate the new electron density from step 2, $n_{KS}(\mathbf{r})=2\sum_i \psi_i^*(\mathbf{r})\,\psi_i(\mathbf{r})$.
4. Compare the calculated electron density, $n_{KS}(\mathbf{r})$, with the electron density used in solving the Kohn-Sham equations, $n(\mathbf{r})$. If the two densities are the same then this is the ground-state electron density and can be used to compute the total energy.
5. Otherwise, the trial electron density must be updated using a chosen algorithm and the iteration routine repeated.

The Kohn-Sham equations are a set of Schrödinger-like independent particle equations which must be solved subject to the condition that the effective potential $V_{eff}^{\sigma}(\mathbf{r})$ and the density $n(\mathbf{r}, \sigma)$ are consistent. This must be solved iteratively by providing an initial guess and using this to calculate the effective potential $V_{eff}^{\sigma}(\mathbf{r})$ which then enables us to solve the KS equation. This means we can calculate the electron density and we are able to see if this is consistent with our initial guess. The loop then re-iterates until the initial and final electron densities are the same. Obviously, this is a very simplified approach but this iterative method is used to solve the Kohn-Sham equations until they are self-consistent.

2.1.4. The Exchange-Correlation Functional

Unfortunately, the true form of the exchange-correlation functional is simply unknown.

However, for a uniform electron gas it can be derived exactly [1]. In this situation, the electron density is constant at all points in space; that is $n(\mathbf{r})$ = constant. This approximation uses only the local density to define the approximate exchange-correlation functional and is called the *local density approximation* (LDA) [2]. However, this does not exactly solve the true Schrödinger equation and the development of functionals that more faithfully represent nature remains an active area of research [3].

A number of approximate functionals have now been developed that give good results in a wide range of physical problems. The best known class of functional after the LDA uses information about the local electron density and the local gradient in the electron density; this approach defines a *generalized gradient approximation* (GGA) [4]. However, there are many ways in which information from the gradient of the electron density can be included in a GGA functional and there are a large number of these functionals. Two of the most widely used of these are the Perdew-Wang functional (PW91) [5] and the Perdew-Burke-Ernzerhof functional (PBE) [6]. Dozens of other GGA functionals have also been developed which give somewhat different results for any particular configuration of atoms. For this reason it is important to specify which functional was used in any particular calculation.

2.1.5. Limitations Of DFT

As successful as DFT calculations can be it must be understood that practical DFT calculations are not exact solutions of the full Schrödinger equation. There are some important situations for which DFT cannot be expected to be physically accurate. The first of these situations where DFT has limited accuracy is in the calculation of electronic excited states. This is due to the basic premise of Hohenberg-Kohn that only applies to the ground-state energy. Standard DFT calculations with existing functionals have limited accuracy for band gaps, with errors >1eV being common [21-22]. However, this is currently an active area of research where considerable progress is being made.

2.1.6. Van der Waals Correction

Another situation where DFT calculations give inaccurate results is associated with the weak van der Waals (vdW) attractions between molecules. These interactions occur because of correlations that exist between temporary fluctuations in the electron density of one molecule and the energy of the electrons in another molecule responding to these fluctuations. Thus, van der Waals interactions are the direct result of long range electron correlation. To accurately calculate the strength of these interactions from quantum mechanics it is necessary to use high-level wave-function-based methods that treat electron correlation in a systematic way [7].

Several versions of the van der Waals density-functional (vdW-DF) exist but in this work we are using the recently implemented one by Stefan Grimme's group [8]. In this vdW-DF, the dispersion corrected total energy is:-

$$E_{MF-D} = E_{MF} + E_{disp} \tag{2.6a}$$

where E_{MF} is the usual mean-field energy (i.e. HF or DFT) and E_{disp} is an empirical dispersion correction given by:-

$$E_{disp} = -s_6 \sum_{i=1}^{N_{at}-1} \sum_{j=i+1}^{N_{nat}} \frac{C_6^{ij}}{R_{ij}^6} f_{dmp}(R_{ij}) \tag{2.6b}$$

where N_{at} is the number of atoms in the system, C_6^{ij} denotes the dispersion coefficient for atom pair ij, s_6 is a global scaling factor and R_{ij} is the interatomic distance. In order to avoid near-singularities for small R, a damping function f_{dmp} must be used, given by:-

$$f_{dmp}(R) = \frac{1}{1+ e^{-\propto(R/R_0-1)}} \tag{2.6c}$$

Where R_0 is the sum of atomic van der Waals radii [9, 10]. Eq. (1.6c) is chosen because it decays at small R fast enough to zero such that dispersion corrections between atoms well below van der Waals distances are negligible and thus, "normal" bonds are not significantly affected by the correction.

2.2. Density Functional Theory (DFT) – Foundations

2.2.1. Thomas-Fermi-Dirac Approximation

The original density functional theory of quantum systems is the method of Thomas and Fermi proposed in 1927. In this model, the Thomas-Fermi method, the kinetic energy of the system of electrons is approximated as an explicit functional of the density, idealized as non-interacting electrons in a homogeneous gas with density equal to the local density at any point. This was further extended to include exchange and correlation among the electrons by Dirac in 1930 who formulated the local approximation for exchange still in use today. However, the Thomas-Fermi type approach starts with approximations that are too crude, missing essential physics and chemistry, such as shell structures of atoms and binding of molecules and thus falls short of the goal of a useful description of electrons in matter.

2.2.2. Hohenberg-Kohn Theorems

The approach of Hohenberg and Kohn is to formulate density functional theory as an exact theory of many-body systems. This applies to any system of interacting particles in an external potential. The two theorems proved by Hohenberg and Kohn provide the basis for density functional theory [8]. These can be stated thus:-

1. For any system of interacting particles in an external potential $V_{ext}(\mathbf{r})$, the potential $V_{ext}(\mathbf{r})$ is determined uniquely, except for a constant, by the ground state particle density $n_o(\mathbf{r})$. Therefore, since the Hamiltonian is fully determined, except for a constant shift of the energy, it follows that the many-body wavefunctions for all states (ground and excited) are determined. Therefore all properties of the system are completely determined given only the ground state density $n_o(\mathbf{r})$.
2. A universal functional for the energy $E[n]$ in terms of the density $n(\mathbf{r})$ can be defined, valid for any external potential $V_{ext}(\mathbf{r})$. For any particular $V_{ext}(\mathbf{r})$, the exact ground state energy of the system is the global minimum value of this functional and the density $n(\mathbf{r})$ that minimizes the functional is the exact ground state density $n_o(\mathbf{r})$. Therefore the functional $E[n]$ alone is sufficient to determine the exact ground state energy and density.

With these simple assertions it follows that by minimizing the total energy of the system with respect to variations in the density function $n(\mathbf{r})$ one could find the exact ground state density and energy. However, as mentioned previously, the functional only determines the ground state properties and not any excited states.

2.3. The Kohn-Sham Ansatz

2.3.1. Overview

Because of Kohn and Sham's approach to replace the original many-body problem by an auxiliary independent particle problem DFT has become the most widely used method for electronic structure calculations. It has led to a self-consistent method involving independent particles but an interacting density, the crucial ingredient being the exchange-correlation energy functional $E_{xc}[n]$.

2.3.2. Kohn-Sham Variational Equations

Solution of the Kohn-Sham system is the problem of minimization with respect to either the density $n(\mathbf{r},\sigma)$ or the effective potential $V_{eff}^{\sigma}(\mathbf{r})$. This leads to the Kohn-Sham Schrödinger-like equations:-

$$(H_{KS}^{\sigma} - \varepsilon_i^{\sigma})\psi_i^{\sigma}(\mathbf{r}) = 0 \tag{2.7}$$

Where ε_i are the eigenvalues and H_{KS} is the effective Hamiltonian:-

$$H_{KS}^{\sigma}(\mathbf{r}) = -\frac{1}{2}\nabla^2 + V_{KS}^{\sigma}(\mathbf{r}) \tag{2.8}$$

With:-

$$V_{KS}^{\sigma}(\mathbf{r}) = V_{ext}(\mathbf{r}) + V_{Hartree}(\mathbf{r}) + V_{xc}^{\sigma}(\mathbf{r}) \quad (2.9)$$

These equations are independent of any approximation to the functional $E_{xc}[n]$ and would lead to the exact ground state density and energy for the interacting system if the exact functional $E_{xc}[n]$ were known. Furthermore, it follows from the Hohenberg-Kohn theorems that the ground state density uniquely determines the potential at the minimum so that there will be a unique Kohn-Sham potential $V_{eff}^{\sigma}(\mathbf{r})|_{min} \equiv V_{KS}^{\sigma}(\mathbf{r})$ associated with any given interacting electron system.

2.3.3. E_{XC} And V_{XC}

By explicitly separating out the independent particle kinetic energy and the long-range Hartree terms the remaining exchange-correlation functional $E_{\mathrm{xc}}[n]$ can be approximated as a local (or nearly local) functional of the density. This means that the energy $E_{\mathrm{xc}}[n]$ can be expressed in the form:-

$$E_{xc}[n] = \int \mathrm{d}\mathbf{r}\, n(\mathbf{r})\epsilon_{\mathrm{xc}}([n],\mathbf{r}) \quad (2.10)$$

Where $\epsilon_{\mathrm{XC}}([n],\mathbf{r})$ is the energy per electron at point r that depends only upon the density $n(\mathbf{r},\sigma)$ in some neighbourhood of point **r**. The exchange-correlation potential $V_{xc}^{\sigma}(\mathbf{r})$ is the functional derivative of E_{xc} which can be written as:-

$$V_{xc}^{\sigma}(\mathbf{r}) = \epsilon_{\mathrm{xc}}([n],\mathbf{r}) + \mathrm{n}(\mathbf{r})\frac{\delta\epsilon_{xc}([n],\mathbf{r})}{\delta n(\mathbf{r},\sigma)} \quad (2.11)$$

where $\epsilon_{\mathrm{xc}}([n],\mathbf{r})$ is defined by the previous equation and is a functional of the density $n(\,r',\sigma'\,)$. The great advance of the Kohn-Sham approach over the Thomas-Fermi approximation is that it is defined by the requirement that it yield the exact charge density. Thus, the application of the Hohenberg-Kohn theorem to the Kohn-Sham non-interacting system implies that the exact density can be fit by only one $V_{xc}^{\sigma}(\mathbf{r})$ which is unique except for an additive term.

2.4. The Exchange Correlation Functional

2.4.1. Overview

The crucial quantity in the Kohn-Sham approach is the exchange-correlation energy which is expressed as a functional of the density $E_{xc}[n]$. In this section we explore some of the relevant approximate functionals. By explicitly separating out the independent particle kinetic energy and the long range Hartree terms the remaining exchange-correlation functional $E_{xc}[n]$ can be approximated as a local (or nearly local) functional of the density. Even though the exact functional $E_{xc}[n]$ will most likely be very complex it is possible to approximate it with much success.

2.4.2. Local Spin Density Approximation (LSDA)

Kohn and Sham showed that solids can be considered approximately as a homogeneous electron gas (HEG) where exchange and correlation effects are local. So a Local (Spin) Density Approximation was proposed (LSDA) in which the exchange-correlation energy is simply an integral over all space with the energy density assumed to be the same as in a HEG with that density. So, for a spin-unpolarized system a local density approximation for the exchange-correlation energy can be written:-

$$E_{xc}^{LDA}[\rho] = \int \rho\,(r)\epsilon_{\mathrm{xc}}(\rho)\mathrm{d}\mathbf{r} \tag{2.12}$$

Where ρ is the electronic density and ϵ_{xc} (the exchange-correlation energy density) is a function of the density alone. The exchange-correlation energy can be separated into the exchange and correlation terms linearly:-

$$E_{xc} = E_x + E_c \tag{12.13}$$

The exchange term (E_x) has a simple analytic form for the HEG but only limiting expressions for the correlation density (E_c) are known exactly.

2.4.3. Generalised-Gradient Approximation (GGA)

The term generalised-gradient approximation (GGA) refers to a variety of ways proposed for functions that modify the behaviour at large gradients in such a way as to preserve desired properties. GGAs are still local but take into account the gradient of the density at the same co-ordinate:-

$$E_{XC}^{GGA}[n_\uparrow, n_\downarrow] = \int \epsilon_{xc}\left(n_\uparrow, n_{\downarrow,} \vec{\nabla} n_\uparrow, \vec{\nabla} n_\downarrow\right) n(\vec{r}) d^3 r \qquad (2.14)$$

GGA has provided good results for molecular geometries and ground-state energies. There are now many GGA functionals in use today, the most widely known being the Perdew and Wang (PW91) [5] and Perdew, Burke and Enzerhof (PBE) [6]. In this thesis the PW91 GGA has been used throughout.

2.5. Vienna Ab-Initio Simulation Package (VASP)

2.5.1. Overview

VASP is a software package which performs ab-initio quantum-mechanical dynamics (MD) simulations using a plane wave basis set. All DFT computations of electronic total energies in this thesis have been performed using this package. The interactions between ions/electrons are described by ultra-soft Vanderbilt pseudopotentials (US-PP) or by the projector-augmented wave (PAW) method. These allow for considerable reduction of the number of plane-waves per atom for transition metals and first row elements. By using such methods as these it is possible to achieve a "well converged" solution. By this we mean one that approximates to the true solution with a specific exchange-correlation functional.

2.5.2. Pseudopotentials

Electrons in matter consist of core electrons (which are strongly localised in the closed inner atomic shells) and valence electrons (which exist further out). A plane wave basis set is

unsuitable for describing the core electron wavefunctions as a prohibitively large number would be required to accurately describe these oscillations. However, the core electron structure remains almost unchanged in different chemical environments and so can be approximated by the use of a pseudopotential approximation. Thus, by using a pseudopotential we can replace the strong Coulomb potential of the nucleus as well as the effects of the tightly bound core electrons by an effective ionic potential acting on the valence electrons.

2.5.3. Ultrasoft Pseudopotentials (USPPs)

The details of a particular pseudopotential define a minimum energy cut-off used in calculations including atoms associated with that pseudopotential. Pseudopotentials requiring high cut-off energies are called hard whilst the more computationally efficient pseudopotentials with lower cut-off energies are called soft. Many modern pseudopotential calculations use the Kleinman-Bylander form, otherwise known as "Ultrasoft" pseudopotentials (USPPs), developed by Vanderbilt in the early 1990s [13]. USPPs attain much smoother (softer) pseudo-wavefunctions and use considerably fewer plane-waves. In this thesis USPP have been used throughout with consistent use of the same type for every simulation.

2.5.4. Reciprocal Space and K-Points

VASP uses density functional theory to provide a good atomic-level description of all types of materials and molecules. By using plane wave basis sets with ultrasoft pseudopotentials calculations are performed in reciprocal space by using Fourier transforms. The reciprocal space that represents the most compact possible cell is called the Brillouin zone (BZ), inside the BZ there are no boundaries, every boundary point is a **k** vector determined from the k-points.

2.5.5. *Energy Cut-Offs*

Bloch's theorem tells us that the solutions of the Schrödinger equation for a periodic system are:-

$$\Phi_k(\mathbf{r}) = \exp(i\mathbf{k}\cdot\mathbf{r})\, u_k(\mathbf{r}) \tag{2.15}$$

with $u_k(\mathbf{r})$ having the same periodicity as the supercell. This periodicity enables us to expand $u_k(\mathbf{r})$ as a set of plane waves:-

$$u_k(\mathbf{r}) = \sum_{\mathbf{G}} c_G \exp[i\mathbf{G}\cdot\mathbf{r}] \tag{2.16}$$

where G represents a reciprocal lattice vector. Combining these last two equations gives:-

$$\Phi_k(\mathbf{r}) = \sum_{\mathbf{G}} c_{\mathbf{k+G}} \exp[i(\mathbf{k}+\mathbf{G})\mathbf{r}] \tag{1.17}$$

However, this summation requires an infinite number of possible values of **G** but because they can be interpreted as the solutions with kinetic energy. With this in mind we can truncate this infinite sum to include only the solutions with kinetic energy less than some value. And hence the infinite sum becomes:-

$$\Phi_k(\mathbf{r}) = \sum_{|\mathbf{G}+\mathbf{k}|<G_{\mathrm{cut}}} c_{\mathbf{k+G}} \exp[i(\mathbf{k}+\mathbf{G})\mathbf{r}] \tag{2.18}$$

This now leads us to a parameter that must be provided, namely the cut-off energy, E_{cut}. This cut-off energy is different for each atomic species because it is determined by how rapidly pseudopotentials vary. Whenever different atomic species are combined in any calculation the highest value should, of course, be used. Also, it is important to remember that whenever DFT calculations for multiple systems are compared to calculate energy differences the same cut-off energy should be used in all calculations.

2.5.6. *Periodic Boundary Conditions*

Since our model of the crystalline surface is infinite in the x and y direction but finite in the z

direction we must take care to correctly model the boundary conditions. Adjacent x and y unit cells must be placed so that adjacent atoms are correctly spaced to correctly account for this. In the z direction we must ensure that the adjacent unit cell does not interact with the one next to it. This is known as the slab model. So, it is important when using such a model to ensure that there is enough vacuum space so that the electron density of the material tails off to zero in the vacuum and that the top of one slab has essentially no effect on the bottom of the next.

2.5.7. Numerical Optimization

Whenever iterative techniques are utilised it is important to be aware of numerical convergence. In order to make practical use of our ability to perform numerical DFT calculations we also need methods where we can search through a problem with many degrees of freedom. Important properties of numerical optimization and convergence include:-

1. The algorithms are iterative so they do not provide an exact solution.
2. An initial estimate (or best guess) must be provided to use the algorithms.
3. The use of a tolerance parameter is required in order to estimate how close the solution is to the exact solution.
4. Choosing an appropriate algorithm can greatly reduce convergence times.

Various methods exist for minimisation of multi-dimensional vectors of which perhaps the best known is called the conjugate-gradient method for minimizing a general function E(**x**) where **x** is an N-dimensional vector [23]. However, in all calculations utilised in this thesis an algorithm known as the Residual Minimization Scheme is used. This involves Direct Inversion in the Iterative Subspace and hence is called the RMM-DIIS scheme for short [24].

2.5.8. Geometry Optimization

Various factors have to be considered when considering the topic of geometry optimization. Are we dealing with an isolated system or a lattice? What is to be our criteria for minimization? Are any of the atoms to be constrained (i.e. fixed in place)? For an isolated

system it is important to be aware that the system will be repeating in x, y and z directions and so a suitable distance should be provided in between the atoms in each periodic image in order to ensure that no interactions occur. In systems where we are dealing with a lattice structure it is even more important to be aware of the exact size of the periodic system as, in order to effectively model this system, adjacent atoms must be placed at the appropriate positions.

A further consideration we must make whenever dealing with atoms is the force on each atom. Indeed, whenever optimizing any geometry to a relaxed state it is this factor more than any other that defines a stable system. In all calculations done in this thesis a cut-off value of 0.01eV/Å has been used. Why this figure? Well, if we change the atom's position by a small amount, say Δr, then the change in the total energy due to this change can be estimated $|\Delta E| \cong |\mathbf{F}||\Delta r|$, where $|\mathbf{F}|$is the force on each atom. This means that if the forces on all the atoms are less than 0.01eV/Å then moving an individual atom by 0.1Å, a relatively significant difference in terms of chemical bond lengths will change the total energy by less than 0.001eV, a small amount of energy.

The final consideration to be made is whether or not we want some of the atoms to remain fixed in place. The only reason for doing this would be if we already knew where the atoms should be prior to optimization. When modelling the surface of a crystal we still need to know how these surface atoms will interact with any molecule placed upon it. However, when considering the bulk of the crystal it is reasonable to assume that these atoms will not significantly interact with the molecules and can thus be held in place. In the first section of this thesis when dealing with thymine it was chosen that the first two layers should be allowed to move and represent the surface and that the lower two layers be constrained and represent the bulk, therefore, with four layers in total representing the entire crystal. However, for the melamine section this was refined to the first three layers representing the surface and the lower two being constrained to represent the bulk. This time therefore having five layers in total.

2.5.9. Choosing K-Points

When we numerically integrate over the Brillouin zone we need a reliable method of choosing K-points. The Monkhorst-Pack method [25] has been used here. When choosing

K-points it's important to remember that smaller supercells will become larger in reciprocal space and so will require proportionally more K-points. For the z-direction it is only necessary to use one k-point because, if the vacuum region is large enough, the electron density tails off to zero a short distance from the edge of the slab and there is very little dispersion in the electronic band structure in this direction.

2.5.10. Surface Relaxation/Energies

When a surface relaxes there is no restriction on the spacing of the atoms like there is in the bulk. It is often the case that the spacings of the layers and separation of the atoms at the surface are somewhat different from those in the bulk. This is known as surface relaxation and occurs because the atoms on the surface are trying to minimise their energies. It is therefore important to use sufficient layers as to effectively model this effect whenever simulating a slab. Also, when choosing the lattice constant, the best approach is to use the value determined by a carefully converged DFT calculation for the bulk material using the same exchange-correlation functional used in the surface calculations. Using the experimental value will lead to artificial stresses within the material.

2.6. Scanning Tunnelling Microscopy (STM) Simulation

Scanning Tunnelling Microscopy (STM) was invented in 1981 by Gerd Binnig and Heinrich Rohrer [14] and has had great influence on surface science as it allowed scientists, for the first time, to study surfaces on a sub-nanometre scale. The mechanics are quite simple, a metal tip is approached very close (~10Å) to a (semi) conducting surface and a bias voltage applied between the tip and surface. Due to the effect known as "quantum tunnelling" there is a small probability that the electrons will penetrate the potential barrier between the tip and the sample.

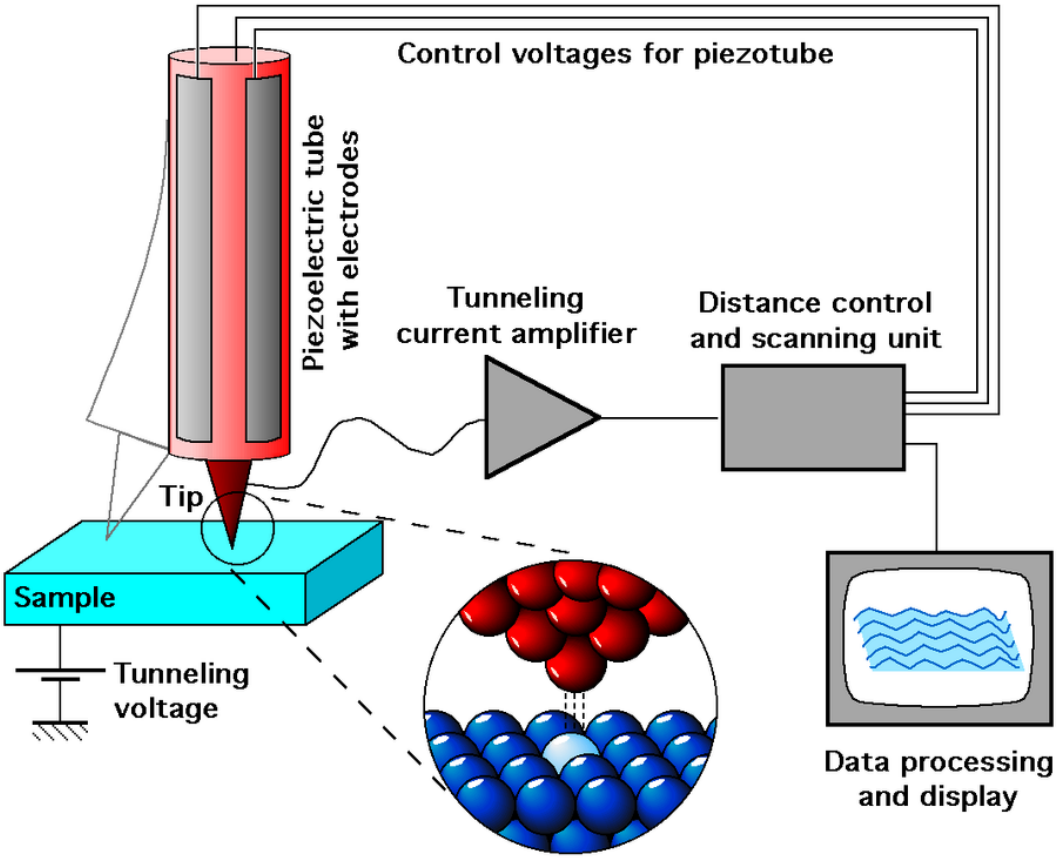

Figure 2.1: A schematic view of a Scanning Tunnelling Microscope.

The probability for tunnelling to occur [26] is given approximately by:-

$$P \propto \exp\left[-d\sqrt{2(v-E)}\right] \tag{2.19}$$

Where d is the width of the barrier, E is the energy of the particle and V is the height of the potential barrier. The equation describes an exponentially decaying probability and decreases by an order of magnitude approximately every Ångström. This allows the STM to produce images on the atomic scale. From first order perturbation theory the tunnelling current if given by Fermi's golden rule as:-

$$I = (2\pi e/\hbar)\sum_{\mu v}\{f(\epsilon_\mu)[1 - f(\epsilon_v + eV)] - f(\epsilon_v)[1 - f(\epsilon_\mu + eV)]\} \times \left|M_{\mu v}\right|^2 \delta(\epsilon_\mu - \epsilon_v) \quad (2.20)$$

Where $f(\epsilon)$ is the Fermi function, V is the applied voltage, $M_{\mu v}$ is the tunnelling matrix element between states ψ_μ of the probe and ψ_v of the sample and ϵ_μ is the energy of state ψ_μ in the absence of tunnelling.

By using Bardeen's approximation [15] of the matrix elements $M_{\mu v}$ and by assuming a spherical tip one can show that the tunnelling current is proportional to the local density of states (LDOS) of the sample:-

$$I(V, \vec{r}_0) \propto \int_{\epsilon_F}^{\epsilon_F + eV} d\epsilon\, \rho(\epsilon, \vec{r}_0) \quad (2.21)$$

And the first derivative of the tunnelling current is given by:-

$$\frac{dI}{dV}(V, \vec{r}_0) \propto \rho(\epsilon_F + eV, \vec{r}_0) = \sum_\alpha |\psi_\alpha(\vec{r}_0)|^2 \delta(\epsilon_F + eV - \epsilon_\alpha) \quad (2.22)$$

where $\rho(\epsilon_F + eV, \vec{r}_0)$ is the LDOS in point $\vec{r}_0$ with energy $\epsilon_F + eV$ and $\psi_\alpha(\vec{r}_0)$ are the wavefunctions of the sample. This is known as the Tersoff-Haman approximation [16,17] and gives reliable STM simulations.

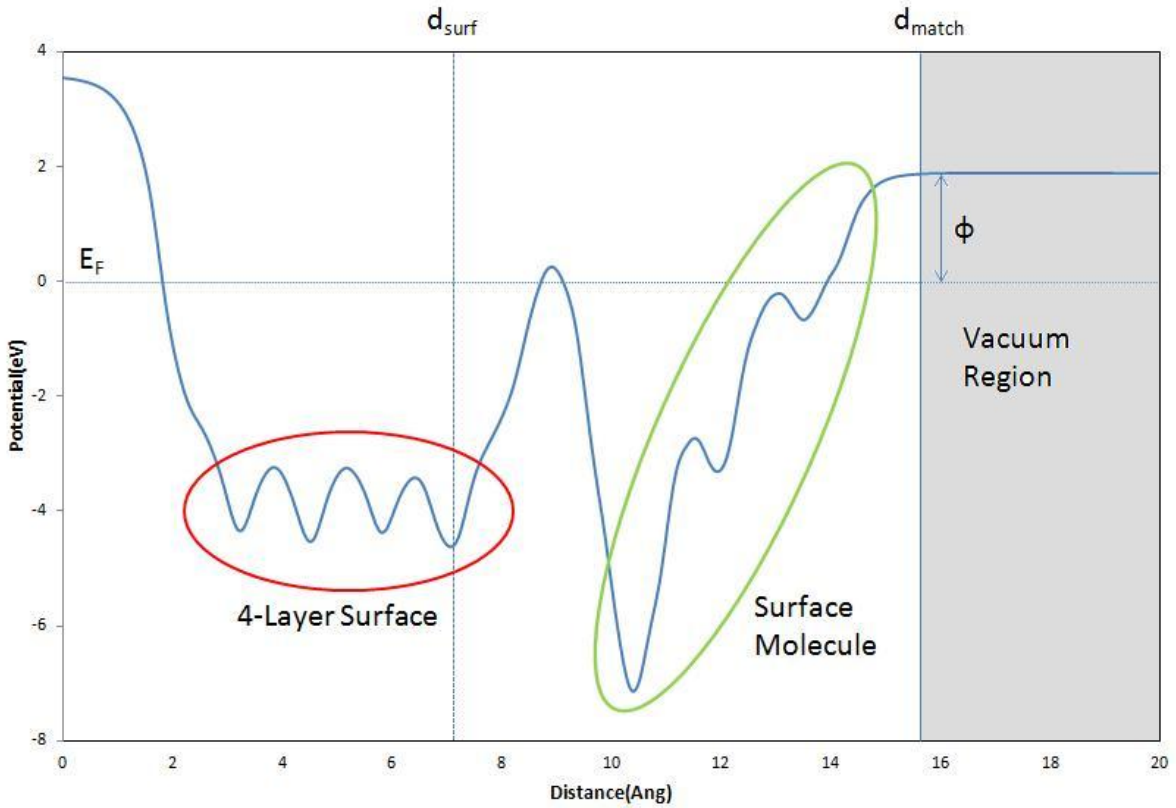

Figure 2.2: Illustration of the electrostatic potential of an adsorbed molecule (thymine) on a 4-layer surface (Cu) taken perpendicular to the surface. The diagram represents a 2D 'slice' through the system. The object within the red circle represents 4 Cu atoms:-

- The left 2 are the Cu atoms that are fixed in place and represent the bulk of the crystal.
- The right 2 are the Cu atoms that are un-fixed in place and represent the surface of the Cu crystal.

The object within the green circle represents the thymine molecule:-

- The first peak is the Oxygen-Nitrogen-Oxygen atoms that are covalently bonded to the Cu surface.
- The second peak is the cyclic ring.
- The third peak is the methyl group.

In figure 2.2 the electrostatic potential has been averaged over the x-y plane along the vector perpendicular to the surface. The surface is Cu(110) and it can be clearly seen that some molecule is placed on the surface. In the STM simulations the wave functions were extrapolated and a matching distance was determined which corresponds to the work function (Φ). This distance occurs when the electrostatic potential becomes constant and is where the

vacuum area begins (grey area).

2.7. X-Ray Photoelectron Spectroscopy (XPS) Simulation

X-ray photoelectron spectroscopy (XPS) measures the energy required to remove core-electrons from atoms within a material. XPS spectra are obtained by irradiating a material with a beam of X-rays while simultaneously measuring the kinetic energy and number of electrons that escape and requires ultra-high vacuum (UHV) conditions. XPS can detect all elements with an atomic number (Z) of 3 and above. It cannot detect hydrogen or helium due to their small atomic radius.

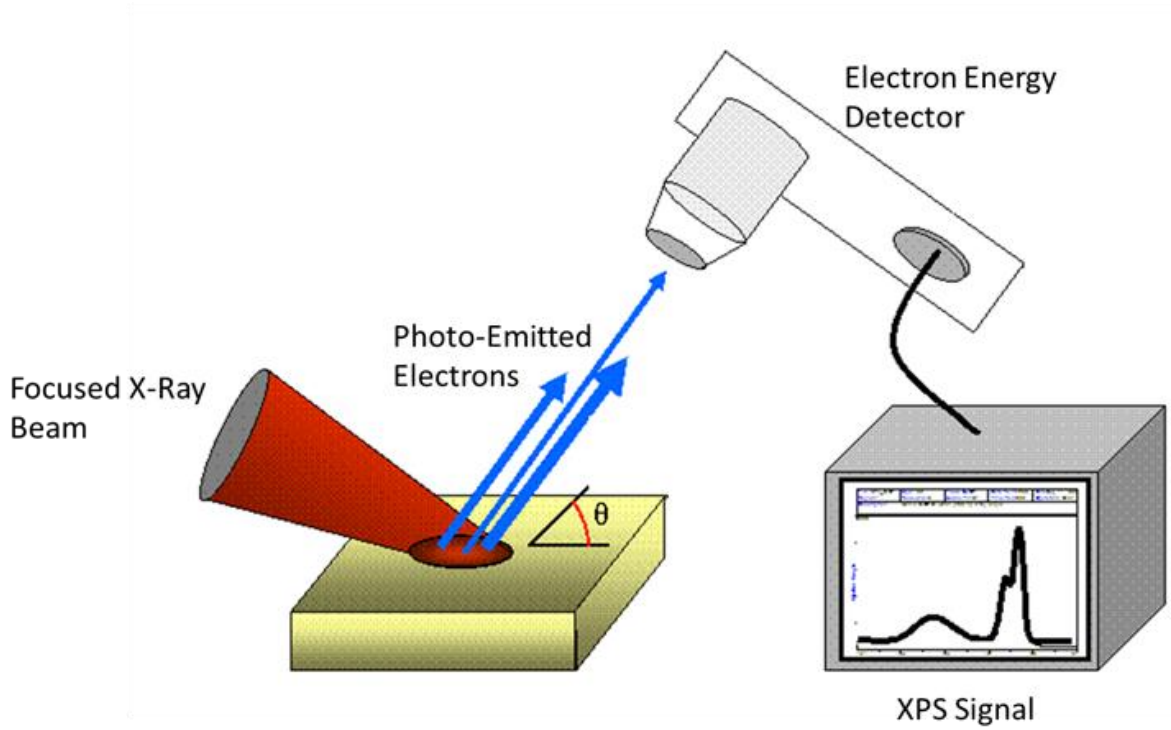

Figure 2.3: The basic components of an XPS system.

Figure 2.3 shows the experimental set up of an XPS system. Since core level shifts are highly sensitive to local electrostatic potentials, it is possible to use XPS to determine the local chemical environments an atom experiences within a molecule. Core level binding energies

can be calculated using DFT and these can then be related to experiment [18]. Figure 2.4 shows the basic principles of the XPS technique. An X-ray with energy *hv* per photon ionises the core of an atom. The kinetic energy E_k of the emitted electron is measured and the core level binding energy E_b (relative to the Fermi level) is given by:-

$$E_b = hv - E_k - \Phi = E(N-1) - E(N) \tag{2.23}$$

where *E(N)* is the total energy of the neutral system and *E(N-1)* is the total energy of the core ionised system and Φ is the work function, i.e. the smallest energy required to generate a photoelectron or to excite an electron at the Fermi level to the vacuum level. However, one must take into account the approximate relation between the measured core level binding energy and that of the occupied core level. The measured core level is related to the *E(N)* level (i.e. full shell) and the *E(N-1)* level (i.e. minus one electron) [18].

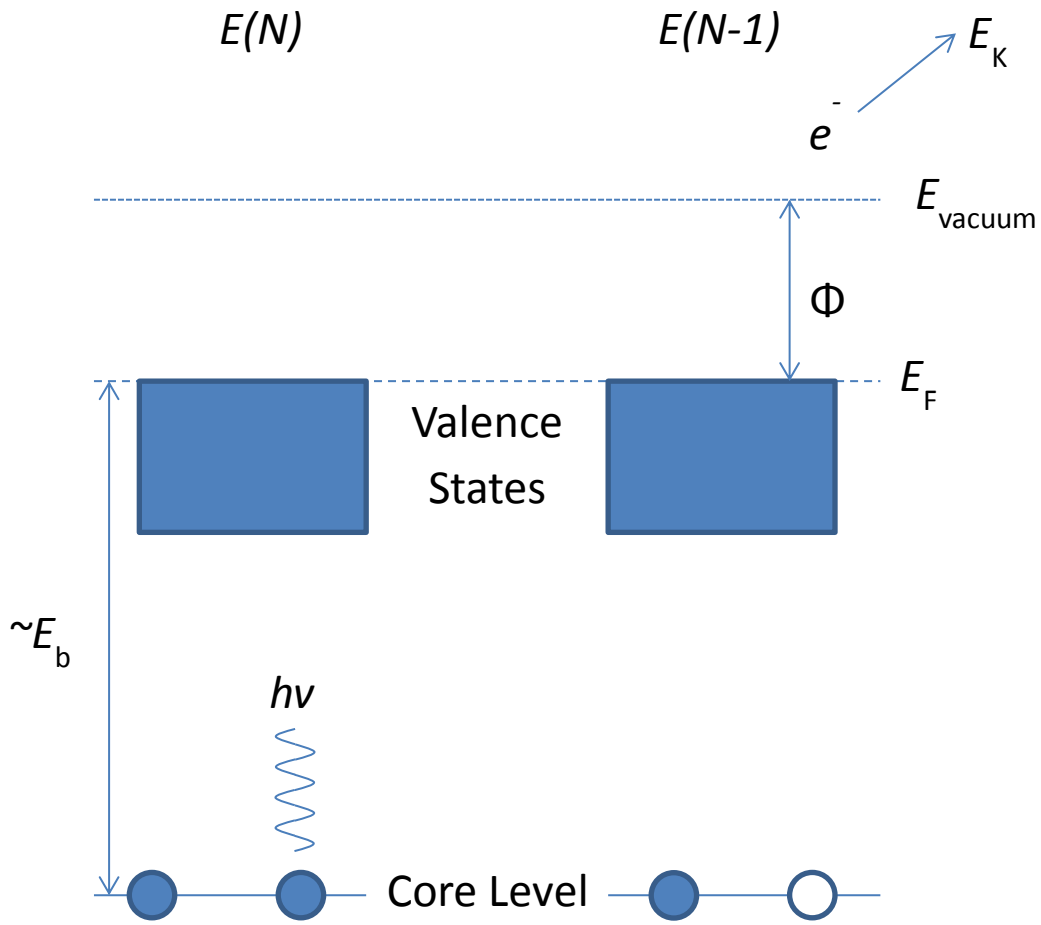

Figure 2.4: Schematic illustration of XPS technique.

There is a subtle difference between a core-ionised atom and a core shifted atom. Equation 2.24 applies to a core-ionised system and not a chemically shifted system:-

$$E_{CLS} = [E^a(N-1) - E^a(N)] - [E^b(N-1) - E^b(N)] \quad (2.24)$$

Where E_{CLS} is the energy if the core level shift, E^a is the energy of system a and E^b is the energy of system b. The total energies of the neutral system are obtained from DFT calculations and the core-ionised system is approximated using the frozen-core approximation [19]. This approximation assumes that the core-hole stays localised when the atom is excited. This approximation is valid for molecules adsorbed on metal surfaces as the substrate acts as an electron reservoir and therefore the total energy of the system remains

relatively constant. In this thesis the Z+1 approximation was used although other methods are available [20]. In this technique the effect of removing a core-electron is approximated by adding a proton to the core of the atom under consideration. This very rough method works by effectively approximating the core-ionised atom with a valence-ionised atom.

2.8. Bibliography

[1] W. Kohn, L. J. Sham. "*Self-Consistent Equations Including Exchange and Correlation Effects*." Physical Review 1965, **140**(4A), A1133-A1138.

[2] W. Kohn. "*Density-Functional Theory for Excited-States in a Quasi-Local-Density Approximation*." Physical Review Letters 1986, **56**(20), 2219-2220.

[3] L. J. Sham, Z. Reut, J. W. Wilkins, "*Density Functionals Beyond the Local Approximation*." Philosophical Transactions of the Royal Society of London Series A Mathematical Physical and Engineering Sciences 1991, **334**(1635), 481-490.

[4] J. P. Perdew, J. A. Chevary, S. H. Vosko. "*Atoms, Molecules, Solids and Surfaces: Applications of the Generalized Gradient Approximation for Exchange and Correlation*." Physical Review B 1992, **46**(11), 6671-6687.

[5] Y. Wang, J. P. Perdew. "*Exchange Potentials in Density-Functional Theory*." Physical Review A 1990, **41**(1), 78-86.

[6] J. P. Perdew, K. Burke, M. Ernzerhof. "*Generalised Gradient Approximation Made Simple*." Physical Review Letters 1996, **77**(18), 3865-3868.

[7] M. Dion, H. Rydberg, E. Schröder. "*Van der Waals Density Functional for Generalised Geometries*." Physical Review Letters 2004, **92**(24), 246401-246404.

[8] S. Grimme. "*Accurate Description of van der Waals Complexes by Density Functional Theory Including Empirical Corrections*." Journal of Computational Chemistry 2004, **25**(12), 1463-1473.

[9] U. Zimmerli, M. Parrinello, P. Koumoutsakos. "*Dispersion Corrections to Density Functionals for Water Aromatic Interactions*." J. Chem. Phys. 2004, **120**(6), 2693-2699.

[10] Q. Wu, W. Yang. "*Direct Method for Optimized Effective Potentials in Density Functional Theory*." Physical Review Letters 2002, **89**(14), 143002/1-143002/4.

[11] P. Hohenberg, W. Kohn. *"Inhomogeneous Electron Gas."* Physical Review 1964, **136**(3B), B864-B871.

[12] K. Burke. *"ABC to DFT"*, http://dft.uci.edu/materials/bookABCDFT/gamma/g1.pdf (2007).

[13] D. Vanderbilt. *"Soft Self-Consistent Pseudopotentials in a Generalized Eigenvalue Formalism."* Phys. Rev. B 1990, **41**(11), 7892-7895.

[14] G. Binnig, H. Rohrer, C. Gerber. "*Surface Studies by Scanning Tunnelling Microscopy*." Physical Review Letters 1982, **49**, 57-61.

[15] J. Bardeen. "*Tunnelling from a Many-Particle Point of View*." Physical Review Letters 1961, **6**(2), 57-59.

[16] J. Tersoff and D. R. Hamann. "*Theory and Application for the Scanning Tunnelling Microscope*." Physical Review Letters 1983, **50**(25), 1998-2001.

[17] J. Tersoff and D. R. Hamann. "*Theory of the Scanning Tunnelling Microscope*." Physical Review B 1985, **31**(2), 805-813.

[18] S. Hüfner. "*Photoelectron Spectroscopy: Principles and Applications 3rd Edition*." Springer-Verlag Berlin Heidelberg, New York, 2003.

[19] L. Köhler, G. Kresse. *"Density Functional Study of CO on Rh(111)."* Physical Review B 2004, **70**(16), 165405, 1-9.

[20] B. Johansson, N. Mårtensson. "*Core-Level Binding Energy Shifts for the Metallic Elements."* Physical Review B 1980, **21**(10), 4427-4457.

[21] P. Rinke, A. Qteish, J. Neugebauer, M. Scheffler. *"Exciting Prospects for Solids: Exact Exchange Based Functional Meet Quasiparticle Energy Calculations."* Phys. Stat. Sol. 2008, **245**(5), 929-945.

[22] J. Uddin, J. E. Peralta, G. E. Scuseria. "*Density Functional Theory Study of Bulk Platinum Monoxide*." Phys. Rev. B 2005, **71**(15), 155112.

[23] C. W. Ueberhuber. Numerical Computation (Volume 2), Chapter 14, Section 4.4 *"Minimization Methods"*, p. 325-335, Springer (1997), ISBN 3-540-62057-5.

[24] G. Kresse, J. Furthmüller. "*Efficient Iterative Schemes for Ab-Initio Total-Energy Calculations Using a Plane-Wave Basis Set."* Phys. Rev. B 1996, **54**(16), 169-186.

[25] H. J. Monkhorst, J. D. Pack, Phys. Rev. B, **13** (1976) 5188.

[26] M. Razavy. *"Quantum Theory of Tunnelling"*, p. 4. World Scientific Publishing Co. 2003.

[27] N. W. Ashcroft and N. D. Mermin, *"Solid State Physics"* Harcourt: New York, (1976).

[28] J.R. Hook, H.E. Hall, *"Solid State Physics (2nd Edition)"*, Manchester Physics Series, John Wiley & Sons (2010).

[29] T. Hahn, *"International Tables for Crystallography, Volume A: Space Group Symmetry, A (5th ed.)"*, Berlin, New York: Springer-Verlag (2002).

3. Chapter Three - Adsorption of Thymine on Cu(110)

3.1. Introduction

Our knowledge of molecular self-assembly on solid surfaces has increased significantly over the last few years. The molecular systems studied have been continuously growing in complexity and one area that has been studied extensively both experimentally and theoretically is self-assembled monolayers of molecules with several kinds of interacting functional groups, such as DNA bases or amino acids. It is generally expected that for such molecules with multifunctional groups a hierarchical self-assembly process exists. During this process directional bonds, i.e. hydrogen bonds, determine the formation of supramolecular structures in the first place (at low surface coverages), while weaker interactions, i.e. van der Waals (vdW) interactions, become more important with increasing surface coverage and then direct the subsequent self-assembly of the supramolecules formed initially. For this kind of experiment, scanning tunnelling microscopy (STM) has proven to be the technique of choice since it allows a direct, real-space determination of the symmetry properties of the molecular network as well as the unit-mesh distances and angles at the atomic scale. However, to obtain further insight into the detailed molecular structures from the STM images, to address questions such as the molecular adsorption conformations and to distinguish the different interactions in self-assembled structures, comparison with advanced theoretical modelling of the STM images is required.

Over the past decade an initial picture has started to build up of how thymine bonds to Cu(110) [1,2,14-16]. However, although many aspects are generally agreed upon, there are still many uncertainties and unresolved questions. There have been several different studies of thymine on Cu(110) now [1,2,14-16], however a definitive study which amalgamates all the various data and resolves many of the questions has not yet been done. Although this study does help to clarify many of these questions it also raises many interesting questions as well. It is well known that many of the nucleotides have the ability to self-assemble into repeating structures on different surfaces [1,2,14-16] and thymine on Cu(110) is no

exception. Using Scanning Tunnelling Microscopy (STM) it has been shown by the Liverpool group that thymine self-assemble into one dimensional (1D) filaments at room temperature (see Figure 3.1a). Upon annealing to 350-400K, the filaments then appear to transform into two distinct directions adjacent to the [001] axis (see Figure 3.1b). By using this data, a basic model is now proposed as to how this process may be occurring. It is consistent with many of the previous studies and also helps to explain many of the results.

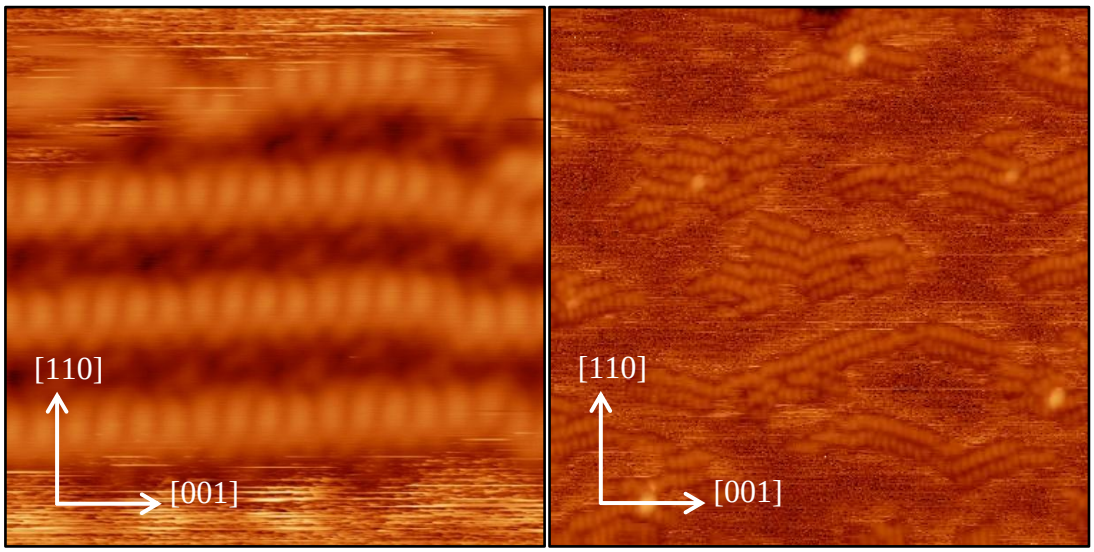

(a) (b)

Figure 3.1: STM images from UHV experiments of the thymine molecule adsorbed on the Cu(110) surface. (a) At room temperature the molecules self-assemble into rows along the [001] direction at a distance of around 3.6Å (-0.3V, -0.33nA, 5x5nm^2). Adjacent rows tend to form in the [110] direction at a distance of around 12Å. (b) After annealing to 350-400K a second phase is observed by STM (-0.27V, -0.45nA, 20x20nm^2) which aligns in two distinct directions at angles ~±20^o to the [001] direction.

The experimental results for thymine adsorbed on Cu(110) for Scanning Tunnelling Microscopy (STM), Reflection Absorption Infra-Red Spectroscopy (RAIRS) and Temperature Programmed Desorption (TPD) are presented and discussed here. The STM data was first taken for a low coverage on an unannealed surface, then for gradually increasing temperature up to ~500K. The RAIRS spectra were taken for an increasing coverage at room temperature and then this was annealed until the thymine completely desorbed at ~640K in a verification of Alex McNutt's [1,2] work. TPD data discussed later shows that hydrogen

desorbs between ~140K and ~370K with a peak at ~230K and then between ~500K and ~700K with an intense peak at ~675K.

3.2. Thymine

Thymine (T, Thy) with chemical formula $C_5H_6N_2O_2$ (see figure 3.2) is one of the four nucleobases in the nucleic acid of DNA. The others are adenine, guanine and cytosine. It is also known as 5-methyluracil and is a pyrimidine nucleobase and can be derived (as the name suggests) by methylation of uracil at the 5^{th} carbon. Both thymine and uracil have very similar molecular structures, with an essentially planar ring or cyclic structure, although for the thymine the tetrahedral methyl group has its hydrogens outside the plane. Both molecules contain two carbonyl groups, two ring nitrogen atoms and a carbon-carbon double bond and possess C_s symmetry. In RNA, thymine is replaced with uracil and in DNA it binds to adenine via two hydrogen bonds stabilising the nucleic acid structures. They are distinguished solely by the introduction of a methyl group at the C5 position in the case of thymine (see Figure 3.2). As such they might reasonably be expected to exhibit similar adsorption behaviour, although the methyl group may have steric effects. Although a small molecule, it has many potential donor and acceptor sites [3] for hydrogen bonding. It is a complex and dynamic molecule and can have a variety of different metal coordination modes due to the tautomeric properties and diversity of functional groups. It can display mono-, bi- and tri-dentate binding interactions with metals.

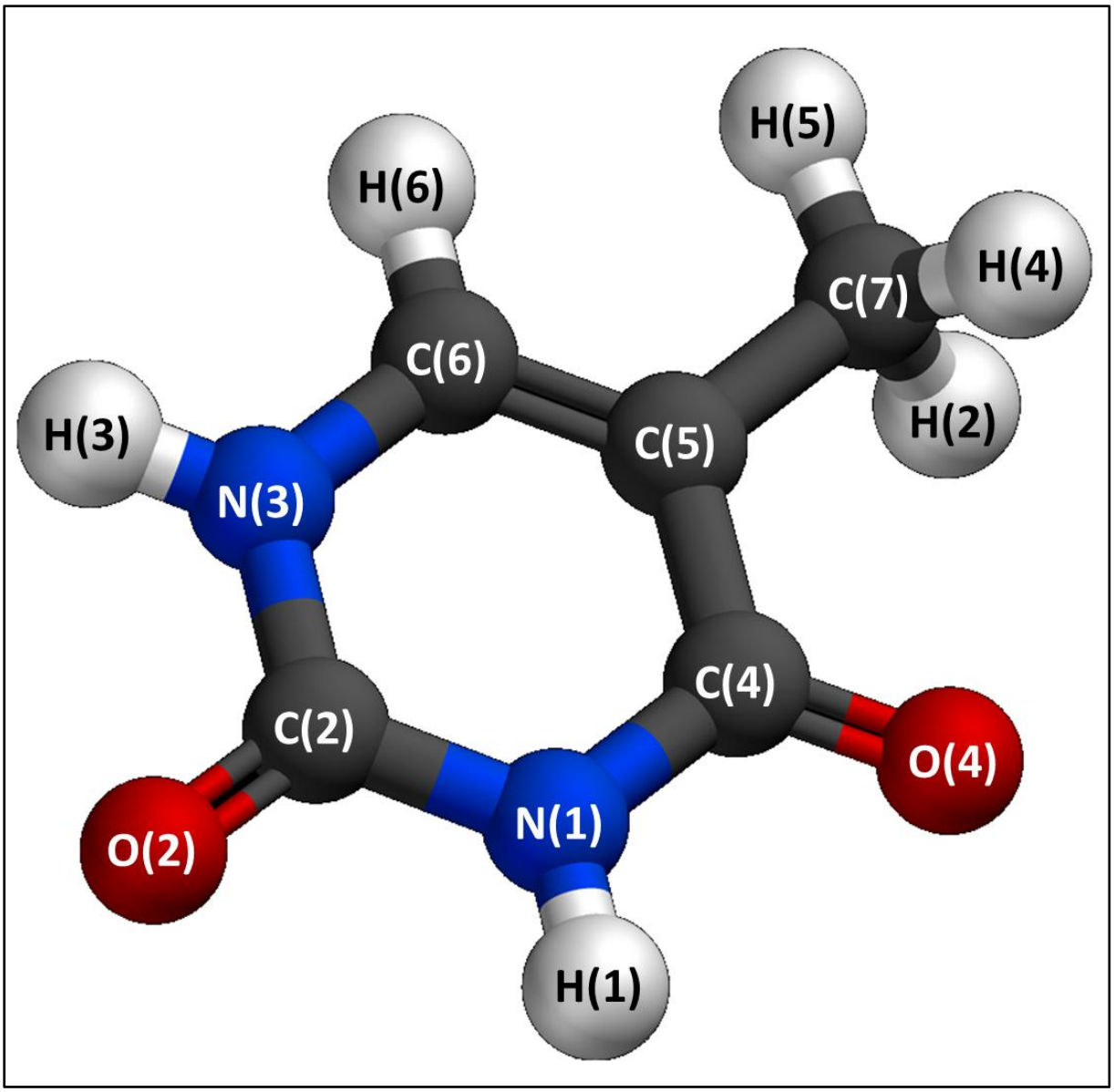

Figure 3.2: The molecular structure of thymine. The carbons (C) are coloured in grey, the nitrogens (N) are coloured in dark blue, the oxygens (O) are coloured in red and the hydrogens are coloured in white. The atoms are numbered in order to distinguish them further.

3.3. The Tautomeric Properties of Thymine

There is also the possibility of tautomerisation as illustrated in figure 3.3. The tautomeric interconversion occurs through the migration of a proton from one/both of the ring nitrogens

of the keto form to one/both of the exocyclic oxygen atoms. This is accompanied by a corresponding shift of electron density between the carbonyl and ring bonds. Thus, it exhibits keto-enol tautomerism. The neutral molecular form is known to exist in the gas phase [4], as well as inert gas matrices [5,6] and solid crystalline state [7-10]. The relative stabilities are such that the neutral form is observed exclusively in its keto form. The relative stabilities of these tautomers have been reported using geometry optimisation techniques [11-13] which show that the keto form is the most stable by 72KJmol^{-1} relative to the next most stable tautomer.

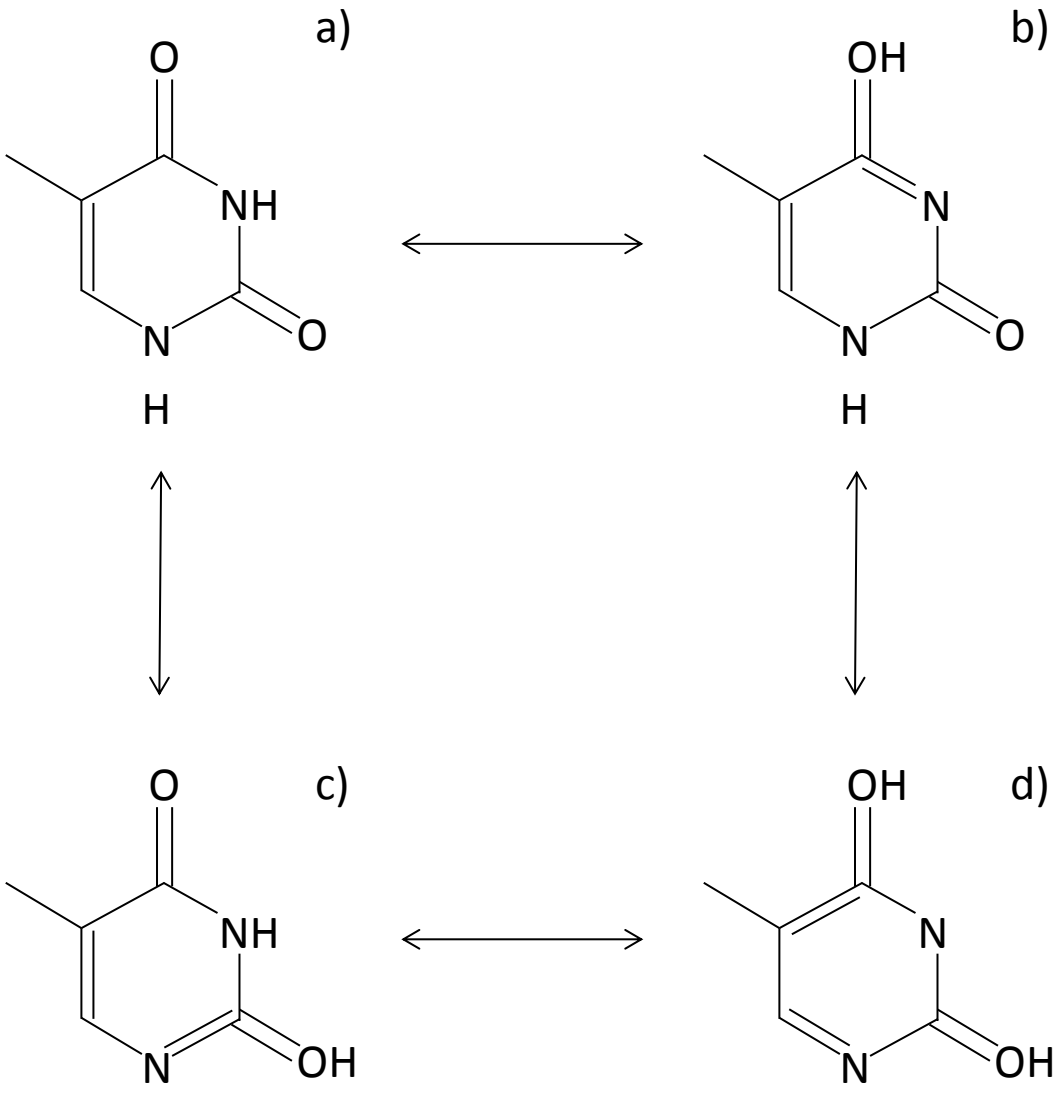

Figure 3.3: The different tautomers of thymine. Image a) shows the stable structure of thymine which can oscillate into the short-lived tautomers shown in image b) and c). It is

then possible for the tautomers shown in b) and c) to oscillate into the even more short-lived tautomer shown in d).

3.4. Previous Experimental Investigations of Thymine on Cu(110)

There have been various experimental investigations into the adsorption of thymine on Cu(110) over the past few years and many studies have been done recently [1,2,14-16]. However, although a consensus on many aspects of this system has now been reached there still remain many unanswered questions on the self-assembly aspects and work is currently continuing into this highly relevant system. Molecular ordering is, in general, controlled by a complex interplay between (weak) intermolecular, non-covalent binding forces (e.g. hydrogen bonding and van der Waals interactions) and molecule-substrate (generally covalent bonding) interactions. STM based studies tend to focus on topographic imaging techniques which normally focus on elucidating possible intermolecular interactions. Spectroscopic studies on the other hand allow for insights into the general arrangement and positioning of the molecule on the surface as well as possible metal-molecule interactions and adsorption configurations.

A series of spectroscopic studies have shown an agreement on an upright positioning of the molecular plane with respect to the surface. These also tend to show that it is the top most surface layer of the Cu(110) to which the thymine bonds to. This is as expected as this is by far the most exposed layer and, as no surface restructuring has been shown to occur in Cu(110), these rows are reasonably spaced apart (i.e. by one lattice constant ~3.6Å). Reflection Absorption Infrared Spectroscopy (RAIRS) [1,14,17], Angle-Resolved Ultra-Violet Photoemission (ARUPS) [18] and Near-Edge X-Ray Absorption Fine Structure (NEXAFS) [15,17] experiments all agree that the thymine molecules have their molecular planes essentially perpendicular to the surface and aligned to the (close-packed) [110] direction. Soft X-Ray Photoelectron Spectroscopy (SXPS) of thymine deposited at room temperature on Cu(110) [15] indicates that the positions of the two oxygen atoms within the thymine molecule are essentially equivalent. That is to say that they are both covalently bonded to one of the outermost Cu atoms and are both positioned essentially atop of one

these. However, these experiments also show that the two nitrogen atoms in the cyclic ring do not bond to the surface in the same positions. This strongly implies a three-point contact configuration for the adsorption of thymine on Cu(110) from room temperature up to ~550K. This consists of both carbonyl atoms O(2) and O(4) and a (deprotonated) N(1) atom with each bonding atom adopting near atop sites on the outermost Cu surface layer [15]. It is essential that the N(1) be deprotonated in order for this configuration to be possible and TPD data (see figure 3.4) reveals that deprotonation does indeed occur at below room temperature.

3.5. Experimental Details

Three multi-analytical UHV chambers with base pressures less than 5 x 10^{-10} mbar were used for this study. RAIRS and TPD studies were carried out using a sample mounting in which a Cu single crystal was fixed to copper supports connected to a Dewar container through Ta wires. STM studies were performed with a different configuration and Tantalum (Ta) wires were used to fix the sample to a Ta plate. Ta was used due to its inertness as well as its high melting point. For all systems Cu(110) crystals were cleaned by cycles of Ar^+ ion bombardment, flashing and annealing to ~800K. LEED was used to confirm sharp (1x1) pattern characteristic of clean Cu(110). Thymine (>99% Sigma-Aldrich) was loaded into a glass crucible in the molecular evaporator. After thorough degassing of the thymine crucible by keeping the crucible at 350−400K for ~24 hours thymine molecules were deposited on the clean Cu(110) substrate by thermal sublimation from the molecular evaporator held at 350-400K. The substrate was held at room temperature in the case of STM and RAIRS, and held at the specified temperatures for LT-RAIRS and TPD.

Reflection Absorption Infrared Spectroscopy (RAIRS) experiments were recorded using a Mattson 6020 FTIR spectrometer, equipped with a liquid nitrogen cooled HgCdTe detector. The spectrometer was operated with a resolution of 4cm^{-1}, with the addition of 256 scans. Spectra were recorded throughout a continuous dosing regimen as sample single beam infrared spectra, and ratioed against a reference background single beam representing the clean Cu(110) surface. TPD data were acquired using a Sensorlab Mass Quadrupole analyser. STM data were collected at room temperature with an Aarhus 150 SPECS STM. All experiments were carried out for coverages up to 1 monolayer (ML).

3.6. Current Experimental Investigations of Thymine on Cu(110)

Electronic structure calculations of infrared spectroscopy were performed with the Gaussian03 package [19] using the hybrid density-functional method B3LYP and the basis set 6-311+G(d,p) [20]. This study was carried out by Prof. Per Uvdal using the Linux cluster at Lunarc, The Centre for Scientific and Technical Computing for Research at Lund University. Calculations were performed using three metal atoms to represent the surface (Figure 3.5e). During the optimization the copper atoms are frozen at the corresponding bulk values (2.55Å and Cu-Cu-Cu bond angle 180˚). This low representation of the surface has been used previously for terminal coordination [21].

TPD data recorded for thymine adsorption on Cu(110) from 100K up to 750K (Figure 3.4) reveal a number of interesting features. The first relevant feature of the spectra corresponds to a broad hydrogen desorption (m/z=2) which begins at just over 100K. This reaches a peak at ~225K. The peak then gradually tapers off until ~300K when a further peak is observed accompanied by a second at ~350K. This is interesting as this is also accompanied by a desorption of thymine (m/z=127) in the range 300K-350K. This feature reveals a first deprotonation of the adsorbed molecule below room temperature, previously reported in the literature under different conditions [1,14-17,23-24]. The molecular desorption spectrum (m/z = 127) only displays a very weak single peak centred at ~350K (in the range of the 10^{-13} mbar) corresponding to a small molecular desorption. There is no sign of change in the molecular adsorption configuration according to IR data (see Figure 3.5). It is unclear whether or not any further hydrogen desorption occurs, however, peaks can clearly be seen at ~560K and ~600K. It is possible that these could correspond to a further deprotonation of the N(3) amide group. A final molecular desorption occurs at ~660K through molecular decomposition as shown by peaks on both spectra 3.4a and 3.4b which represents the formation and desorption of H_2 and CO respectively on the process.

Reflection Absorption Infrared Spectroscopy (RAIRS) data for thymine adsorbed on Cu(110) has been collected in order to establish its adsorption state for every phase observed in the thermodesorption spectra. Figure 3.5a shows RAIRS data for a multilayer of thymine recorded at low temperature (213K). Desorption of the condensed layer by annealing to room

temperature is shown in figure 3.5b. A further annealing of the monolayer to 373K is shown in figure 3.5c. The RAIRS spectrum for thymine adsorption on Cu(110) at room temperature, figure 3.5b, is principally characterised by two very intense peaks corresponding to the stretching vibration of both carbonyl groups (C2=O and C4=O), at 1658cm^{-1} and 1623cm^{-1} respectively, suggesting a very intense perpendicular component of both the exocyclic groups with respect to the surface. This orientation is supported by the high intensity of all in plane modes in contrast to the weak intensity of those out-of-plane modes, agreeing with most spectroscopic studies in the literature [14,22A downward shift of both C=O stretching vibrations has been detected with respect to those on the multilayer (1678cm^{-1} and 1709cm^{-1}) and polycrystalline (1678cm^{-1} and 1731cm^{-1}) [25] species. These quite large shifts have been recorded for thymine, uracil and derivates in a variety of coordination forms in the literature [14,22-23,26-30], indicating that both carbonyl groups interact with the surface, probably through the lone electron pair of the oxygen atoms [18].

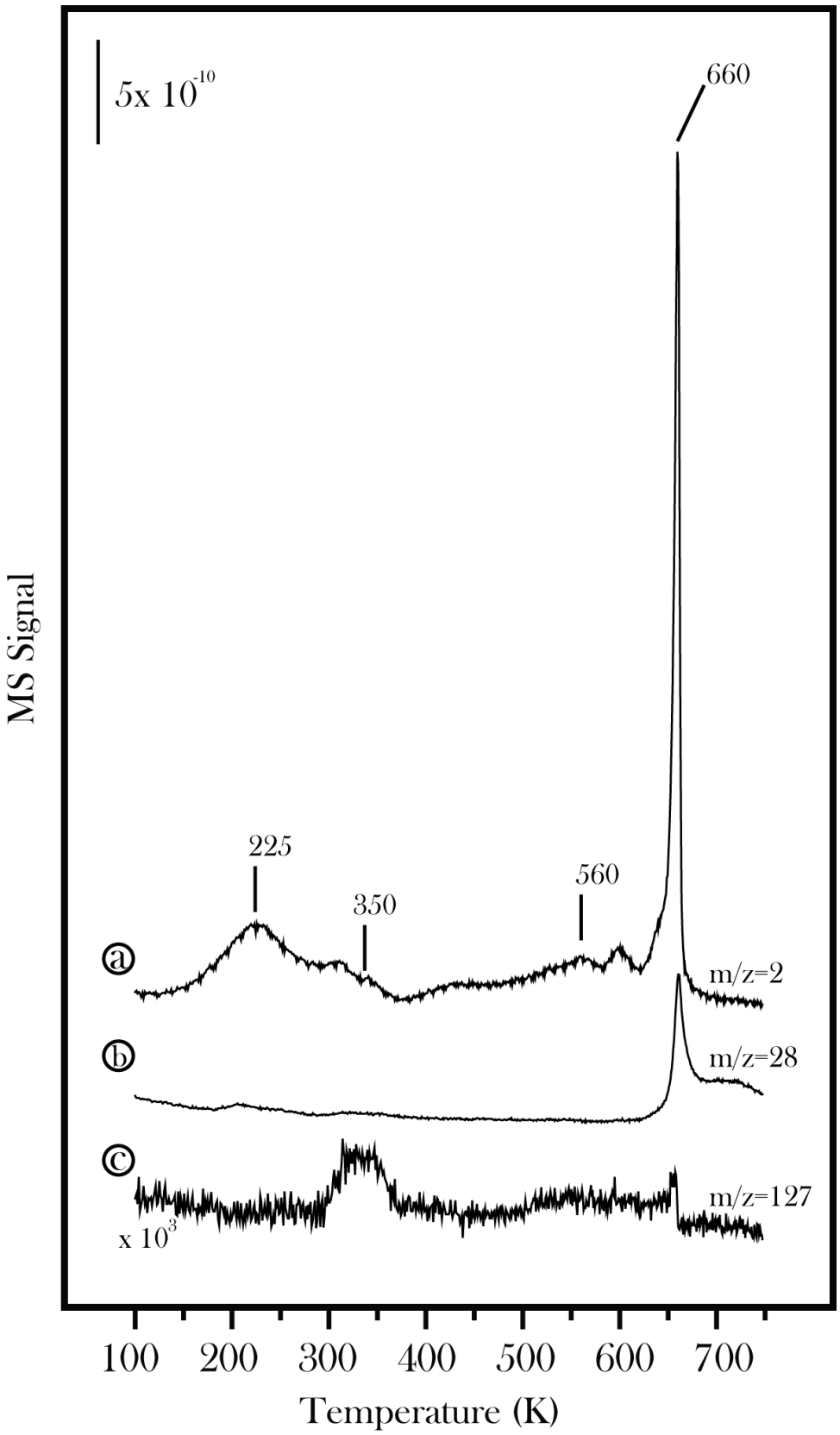

Figure 3.4: TPD spectra obtained for a saturated monolayer of thymine adsorbed from 100-750K. Masses corresponding to the desorption of (a) H_2 (m/z= 2), (b) CO (m/z= 28) and (c) the molecular peak (m/z= 127).

The relative intensities of both carbonyl peaks provide a further insight for the assignment of these peaks. According to the theoretical calculations by Prof. Per Uvdal, spectrum 3.5d, and literature assignments [1,22-25], the more intense peak at 1623cm^{-1} corresponds to the carbonyl in position 4 (C4=O), whereas the weaker peak at 1658cm^{-1} is assigned to the stretching vibration from the carbonyl group in position 2, this being later shifted from 1709cm^{-1} in the multilayer spectrum. The difference in intensity between these two stretching vibrations arises from the coupling of the carbonyl group in position 4 and the double bond between positions 5 and 6 (νC4O + νC5C6) (1678cm^{-1} in the multilayer). This assignment allows us to ascertain that both stretching vibrations suffer very similar downshifting (around 55cm^{-1} each), suggesting that the contribution of both carbonyl groups to the metal-molecule interaction are very similar and that both sites remain very close to the surface.

The proposed three-point contact adsorption configuration (Figure 3.5e) is also supported by the equal contribution of both carbonyl groups in the molecule-metal interaction. Direct evidence of an N(1) deprotonated state by infrared spectroscopy arises from the appearance of two new peaks associated with the symmetric and asymmetric stretching vibrations of the [OCNCO]$^{-}$ moieties, at 1392cm^{-1} and 1545cm^{-1} respectively (1380cm^{-1} and 1507cm^{-1} in the calculated spectrum). This conjugated system has also been detected in other IR studies in the literature. Lippert et al. [23] observed an intense band around 1500cm^{-1} for 1-methyl thymine complex of (Pt, Ag), in which proof of the deprotonated N3 group bonded to Pt or Ag is given by X-ray diffraction. In another infrared study of anionic thymine derivates in alkali medium, Wierzchowski et al. [24] detected two bands corresponding to the anionic thymine species at 1384cm^{-1} and 1581cm^{-1}, and again 1384cm^{-1} and a combination of 1574cm^{-1} and 1593cm^{-1} for the 1-methyl thymine, whereas these bands were absent in the case of 3-methyl thymine. The IR spectrum shown in figure 3.5c recorded at 373K reveals no substantial change in the adsorption configuration. The principal features remain unchanged and the overall interpretation of the spectrum with respect to the one at room temperature (see figure 3.5b) remains the same. This suggests that the molecule-surface interaction remains essentially unvaried in this range of temperatures.

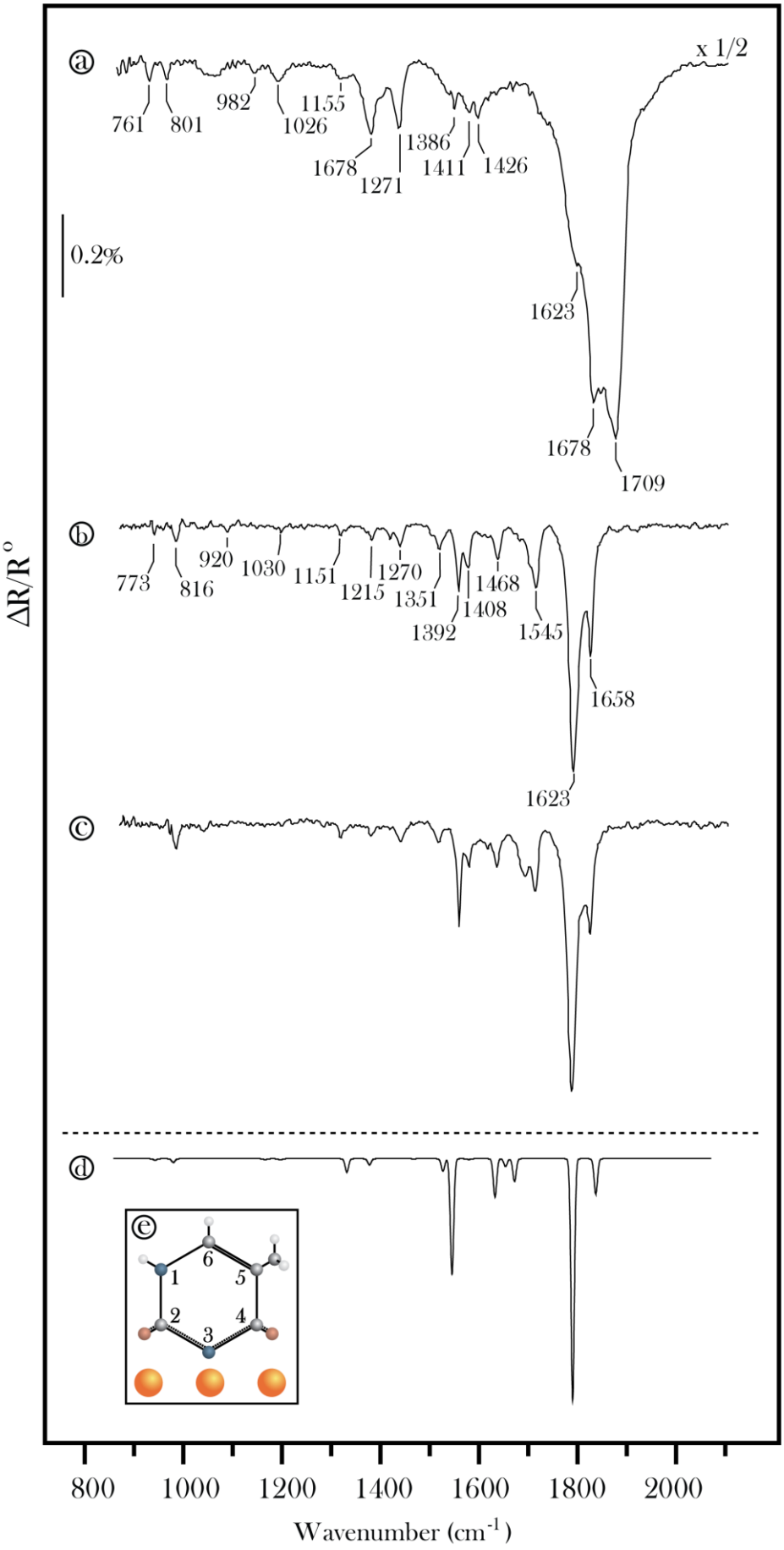
ⓐ
x 1/2
761
801
982
1026
1155
1678
1271
1386
1411
1426
0.2%
1623
1678
1709
ⓑ
773
816
920
1030
1151
1215
1270
1351
1392
1408
1468
1545
1658
1623
ⓒ
ⓓ
ⓔ
1
2
3
4
5
6
ΔR/R°
800
1000
1200
1400
1600
1800
2000
Wavenumber (cm-1)

Figure 3.5: RAIRS spectra obtained for a saturated monolayer of thymine adsorbed at 213K (a) and subsequent annealing to 300K (b) and 373K (c). Spectrum (d) corresponds to a theoretical calculation on the presumed anionic species adsorbed on Cu(110) at room temperature via a three-point contact interaction with the surface, represented in (e).

The presence of two exocyclic oxygens, two ring nitrogens, and a conjugated π-system in the molecular plane gives rise to a multitude of bonding possibilities with the surface. The calculations by Prof. Per Uvdal yielded the spectrum shown in figure 3.5d which, upon comparison with experimental evidence shows very good agreement and gives evidence to the adsorption geometry shown in figure 3.5c. These results suggests a molecule-surface interaction that includes the two carbonyl groups and the deprotonated N(1) nitrogen bonding with consecutive Cu atoms aligned on the [110] direction as shown in Figure 3.5e, in agreement with the literature [15-18]. The anharmonicity of the vibrational modes of the present system is treated by an experimental scaling factor of 0.9941 which brings the υ_s(C-O) + δ(NH) mode into complete agreement with the experimental value. This scaling factor gives a better agreement with experiment than the general scaling factor 0.9679 determined with the 6-311+G(d,p) basis set [20] making the mode assignment more transparent (Table 3.1). The intensities include only the components of the dynamic dipole moments normal to the surface, that is, in the C_s plane of the molecule and perpendicular to the Cu-Cu-Cu bond direction. The mode assignments are approximate and based on inspection using GaussView [31].

High resolution STM images (Figures 3.6-3.8) show thymine molecules adsorbed on Cu(110) imaged as oval protrusions. The size of these protrusions is approximately (2±0.2)x(5±0.5)$Å^2$, as expected for an upright positioning of the molecule, with the molecular plane roughly aligned along the [110] direction as described above (Figure 3.5e). The shapes of the protrusions are also in agreement with the literature. Notably, Li et al. [22] have found thymine to show the same shape when adsorbed on Au(111), and Caciuc et al. [16] reported simulated STM topographies for the same three-point adsorption model of thymine on Cu(110) which matches the observations reported in this study. The size of the molecule remains unvaried under the different conditions studied, reinforcing the observation that no change in the adsorption state occurs below ~400K.

Multilayer 213K	Monolayer 300K	Calculation	Polycrystalline [25]	Assignments
761	773	777	761	ι ring
801	816	814	814	β ring, ν ring
875	-	-	847	γ C_2O, γC_4O
-	920	-	935	γ C_6H
982	-	1000	984	γ NH
1026	1030	1031	1030	β ring, ν ring
-	-	-	1048	γ CH_3
1155	1151	1166	1152	ι CH_3
1215	1215	1212	1215	ν C_5C_{11}
-	1250	-	1246	ν ring
1271	1270	-	1257	ν ring
-	1351	1362	1366	β CH_3^{sym}, β C_6H
1386	-	-	1383	β CH_3^{ass}
-	1392	1380	-	ν CO^{sym} $[OCNCO]^-$
1411	1408	1414	1406	β N_3H
1426	-	-	1428	β CH_3^{ass}
1462	1468	1467	1447	β N_1H
1480	-	1489	1482	ν ring
-	1545	1507	-	ν CO^{ass} $[OCNCO]^-$
1678	1623	1625	1678	ν C_4O + ν C_5C_6
1709	1658	1672	1731	ν C_2O

Table 3.1: Vibrational assignments for RAIRS data obtained for a saturated monolayer of thymine adsorbed at 213K (a) and subsequent annealing to 300K (b). Reference data from a model N(1) deprotonated system adsorbed on Cu(110) at room temperature and polycrystalline thymine are also shown for comparison.

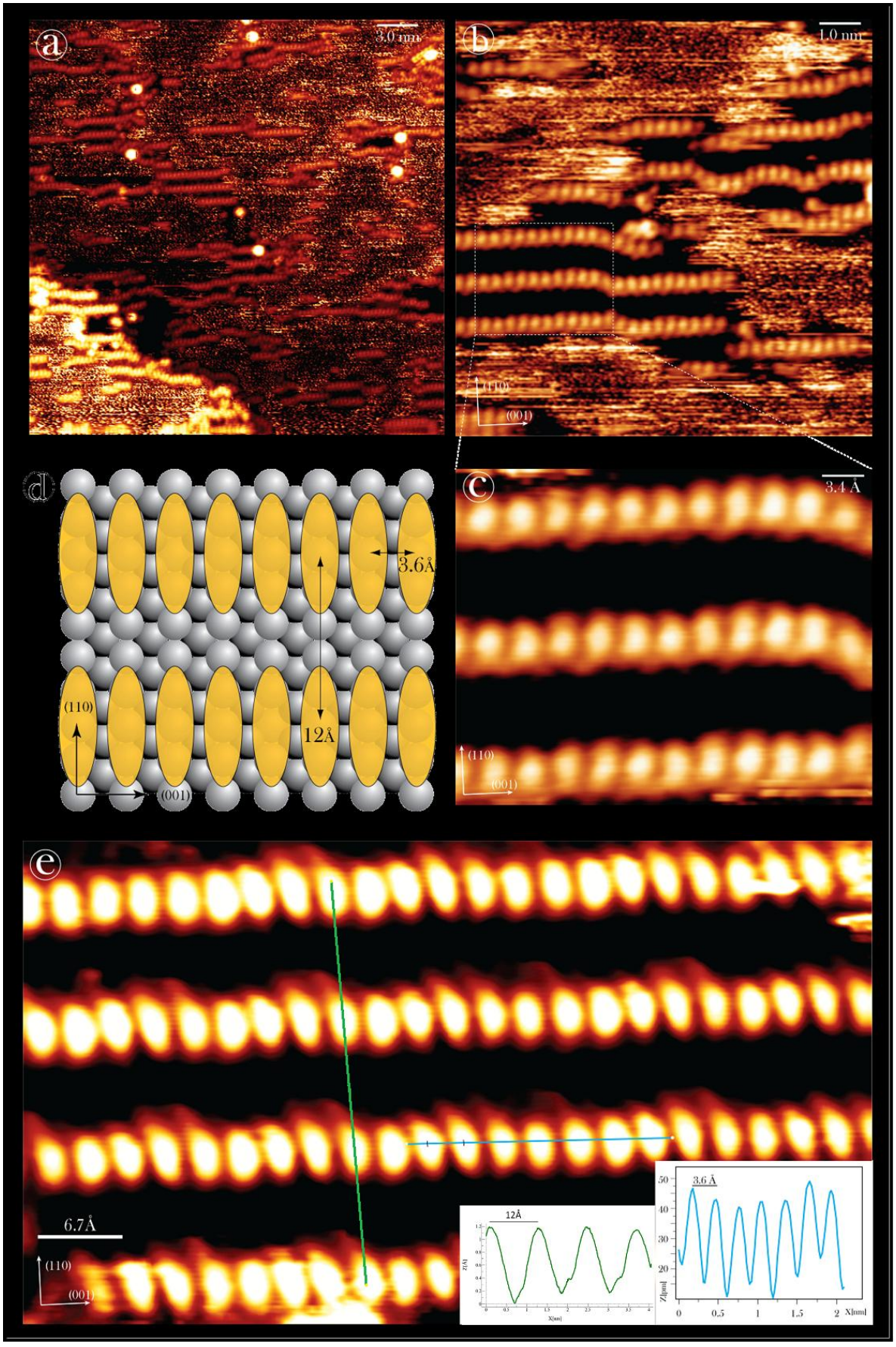
a
3.0 nm
b
1.0 nm
(110)
(001)
d
3.6Å
12Å
(110)
(001)
c
3.4 Å
(110)
(001)
e
6.7Å
(110)
(001)
12Å
3.6 Å
Z[pm]
X[nm]

Figure 3.6: Constant current STM images of thymine adsorbed on a saturated Cu(110) surface dosed and recorded at room temperatures. The figure shows:-

a) A 30x30nm^2 image (I_t: -0.430nA; V_t: -611.3mV) of several thymine arrangements including a step edge with assembled molecules following the contour.
b) A 10x10nm^2 image (I_t: -0.330nA; V_t: -305.8mV) showing in more detail the self-assembly and the constant separation between these 1D chains.
c) A higher magnification 3.4x2.8nm^2 image of the previous image showing in greater detail the molecular arrangement in every chain.
d) A schematic representation of the molecular positioning with respect to the Cu(110) reconstruction.
e) A 6.7x3.8nm^2 image (I_t: -0.390nA; V_t: -437mV) of four consecutive chains with two line profiles. The blue line profile represents the variation in intensity along the (001) direction. The green line represents the variation in intensity along the (110) direction.

The self-assembly of thymine on Cu(110) under UHV conditions consists of 1D chain-like structures for temperatures ranging from room temperature up to ~400K (Figures 3.6-3.8). We can, however, distinguish two different phases from the STM images under these conditions. A first phase is observed at room temperature (Figure 3.6) showing thymine molecules arranging mainly in rows along the [001] direction as well as a second phase, where the chain-like structures align approximately along both the [112] and [-1-12] directions upon annealing of the substrate to temperatures over ~350K (see figures 3.7-3.8).
Phase 1 (Figure 3.6), observed from room temperature up to ~350K, has domains consisting of 1D chains with every molecule separated by ~3.6Å. This implies a close packing alignment of thymine molecules on consecutive Cu rows, with sets of rows separated by over 12Å. This suggests that long distance interactions occur between rows. Molecules in this phase are believed to interact only weakly since there´s a high mobility of these structures along the [110] direction and molecules inside the chains can occasionally drift up or down briefly before going back to their original positioning. Furthermore, it is clear that molecular assemblies follow the contour of step edges (Figure 3.6a), indicating that the driving force for the self-assembly across the [001] direction isn´t strong enough to prevail on the irregular edges of a terrace.

Further insight into the assembly of the phase 1 strands was gained during STM investigations. Figure 3.7 is a series of images taken at approximately 1 minute intervals (the length of time required to scan an image) and shows the stages in which a filament is forming. The images give some insight into how this process may be occurring. A brief description of this process follows:-

a) Filament is formed except for a break in the top strand.
b) This break is reformed and another short strand comes in from the right close to the lower strand.
c) This then appears to cause the lower strand to detach and a short double-strand is formed.
d) The top of this strand breaks off slightly.
e) The lower strand reattaches itself and the top strand reforms.
f) The top strand now attaches and a complete double strand is now formed.

This is only one example of the process and a whole series of images were made during the analysis which seemed to be showing that thymine molecules, although in a constant state of flux, demonstrated that they were being guided to attach onto the ends of existing filaments. It can only be speculated as to what interaction is causing this to occur but directional hydrogen bonding or van der Waals interactions are the most likely candidates.

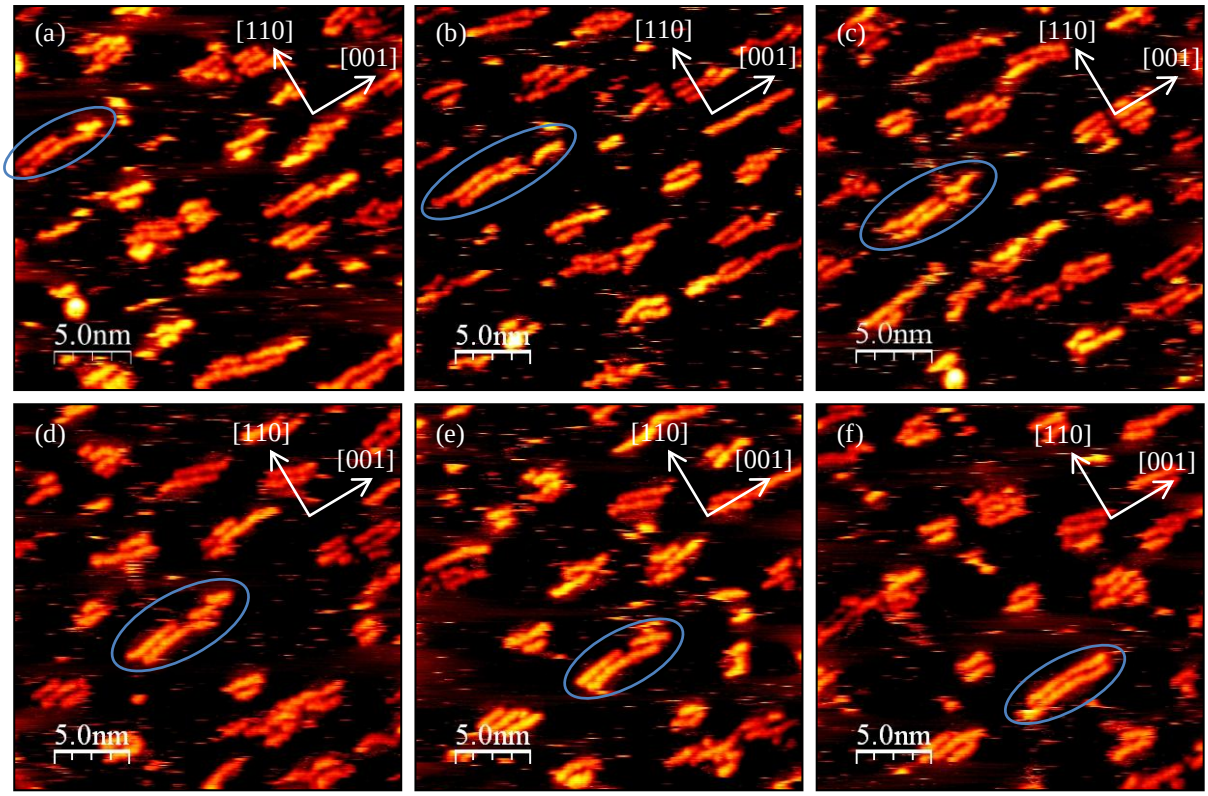

Figure 3.7: STM images (V_t = -1.50V, I_t = 0.20nA) showing assembly of thymine molecules on Cu(110) adsorbed at room temperature. The images were taken at approximately 60 second intervals. The highlighted regions correspond to the same filament structure and show how it can self-assemble and disrupt on a timescale of seconds/minutes.

A different molecular arrangement appears when the system is annealed over 350K. This second phase is characterized by 1D molecular arrangements disposed approximately along the [112] and [-1-12] directions. These rows are formed out of pairs of thymine molecules equally placed on consecutive [110] rows, separated by ~3.6Å the same as for the room temperature phase, with a subsequent pair orientated one Cu atom up in the [-1-14] or down in the [114] direction. This arrangement aligns along overall directions of [-1-12] and [112] and thus disrupts the mirror symmetry of the underlying Cu(110) surface. Rows are separated by ~7Å which suggests stronger interactions between rows than in the case of the lower temperature phase. The appearance of this second phase is hinted by TPD data (see figure 3.4) where a small simultaneous hydrogen and molecular desorption is observed at ~350K.

Considering the low temperature of the transition between phases 1 and 2, it is reasonable to assume that phase 1 may be a kinetic assembly, whereas phase 2 may be the more stable thermodynamic product and the mild annealing required to switch between the two phases reflects the low barrier for this transition.

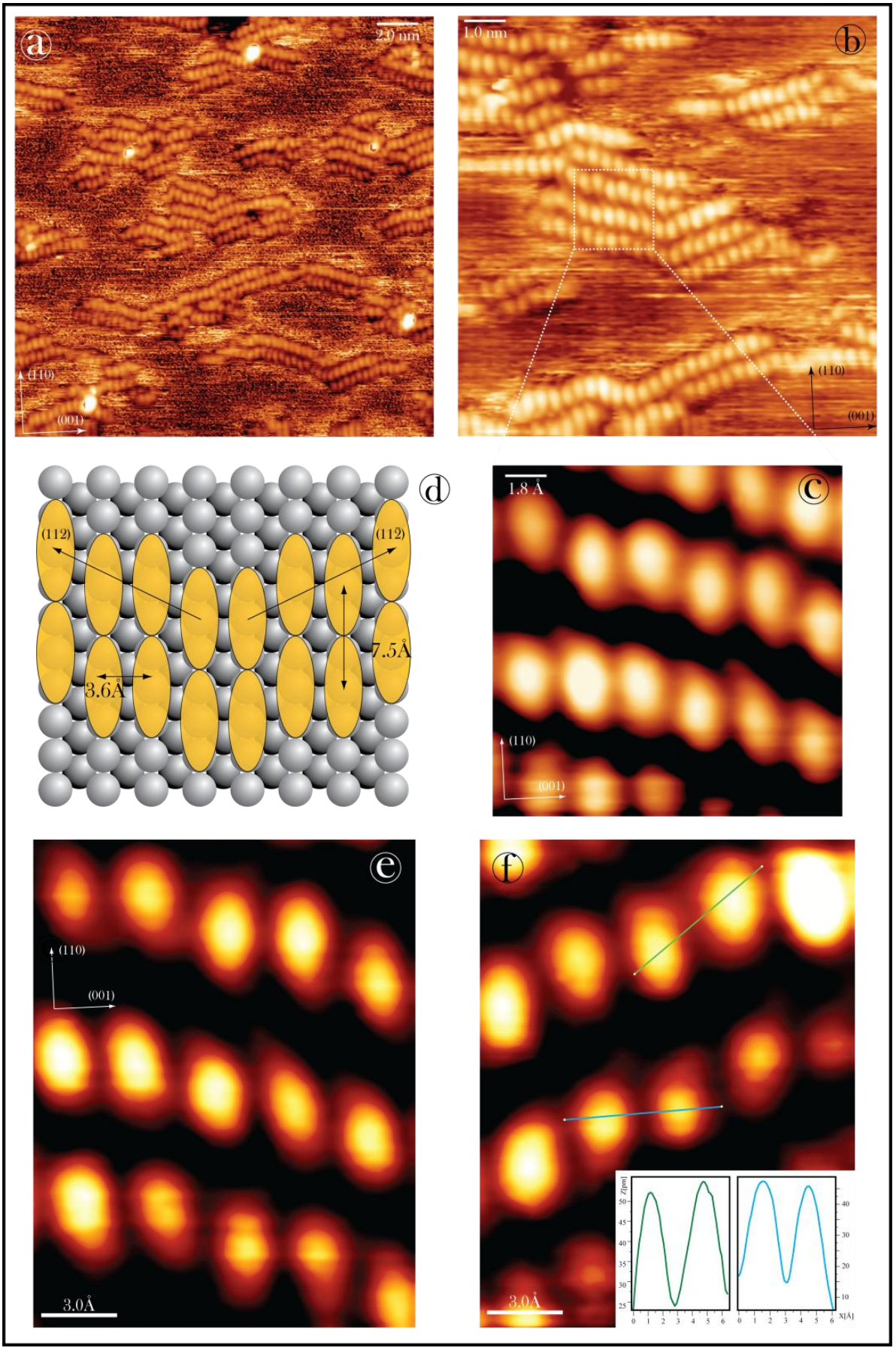
a
2.0 nm
(110)
(001)
b
1.0 nm
(110)
(001)
d
(112)
(11$\bar{2}$)
7.5Å
3.6Å
c
1.8 Å
(110)
(001)
e
(110)
(001)
3.0Å
f
3.0Å
Z[pm]
X[Å]

Figure 3.8: Constant current STM images of thymine adsorbed on a saturated Cu(110) surface dosed and recorded at room temperatures after annealing to ~370K. The figure shows:-

a) A 20x20nm^2 image (I_t: -0.450nA; V_t: -273.4mV) of a highly covered surface. Thymine arrangements in both [112] and [-1-12] directions are observed.
b) A 10x10nm^2 image (I_t: -0.400nA; V_t: -273.4mV) reveals more insights into both directional arrangements.
c) A higher magnification 1.8x1.8nm^2 of the previous image shows in greater detail the molecular arrangement in every chain.
d) A schematic representation of the molecular positioning with respect to the Cu(110) reconstruction.
e) A high definition 1.5x1.9nm^2 image (I_t: -0.410nA; V_t: -273.4mV) of the [112] arrangement.
f) The [-1-12] arrangement with line profile showing the dimer-like structure of every 1D chain with two line profiles. The blue line profile represents the variation in intensity along the (001) direction. The green line represents the variation in intensity in between thymines on different Cu rows, i.e. 1 Cu in the (001) direction and 1 Cu in the (110) direction.

3.7. Thymine Bonding to Cu(110)

Experimental techniques have managed to ascertain how the thymine molecules are adsorbed on the Cu(110). These have determined that the molecule is bonded covalently to the outermost layer of the Cu(110) surface via the lone pair electrons of the O(2) and O(4) oxygen molecules and the deprotonated N(1) nitrogen in-between the two (see figure 3.2) aligned along the [110] direction. Although the single molecule is most likely aligned with the cyclic group perpendicular to the surface, previous studies [1,2,14-16] seem to indicate that intermolecular forces probably caused this to angle up to ~±20^o to the vertical. The object of this PhD was to investigate the energetics of thymine assembly at the surface, including various different arrangements and orientations.

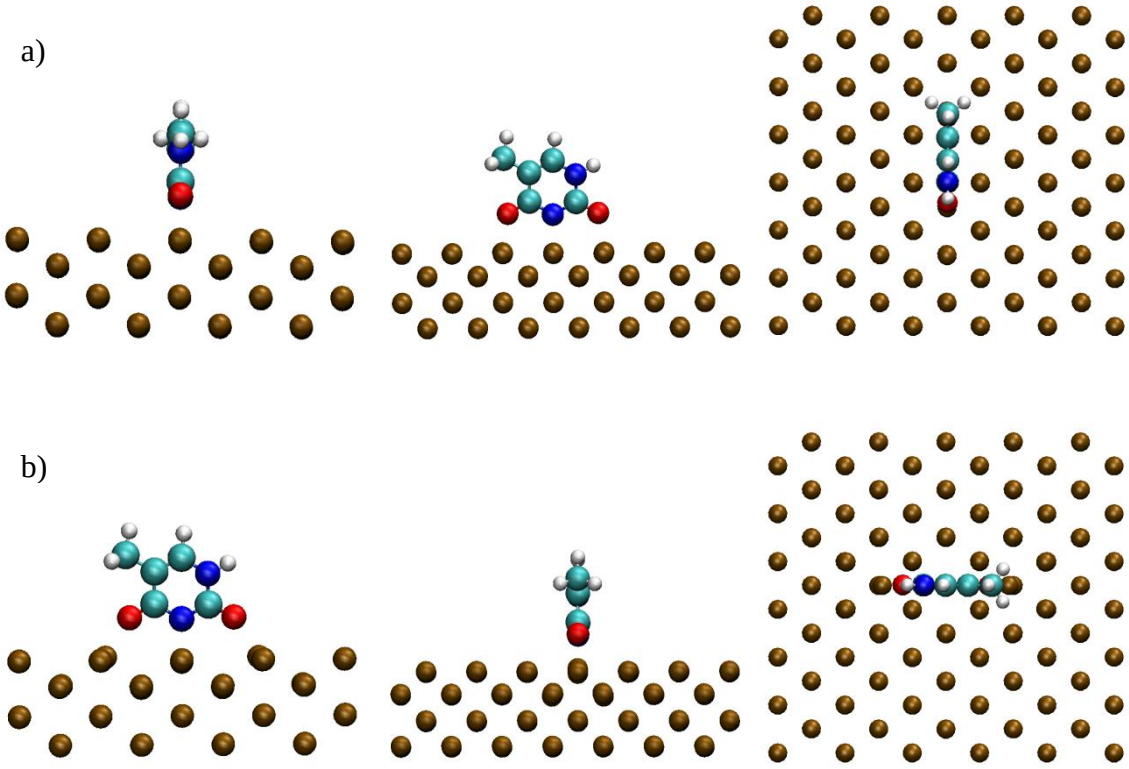

Figure 3.9: Single thymine molecule adsorbed on a 5x7 Cu(110) surface. In a) the thymine is bonded with the cyclic plane aligned along the [110] direction. Here ΔE_{Tot}=-1.990eV (calculated). In b) the thymine is bonded with the cyclic plane aligned along the [001] direction. Here ΔE_{Tot}=-1.416eV (calculated).

By relaxing the separate components of the system (i.e. the surface and the molecule) and then combining the systems an enthalpy of formation was calculated. If the reaction is exothermic (i.e. the total energy of the separate systems being greater than that of the combined components) the value will be negative. If the reaction is endothermic (i.e. the total energy of the separate systems being lower than that of the combined components) the value will be positive. Therefore, if the energy of the combined system is subtracted from the separate systems the difference between the two results in a representation of the overall stability of the system being analysed. The thymine molecule is deprotonated at the N(1) site so the molecule undergoes dehydrogenation during the dosing process. Therefore, a simulation of both an isolated thymine and a hydrogen molecule were required.

The reaction can be summarised as follows:-

$$\Delta E_{SC} + \Delta E_{TM} \longrightarrow \Delta E_S + \tfrac{1}{2}\Delta E_{HM} \quad (2)$$

And the overall enthalpy of formation is therefore:-

$$\Delta E_{Tot} = \Delta E_{SC} + \Delta E_{TM} - \Delta E_S - \tfrac{1}{2}\Delta E_{HM} \quad (3)$$

Here ΔE_{Tot} is the enthalpy of formation of the chemisorbed thymine molecule on the Cu(110) surface, ΔE_{SC} is the enthalpy of formation of the Cu(110) surface, ΔE_{TM} is the enthalpy of formation of the thymine molecule, ΔE_S is the enthalpy of thymine and Cu(110) surface and ΔE_{HM} is the enthalpy of the hydrogen molecule. This basic analysis technique was utilised throughout and gave results reflective of the stability of the particular orientation. The simulations began with a single molecule on a 5×7 unit cell. As it was believed that the molecule was oriented along the [110] direction, a comparison was first made with another possible orientation, i.e. along the [001] direction. A simulation with the thymine bonded directly above the second row of Cu atoms was also performed but failed to converge, further demonstrating a preference for the thymine bonding to the top layer of Cu atoms.

The relative stabilities demonstrate clearly that the [110] alignment is the preferred orientation in accordance with experimental data. The images of the relaxed thymine molecule oriented in the [110] direction show that the oxygen atoms slightly contort the outermost Cu layer by slightly pulling the Cu atoms below in an upward direction. However, with the thymine orientated in the [001] direction the surface is much more dramatically restructured with an upward and a lateral displacement of the outermost Cu layer. This leads to some restructuring of the second layer also.

3.8. Theoretical Data and Analysis

3.8.1. Overview

Many VASP simulations of thymine on Cu(110) have been carried out. Although these have been done on many different unit cell sizes they have all been done on unit cells with 4 layers of Cu atoms. The lower two have been fixed in place and represent the bulk of the crystal. However, the upper two were allowed to move and represent the surface of the crystal. The first few simulations were carried out in order to test and to verify the accumulated experimental data on how it was thought that the thymine bonded to the surface. Various stretches had been observed on RAIRS images and NEXAFS experiments had further narrowed down the possible ways that the thymine molecule was arranged upon the surface. So, it seemed logical to begin with as small a unit cell as possible in order to isolate a single thymine molecule. NEXAFS, TPD and RAIRS data strongly suggested that the thymine was bonded to the surface via the two oxygen molecules O(2) and O(4) and a deprotonated N(1) atom along the [001] direction. NEXAFS data also suggested that the molecule was angled in some way, however, the exact amount of angling was unclear. Also, NEXAFS data suggested that the amount of angling in all but the [001] axis was relatively small. It seemed reasonable, therefore to begin by positioning the thymine as close to these values as possible.

Many parameters had to be set before this system could successfully be used to model this system and these were altered and improved upon during the course of simulations. The system consisted of 5 separate atomic species in total. The surface contained just one, namely Cu, however, the thymine molecule contained 4 separate atomic species, namely Carbon (C), Nitrogen (N), Oxygen (O) and Hydrogen (H). All relevant criteria of these 5 different atomic species had to be defined and these are all contained in four files. The simplest of these files was the file called KPOINTS. VASP uses Fast Fourier Transforms (FFTs) in order to efficiently compute an inverse matrix of our system. This radically improves the speed of calculations. However, the number of "k-points" must be specifically defined as well as their exact nature. These are set in the KPOINTS file and are unique to each different unit cell. Also, in order to keep processing speed to a minimum these must be set to the minimum possible (integer) values. A rough formula was used throughout which was later refined. However, this can produce accuracy problems when comparing simulations performed on

different sizes of unit cells so it is always advisable to use the same size unit cell wherever possible.

The POSCAR file is another relatively simple file that is used throughout the analysis. This file sets the number, type, positions and size of unit cell to be used. It also specifies which atoms are to be held in place and which are to be allowed to move freely. Another, related file is called the CONTCAR file. Each structural iteration generates a new CONTCAR file containing the new positions of the atoms. To begin a new series of iterations the CONTCAR file must be renamed the POSCAR file. The third necessary file is called the INCAR file. This specifies the number of iterations to be made, the criteria for terminating structural relaxation and the type of algorithm to be used. It also sets the Wigner Seitz radius for each type of atom in the simulation. The final (and largest) file needed is called the POTCAR file. This contains all the information for each pseudopotential to be used for each atomic species. It also contains the mass, valence and energy of the reference configuration for which the pseudopotential was created.

Two further files are worth mentioning briefly as they can speed up structural relaxations somewhat. Each iteration generates a file called CHGCAR which contains the lattice vectors, atomic co-ordinates and the total charge density (multiplied by the volume) of the system. It also generates a file called WAVECAR which contains the initial eigenvalues, Fermi-weights and wavefunctions of the system. Both these files are very large (especially the WAVECAR file which can be <1Gb) and take much processing power to generate. Each iteration generates a modified version and so, if stored from a previous series of iterations, can often reduce the time taken to create the first iteration by at least an order of magnitude.

Due to the inaccuracies of DFT it is not always best to use the same lattice spacing in simulations as in experiment. The experimentally determined lattice spacing for Cu is ~3.61Å. However, when simulations are run using this value, the measured interatomic forces in the lattice are very high. Thus, it is necessary to use a slightly different value when modelling the surface. The most effective value (i.e. the one that relaxes to the lowest energy) is 3.64Å, which is the compiled lattice constant for bulk Cu. This is a systematic error and means that distances can never be realistically gauged to more than ~±0.05Å. Allowing for other non-systematic errors it seems reasonable to approximate all errors in distance in our calculations to ~±0.1Å.

Symmetry arguments are used throughout this thesis in order to justify the universality of our models. Also, attempts are made to justify many of the simplifications used, mainly in order to minimise the amount of processing power used. Even using many high speed processors operating in tandem it would still often take several hundred iterations and many days (weeks or even months) to run some of these simulations so it became necessary to keep these models as simple as possible whilst still being realistic enough to give accurate values for both the energies and bonding positions of the molecules involved.

3.8.2. Gas Phase Thymine And Hydrogen

The gas phase thymine molecule was modelled in a 15x15x15$Å^3$ unit cell which allowed for a minimum separation of <9Å. As the x, y and z directions are non-concomitant, the K-points were all set to 1. As accurate as possible values were necessary for this particular simulation as it was to be used for reference in all our thymine simulations. Initial models did not incorporate non-ab-initio corrected dispersion interactions. Although the gas phase unit cell size was determined to eliminate any long-range interactions between adjacent thymine molecules there is the possibility of self-interaction within the molecule itself and when these were accounted for the molecule was found to be almost 0.25eV more stable.

For consistency, the gas phase hydrogen was modelled in exactly the same way as the gas phase thymine in a 15x15x15Å. Self-interaction via dispersion interactions in such a small and symmetric molecule is unlikely to be an issue but a simulation was run correcting for such issues nonetheless. A much larger issue is whether one of the final products is indeed H_2 gas. Although H_2 gas was observed being emitted during TPD experiments (see figure 3.4) the question as to whether all the hydrogen leaves the surface has not yet been fully resolved. If indeed some of the hydrogen remains on the surface (as seems quite likely) then this is a source of systematic of error. Hydrogen bonded onto the Cu surface forms a much less localised (and thus weaker) bond than H_2 gas. However, our models are static in nature and are trying to simulate two relatively stable states, an initial one and a final one. If one of the states is dynamic in nature (i.e. hydrogen atoms moving around on the surface) then it is very difficult to accurately measure its actual stability.

3.8.3. Isolated Thymine Bonded to Cu Surface

Throughout this thesis the systems that were modelled became progressively more and more complex so arguments are constantly used to justify these various simplifications. The first dozen or so simulations were performed in order to try and familiarise ourselves with the system and to attempt to verify much of the experimental data. The first thing that had to be determined was what size unit cell to use. The first unit cell contained 60 Cu atoms in 4 layers (2 fixed, representing the bulk and 2 were allowed to move, representing the surface). Each layer therefore contained 15 Cu atoms. These were arranged 3 rows in the [110] direction and 5 rows in the [001] direction. No surface reconstruction has been observed for Cu(110) and this was further confirmed when this unit cell was relaxed. This effectively produced a model of an infinite sheet of Cu atoms with a single thymine bonded along both the [001] and the [110] direction, separated by <7Å to be created (see figure 3.10).

The first simulations involved placing a single thymine upon this surface. It seemed reasonable to begin by placing the molecule close to the position suggested by previous literature. This involves deprotonation at the N(1) position and covalently bonding to the top most layer of the crystal. Resulting geometry is shown in figure 3.10a with ΔE_{Tot} = -2.328eV. The O-Cu bonds are found to be ~2.0Å in agreement with NEXAFS data [15]. The STM simulation for this configuration (see figure 3.11) shows a double lobed feature. Additionally, the thymine was placed on the surface at a slight angle (~6^o along the y-axis as shown in figure 3.12 to determine:-

a) If this was a stable position.
b) If it preferred the untilted geometry shown in figure 3.10.
c) What this energy was.

Here ΔE_{Tot} = -1.981eV, showing that the tilted position is not preferred in the isolated thymine molecule. We also examined a possible alternative bonding position. When the thymine was rotated 90^o about the z-axis through the N(1) atom and placed with the plane of the molecule aligned along the [110] direction of the crystal. In figure 3.10b, the ΔE_{Tot} for this geometry is -1.416eV and is substantially unfavoured w.r.t. the previous geometry. Also that the covalent bonds between the O(2) and O(4) oxygens and the Cu surface are longer than in our previous model (see figure 3.10) and the oxygens also distort the bonding Cu

atoms and effectively pull them ~0.25Å from their preferred lattice positions, a relatively large distance.

a)

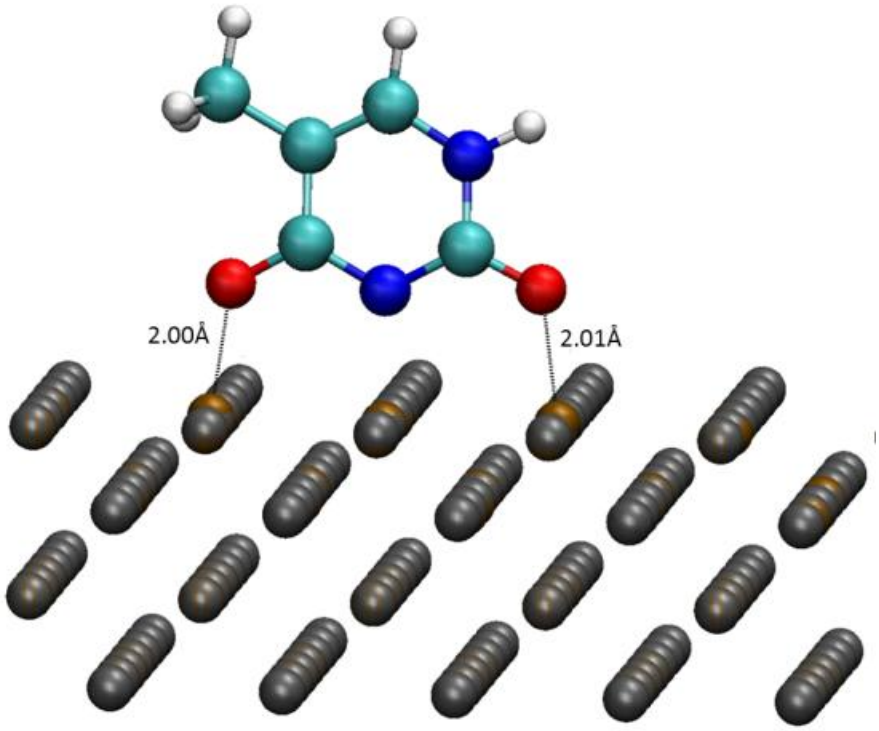

b)

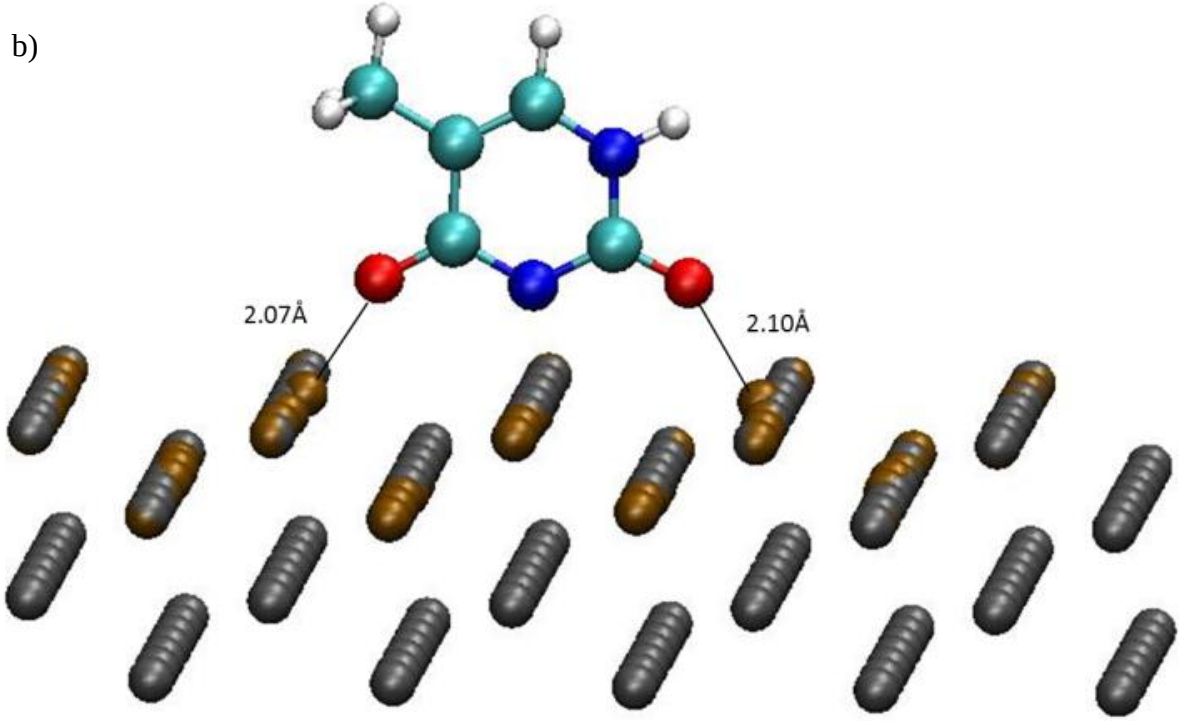

Figure 3.10: Isolated thymine chemisorbed onto the Cu(110) surface. Grey spheres represent Cu atoms undeviated from original positions. Copper coloured spheres represent positions of Cu atoms after relaxation of thymine on the surface. In a) thymine is bonded with the cyclic plane parallel to the [110] direction and in b) the thymine is bonded with the cyclic plane parallel to the [001] direction. In a) ΔE_{Tot} = -2.328eV (calculated) and in b) ΔE_{Tot} = -1.416eV (calculated).

As determined by spectroscopic observations we have to assume that the difference between these two phases is due to inter-molecular forces and thus it has nothing to do with the adsorption configuration which remains unchanged at this stage. This fact suggests that the driving force for the formation of both self-assembled structures partly comes from some attractive intermolecular interactions during diffusion processes at room temperature since no individual molecules are found under the studied conditions. No change in the assembly properties has been observed to be dependent on the coverage. However, the high molecular mobility of rows observed in phase 1 suggests the presence of a mildly strong interaction between molecules. In opposition molecules in phase 2 appear to be more strongly bonded and no molecular diffusion has been observed on molecules forming part of the 1D superstructures. Some diffusion on small 1D rows leading to the merging of two rows have been witnessed, but molecules seem to be fixed once they form part of these structures. Considering now the low temperature of the transition between phases 1 and 2, it is reasonable to assume that phase 1 may be a kinetic assembly, whereas phase 2 may be the more stable thermodynamic product and the mild annealing required in order to switch between the two phases to be the barrier for this state.

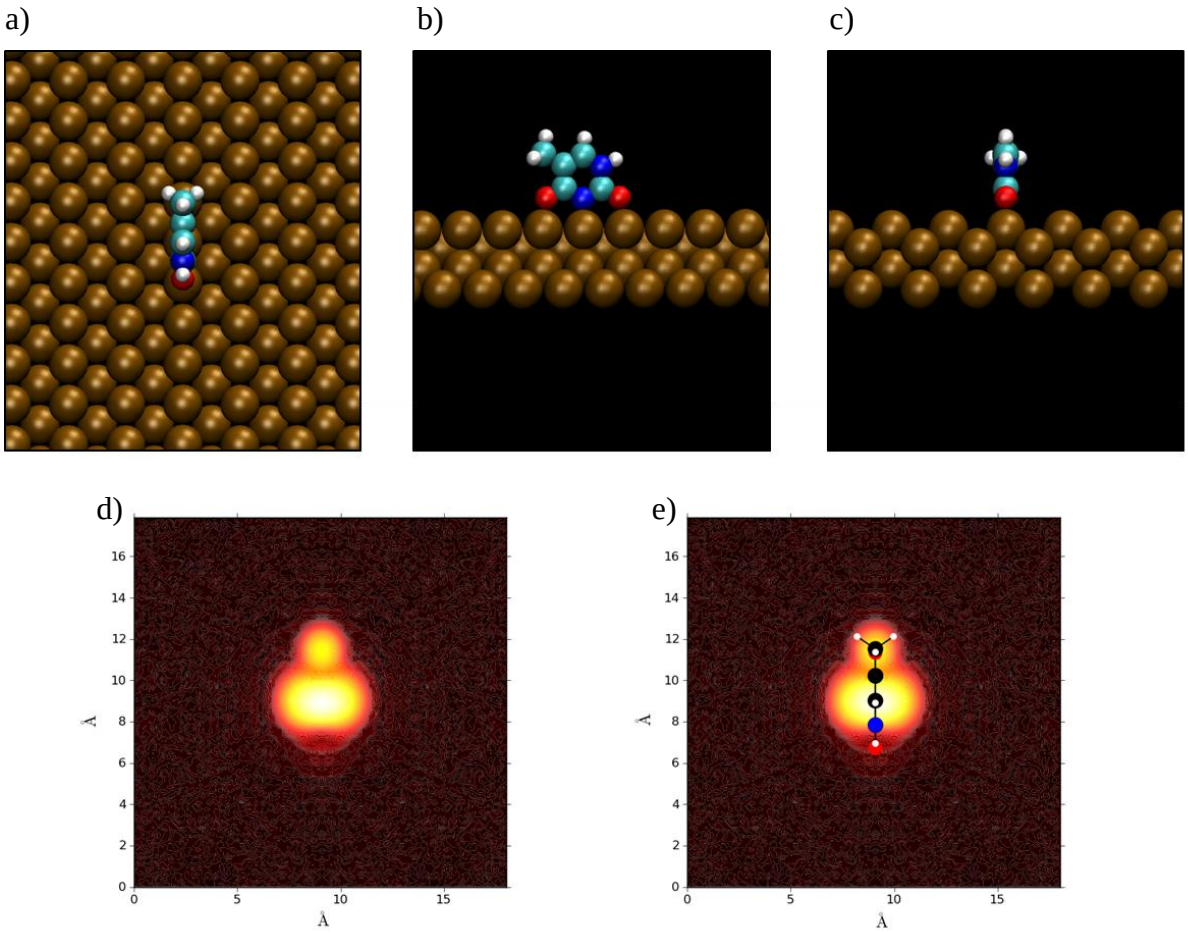

Figure 3.11: Diagram illustrating a fully relaxed single deprotonated thymine molecule bonded with the cyclic plane parallel to the [110] direction of Cu surface. When viewed from a) above, b) along the [001] direction and c) along the [110] direction the diagram shows thymine bonded at 90^{o} to the surface. In d) and e) simulated STM images (V_t: -0.3V) both with and without the thymine superimposed show the thymine creates a large image for the cyclic ring and a smaller image associated with the methyl group. Here ΔE_{Tot} = -2.328eV (calculated).

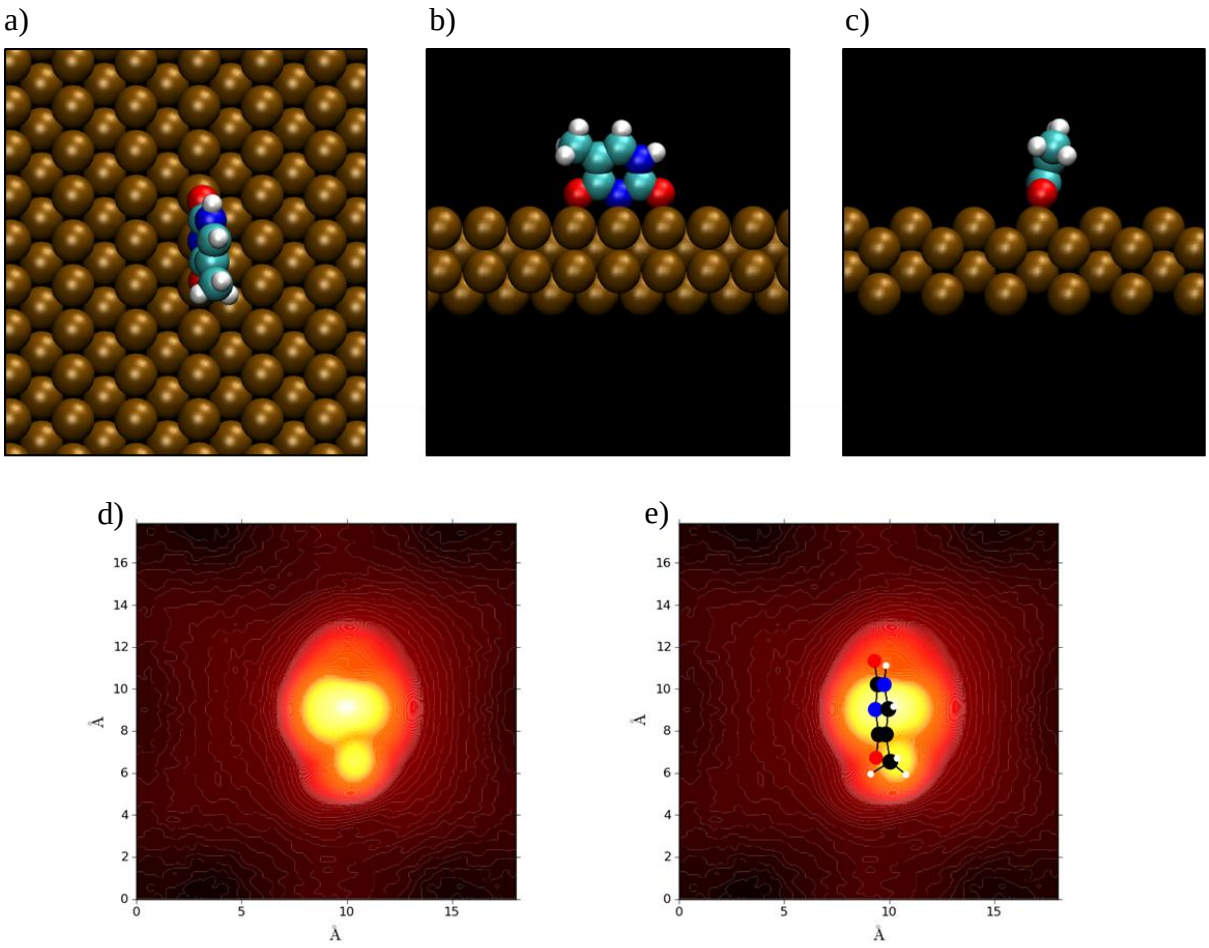

Figure 3.12: Diagram illustrating a fully relaxed single deprotonated thymine molecule bonded with the cyclic plane tilted with respect to the surface normal along the [110] direction of Cu surface. When viewed from a) above, b) along the [110] direction and c) along the [110] direction. In d) and e) simulated STM images (V_t: -0.3V) both with and without the thymine superimposed show the thymine creates a large image for the cyclic ring and a smaller image associated with the methyl group. Here ΔE_{Tot} = -1.981eV (calculated).

Further investigations of the isolated thymine molecule bonded to the surface involved using simulated X-Ray Photoelectron Spectroscopy (XPS). This involved using a computational technique that closely resembled the experimental technique and when plotted for an isolated thymine molecule arranged with the cyclic plane perpendicular to the Cu(110) surface produced an image very similar to the experimental one (see figure 3.13). This strongly suggested that the thymine was arranged on the Cu surface in this approximate orientation.

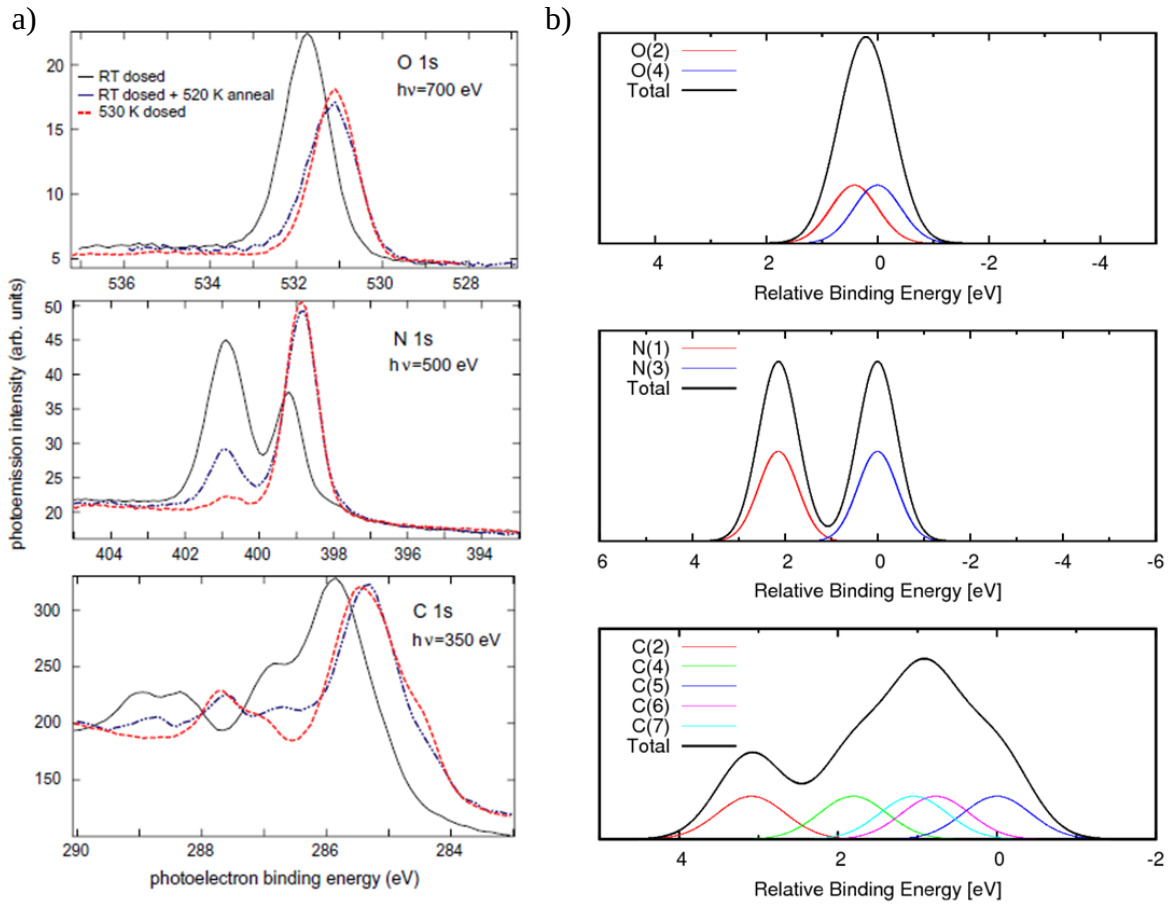

Figure 3.13: Shows both an experimental (a) [15] and a simulated (b) XPS image of thymine adsorbed on the Cu surface. In the top images both the experimental and simulated XPS show that that the core shift of both the O(2) and O(4) are about the same. In the middle images both the experimental and simulated XPS show that the core shifts of the N(1) and N(3) atoms are significantly different. In the bottom images the C(2), C(4), C(5), C(6) and C(7) atoms in the experimental and simulated XPS are all arranged in a similar way.

3.8.4. Phase 1 Structure

The next stage in the investigation considered the self-assembly process, which involved calculations on 1D rows of thymine molecules on the surface in various different configurations. First, thymine molecules were placed on adjacent top rows on the Cu surface in the most stable configuration determined in the previous section, i.e. with the plane of the molecule aligned along the [001] axis as shown in figure 3.11. Two obvious self-assembly

orientations of neighbouring molecules presented themselves here, those with the methyl groups parallel to one another and the other with the methyl groups in an anti-parallel configuration. However, there seemed to be very little difference in the stability of the two systems, with the one with the anti-parallel methyl group being only ~10meV more stable (see figure 3.14).

Although Density Functional Theory is now recognised as the state-of-the-art method for modelling systems of this type it does have inherent weaknesses. Weaker, long-distance interactions, like van der Waals (vdW), are not accurately measured. When dealing with systems of this type, these types of inter-molecular forces can play a very significant part in the arrangement of molecules on surfaces. Recent developments in algorithms modelling these types of interactions have been made [32,33] and have been incorporated into later versions of VASP. When these new algorithms were used in our system it became apparent that these played a very important role in the stability of our system. When thymine molecules were placed on adjacent rows with the cyclic rings aligned the stability increased by ~200 meV and it immediately became apparent that dispersion forces played a crucial role in the subsequent self-arrangement of thymine on the surface.

The first repeating chain structure that was simulated consisted of a single thymine molecule on a 1x7 unit cell. This particular simulation angled the cyclic plane of the thymine ~20^{o} to the vertical. Although the simulation did not demonstrate any remarkable difference in stability when dispersion corrections were accounted for [32,33] the structure showed itself to be significantly more stable (with an increase ΔE_{Tot} of ~0.25eV) than any of the previous structures. It was decided at that point to simulate a structure that contained two thymine molecules. The reason for this was due to the high distribution of charge around the end of the molecule containing the methyl group. Thymine is not a completely planar molecule and contains a methyl group bonded to the C(5) atom. This methyl group has three hydrogen atoms so placed as to be out of the plane of the molecule. It was believed that a structure where these were placed further apart may be more stable. A unit cell of size 2×7 was constructed and thymine placed so that the methyl group would be on alternate sides of the chain. As with the previous repeating structure, once dispersion effects were taken into account this structure proved to be significantly more stable (with an increase ΔE_{Tot} of ~0.2eV) than an isolated pair of thymine molecules (the slightly lower increase than for the previous simulation being accounted for by the steric hindrance of the two adjacent methyl

groups). Also, a further simulation was run with the molecule perpendicular to the surface, however, this proved to be of exactly the same stability. This seemed to re-enforce the theory that it was the π dispersion interactions that was the important factor in the self-assembly of the phase 1 structures and not any directional hydrogen bonding due to the angling and rotation of the molecule with respect to the surface.

STM images had repeatedly shown that Phase 1, present from room temperature up to ~350K, has network structures consisting of 1D chains parallel to the [001] direction, with every molecule separated by ~3.6Å. This implies that subsequent molecules of each row are located in consecutive Cu rows, with sets of rows separated by over 12Å, suggesting that little interaction occurs between rows. Molecules in this phase are believed to interact only weakly since there is a high mobility of these structures alongside the [110] direction and molecules can occasionally drift up or down briefly before going back to their original positioning. This first phase doesn't modify the main direction of the underlying surface.

The STM images clearly show that the phase 1 chains are often grouped together, separated by a constant distance of over 12Å. This corresponds to five rows of Cu atoms. As each thymine molecule occupies three rows, the rows are therefore separated by two empty Cu rows. Due to the repeating nature of the simulating technique used, both the simulations of the chain structures effectively modelled rows separated by four empty Cu rows. The next series of simulations focused in on this slight disparity between experimental observation and theoretical simulation. A series of unit cells from 2×3 to 2×8 were created and two thymine molecules placed on each in a similar manner to previously. This effectively simulated the moving of the infinite chain structure, observed in the formation of phase 1, closer together. A graph of the adsorption energies was thus produced (see Figure 3.14). What was observed was that the stability reached a minimum at the 2x4 unit cell. Although there seems to be some disparity between the theoretically predicted most stable unit cell size and that observed experimentally there does appear to be a kinetic barrier between the 2x3 and the 2x5 unit cells which might explain why annealing is necessary to get from phase 1 to phase 2. A possible explanation as to why this kinetic barrier is observed is that the surface Cu atoms are displaced slightly from their original positions as observed in figure 3.10 and that this displacement causes the relative instability of the 2x4 unit cell and thus causes the creation of a kinetic barrier.

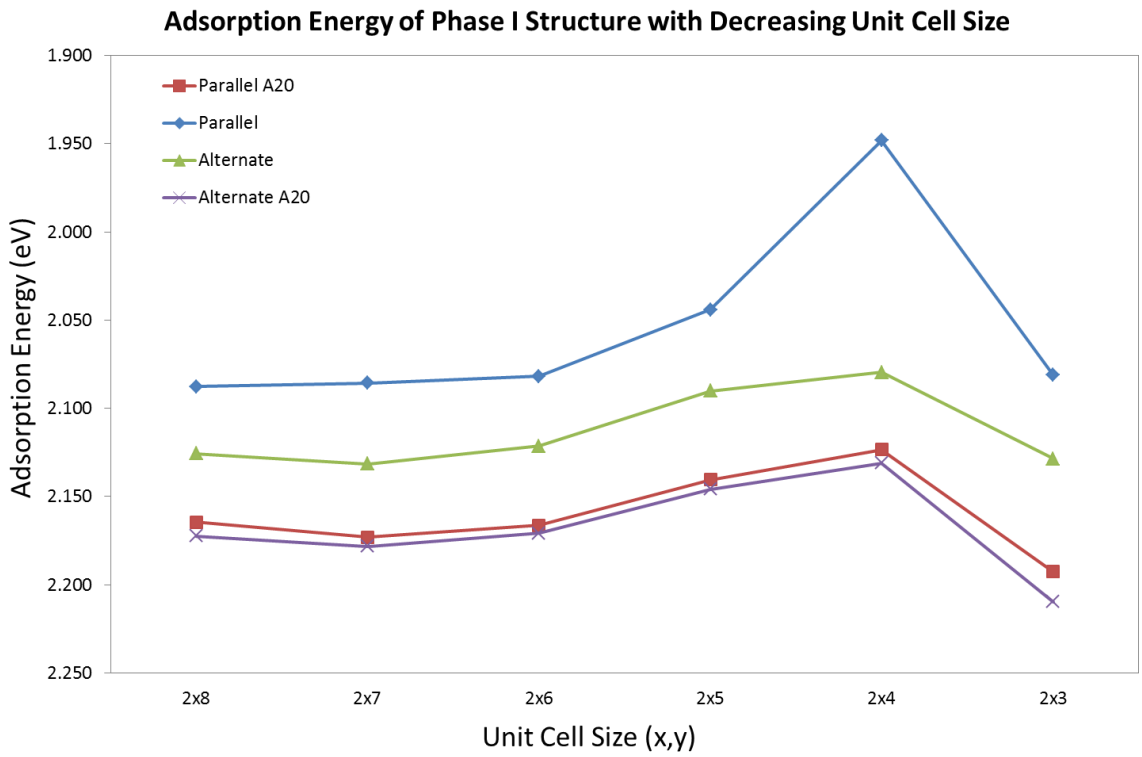

Figure 3.14: Shows the variation in stability for adsorbed thymine. The blue line shows thymine with the methyl groups parallel and the red line with the cyclic plane of the thymine angled at ~20^{o} to the vertical. The green line shows the thymine when the methyl groups are arranged on alternate sides and the purple line with the cyclic plane of the thymine angled at ~20^{o} to the vertical.

The first investigations were performed on a 1x5, 2x5 and 4x5 unit cells as this corresponded to the experimentally observed separation of the phase 1 rows. Initial investigations took 3 variations; the first, in a 1x5 unit cell, was angled (~20^{o}) and represented thymine with the methyl group along the same side (see figure 3.15a-b). The second, in a 2x5 unit cell, was also angled (~20^{o}) and represented thymine with the methyl group along alternating sides (see figure 3.15c-d). The third, in a 4x5 unit cell, was also angled (~20^{o}) and also represented thymine with the methyl group along alternating sides only this time in pairs (see figure 3.15e-f). The order of stability was 2x5 > 4x5 > 1x5. This suggested that the methyl group may be affecting the stability of the structure via steric repulsion of the methyl hydrogens.

Very little difference in stability was observed between the three structures and the original STM images were of insufficient resolution to definitively say whether any one structure

more closely resembled the experimental data. However, it seems reasonable to assume that there is probably a certain degree of randomness occurring in the orientation of the molecules along the chain. However, later investigations did seem to show that this may not be the case and some images showed that a repeating structure of 4 thymine molecules may occur. A series of simulated STM images of the phase 1 structures were then conducted in order to ascertain which of the two possible configurations most closely corresponded to the experimental data. Most interestingly, the bright spots observed on the STM images seemed to correspond, not necessarily with the thymine molecule, but with the delocalised electrons both above and below the cyclic ring (see figure 3.15).

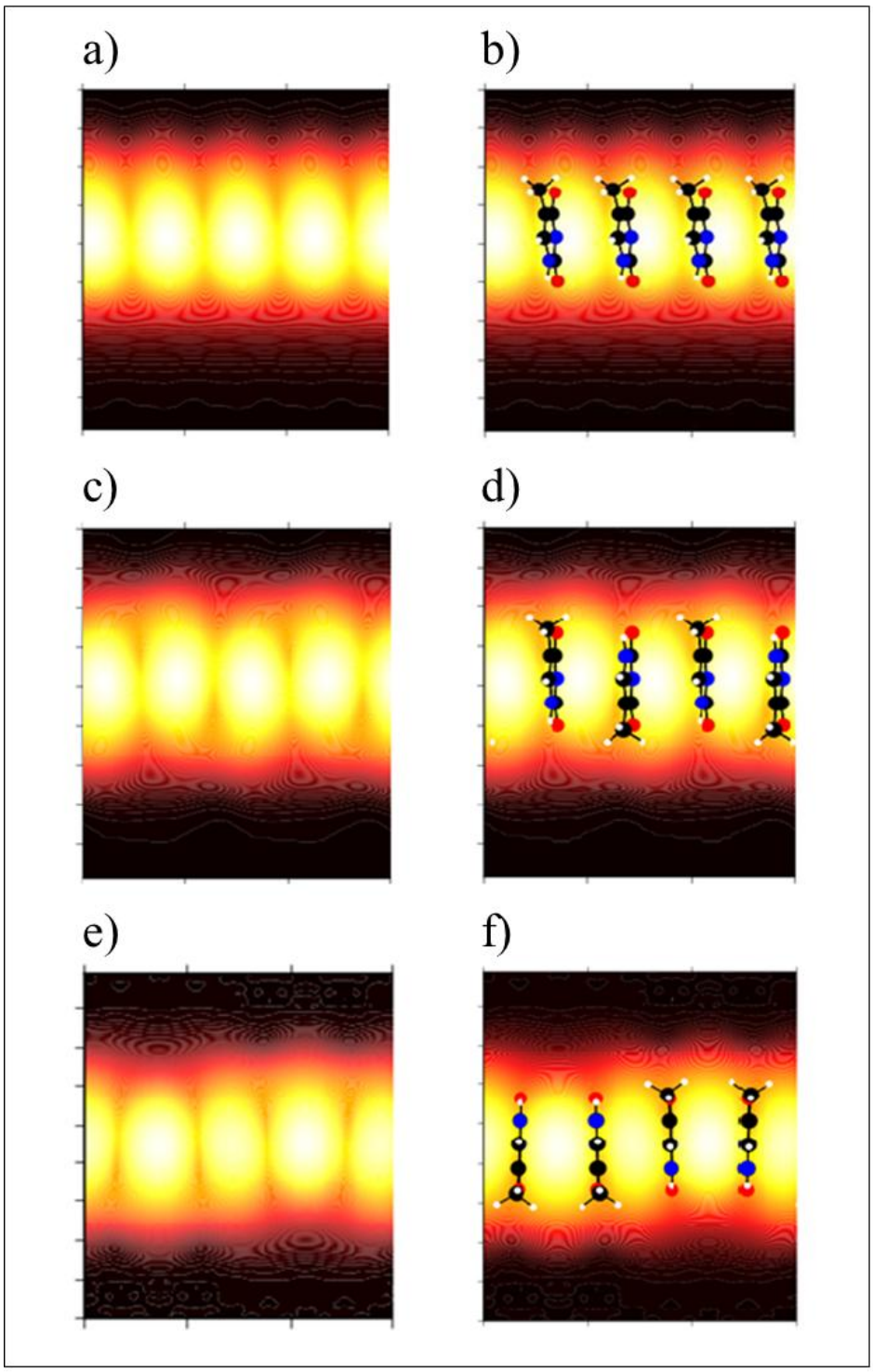

Figure 3.15: Simulated STM images for phase 1 structure. In a) and b) the thymine molecules are aligned with the methyl group along the same side. Here ΔE_{Tot} = -1.242eV (calculated). In c) and d) the thymine molecules are aligned with the methyl group on alternating sides. Here ΔE_{Tot} = -1.309eV (calculated). In e) and f) the thymine molecules have the methyl group paired on alternating sides. Here ΔE_{Tot} = -1.293eV (calculated).

The second stage in the investigations of phase 1 focused primarily on comparing the stabilities of structures with the methyl group along the same side and on alternating sides. These simulations were done using the Grimme correction in order to more accurately simulate the inter-molecular forces between both the molecules as well as the surface [32,33]. Also, on comparing the stabilities of structures where the plane of the molecule was at 90^{o} to the surface and where it was angled 20^{o}. The following images illustrate a detailed investigation using STM simulations to carefully scrutinise the various possible arrangements of the phase 1 structure. Unless stated otherwise, all the images were simulated with a bias voltage of -0.3eV.

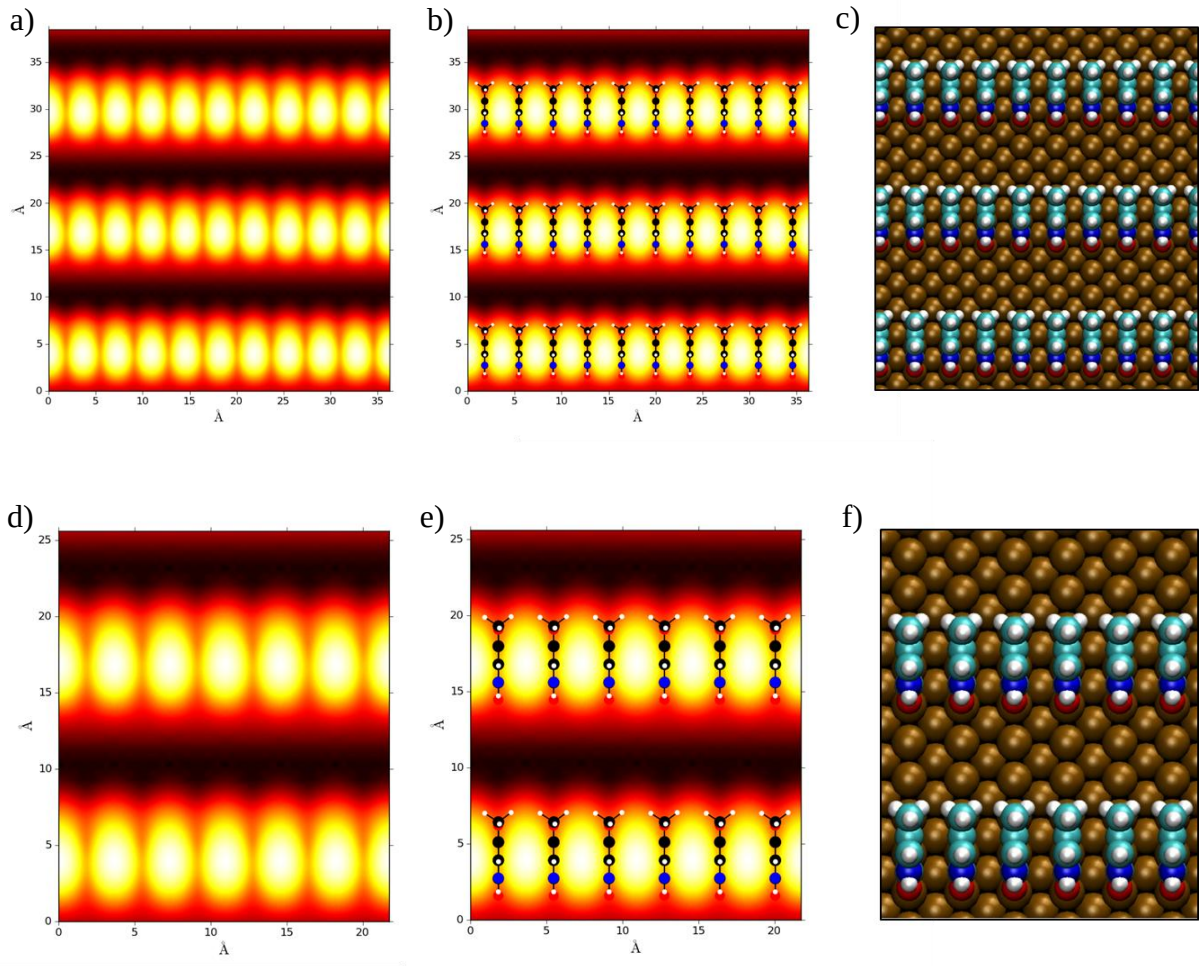

Figure 3.16: Illustration of phase 1 structure with methyl group aligned and at 90^{o} to the Cu surface. Here ΔE_{Tot} = -2.044eV (calculated).

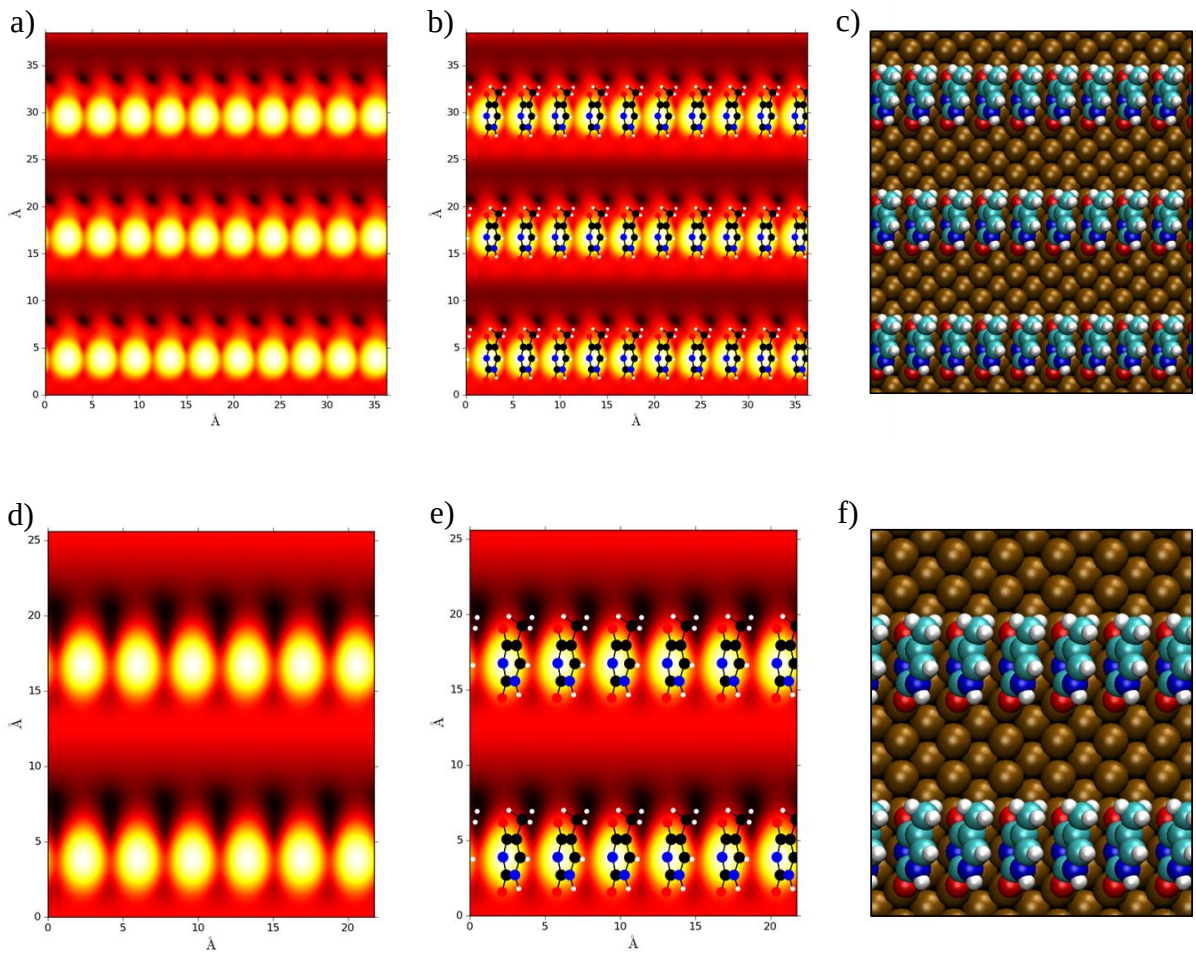

Figure 3.17: Illustration of phase 1 structure with methyl group aligned and at 70^{o} to the Cu surface. Here ΔE_{Tot} = -2.140eV (calculated).

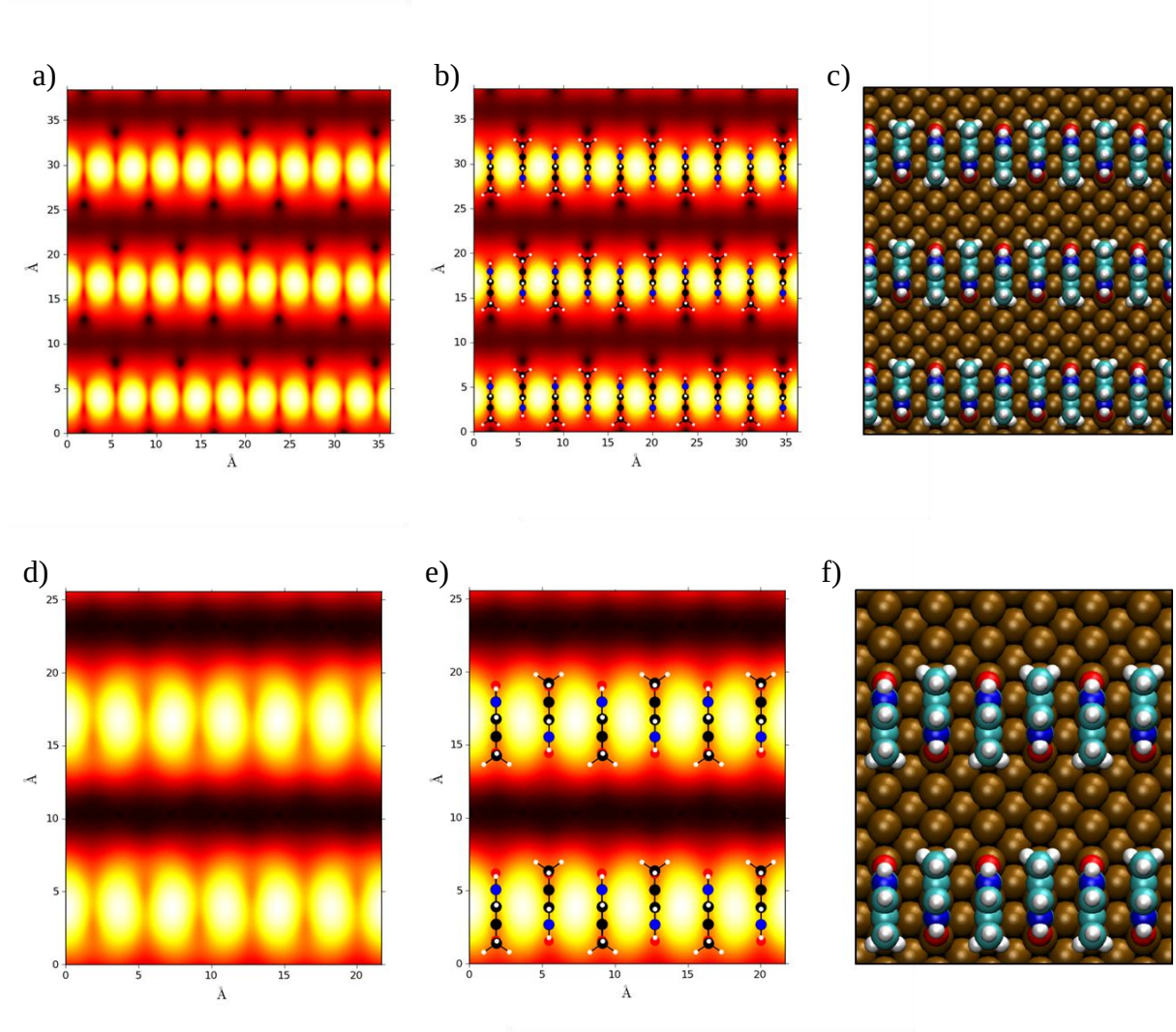

Figure 3.18: Illustration of phase 1 structure with methyl group on alternating sides and at 90^{o} to the Cu surface. Here ΔE_{Tot} = -2.090eV (calculated).

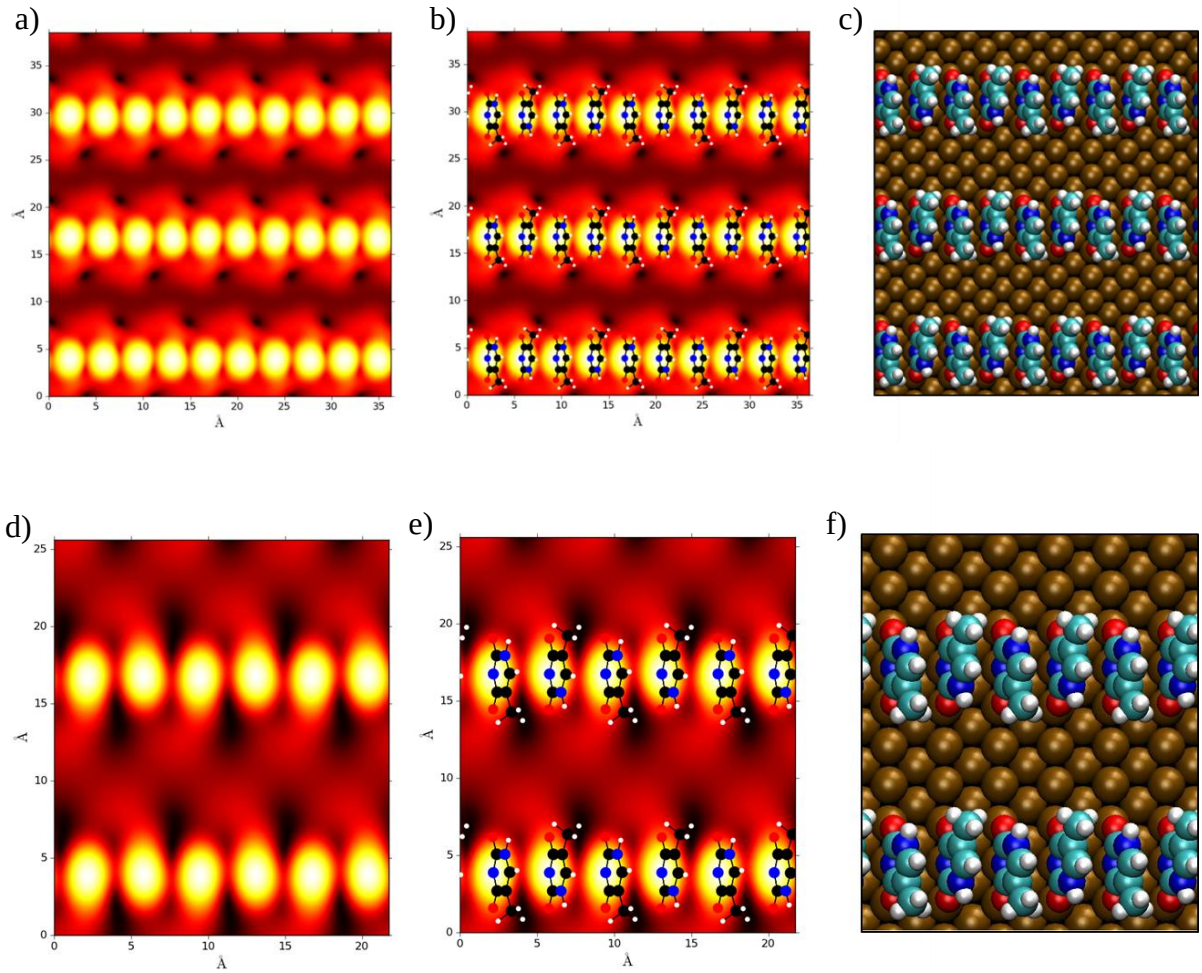

Figure 3.19: Illustration of phase 1 structure with methyl group on alternating sides and at ~70^{o} to the Cu surface. Here ΔE_{Tot} = -2.146eV (calculated).

This series of simulations (figures 3.16-3.19) showed a slight preference for the thymine to arrange with the methyl group on alternating sides of the chain (~5-10 meV) and a strong preference to arrange with the cyclic plane of the molecule angled at ~20^{o} to the vertical (~50-100 meV). Thus, it is possible to conclude that inter-molecular forces play a strong part in the self-assembly and positioning of the thymine chains (see table 3.2). As isolated thymine molecules prefer to position themselves at 90^{o} to the Cu surface then the preference for angling must be due to vdW forces between the molecules. The slight preference for the methyl group to position on alternating sides is most likely due to steric repulsion between the hydrogen in the (non-planer) methyl group.

Figure Number	Molecular Orientation*	Energy of Structure (eV)
3.16	P90	2.044
3.17	P70	2.140
3.18	A90	2.090
3.19	A70	2.146

Table 3.2: This is a summary of the previous four simulations of thymine on Cu(110) in table format.

* - The molecular orientation code corresponds to P meaning the methyl group is aligned on the same side (i.e. parallel), A meaning the methyl group is on opposite sides (i.e. alternating) and the 90 means that the thymine molecule has its cyclic plane angled at ~90^{o} to the surface and 70 means that the thymine molecule has its cyclic plane angled at ~70^{o} to the surface.

The third and final stage, of this investigation involved more carefully scrutinising the most stable of these structures with simulated STM. Different bias voltages and mean distances of the STM tip over the surface could, conceivably affect the image and so this was investigated. Three negative bias voltages were chosen (-0.3eV, -0.65eV, -1eV) and three mean distances (~6.5Å, ~8Å, ~9.5Å).

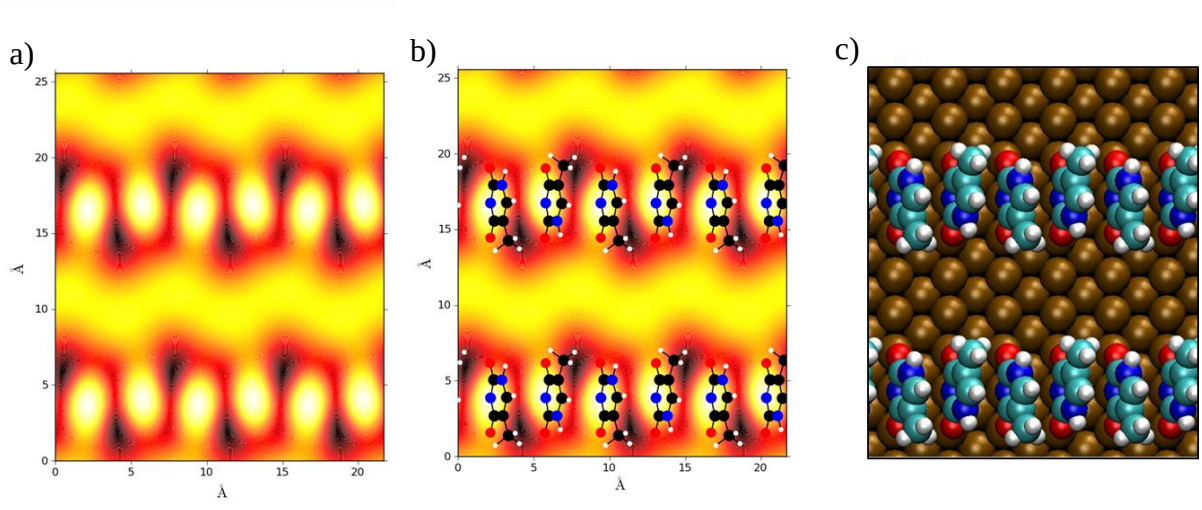

Figure 3.20: Illustration of phase 1 structure with methyl group on alternating sides and at 70^{o} to the Cu surface (~9.5Å) with a bias voltage of -0.3eV.

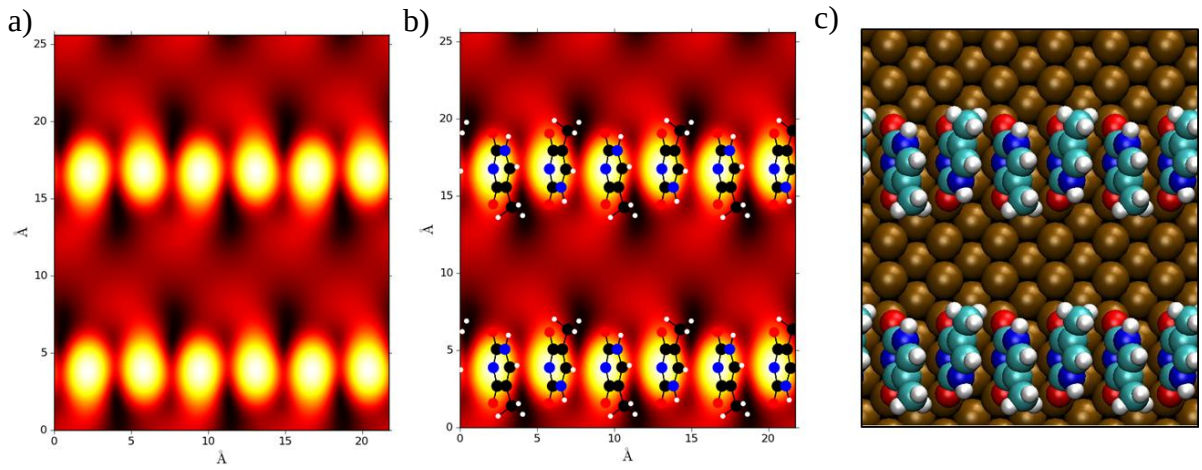

Figure 3.21: Illustration of phase 1 structure with methyl group on alternating sides and at 70^{o} to the Cu surface (~8Å) with a bias voltage of -0.3eV.

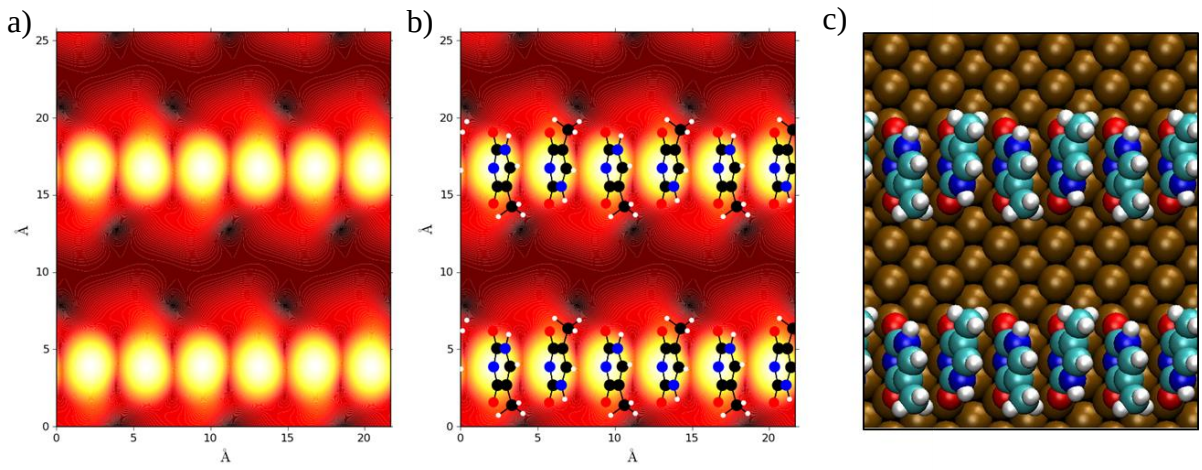

Figure 3.22: Illustration of phase 1 structure with methyl group on alternating sides and at 70^{o} to the Cu surface (~6.5Å) with a bias voltage of -0.3eV.

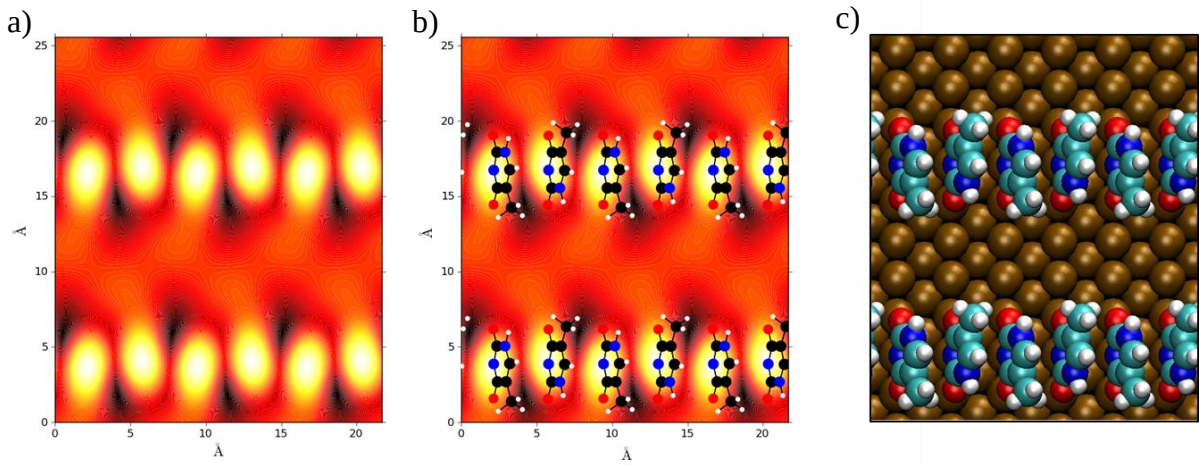

Figure 3.23: Illustration of phase 1 structure with methyl group on alternating sides and at 70^{o} to the Cu surface (~9.5Å) with a bias voltage of -0.65eV.

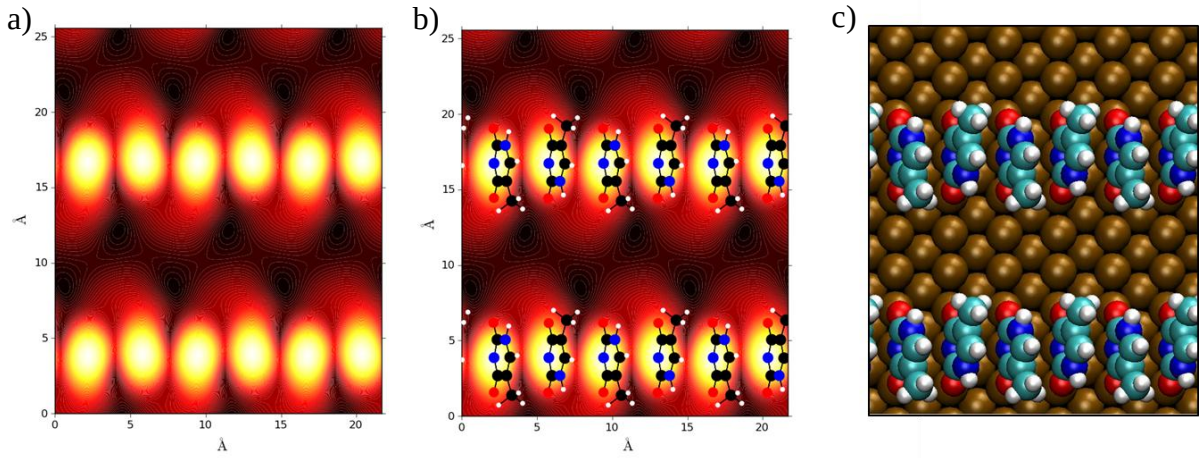

Figure 3.24: Illustration of phase 1 structure with methyl group on alternating sides and at 70^{o} to the Cu surface (~8Å) with a bias voltage of -0.65eV.

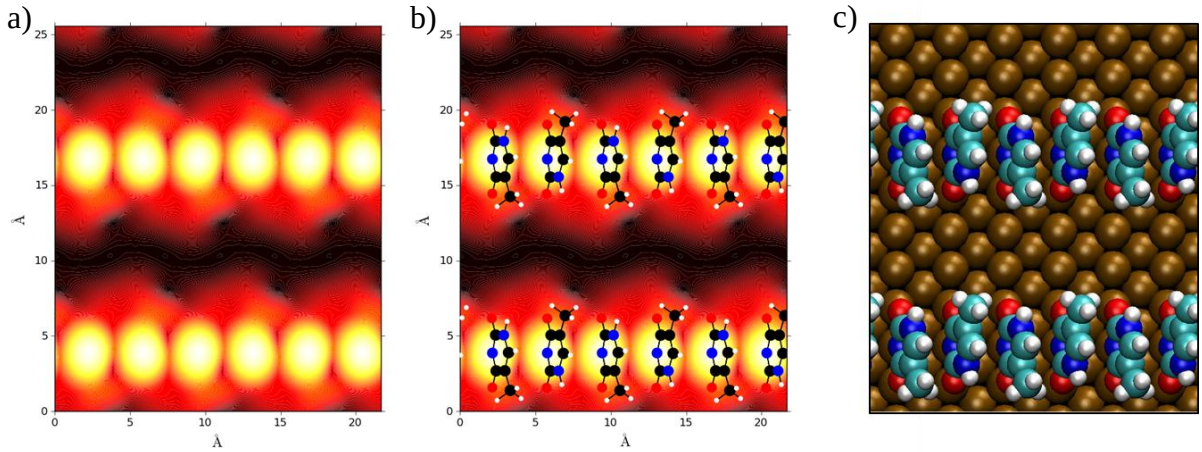

Figure 3.25: Illustration of phase 1 structure with methyl group on alternating sides and at 70^{o} to the Cu surface (~6.5Å) with a bias voltage of -0.65eV.

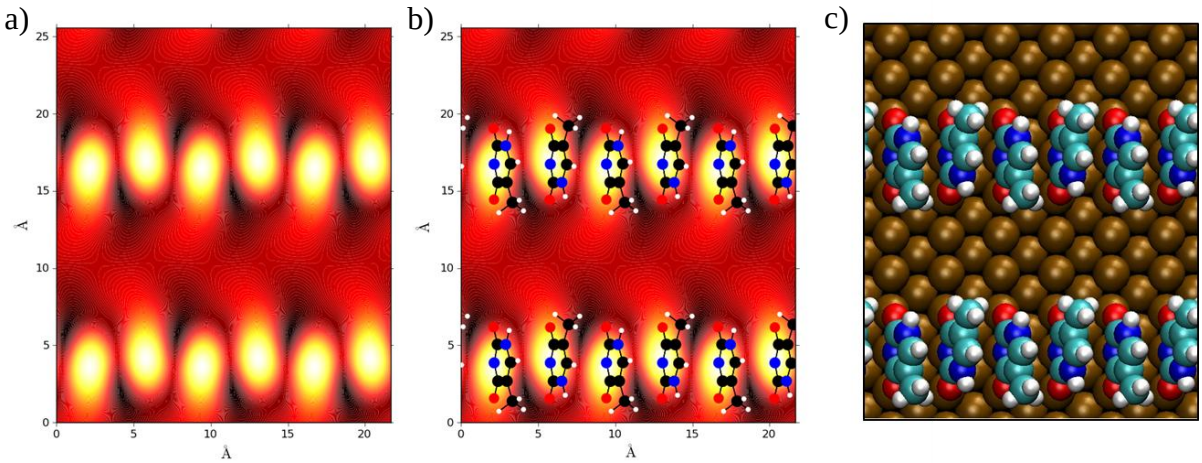

Figure 3.26: Illustration of phase 1 structure with methyl group on alternating sides and at 70^{o} to the Cu surface (~9.5Å) with a bias voltage of -1eV.

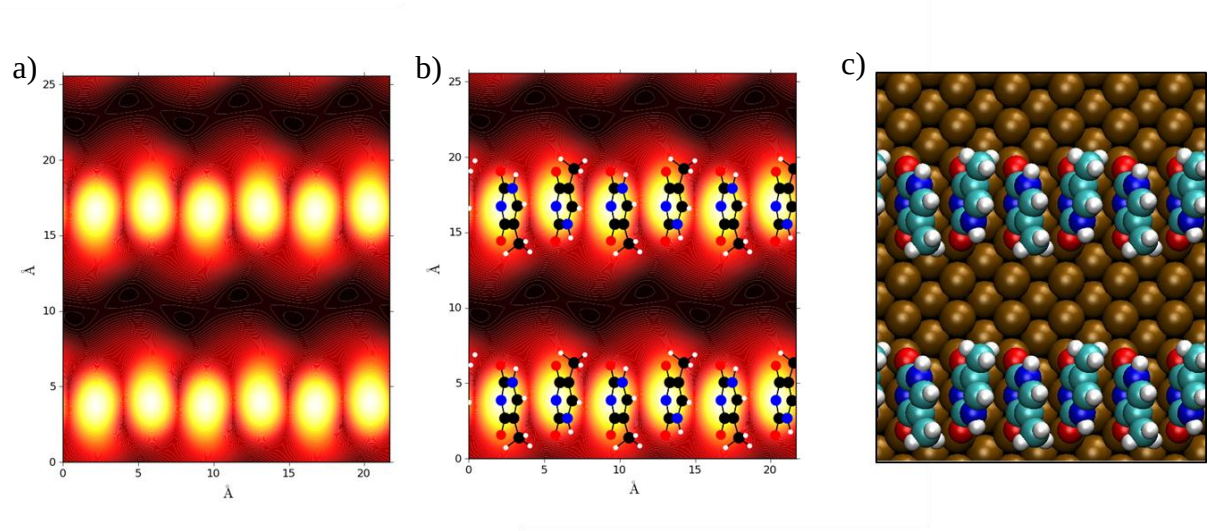

Figure 3.27: Illustration of phase 1 structure with methyl group on alternating sides and at 70^{o} to the Cu surface (~8Å) with a bias voltage of -1eV.

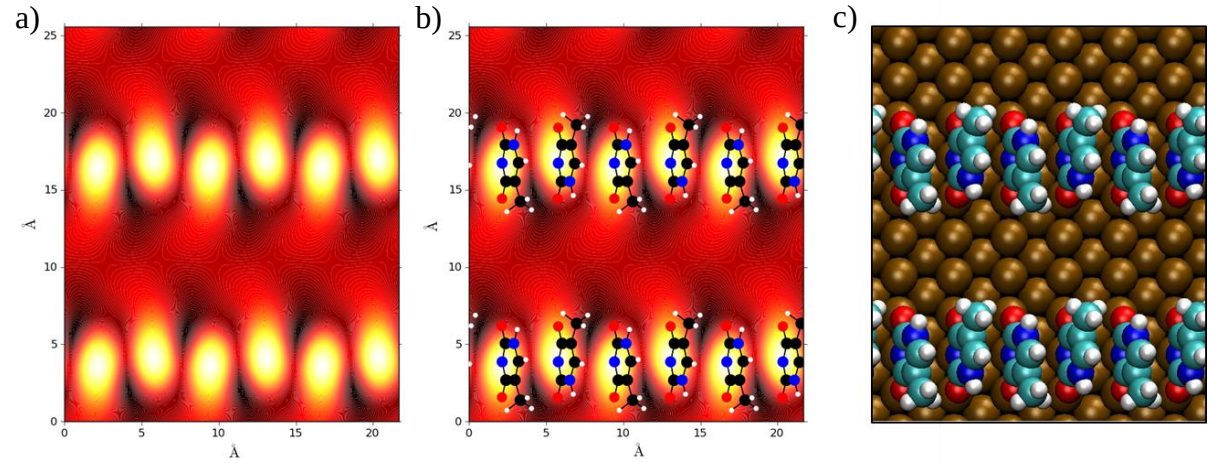

Figure 3.28: Illustration of phase 1 structure with methyl group on alternating sides and at 70^{o} to the Cu surface (~6.5Å) with a bias voltage of -1eV.

As can be seen, increasing the bias voltage does not significantly alter the image and the thymine appears as a bright spot on all the images. However, as the tip is brought closer to the surface this alters the shape and intensity of the images produced in-between the rows. The images also demonstrate that great variation is produced in-between the rows depending on the bias voltage and the tunnelling current. Although this investigation into the shapes

observed in-between the phase 1 rows in some of the STM images (see figure3.1a) does not explain their periodicity (occurring every fourth Cu row) or their shape, it does illustrate how they seem to be formed by the position of the methyl group. Also, it is a clear indication that further investigations (both experimental and theoretical) are warranted in order to produce a concise analysis of this system.

Yet another simulated technique was utilised in our investigation of thymine adsorbed on the Cu surface. Namely the scrutinisation of the Density Of States (DOS) of various orbitals associated with the bonding of thymine on the Cu surface (see figures 3.29-3.32). These clearly showed a shift in the bonding orbitals when the thymine goes from the gas phase to being adsorbed on the Cu surface. However, when going from an isolated adsorbed thymine molecule to being in a phase 1 chain there is a more subtle change in the DOS. The orbitals that are parallel to the cyclic ring (namely the s, p_y and p_z orbitals) show very little change. However, the orbitals tangential to the cyclic ring (namely the cyclic ring and p_x orbitals) show a marked change in energy.

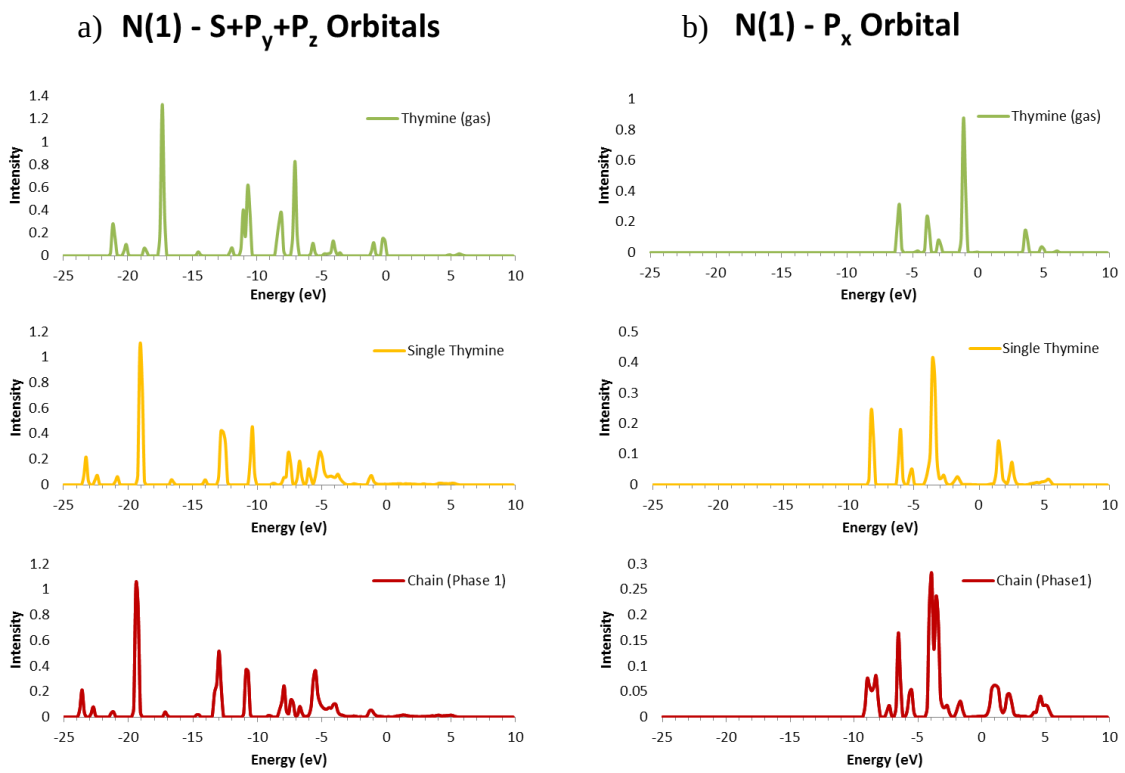

Figure 3.29: Shows bonding orbitals for N(1) thymine atom.

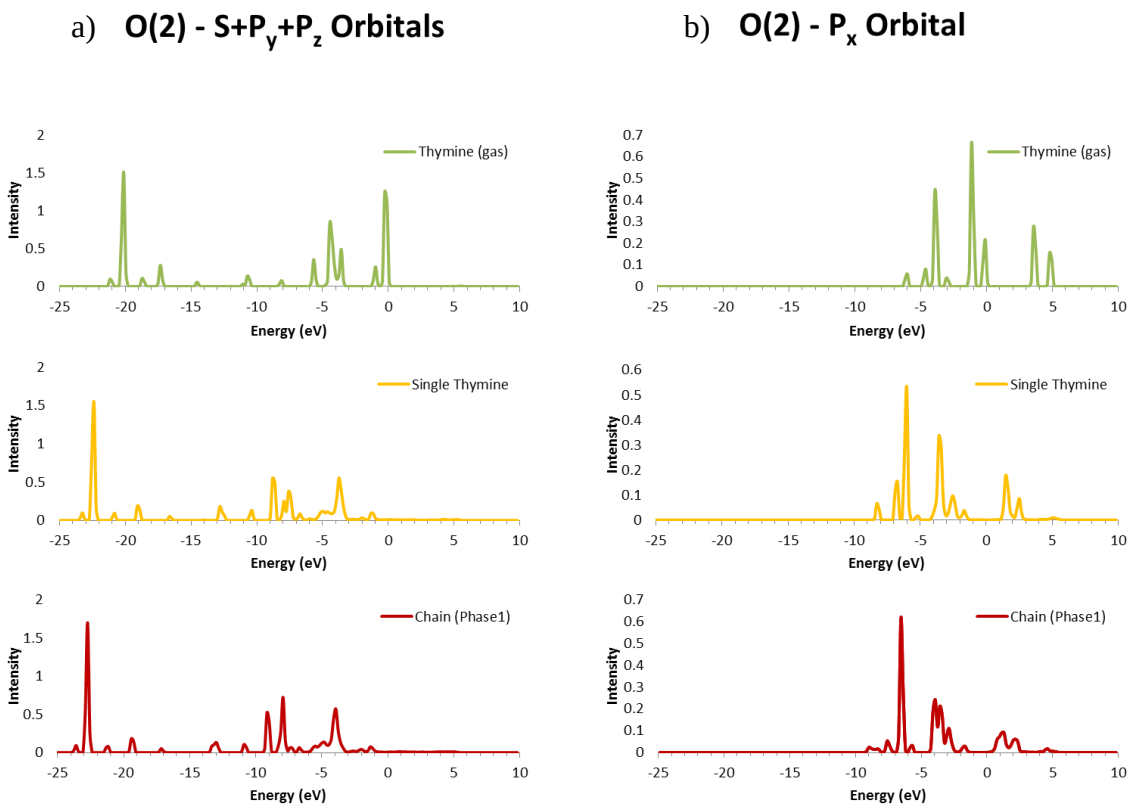

Figure 3.30: Shows bonding orbitals for O(2) thymine atom.

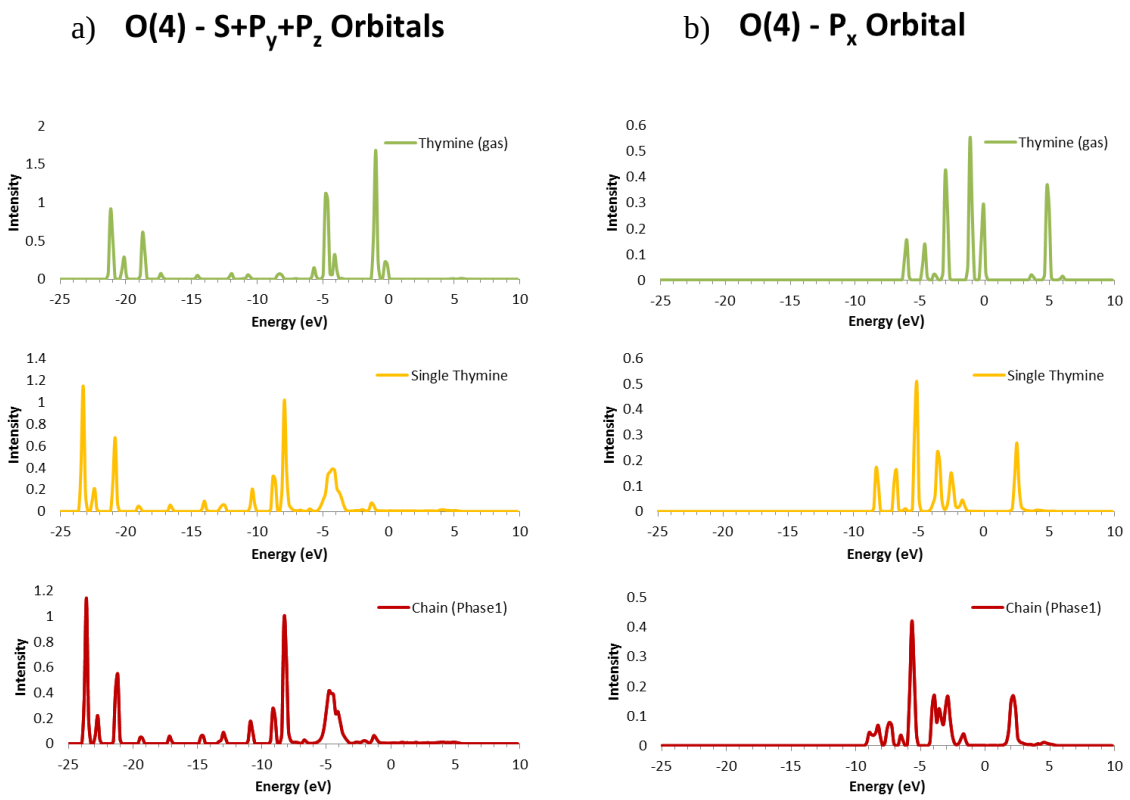

Figure 3.31: Shows bonding orbitals for O(4) thymine atom.

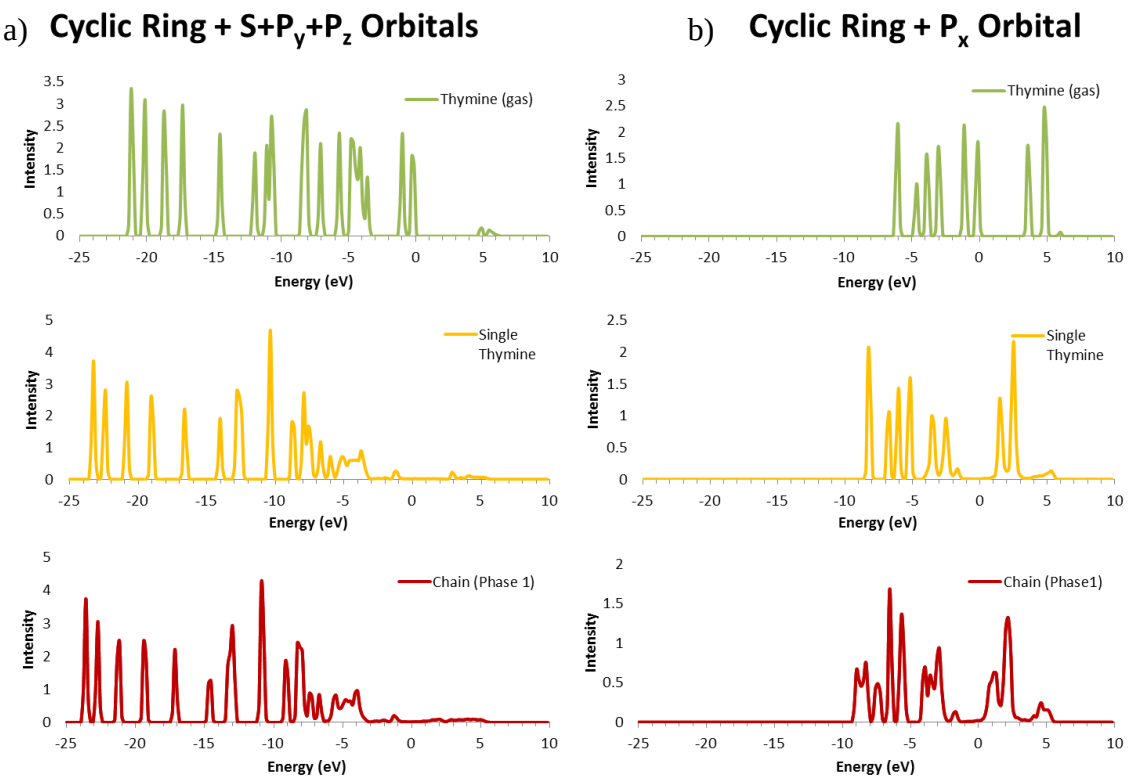

Figure 3.32: Shows bonding orbitals for cyclic ring and oxygen atoms of thymine atom.

3.8.5. Phase 2 Structure

After the substrate had been annealed to a higher temperature (between 350K-400K) another structure was observed. This involved similar chains of varying length, however, rather than being aligned along the [001] direction the chains were angled at ~±20^o to this axis. These were usually arranged in pairs but could be grouped together in three or even four rows. However, single rows were almost never observed. The direction of formation showed no regional preference and the two varieties seemed to be mixed together at random. Each grouping of thymine molecules seemed to correspond with a Cu row. These would usually occur in pairs but could also be seen as single, triple or (occasionally) quadruple molecules on the same row adjacent to one another. Interestingly, although close inspection revealed a certain degree of randomness in the structures when larger images were viewed the chains were observed to follow approximately the same direction (see figure 3.8). However, many of the images showed a definite tendency to form rows with pairs of adjacent thymine molecules and figure 3.8d shows a model of how these chains may be arranged on the Cu(110) surface.

The first stage in the STM simulation investigation into the phase 2 structure involved using an angled unit cell. The unit cell was 4 lattice spacings in the [001] direction and 2 lattice spacings in the [110] direction thus creating a downward sloping cell (see figure 3.28). The unit cell was 6 lattice spacings in the [110] direction thus creating a 4(-2)x6 unit cell. Although the phase 2 structure had a tendency to angle both upwards and downwards (i.e. at $\sim\pm20^{o}$ to the [001] direction) each is a mirror image of the other in both the planes [110] and [001]. For this reason, it was only necessary to simulate one of the two directions in order to be completely representative of both systems.

Each unit cell could fit up to 8 thymine molecules bonded to the Cu surface in a similar way as the phase 1 structure (i.e. deprotonated at the N(1) atom). Once again various different potential orientations were tried with different sized unit cells. In figure 3.33a-b, the unit cell consisted of only two thymine molecules with the methyl group on adjacent sides. The Grimme corrected adsorption energies [32-33] produced a very stable structure (ΔE_{Tot} = -2.251eV) which suggested that the phase 2 structure was more stable than phase 1. Figure 3.28c-d uses the same size unit cell and shows a slightly different configuration with the methyl group now on opposite sides. This structure proved to be slightly less stable (ΔE_{Tot}= -2.186eV) but still more stable than phase 1. Figure 3.28e-f shows a slightly larger unit cell containing four thymine molecules with pairs of thymine molecules with the methyl group on adjacent sides. This proved to be of exactly the same stability (ΔE_{Tot} = -2.186eV). Figure 3.18g-h was the most stable structure (ΔE_{Tot} = -2.266eV). This structure had the methyl groups reasonably well spaced apart and it is interesting to note that the methyl group forms a chain along the centre of the structure, again suggesting that this non-planar part of this otherwise planar molecule is an important factor in the self-assembly process.

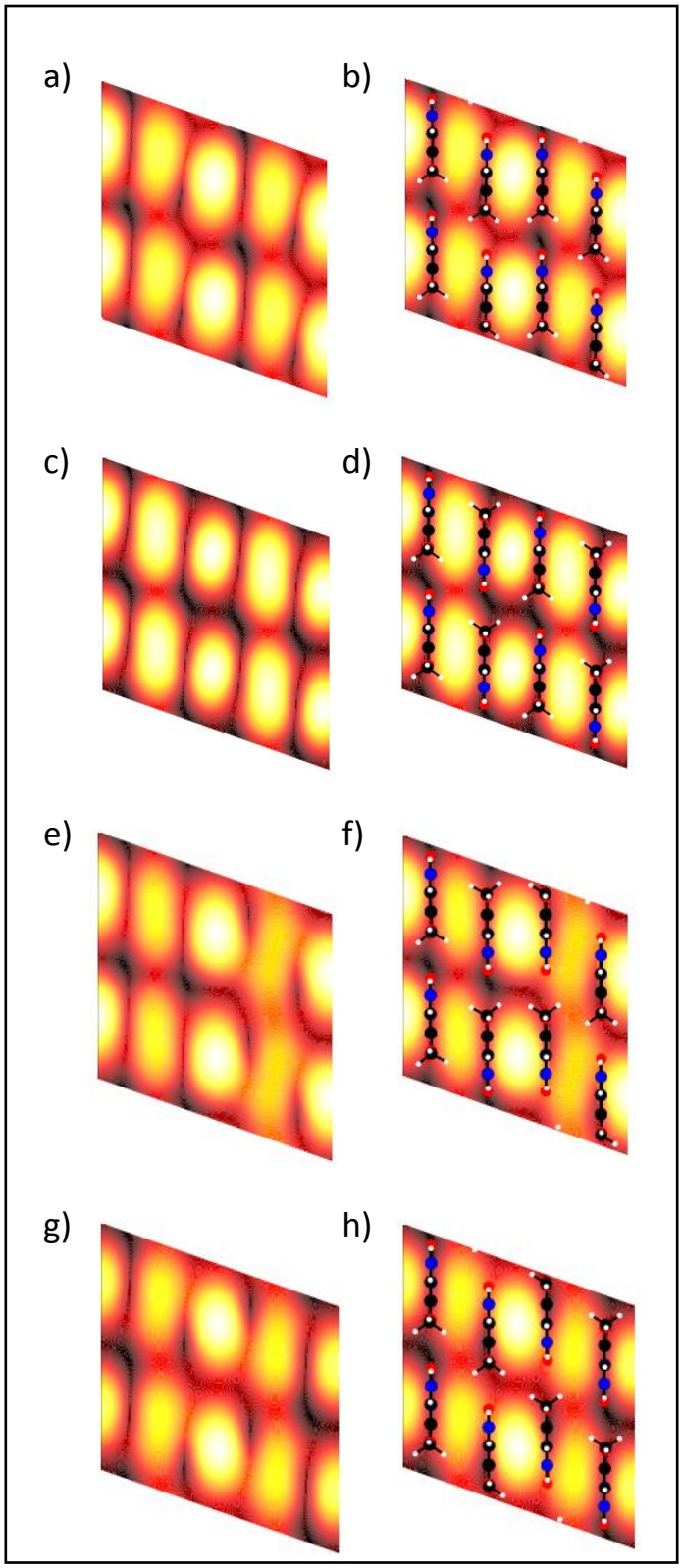

Figure 3.33: Simulated STM images for various possible phase 2 structures. The stability of a) and b) was ΔE_{Tot} = -2.251eV (calculated). The stability of c) and d) was ΔE_{Tot} = -2.186eV (calculated). The stability of e) and f) was ΔE_{Tot} = -2.186eV (calculated). The stability of a) and b) was ΔE_{Tot} = -2.266eV (calculated).

Although the STM images produced for the phase 2 simulation do closely resemble the experimental images certain discrepancies are apparent. Not only do some of the images display variations in the intensity of the bright spots but also in the size and shape. More importantly, the bright spots appear to align in the [110] direction in the STM images, whereas in the experimental images they do not (see Figure 3.8c). The second stage in the STM investigation into the phase 2 structure involved reducing the size of the unit cell by half, in accordance with the LEED data [2]. The unit cell was now a 2(-1)x6. A new set of (4) potential structures were now investigated as before, both with the plane of the molecule angled at 90^{o} to the Cu surface and at $\sim 70^{o}$. However, this system could conceivably have been modelled on a 2(1)x3 unit cell if both rows were angled in the same direction, the top row would be angled at $+70^{o}$ and the bottom row at -70^{o}. The same could be said of the simulation angled at 90^{o} to the Cu surface, however, these were just used in order to compare the stability of the angled simulations as well as the STM simulation. Again, all the images (figures 3.34-3.45) were simulated with a bias voltage of -0.3eV and each of these figures can be summarised as follows:-

a) This image shows a simulated STM image without the thymine molecules superimposed. Along the [001] direction (x-axis) are 4 unit cells and along the [110] (y-axis) are 2 unit cells.
b) This image shows a simulated STM image with the thymine molecules superimposed. Along the [001] direction (x-axis) are 4 unit cells and along the [110] (y-axis) are 2 unit cells.
c) This image shows a view of the surface with the thymine molecules superimposed. Along the [001] direction (x-axis) are 4 unit cells and along the [110] (y-axis) are 2 unit cells.
d) This image shows a simulated STM image without the thymine molecules superimposed. Along the [001] direction (x-axis) are 3 unit cells and along the [110] (y-axis) is 1 unit cell.
e) This image shows a simulated STM image with the thymine molecules superimposed. Along the [001] direction (x-axis) are 3 unit cells and along the [110] (y-axis) is 1 unit cell.
f) This image shows a view of the surface with the thymine molecules superimposed. Along the [001] direction (x-axis) are 3 unit cells and along the [110] (y-axis) is 1 unit cell.

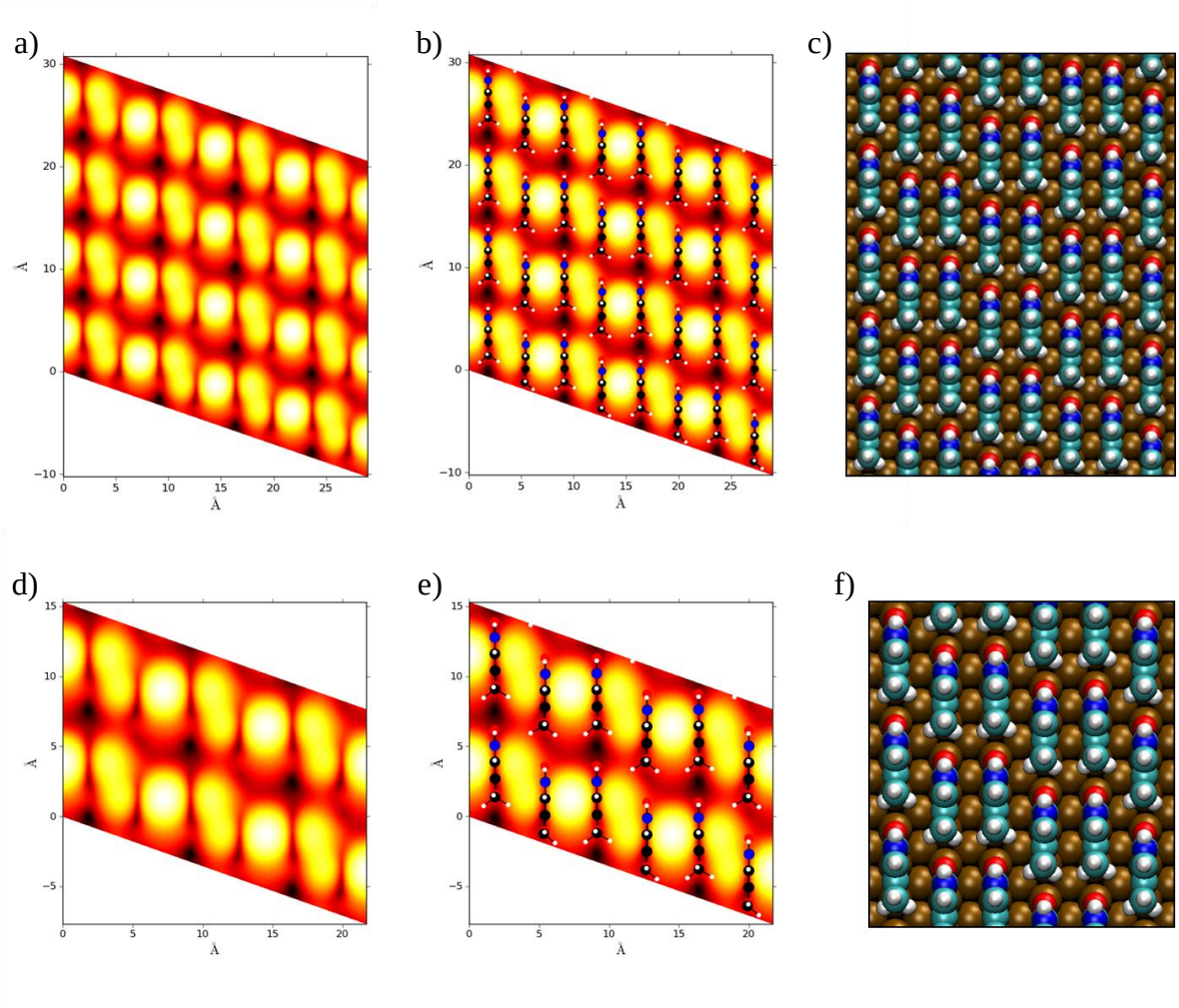

Figure 3.34: All thymine molecules are aligned in the same direction and with the cyclic plane at ~90^{o} to the Cu surface. Here ΔE_{Tot} = -2.115eV (calculated). This simulation is not very stable and produces one image that is very bright (in between the adjacent thymines) and another that is slightly elongated and more diffuse (in between the thymines on adjacent rows). This is in contradiction to the experimental image in which all the images are of approximately the same size and intensity.

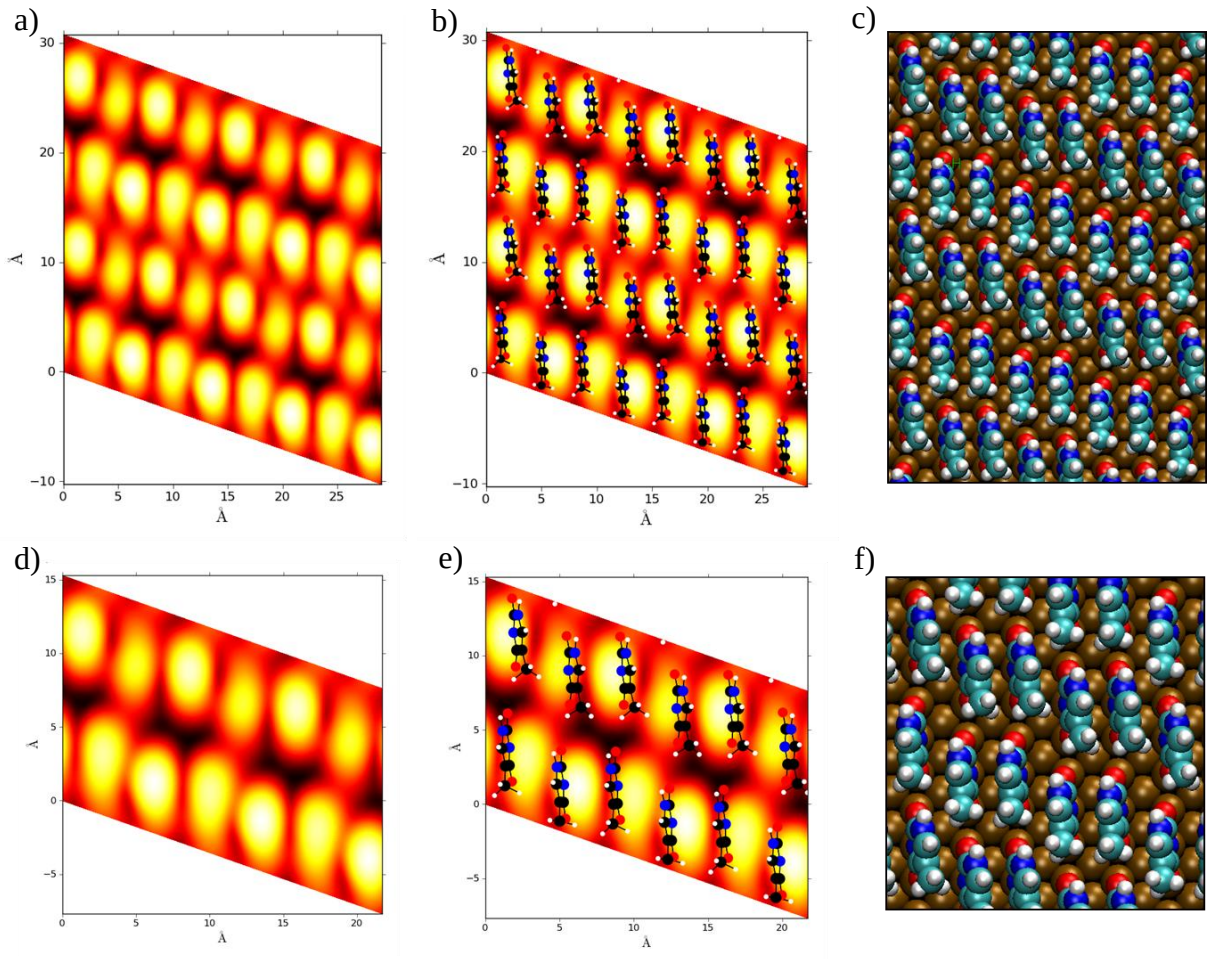

Figure 3.35: All thymine molecules are aligned in the same direction and with the upper row cyclic plane at ~+70^{o} to the Cu surface and the lower row cyclic plane at ~-70^{o} to the Cu surface. Here ΔE_{Tot} = -2.109eV (calculated).

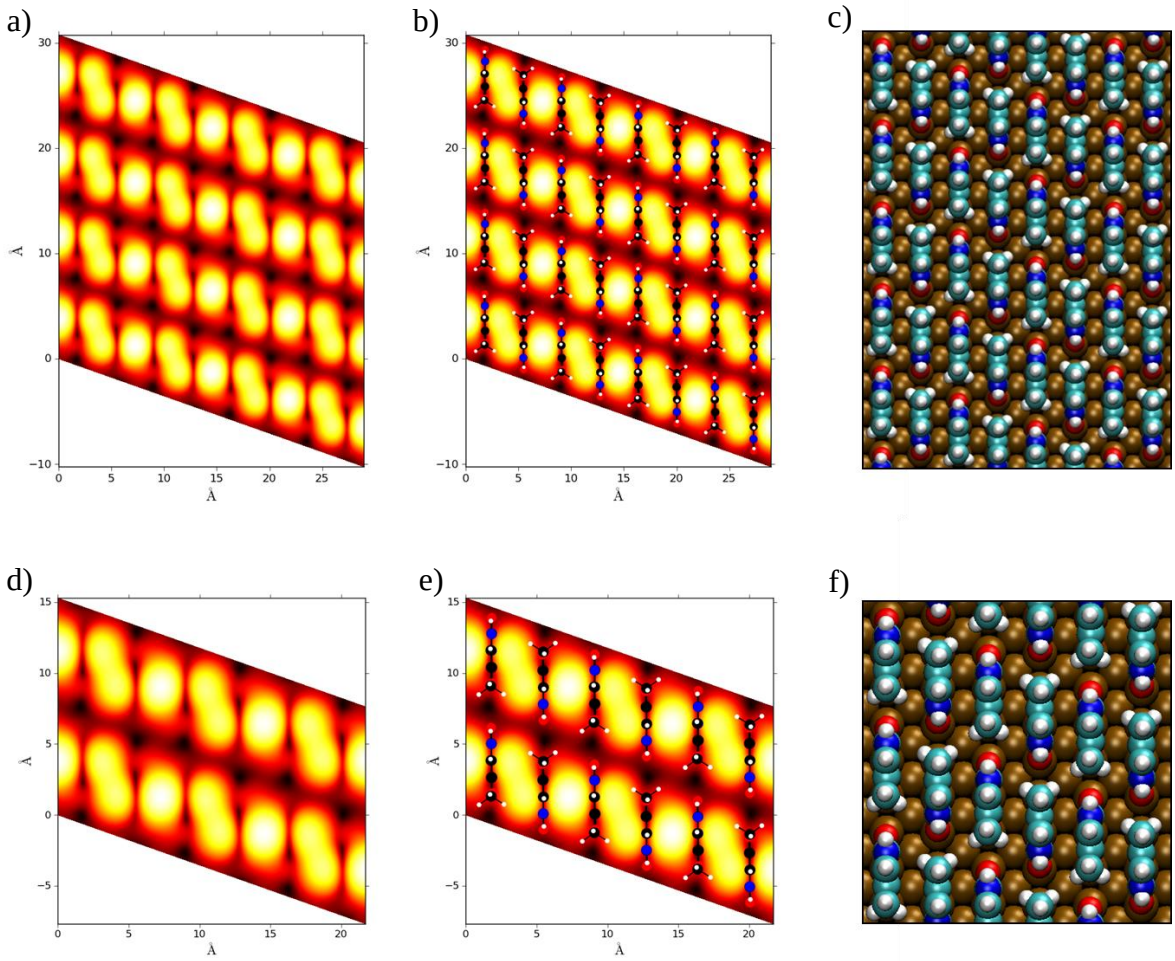

Figure 3.36: All thymine molecules are aligned in opposite directions and the cyclic plane at ~90^{o} to the Cu surface.Here ΔE_{Tot} = -2.130eV (calculated).

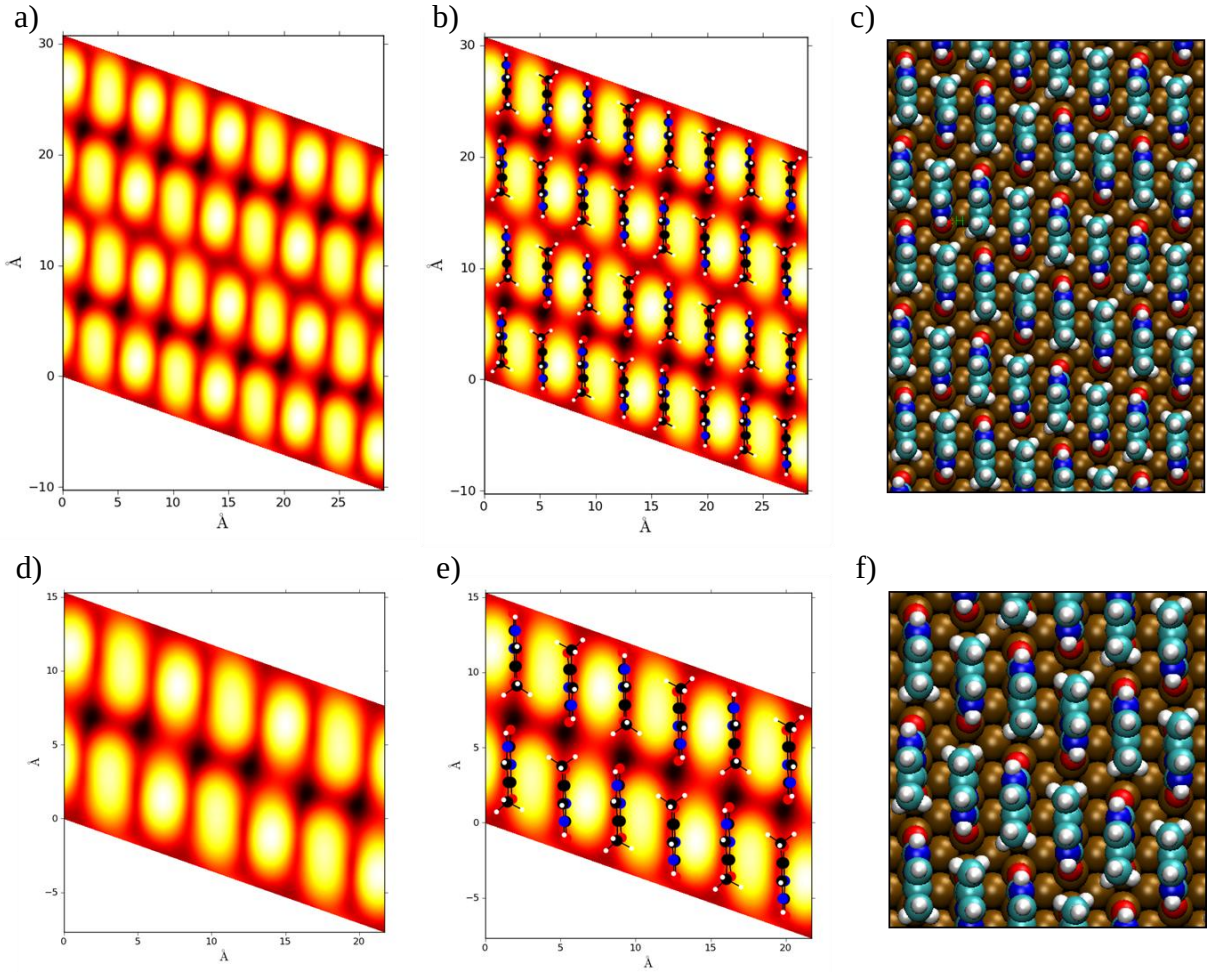

Figure 3.37: The thymine molecules are aligned in the opposite directions and with the upper row cyclic plane at ~+70^{o} to the Cu surface and the lower row cyclic plane at ~-70^{o} to the Cu surface. Here ΔE_{Tot} = -2.128eV (calculated).

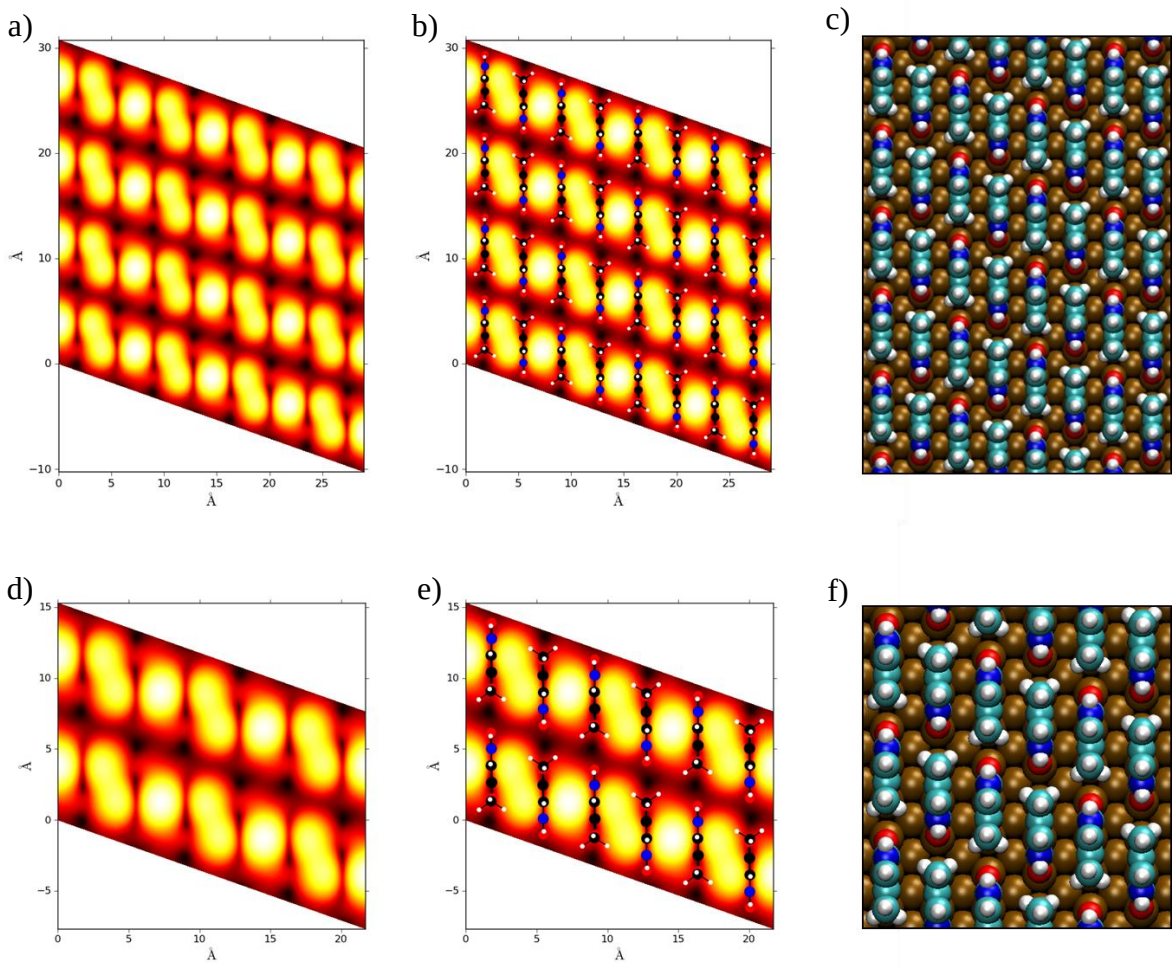

Figure 3.38: The thymine molecules are aligned in the opposite directions and with the cyclic plane at ~90^{o} to the Cu surface. Here ΔE_{Tot} = -2.128eV (calculated).

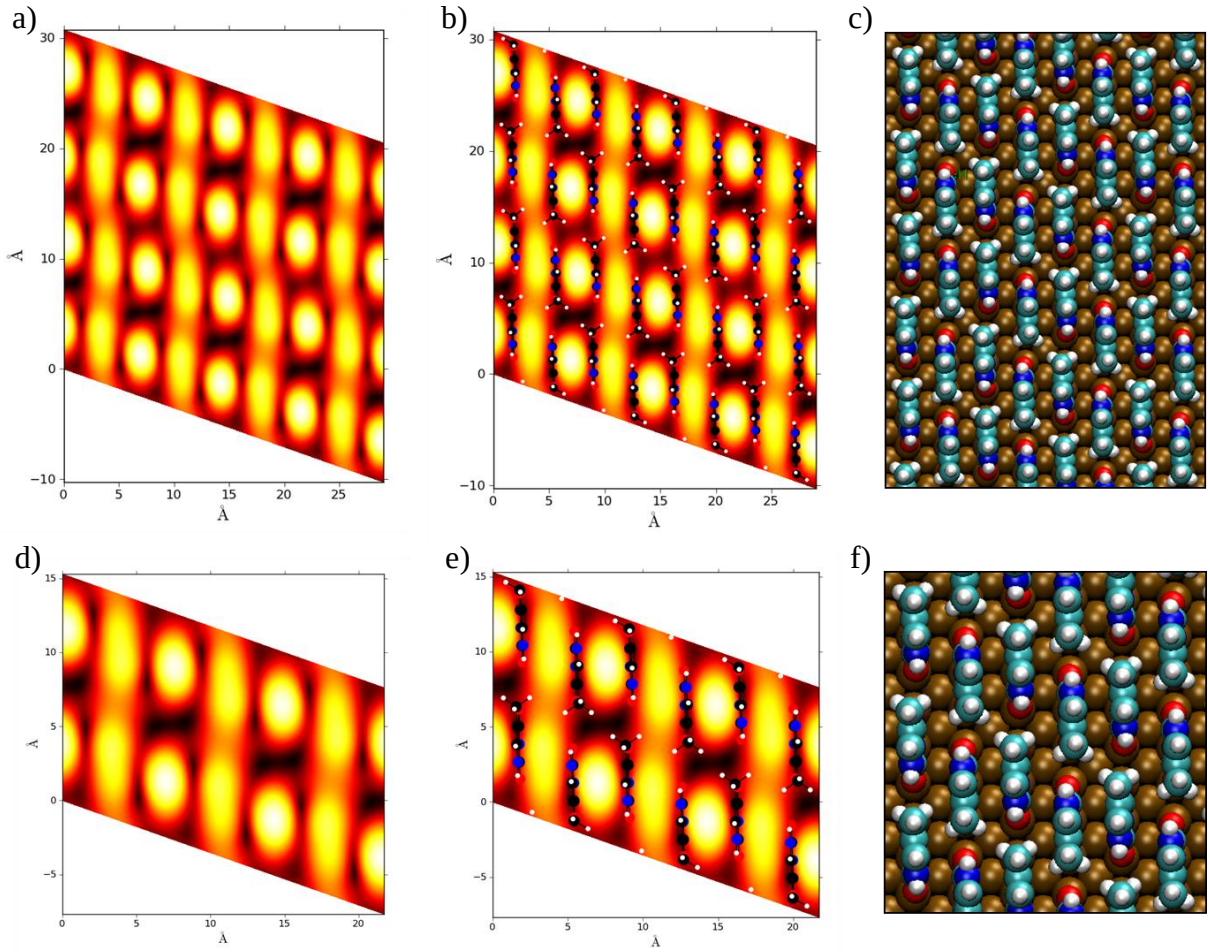

Figure 3.39: The thymine molecules are aligned in the opposite directions and with the upper row cyclic plane at ~+70^{o} to the Cu surface and the lower row cyclic plane at ~-70^{o} to the Cu surface. Here ΔE_{Tot} = -2.127eV (calculated).

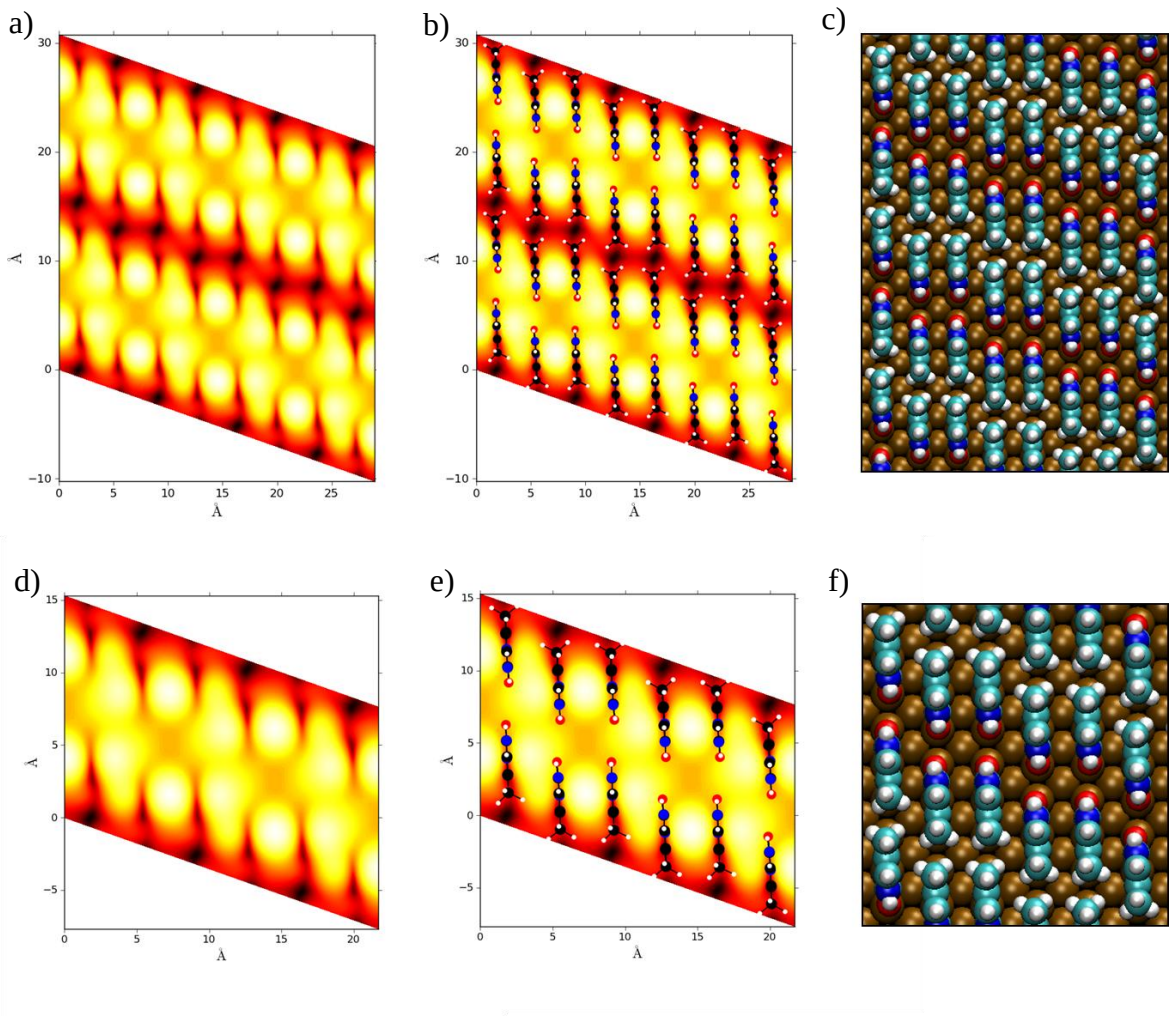

Figure 3.40: The thymine molecules are aligned in the opposite directions and with the cyclic plane at ~90^{o} to the Cu surface. Here ΔE_{Tot} = -2.010eV (calculated).

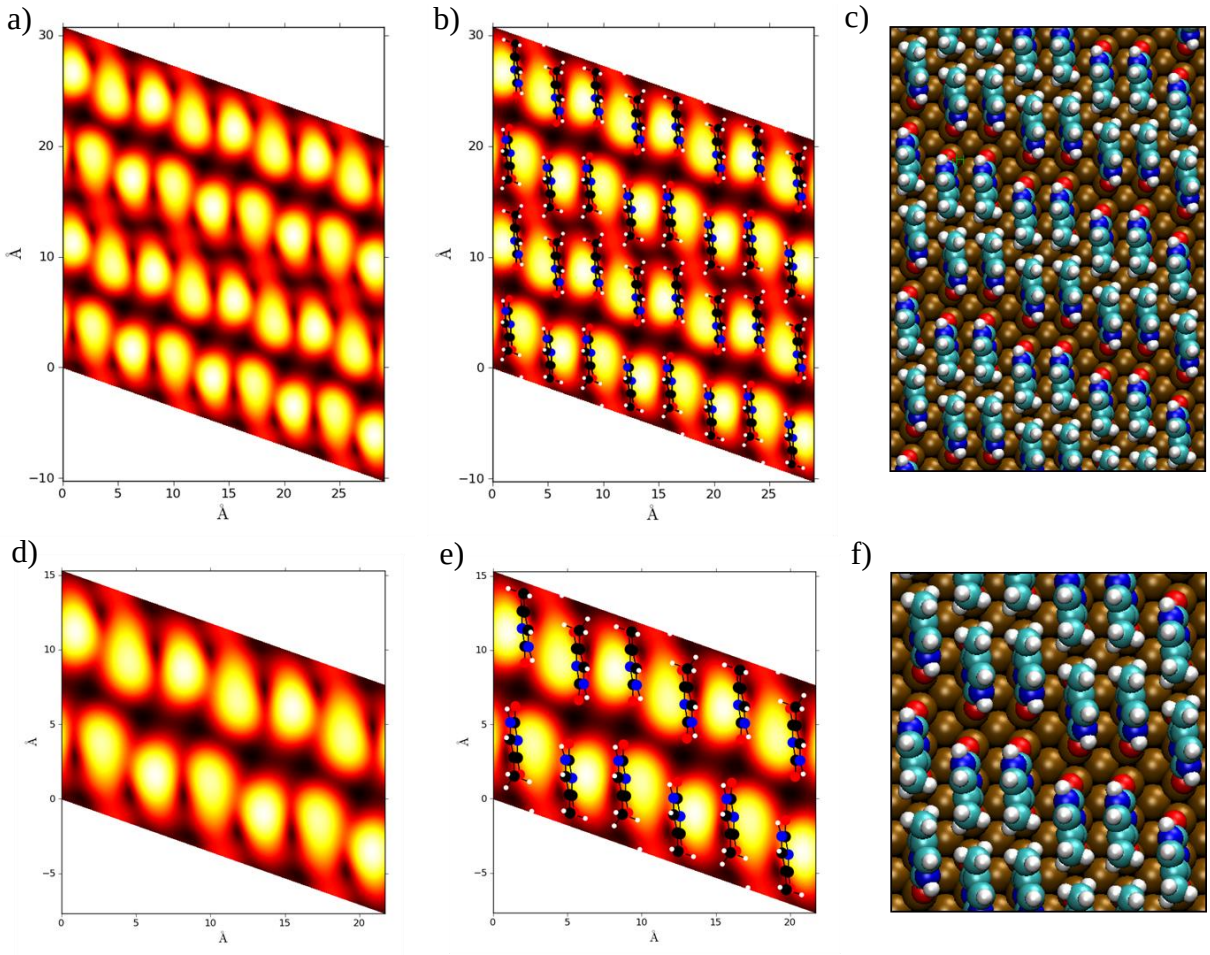

Figure 3.41: The thymine molecules are aligned in the opposite directions and with the upper row cyclic plane at ~+70^{o} to the Cu surface and the lower row cyclic plane at ~-70^{o} to the Cu surface. Here ΔE_{Tot} = -2.025eV (calculated).

Figure Number	Molecular Orientation*	Energy of Structure (eV)
3.34	Pa90	2.115
3.35	Pa70	2.109
3.36	Aa90	2.130
3.37	Aa70	2.128
3.38	Ab90	2.128
3.39	Ab70	2.127
3.40	Pb90	2.010
3.41	Pb70	2.025

Table 3.3: This is a summary of the previous eight simulations of thymine on Cu(110) in table format.

* - The molecular orientation code corresponds to P meaning the methyl group is aligned on the same side (i.e. parallel), A meaning the methyl group is on opposite sides (i.e. alternating) and the 90 means that the thymine molecule has its cyclic plane angled at ~90^{o} to the surface and 70 means that the thymine molecule has its cyclic plane angled at ~70^{o} to the surface. The lower case a and b means that the there are two different orientations that correspond to this structure (see the relevant figure for more information).

The results of these simulations are summarised in table 3.3 (see above). However, due to the fact that these structures proved to be less stable than the phase 1 a third stage of this investigation involved looking more closely at the most stable configuration (see figure 3.36). This involved placing the structure on a larger unit cell, 2(-1)x12 which enabled two pairs of rows to be isolated, as this was what was observed experimentally. These were then angled in four different potential orientations. In this set of simulations three main conclusions could be made. Firstly, they are all more stable when the pairs of rows are isolated. This explains why the phase 2 structure seems to prefer being in pairs. Secondly, when the cyclic plane of the thymine molecule is angled ~20^{o} to the vertical it does not matter whether it is angled +20^{o} or -20^{o} (see figures 3.42 and 3.43) as the ΔE_{Tot} value is identical in both cases. Thirdly, when the two rows at opposite angled (i.e. ±20^{o}) the stability of the structures reduces. This indicates that the chains are angled in the same direction.

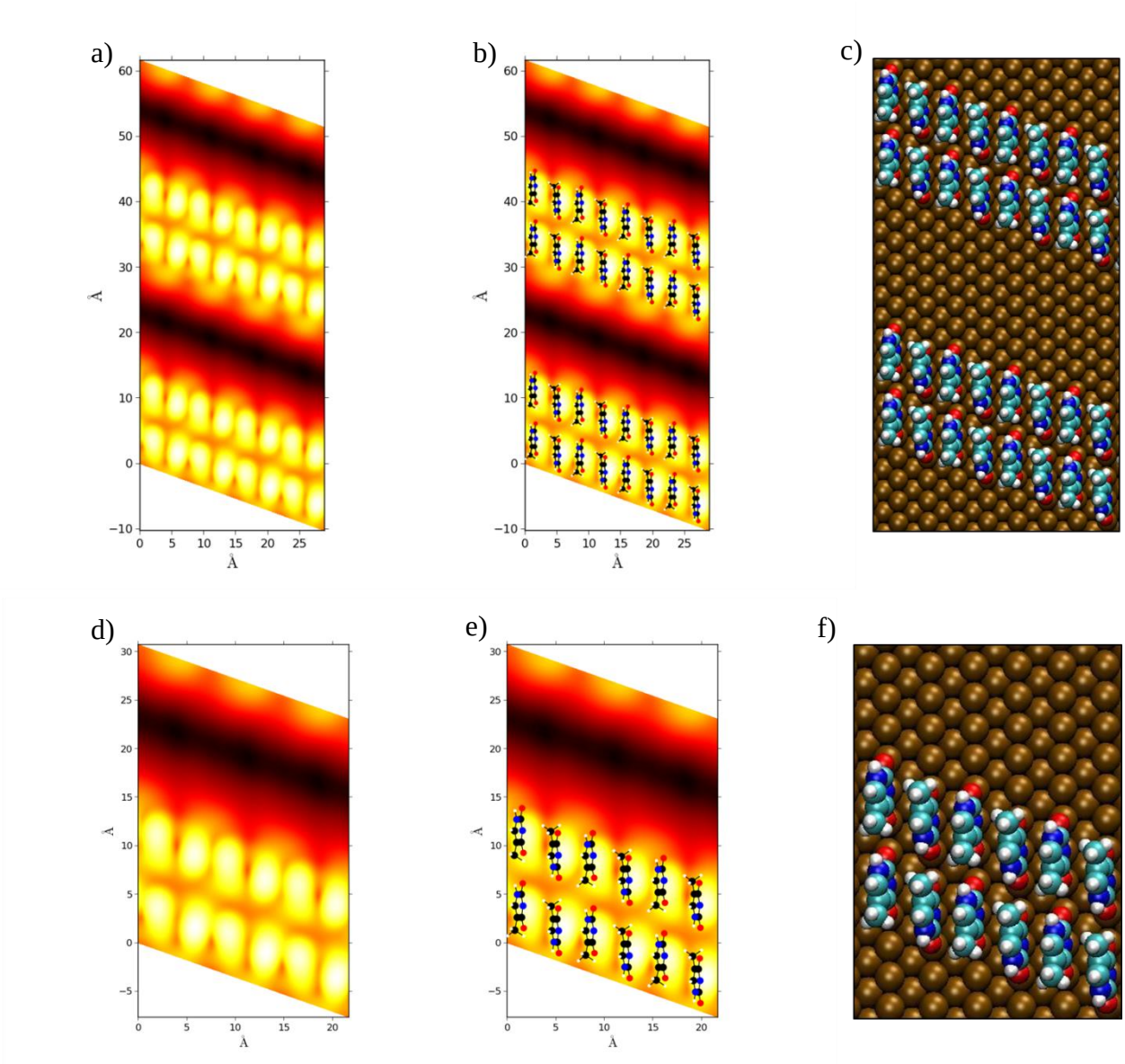

Figure 3.42: This structure involved having the cyclic plane of all the thymine molecules angled ~20^{o} to the vertical to the left. Here ΔE_{Tot} = -2.173eV (calculated).

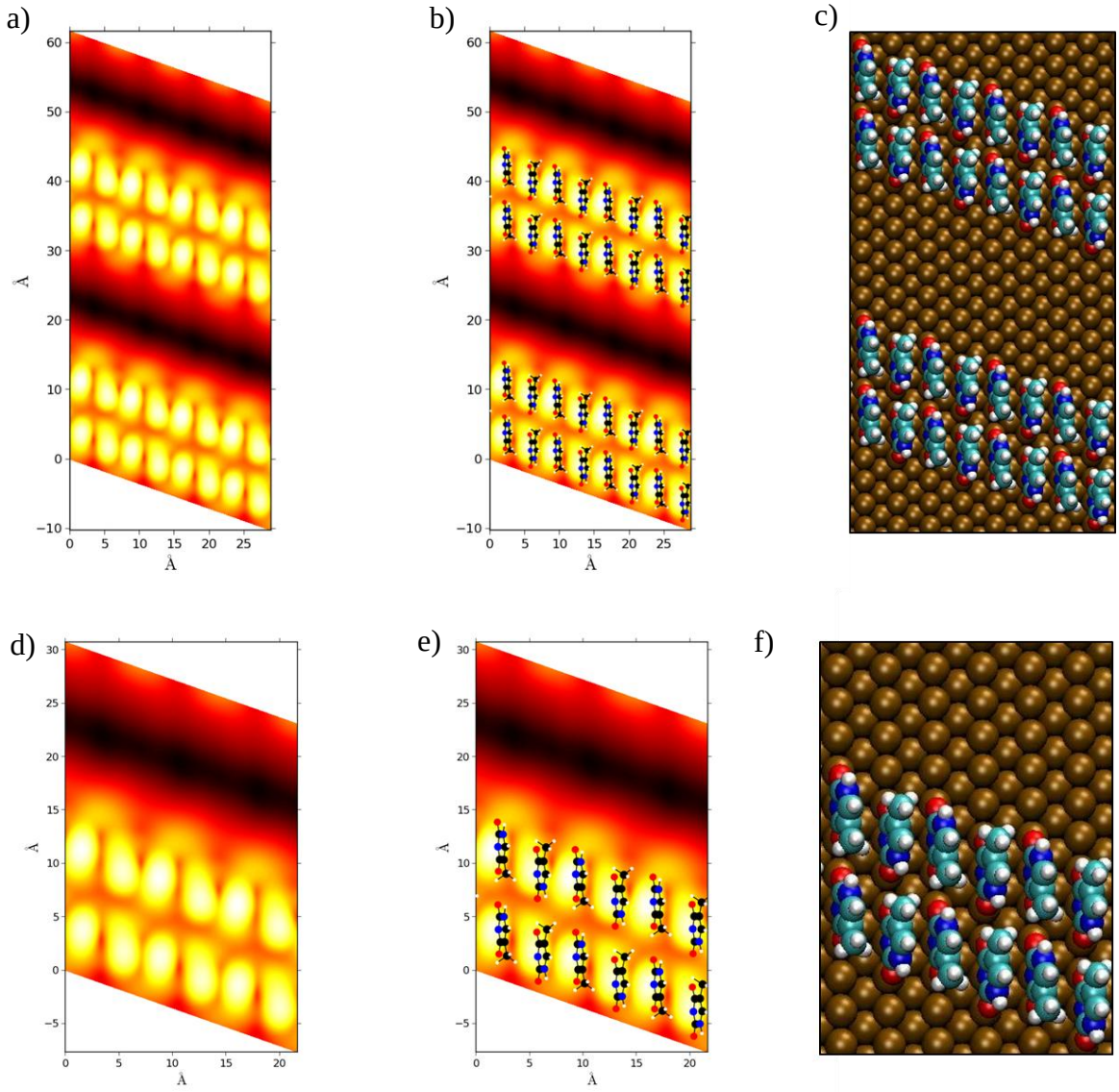

Figure 3.43: This structure involved having the cyclic plane of all the thymine molecules angled ~20^{o} to the vertical to the right. Here ΔE_{Tot} = -2.173eV (calculated).

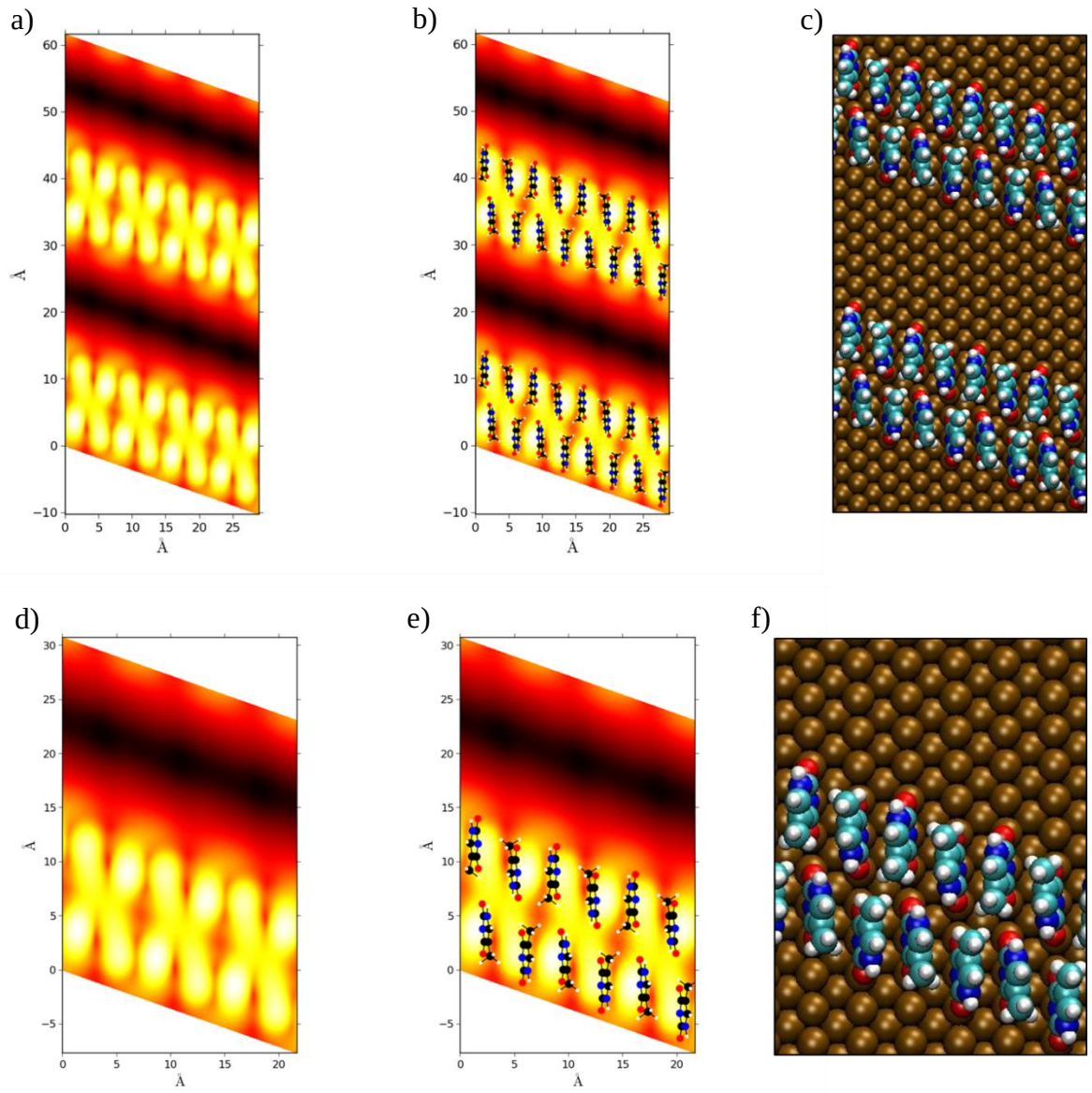

Figure 3.44: This structure involved having the cyclic plane of the top row of the thymine molecules angled ~20^{o} to the vertical to the left and the bottom row angled ~20^{o} to the vertical to the right. Here ΔE_{Tot} = -2.145eV (calculated).

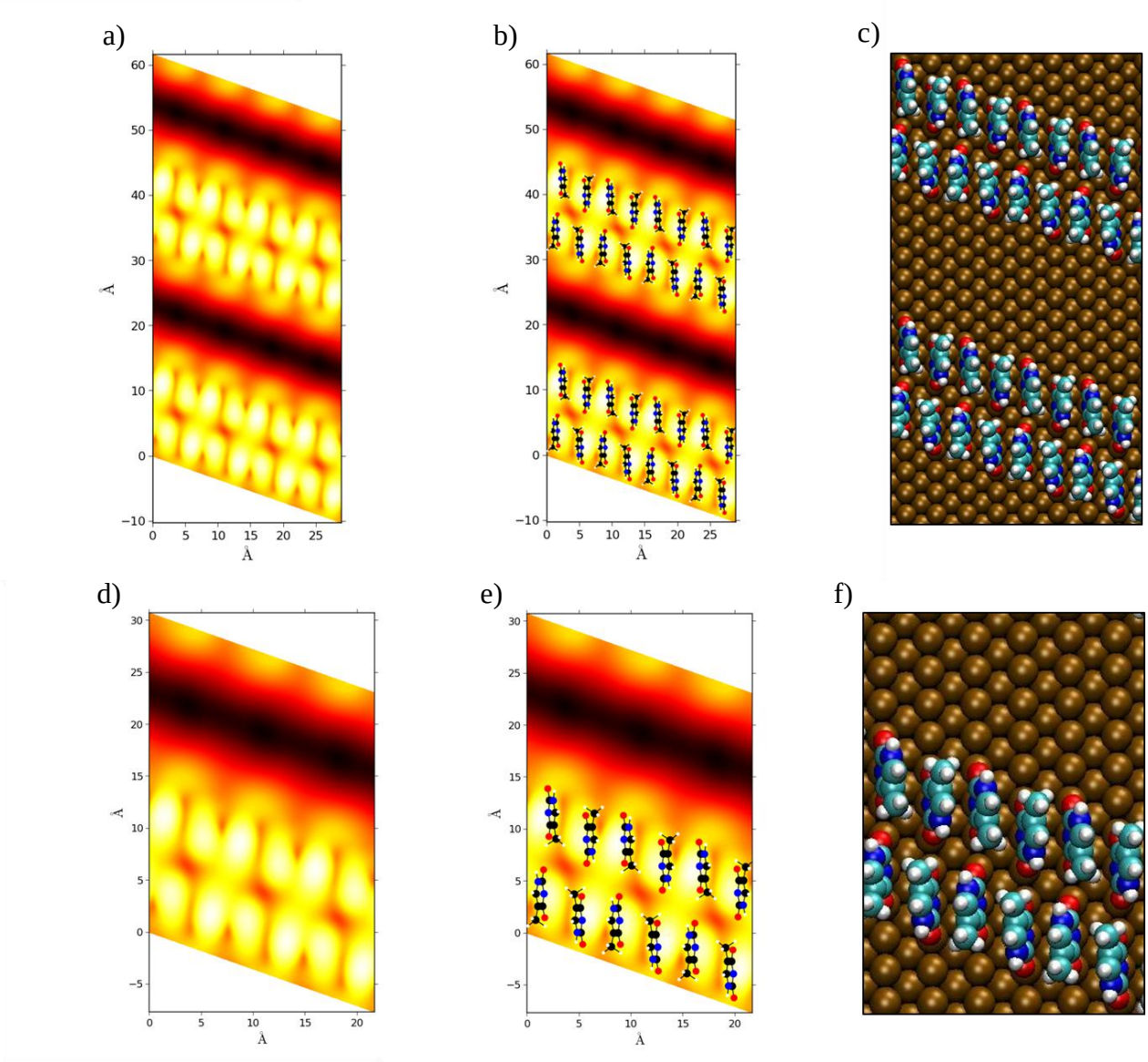

Figure 3.45: This structure involved having the cyclic plane of the top row of the thymine molecules angled ~20^{o} to the vertical to the right and the bottom row angled ~20^{o} to the vertical to the left. Here ΔE_{Tot} = -2.157eV (calculated).

The table below (see table 3.4) summarises the results of the previous 4 simulations.

Figure Number	Molecular Orientation*	Energy of Structure (eV)
3.42	A70	2.173
3.43	A70	2.173
3.44	A±70	2.145
3.45	A±70	2.157

Table 3.4: This is a summary of the previous four simulations of thymine on Cu(110) in table format.

* - The molecular orientation code corresponds to A meaning the methyl group is on opposite sides (i.e. alternating) and the 70 means that the thymine molecule has its cyclic plane angled at ~70^{o} to the surface. The ± means that one row is angled 70^{o} in one direction and the adjacent row is angled 70^{o} in the opposite direction.

3.9. Conclusions

The thymine molecule chemisorbs to the Cu(110) surface via a deprotonated nitrogen and the two oxygen atoms along the [110] direction with the plane of the cyclic ring approximately perpendicular to the surface. It also seems reasonable to assume that the self-assembly process is dominated by vdW interactions between the thymine molecules. It seems unlikely that vdW interactions are solely responsible for the kinetic barrier to the formation of the phase 2 structure due to the distance between the phase 1 rows. Therefore, it seems reasonable to assume that the surface plays a major role in this. The pairing of the rows as well as the angling in the phase 2 structure seems to demonstrate that the dispersion interactions occur not only parallel to the rows but may also have a tangential component and that the surface may have an important part to play in this too.

A phase 2 structure was found that was more stable than the most stable phase 1 structure although only on the 2(-2)x12 unit cell. This is in conflict with the LEED data which predicts the 2(-1)x6 and the 2(1)x6 unit cells. However, since that data was taken STM images have

revealed that the phase 2 structure does not form long-range structures in the [110] direction. The explanation for this may lie in the high stability of the structures observed in figures 3.42 and 3.43 which are both on a 2(-2)x12 unit cell. Indeed, they are both exactly the same structure when rotated about the z-direction. The high stability of this structure probably explains why the phase 2 tends to form isolated chains of thymine two molecules thick.

However, questions still remain. Why does the phase 1 structure not go on to form parallel chains on a 2x3 unit cell as figure 3.14 might suggest? What are the anomalous bright spots observed in-between the phase 1 rows that correspond to a 4x5 periodicity? Obviously further investigation into this system is required.

3.10. Bibliography

[1] A. McNutt, S. Haq, R. Raval. *"High Temperature Phase of the DNA Base Thymine on Cu(1 1 0): A Resonance Delocalised Bonding System."* Surface Science 2002, **502-503**, 185-192.

[2] A. McNutt. *"Structural Studies of the Adsorption of the Nucleic Acid Bases on Cu(110)."* PhD thesis, University of Liverpool, 2002.

[3] R. E. Kelly, L. N. Kantorovich. *"Homopairing Possibilities of the DNA Base Thymine and the RNA Base Uracil: An Ab-Initio Density Functional Theory Study."* J. Phys. Chem. B 2006, **110**(5), 2249-2255.

[4] P. Colarusso, K. Zhang, B. Guo, P. F. Bernath. *"The Infrared Spectra of Uracil, Thymine and Adenine in the Gas Phase."* Chem. Phys. Letters 1997, **269**(1-2), 39-48.

[5] A. Les, L. Adamowicz, M. Nowak, L. Lapinski. *"The Infrared Spectra of Matrix Isolated Uracil and Thymine: An Assignment Based on New Theoretical Calculations."* Spectrochimica Acta 1992, **48**(10) 1385-1395.

[6] M. Nowak. *"IR Matrix Isolation Studies of Nucleic Acid Constituents: The Spectrum of Monomeric Thymine."* J. Molecular Structure 1989, **193**(C), 35-49.

[7] S. L. Zhang, K. H. Michaelian, G. R. Loppnow. *"Vibrational Spectra and Experimental Assignments of Thymine and Nine of its Isotopomers."* J. Phys. Chem 1998, **102**(2), 461-470.

[8] J. Florian, V. Hrouda. *"Scaled Quantum Mechanical Force Fields and Vibrational Spectra of Solid State Nucleic Acid Constituents V: Thymine and Uracil."* Spectrochimica Acta 1993, **49**(7), 921-938.

[9] H. Susi, J. S. Ard. *"Vibrational Spectra of Nucleic Acid Constituents-I. Planar Vibrations of Uracil."* Spectrochimica Acta 1971, **27**(9), 1549-1562.

[10] H. Susi, J. S. Ard. *"Planar valence force constants and assignments for pyrimidine derivatives."* Spectrochimica Acta 1974, **30**(9), 1843-1853.

[11] M. J. Scanlan, I. H. Hillier. *"An Ab-Initio Study of Tautomerism of Uracil, Thymine, 5-Fluorouracil and Cytosine."* J. Am. Chem. Soc. 1984, **106**(13), 3737-3745.

[12] M. J. Scanlan, I. H. Hillier. *"Accurate Prediction of the Relative Energies of the Six Tautomers of Uracil."* Chem. Phys. Letters 1983, **98**(6), 545-547.

[13] L. Snyder, R. Shulman, D. Neumann. *"Electronic Structure of Thymine."* J. Chem. Phys. 1970, **53**(1), 256-267.

[14] T. Yamada, K. Shirasaka, A. Takano, M. Kawai. *"Adsorption of Cytosine, Thymine, Guanine and Adenine on Cu(110) Studied by Infrared Reflection Absorption Spectroscopy."* Surface Science 2004, **561**(2-3), 233-247.

[15] F. Allegretti, M. Polcik, D. P. Woodruff. *"Quantitative Determination of the Local Structure of Thymine on Cu(110) Using Scanned-Energy Mode Photoelectron Diffraction."* Surf. Sci. 2007**, 601**(17), 3611-3622.

[16] V. Caciuc, N. Atodiresei, P. Lazic, Y. Morikawa, S. Blugel. *"First-Principles and Semi-Empirical van der Waals Study of Thymine on Cu(110) Surface."* arXiv:0811.3088v1 2008.

[17] M. Furukawa, H. Fujisawa, S. Katano, H. Ogasawara, Y. Kim. *"Geometrical Characterization of Pyrimidine Base Molecules Adsorbed on Cu(110) Surfaces: XPS and NEXAFS Studies."* Surface Science 2003**, 532-535**, 261-266.

[18] M. L. M. Rocco, R. Dudde, K. H. Frank, E. E. Koch. *"Angle-Resolved Photoemission from Uracil and Thymine Adsorbed on Cu(110)."* Chemical Physics Letters 1989, **160**(4), 366-370.

[19] M. J. Frisch, G. W. Trucks, H. B. Schlegel et al. Gaussian 03, Pittsburg PA, 2003.

[20] M. P. Andersson, P. Uvdal. *"New Scale Factors for Harmonic Vibrational Frequencies Using the B3LYP Density Functional Method With the Triple-Z Basis Set 6-311+G(D,P)."* The Journal of Physical Chemistry A 2005**, 109**(12), 2937-2941.

[21] P. Gazdzicki, P. Uvdal, P. Jakob. *"Adsorption of Intact Methanol on Ru(0001)."* J. Chem. Phys. 2009**, 130**(22), 224703.

[22] W. H. Li, W. Haiss, S. Floate, R. J. Nichols. *"In-Situ Infrared Spectroscopic and Scanning Tunnelling Microscopy Investigations of the Chemisorption Phases of Uracil, Thymine and 3-Methyl Uracil on Au(111) Electrodes."* Langmuir 1999**, 15**(14), 4875-4883.

[23] B. Lippert, D. Neugebauer. *"Simultaneous Binding of Two Different Transition Metals to the DNA Model Base 1-Methylthymine: The X-Ray Structure of Bis[Bis(M-1-Methylthyminato-N3,O4) Cis-Diammine Platinum(II)] Silver Nitrate Pentahydrate."* Inorganica Chimica Acta 1980**, 46**(C), 171-179.

[24] K. L. Wierzchowski, E. Litonska, D. Shugar. *"Infrared And Ultraviolet Studies on the Tautomeric Equilibria in Aqueous Medium Between Monoanionic Species of Uracil, Thymine, 5-Fluorouracil and Other 2,4-Diketopyrimidines."* Journal of the American Chemical Society 1965**, 87**(20), 4621-4629.

[25] S. L. Zhang, K. H. Michaelian, G. R. Loppnow. *"Vibrational Spectra and Experimental Assignments of Thymine and Nine of its Isotopomers."* The Journal of Physical Chemistry A 1998, **102**(2), 461-470.

[26] B. Lippert. "*On the Tautomerism of the Thymine Anion in the Solid State: A Raman and Infrared Study."* Journal of Raman Spectroscopy 1980, **9**(5), 324-333.

[27] A. R. Sarkar, P. Ghosh *"Interaction Of Divalent Metal Ions With Uracil. I. Oxygen Coordinating Uracil Complexes Of Mn(II), Fe(II), Co(II), Ni(II) And Cu(II)."* Inorganica Chimica Acta 1983**, 78**(C), L39-L41.

[28] M. Gupta, M. N. Srivastava. *"Synthesis and Characterization of Mixed Ligand Complexes of Copper(II), Nickel(II), Cobalt(II) And Zinc(II) With Glycine and Uracil or 2-Thiouracil."* Polyhedron 1985**, 4**(3), 475-479.

[29] A. R. Dias, M. T. Duarte, A. M. Galvão. *"Uracil and Thiouracil Complexes of Dicyclopentadienyl Molybdenum and Tungsten: Preparation and Electrochemistry. The Structures of [M(H5-C5H5)2(2-SN2OC4H3)][PF6], [M(H5-C5H5)2{2-S(CH3)N2OC4H2}][PF6],..."* Polyhedron 1995**, 14**(5), 675-685.

[30] P. Ghosh, T. K. Mukhopadhyay, A. R. Sarkar. *"Interaction of Divalent Metal Ions with Uracil III. Complexes of Mn II, Fe II, Co II, Ni II And Cu II with Uracil Acting as Bidentate Ligand."* Transition Metal Chemistry 1984**, 9**(2), 46-48.

[31] A. Frisch, A. B. Nielson, A. J. Holder. *"GAUSSVIEW User Manual"* Gaussian Inc. Pittsburgh, PA, 2000.

[32] S. J. Grimme, J. Antony. *"Density Functional Theory Including Dispersion Corrections for Intermolecular Interactions in a Large Benchmark Set of Biologically Relevant Molecules."* Phys. Chem. Chem. Phys. 2006, 8(45), 5287-5293.

[33] S. J., Grimme. *"Accurate Description of van der Waals Complexes by Density Functional Theory Including Empirical Corrections."* Comp. Chem. 2004, 25(12), 1463-1473.

4. Chapter Four – Adsorption Of Melamine on Cu(110)

4.1. Introduction

Another self-assembled molecular system that has been studied recently, both experimentally and theoretically, which also has several kinds of interacting functional groups, are organic bases. Supramolecular structures grown on metallic surfaces have been studied intensely over the last decade, and, by means of STM considerable insight has been gained into mechanisms guiding the self-assembly of molecular nanostructures on surfaces [1-3]. Various investigations into how melamine arranges on conducting surfaces [4-11], semi-conducting surfaces [12] and non-conducting surfaces [13] have recently been done. However, only one study had looked at how melamine arranges and bonds to a Cu surface [5] prior to this investigation.

Investigations carried out at Liverpool University by Dr. Matt Dyer had shown that, for single molecules of melamine bonding to Cu(110), an upright position was favoured. However, RAIRS simulations of dimers of melamine in the gas phase indicate that there could be at least some hydrogen bonding of monolayers of melamine on Cu(110), which would suggest that the melamine was not completely upright, but was instead, angled in some way. On top of this, there was also the possibility of some van der Waals (vdW) interactions between the melamine. This could further modify the position of the melamine on the surface. Thus, a more detailed DFT investigation was undertaken. Using Scanning Tunnelling Microscopy (STM) it has been shown by the Liverpool group that melamine molecules self-assemble into a two dimensional (2D) structure at room temperature (see figure 4.1). By using this data, a basic model is now proposed for this structure.

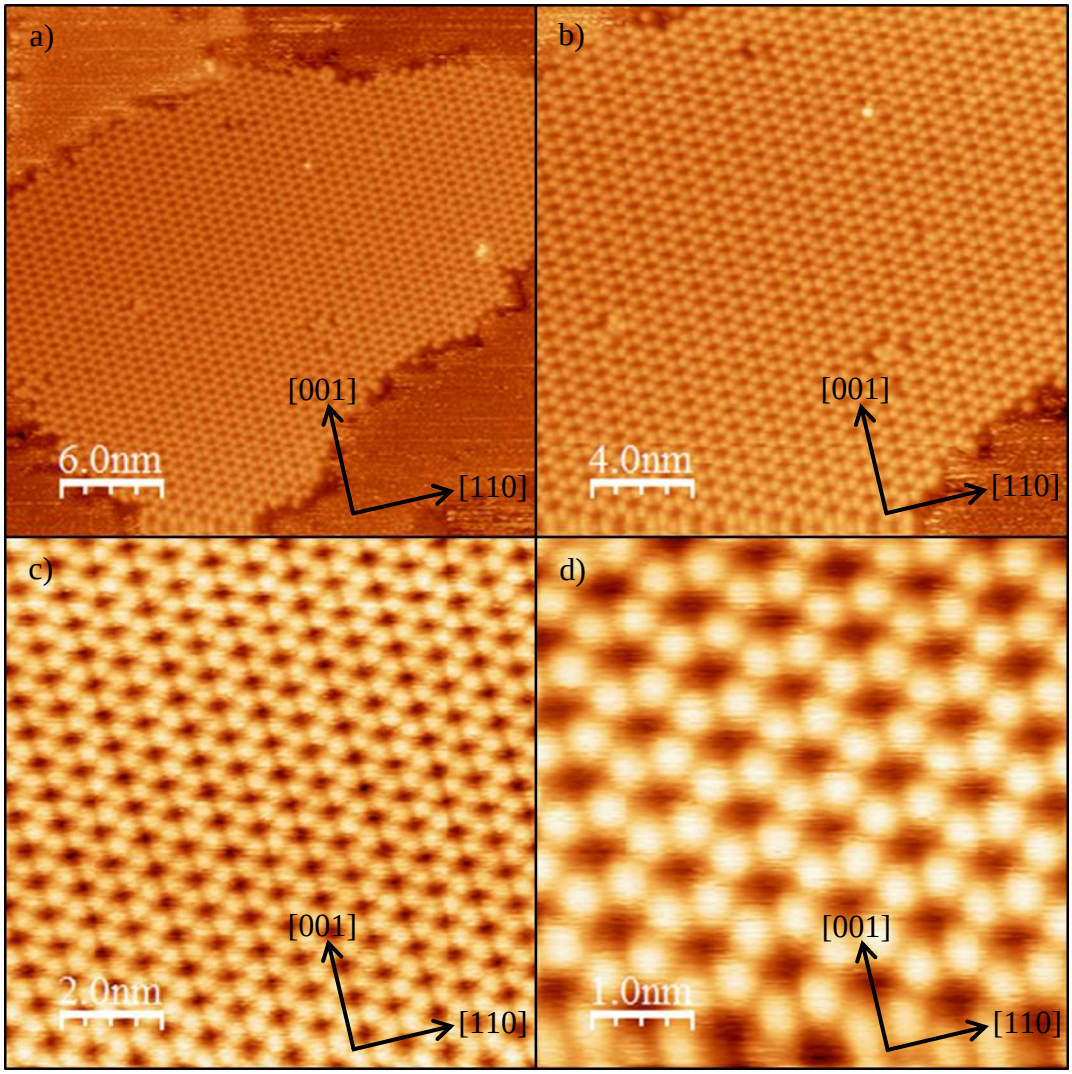

Figure 4.1: Some STM images of melamine adsorbed on the Cu(110) surface. Each of the images a) – d) shows a section of one such 2D structure in increasingly higher resolution. The bias voltage is -0.3V on all four images.

4.2. Melamine

Melamine (2,4,6-triamino-s-triazine) with chemical formula $C_3H_6N_6$, is an organic base and a trimer of cyanamide and is part of a family of triazine compounds. The others being cyanuric acid, ammelide and ammeline but is the only molecule to contain only carbon, nitrogen and hydrogen and no oxygen. It has a 1,3,5-triazine skeleton and, like cyanamide, it contains 66% nitrogen by mass. It is a complex biological molecule, containing an aromatic ring and three

side chain amino groups. The molecular properties of this molecule are interesting, in particular the possible conjugation or the interaction between the π electrons in the triazine ring as well as the lone pair electrons of the amino nitrogens. The extension of the conjugation to the side chain nitrogen atoms and the resultant effect on the hybridisation characteristics of the amino nitrogens, i.e. either the sp^2 or sp^3, has interesting geometric implications.

If mixed with resins it has fire retardant properties due to its release of nitrogen gas when burned or charred and has several other industrial uses. It is a heterocyclic triazine used primarily in the synthesis of melamine-formaldehyde resins (MFR) for the manufacture of laminates, plastics, coatings, commercial filters, glues or adhesives and moulding compounds [14]. It can also be used as a colorant and a fertilizer. Melamine is a metabolite of cryomazine (a pesticide) and is found in mammals that have ingested cryomazine. It contains a cyclic ring structure containing alternating carbon and nitrogen atoms forming a delocalised hybridised electron planar ring. Thus, the centre of the molecule contains a series of carbon-nitrogen bonds. An amine group is additionally bonded to each of the carbons in the cyclic ring and melamine is thus a completely planar molecule. Melamine and related triazine derivates are able to form self-assembling, high molecular weight complexes via organized intramolecular networks of hydrogen bonds as well as π-π aromatic ring stacking [15,16].

The unique capabilities exhibited by melamine provide useful molecular scaffolding components (exploited by the field of supramolecular chemistry) to produce a variety of sophisticated nano-scaled molecular complexes. Known triazine-based self-assembling supramolecular complexes include rosettes [17,18], crinkled tapes [19], nanoropes and nanoribbons [20], propeller-like banana complexes [21], molecular guest boxes [22], channel structures [23], hydrogels [24] and supramolecular membranes [25,26]. The hydrogen bond forming properties of melamine allow it to interact with nucleobases, such as uracil [23].

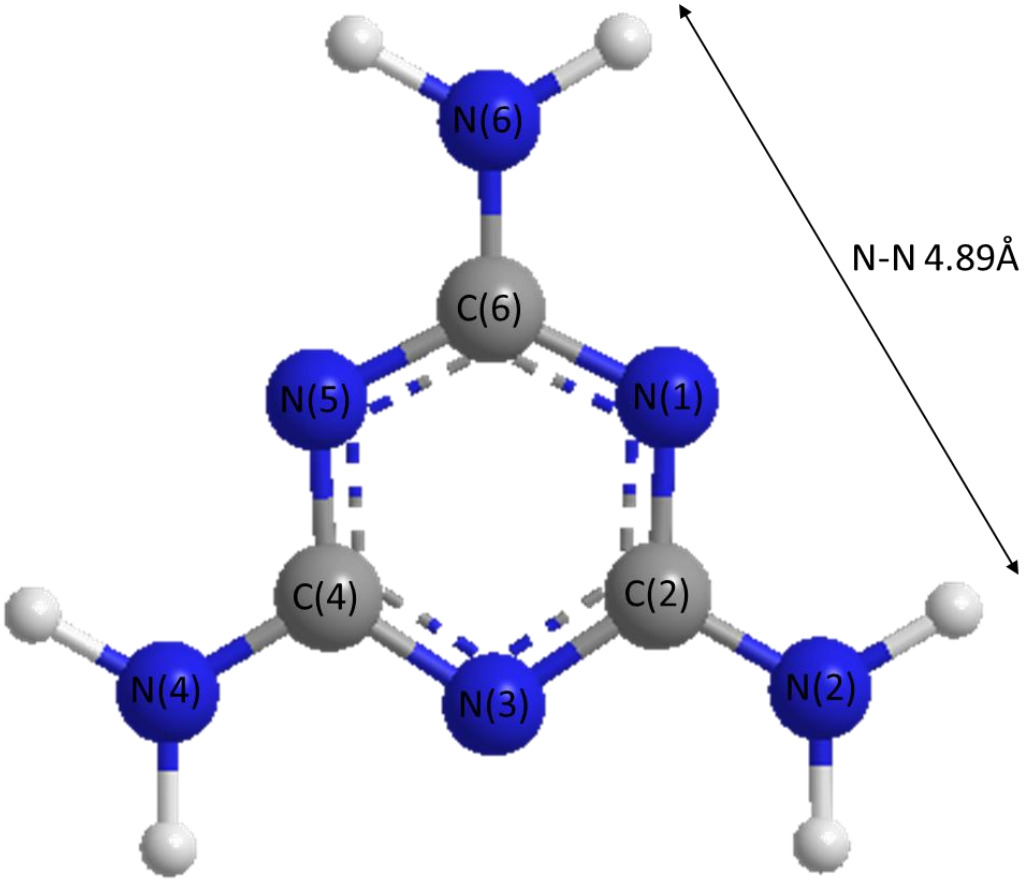

Figure 4.2: The molecular structure of melamine.

Although the chemical structures of melamine and related triazines are subject to tautomeric equilibrium [27] spectroscopic studies [29] confirmed that the enamine form of melamine and the keto form of cyanuric acid are the resonance structures favoured in acidic to neutral solutions, consistent with the enthalpy difference required for hydrogen transfer from an amide to imide configuration ($\Delta H = 0$) compared with those for the more favourable enol to keto conversion ($\Delta H = -42$KJ/mol). Via the sp^2 hybridized nitrogen atoms of its triazine ring, each melamine monomer provides three unshared pairs of electrons available as hydrogen bond acceptors. In addition, unsubstituted melamine includes three exocyclic primary amines, each with the potential to provide a pair of hydrogen bond donors. A useful and simplified paradigm to appreciate the hydrogen-bonding pattern of melamine is that of an equilateral triangle, with each 4.89 Å side (see figure 4.2) providing an offset triplet of hydrogen bond donor–acceptor–donor groups (D-A-D) available to form complementary intermolecular

bonds with appropriately spaced functional group triplets comprising a hydrogen bond acceptor–donor–acceptor (A-D-A) motif [30].

Melamine (as well as its derivatives) has various industrial applications [31-38]. It is categorized as a spumific compound which means that when it decomposes it releases non-flammable gases in large quantities and produces a thick insulating coating [31]. It is for this reason that it has developed into a flame and heat retardant [32] as well as a thermosetting cross-linked polymer (soluble in water and resistant to crease and wrinkle) which can be applied to textile fabrics in aqueous form [33, 34]. Thus, its industrial relevance has fuelled scientific interest and research into this molecule. However, most recently, attention has focused on its ability to form supramolecular networks due to its ability to readily form hydrogen bonds both with itself and a variety of other organic molecules (or ligands) on metal surfaces [39-42].

4.3. The Molecular Properties of Melamine

Melamine possesses a number of symmetry elements which are considered in its vibrational assignment. Bond lengths exhibit a large degree of π electron delocalisation [43] and molecular orbital calculations confirm that N atoms are sp^2 hybridised and that the NH_2 groups are in approximately the same plane as the cyclic ring structure [44-46]. According to Jiang et al [47] the molecule exhibits D_{3h} symmetry and considered the molecule to be somewhat 'floppy'. However, this is effectively an averaged model of two optimised conformers with pyramidal amino groups and it is also possible that the molecule exhibit C_s as well as C_{3v} symmetry. It is also possible, of course, that the Cu surface may distort melamine away from a planar arrangement causing a further loss of symmetry. Regardless of this an assignment of possible modes of vibration according to various D_{3h} symmetry classes has been made (see table 4.1).

Melamine on Cu(110)		Vibrational Mode	Symmetry Class	Solid-State Melamine
Low Coverage ν (cm^{-1})	Saturation Coverage ν (cm^{-1})			
		νNH_2 ass	E’	3464
3443	3403	νNH_2 sym	E’	3416
			E’	3320
			A_1’	1660
	1647	δNH_2	E’	1643
1616	1617	δNH_2	E’	1626
		V_1CN	E’	1583
	1559	V_1CN	E’	1565
	1549	V_3CN	E’	1549
1532	1534	V_3CN	E’	1531
	1496			
	1488			
		V_4CN	A_1’	1469
1440	1436	V_2CN	E’	1434
	1421			
	1368			
		rNH_2	E’	1190
		r NH_2	E’	1175
	1066			
		α_2CN	A_1’	1022
	991			
	817	α_1CN	E’	813
762		γCN	A_2’’	760
		φCN	A_2’’	730

Table 4.1: A list of possible vibrational modes for melamine on Cu(110) [47–50].

Melamine has a total of 39 normal modes of vibration, 18 associated with the NH_2 groups and 21 with skeletal vibrations. Each NH_2 group has 6 vibrational modes, 2 stretching, 2 bending (in and out of plane) and 2 twisting/wagging (out of plane). The 3 NH_2 groups therefore result in both in and out of phase modes. These are illustrated in figure 4.3.

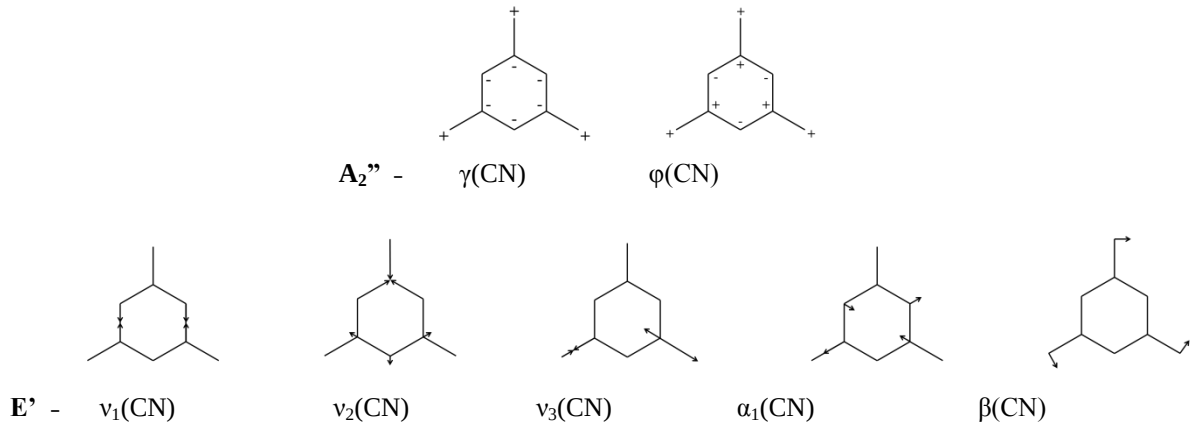

Figure 4.3: Schematic representation of various different vibrational modes of the D_{3h} symmetry class [47–50].

The non-planar A_2" vibrations consist of a side chain bending mode, γ, and a ring bending mode, φ. The planar E' vibrations consist of two ring (ν_1 and ν_2), a side chain (ν_3), a ring bending (α) and a side chain (β) mode. However, distortions in the molecule could (potentially) result in more vibrational modes being visible. There is also the possibility of tautomerisation. The tautomeric interconversion occurs through the migration of a proton from one or more of the side chain nitrogens to one or more of the ring nitrogens. This is accompanied by a corresponding shift of electron density between the carbonyl and ring bonds. Thus, the cyclic ring nitrogens can be bonded to 1, 2 or 3 hydrogens. Any of these states is a potential structure and thus, must be considered in a complete analysis of the system.

4.4. Experimental Details

For all systems Cu(110) crystals were cleaned by at least 3 cycles of Ar^+ ion bombardment, flashing and annealing to ~900K. LEED images were used to confirm a sharp (1x1) pattern that is characteristic of clean Cu(110). Various multi-analytical UHV chambers with base pressures $<5 \times 10^{-10}$ mbar were used for this study. RAIRS and TPD studies were carried out using a sample mounting in which a Cu single crystal was fixed to Cu supports connected to a Dewar container through Ta wires. STM studies were performed with a different configuration and Ta wires were used to fix the sample to a Ta plate. Melamine (>99% Sigma-Aldrich) was sublimed onto a clean Cu(110) surface, held at room temperature in the case of STM and RAIRS, and held at the specified temperatures for LT-RAIRS and TPD.

Reflection Absorption Infrared Spectroscopy (RAIRS) experiments were recorded using a Mattson 6020 FTIR spectrometer, equipped with a liquid nitrogen cooled HgCdTe detector. The spectrometer was operated with a resolution of $4cm^{-1}$, with the addition of 256 scans. Spectra were recorded throughout a continuous dosing regimen as sample single beam infrared spectra, and ratioed against a reference background single beam representing the clean Cu(110) surface. TPD data were acquired using a Sensorlab Mass Quadrupole analyser. STM data were collected at room temperature with an Aarhus 150 SPECS STM. All experiments were carried out for coverages up to 1 monolayer (ML).

4.5. Current Experimental Investigations of Melamine on Cu(110)

Before the determination of the exact geometry could be ascertained as much experimental information as possible was gathered. RAIRS experimental data gave some information as to how the melamine may bond to the Cu(110) surface. This came in the form of how the various amplitudes of the different “stretches” varied and at what frequency they occurred (see figures 4.4 and 4.5). The strong presence of a hydrogen bonded scissor stretch at $1646cm^{-1}$ on the simulated RAIRS (figure 4.4) corresponded well with the large peak seen at $1647cm^{-1}$ on the experimental data (figure 4.5). However, the large stretch seen at $3157cm^{-1}$

on the simulated RAIRS (figure 4.4) was not observed at all on the experimental data (figure 4.5). However, as the molecule was unlikely to be orientated like this on the surface the existence of at least some hydrogen bonding could not be ruled out entirely.

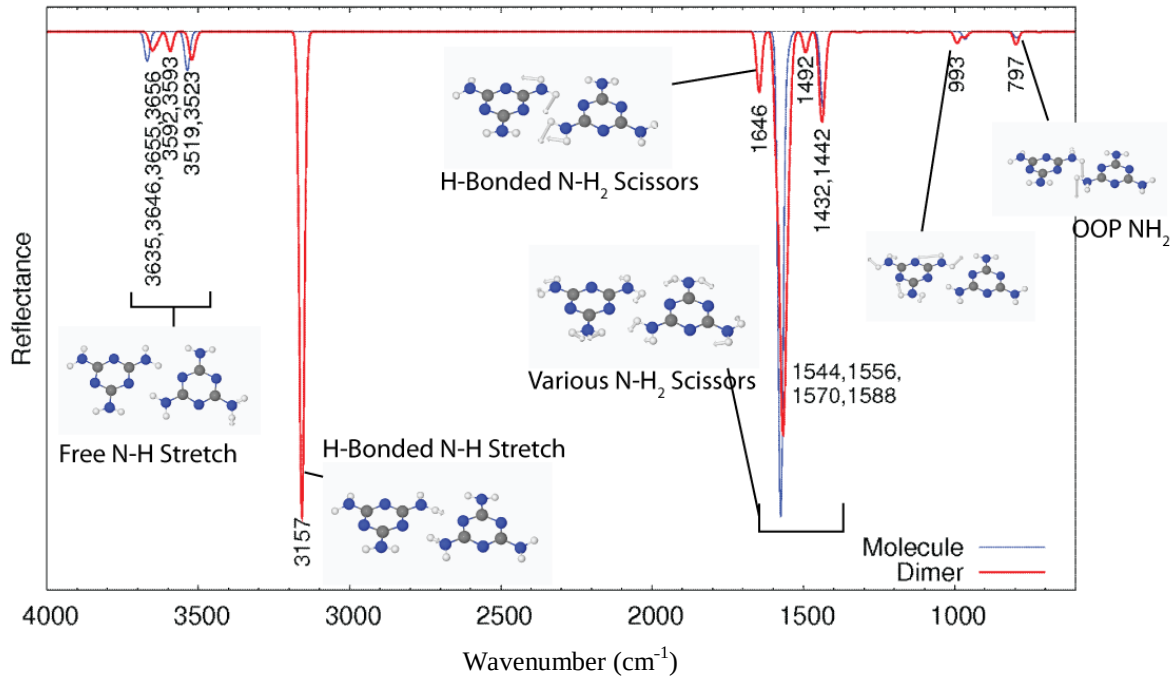

Figure 4.4: RAIRS spectrum generated for a melamine dimer compared to an isolated molecule. The blue line represents the peaks generated for an isolated melamine molecule. The red line represents the peaks generated for a melamine dimer aligned in the same plane and placed adjacent to it. For the dimers each range of peaks is allocated to a different stretch mode.

A detailed analysis of the RAIRS data shows a number of absorption bands between 1650cm^{-1} and 800cm^{-1} and a weaker one at 3400cm^{-1}. These bands all correspond to in-plane vibrational modes and thus rules out the possibility that the melamine adsorbs onto the Cu(110) in a flat lying orientation. However, the presence of a weak out-of-plane mode at 762cm^{-1} suggests that the melamine is slightly tilted. The additional (weak) bands that have not been assigned suggest there is some deviation from the D_{3h} symmetry due to the NH_2 groups being deformed in some way due (most likely) to interactions with the surface. However, intramolecular interactions could also be responsible.

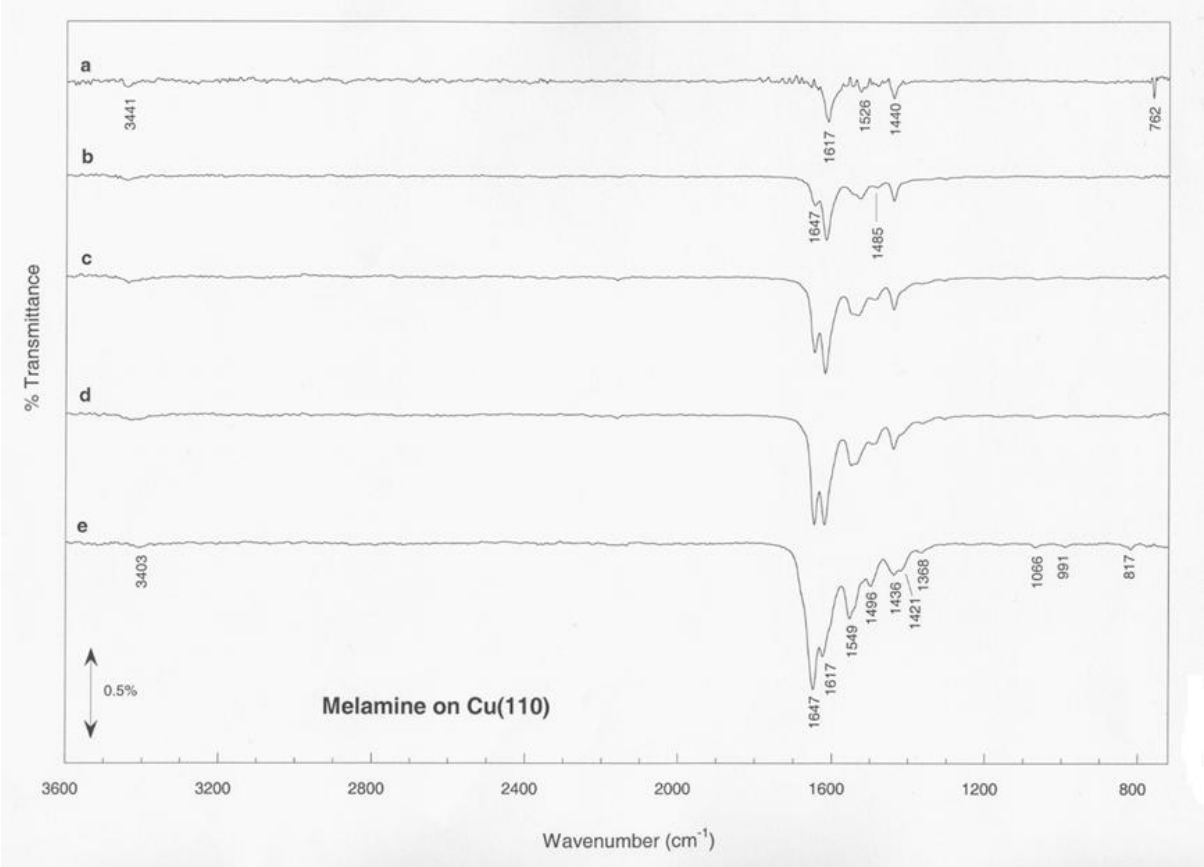

Figure 4.5: RAIRS spectrum generated for a melamine on Cu(110) at increasing coverage [47–50]:–

a) Very low coverage (~20%). Two very small peaks at 1526 cm^{-1} and 3441cm^{-1} with two slightly larger ones at 762 cm^{-1}, 1440 cm^{-1} and 1440 cm^{-1} with quite a large one at 1617 cm^{-1}.
b) Low coverage (~40%). The peaks at 762 cm^{-1} and 3441cm^{-1} have disappeared and two new peaks at 1647cm^{-1} and 1485cm^{-1}.
c) Medium coverage (~60%). The existing peaks have continued to increase in size with additional peaks at 1549cm^{-1}, 1496cm-1 and 1436cm^{-1} starting to emerge.
d) High coverage (~80%). The existing peaks have continued to increase in size.
e) Very high coverage (~100%). The existing peaks have continued to increase in size with additional peaks at 1421cm^{-1}, 1368cm^{-1} emerging. Also, three small peaks at 1066cm^{-1}, 991cm^{-1} and 817cm^{-1} have appeared.

LEED experiments also gave some information about potential symmetries of long-range structures. The LEED pattern is a (6x2) (see figure 4.6). Various missing spots observed in both the [110] and [001] directions ruled out certain symmetries. Glide lines are observed in

the [110] direction and reflectional symmetry lines in the [001] direction are consistent with pmg symmetry (see figure 4.6).

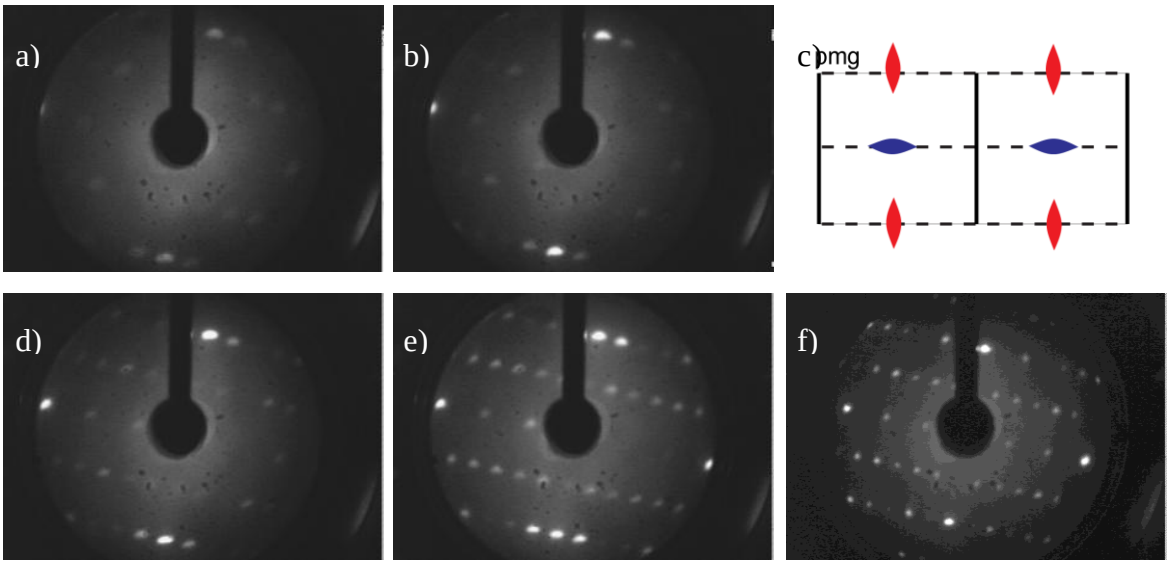

Figure 4.6: LEED images of melamine on Cu(110) of increasing energy showing the (6x2) unit cell with various missing spots. This is consistent with pmg symmetry [47–50] which is shown in image c). Image a) is taken at 37eV, image b) at 40eV, image d) at 42eV, image e) at 44eV, image f) at 58eV.

TPD experiments also revealed a deprotonation event between 500K and 700K (see figure 4.7). The other experimental data available on this system were STM (see figure 4.8). This consisted of a series of hexagonal bright spots arranged on a repeating (6x2) unit cell in accordance with the LEED data. In the [110] direction the bright spots would appear "pair-wise" and in the [001] direction the bright spots would appear to "zig-zag". Thus, after calibration, a (6x2) unit cell was proposed for the room temperature arrangement of melamine on the Cu(110) surface with dimensions of 15.4Å in the [110] direction and 7.24Å in the [001] direction (see figure 4.8).

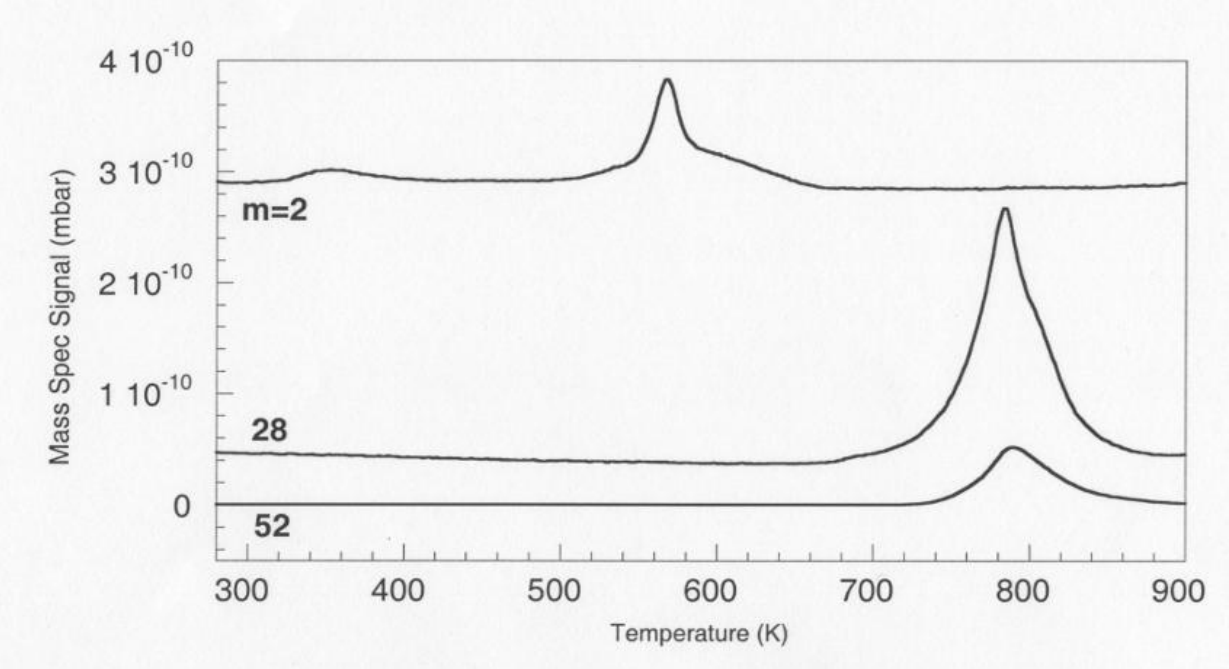

Figure 4.7: Temperature programmed desorption (TPD) shows a deprotonation event at between 500K and 700K [50].

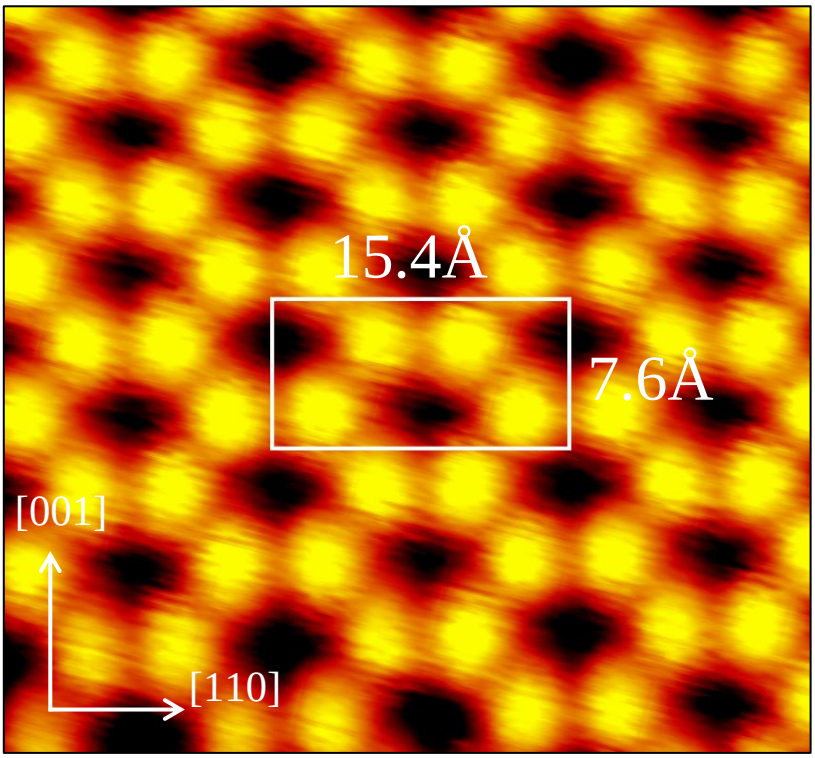

Figure 4.8: An STM image of a monolayer of melamine on Cu(110). This is consistent with a (6x2) unit cell.

4.6. Theoretical Data and Analysis

4.6.1. Overview

Before attempting to determine the exact structure of how melamine self-arranges on the Cu(110) surface a series of simulations were first run to try and determine the most stable structure for an isolated molecule adsorbed on the surface. A series of previous simulations conducted by Dr. Matt Dyer had determined that the N-group of the cyclic ring bonded directly over a Cu atom on the uppermost layer of the Cu(110) surface. However, it was not clear whether the cyclic plane of the melamine aligned along the [110] direction or the [001] direction or somewhere in-between. So, three simulations were conducted for the undeprotonated melamine where the molecule was aligned exactly with the [110] direction, exactly with the [001] direction and exactly half-way in-between these two directions. K-points were determined in accordance with the same criteria used with thymine and the same lattice spacing used (i.e. 3.64 Å). The only difference was that an extra layer to the surface was used in these latter simulations. The top 3 layers were allowed to move (representing the surface) and the lower 2 were fixed (representing the bulk). A unit cell with 6 Cu atoms in the [001] direction and 4 in the [110] direction was used. This was sufficient to isolate each melamine molecule from the one on each adjacent side by >8Å and thus any long-range dispersion interactions should be negligible.

In all cases the melamine N-group bonded just over 2Å directly above an uppermost Cu atom. The least stable of these three simulations occurred when the plane of the melamine was bonded along the [001] direction of the crystal (see figure 4.11c and 4.11f). In this geometry, the molecule pulled the uppermost Cu ~0.3Å towards the molecule and some distortion in the shape of the melamine was also observed. The molecule was also angled slightly ~10^{o} to the vertical. The simulations of the melamine aligned along the [110] direction (see figure 4.11a and 4.11d) and at 45^{o} to it (see figure 4.11b and 4.11e) were both very similar in energy, only ~25meV separated the two. Although no hydrogen desorption was observed until ~550K it was still uncertain whether:-

a) The melamine deprotonated below room temperature.
b) The melamine tautomerised.
c) What angle the molecule was orientated.

A series of similar simulations were run with a melamine molecule singly deprotonated and doubly deprotonated (see figures 4.12-4.14). Although the energies did not favour a double deprotonation they did not rule out a single deprotonation of the melamine molecule. Although, although deprotonation was observed at ~550K it seemed reasonable to assume that the molecule only deprotonated at higher temperatures and that the room temperature self-assembly was of an intact melamine molecule.

4.6.2. Gas Phase Melamine And Hydrogen

The gas phase melamine molecule was modelled in a 15x15x15Å unit cell which allowed for a minimum separation of <9 Å. As the x-, y- and z-directions are non-repeating the k-points were all set to 1. As accurate as possible values were necessary for this particular simulation as it was to be used for reference in all our melamine simulations. For consistency the gas phase hydrogen was modelled in exactly the same way as the gas phase melamine in a 15x15x15Å unit cell.

4.6.3. Isolated Melamine Bonded to Cu Surface

In order to test whether the melamine bonded with the cyclic plane parallel to or perpendicular to the surface 2 simulations were carried out. These were then STM simulated (figures 4.9 and 4.10) in order to determine both the stability and the correspondence to the experimental STM images taken. It can be seen that when the melamine has its cyclic ring perpendicular to the Cu surface, an almost completely round image is produced. However, when it has its cyclic ring parallel to the Cu surface the image is more triangular in shape.

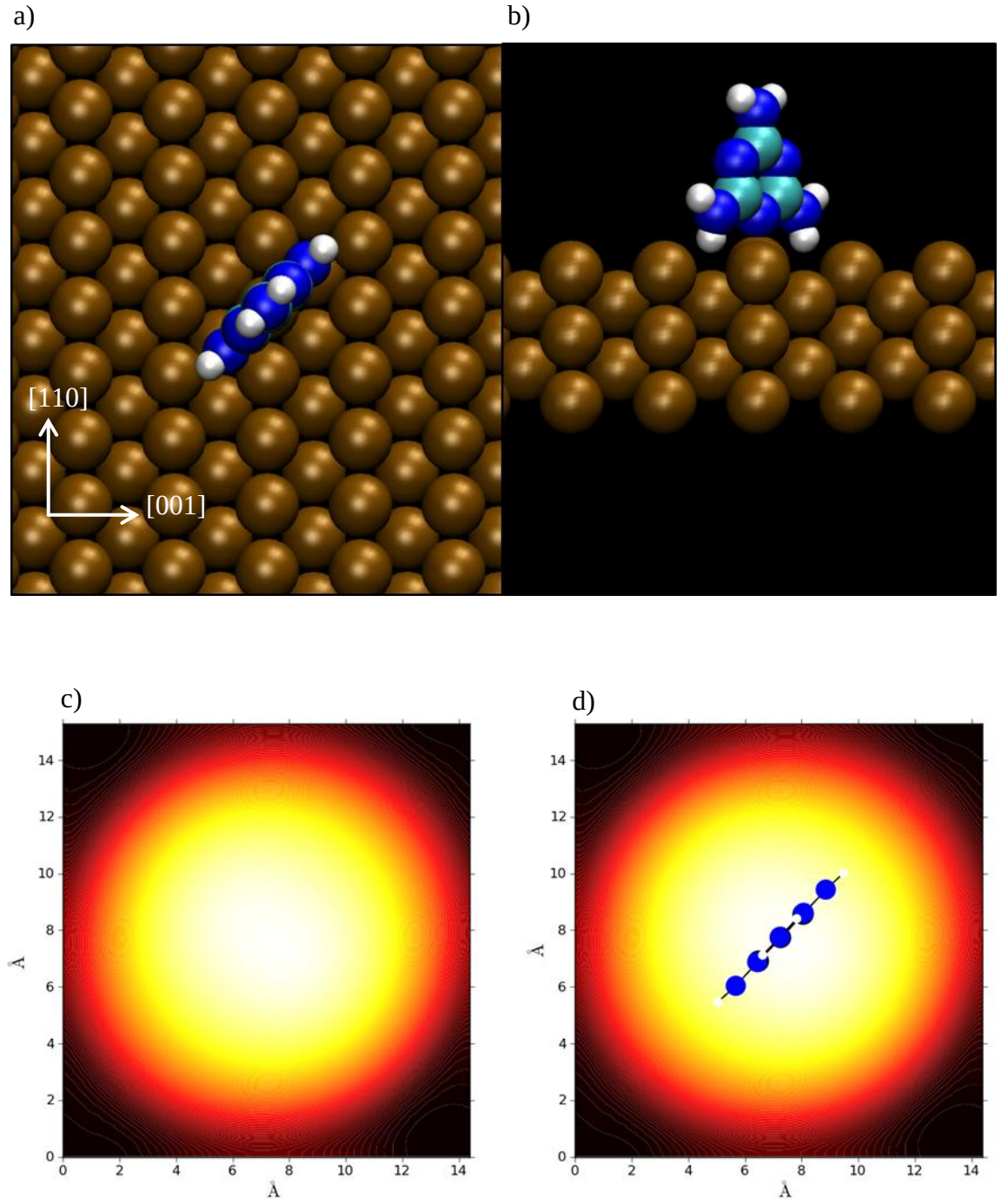

Figure 4.9: Undeprotonated melamine bonded to Cu(110) surface with cyclic ring perpendicular to the surface. Here V_t= -0.3 V and ΔE_{Tot} = -1.759eV (calculated).

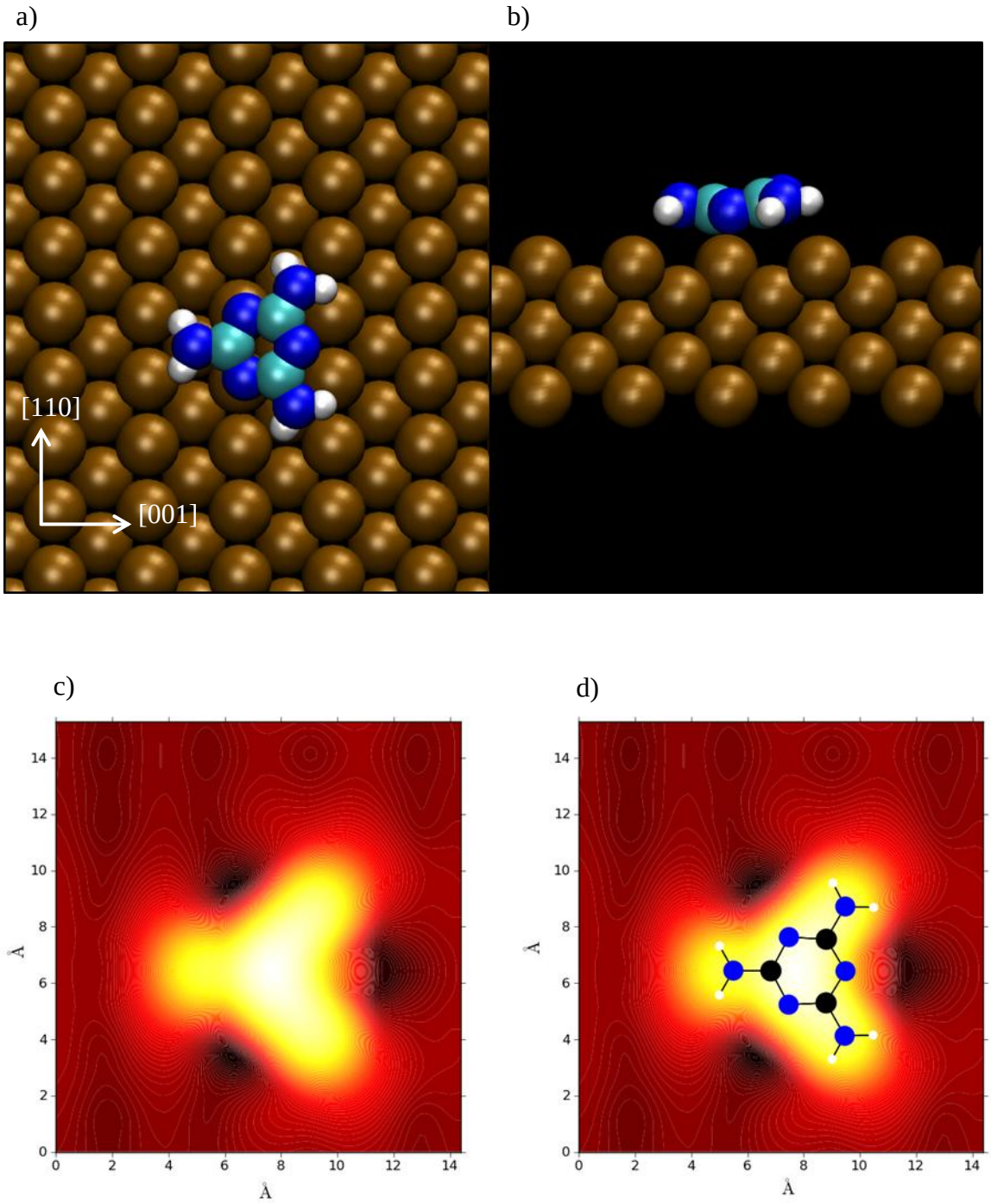

Figure 4.10: Undeprotonated melamine bonded to Cu(110) surface with cyclic ring perpendicular to the surface. Here V_t= -0.3 V and ΔE_{Tot} = -1.846eV (calculated).

4.6.4. The Undeprotonated Simulations

Although the flat lying simulation was slightly more stable than the upright one the simulated STM image suggested a more upright orientation. Various arrangements of (undeprotonated) melamine molecules were simulated on the Cu(110) surface (see figure 4.11). These tended to orient with the N(1)/N(3)/N(5) atom ~2Å above the uppermost Cu atom.

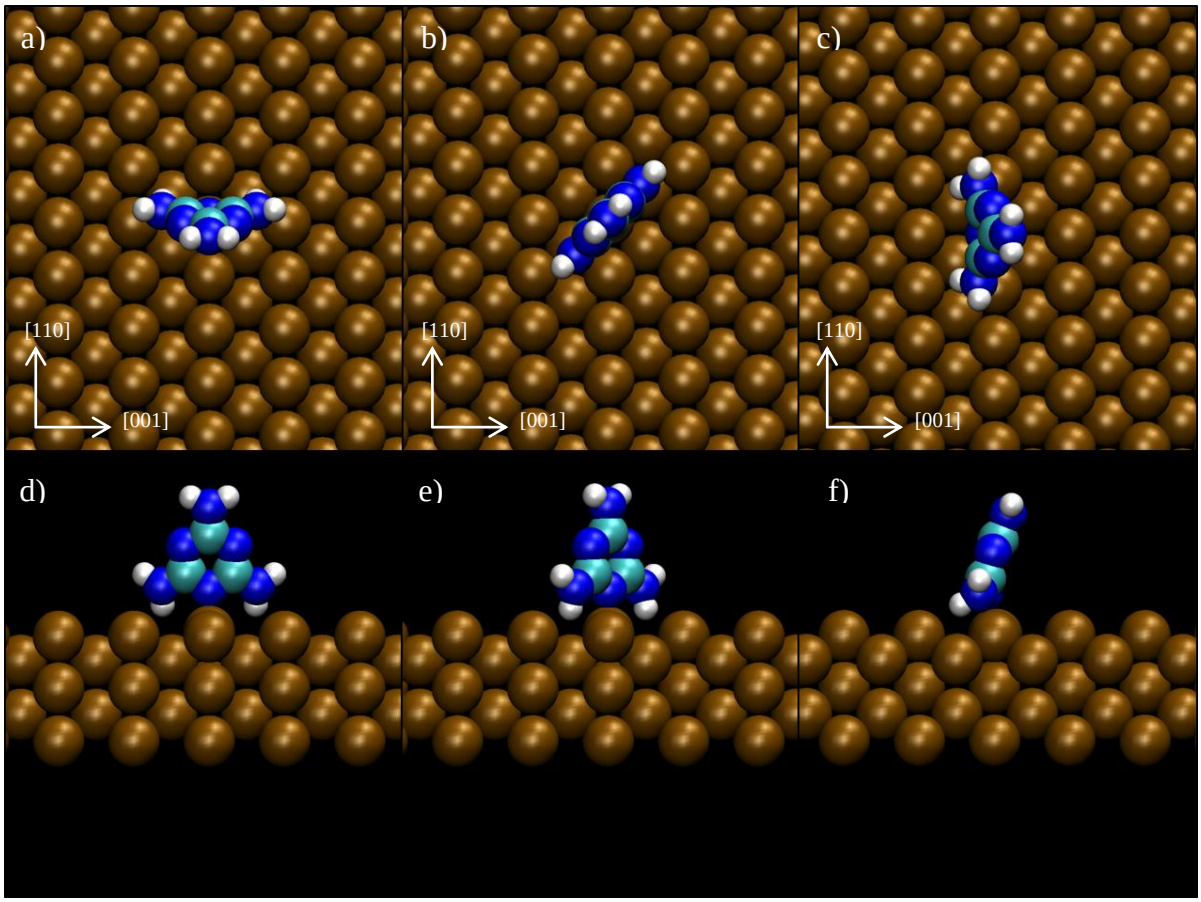

Figure 4.11: Undeprotonated melamine bonded to Cu(110) surface with cyclic ring perpendicular to the Cu surface. In a) and d) ΔE_{Tot} = -1.784eV (calculated). In b) and e) ΔE_{Tot} = -1.759eV(calculated). In c) and f) ΔE_{Tot} = -1.583eV (calculated).

4.6.5. Single Deprotonated Simulations

Various arrangements of deprotonated melamine molecules were also simulated on the Cu(110) surface (see figure 4.12). Again, these tended to orient with the N(1)/N(3)/N(5) atom ~2Å above the uppermost Cu atom. However, this time the symmetrical appearance was lost and the molecules tended to angle in various different ways.

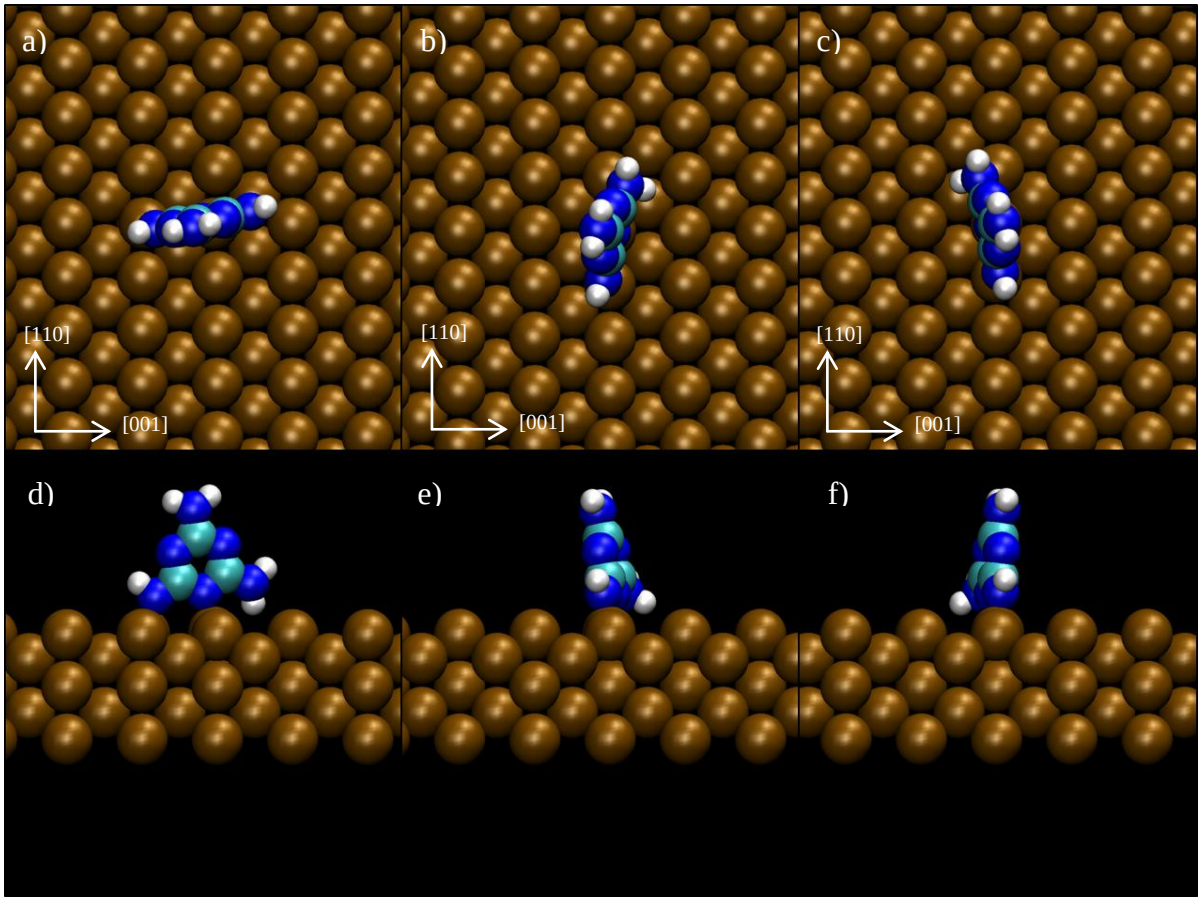

Figure 4.12: Singly deprotonated melamine bonded to Cu(110) surface with cyclic ring perpendicular to the Cu surface. In a) and d) ΔE_{Tot} = -1.706eV (calculated). In b) and e) ΔE_{Tot} = -1.994eV (calculated). In c) and f) ΔE_{Tot} = -1.984eV (calculated).

4.6.6. Double Deprotonated Simulations – Part 1

Various arrangements of doubly deprotonated melamine molecules were also simulated on the Cu(110) surface (see figure 4.13). In this series of simulations different NH_2 groups would be deprotonated. Again, these tended to orient with the N(1)/N(3)/N(5) atom ~2Å above the uppermost Cu atom. However, this time also the N(2)/N(4)/N(6) atom also would align with an uppermost Cu atom even when the simulation was started at 45^o to the [110] direction (see figure 4.13c and 4.13f).

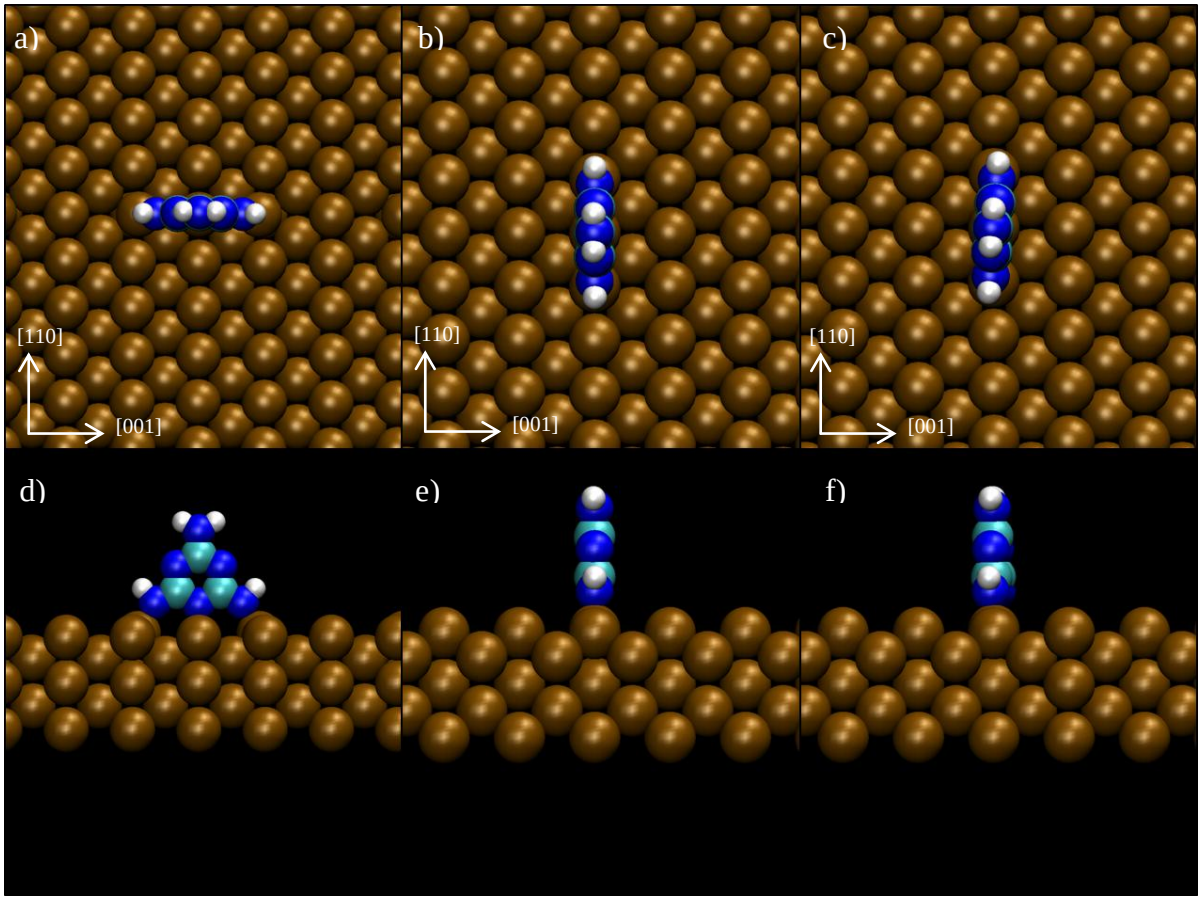

Figure 4.13: Double deprotonated melamine bonded to Cu(110) surface with cyclic ring perpendicular to the Cu surface. In a) and d) ΔE_{Tot} = -1.171eV (calculated). In b) and e) ΔE_{Tot} = -1.631eV (calculated). In c) and f) ΔE_{Tot} = -1.634eV (calculated).

4.6.7. Double Deprotonated Simulations – Part 2

Various arrangements of doubly deprotonated melamine molecules were simulated on the Cu(110) surface (see figure 4.14). In this series of simulations the same NH_2 group would be deprotonated. The melamine would angle in various lop-sided orientations but would remain with the cyclic group approximately perpendicular to the Cu surface. Again, these tended to orient with the N(1)/N(3)/N(5) atom ~2Å above the uppermost Cu atom. However, this series of simulations were highly unstable.

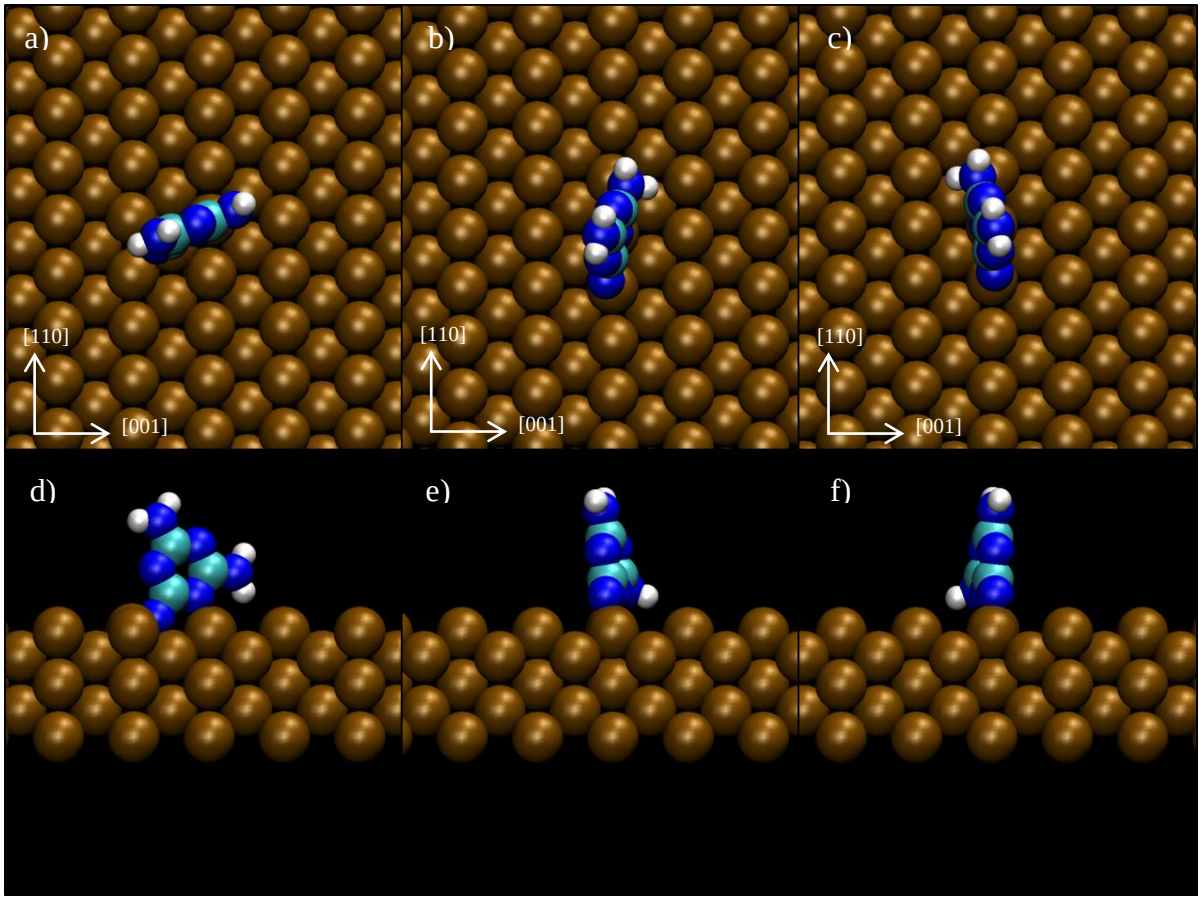

Figure 4.14: Double deprotonated melamine bonded to Cu(110) surface with cyclic ring perpendicular to the Cu surface. In a) and d) ΔE_{Tot} = -1.352eV (calculated). In b) and e) ΔE_{Tot} = -0.142eV (calculated). In c) and f) ΔE_{Tot} = -0.136eV (calculated).

4.6.8. Tautomer Simulations – Part 1

Two separate tautomers were simulated. The first was essentially undeprotonated and simply involved moving a hydrogen off two NH_2 groups onto an adjacent nitrogen (see figure 4.15). These were simulated with the cyclic group aligned along both the [001] directions and the [110]. Both orientations relaxed with the plane of the cyclic group aligned at ~60^o to the Cu surface. However, neither simulations were very stable.

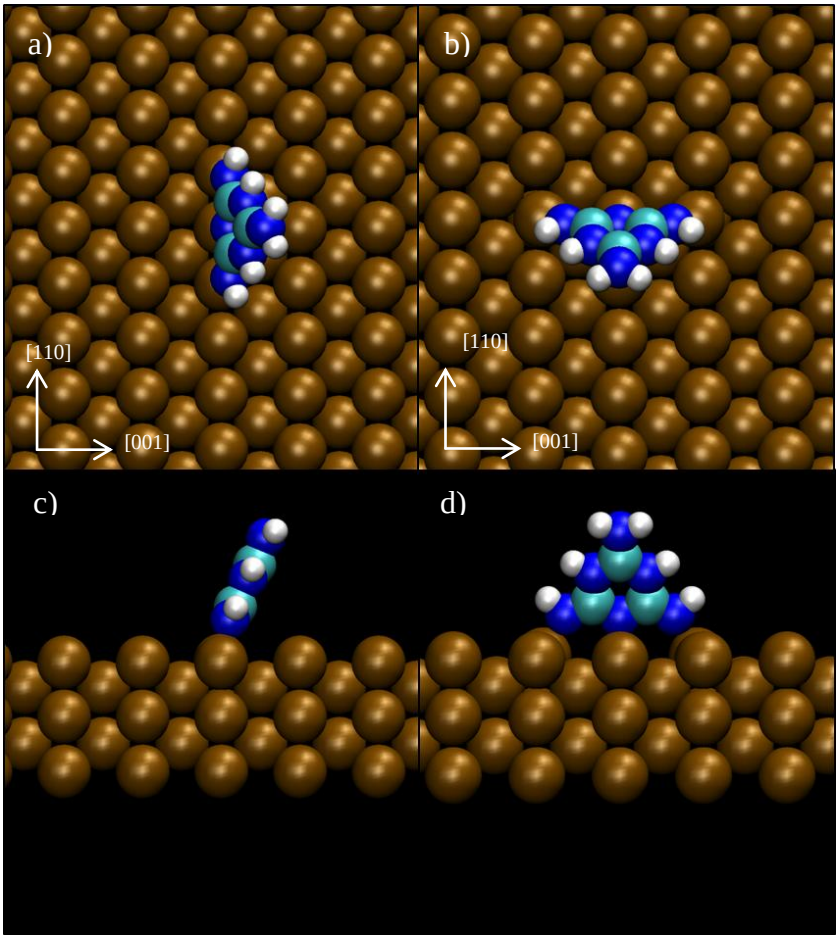

Figure 4.15: A tautomer of melamine bonded to Cu(110) surface with cyclic ring angled at ~60^{o} to the Cu surface. In a) and c) ΔE_{Tot} = -0.527eV (calculated). In b) and c) ΔE_{Tot} = 0.206eV (calculated).

4.6.9. Tautomer Simulations – Part 2

The second tautomer was single deprotonated and involved moving a hydrogen off one NH_2 group onto an adjacent nitrogen (see figure 4.16). These were simulated with the cyclic group aligned along both the [001] and the [110] directions. Both orientations relaxed with the plane of the cyclic group aligned at ~60^{o} to the Cu surface. This time the simulations were relatively stable and the one where the plane of the cyclic group is aligned with the [110] direction was highly stable.

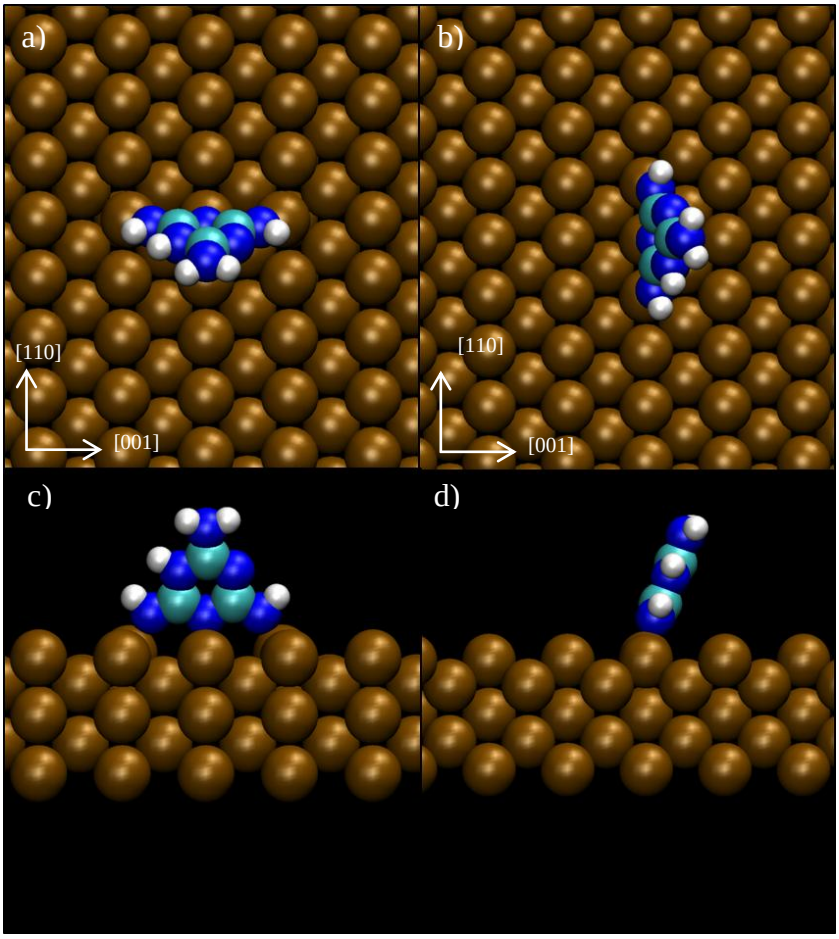

Figure 4.16: A tautomer of melamine bonded to Cu(110) surface with cyclic ring angled at ~60^{o} to the Cu surface. In a) and c) ΔE_{Tot} = -1.224eV (calculated). In b) and c) ΔE_{Tot} = -1.915eV (calculated).

4.7. Additional Simulations

Various simulations of melamine bonded to the surface in a horizontal orientation were also run. One proved to be highly stable (see figure 4.10). Some simulations of pairs of melamine molecules in the gas phase were investigated. This was to examine the possibility of dispersion interactions between the melamine cyclic rings. Three separate simulations were run which clearly showed that isolated pairs of melamine molecules were more stable when aligned parallel and stacked (ΔE_{Tot} = -0.066eV), more stable still when shifted in the x-direction (ΔE_{Tot} = -0.150eV) and more stable still when shifted in both the x-direction and the y-direction (ΔE_{Tot} = -0.162eV).

4.8. Conclusions – Part 1

From these series of simulations the following may be concluded:-

a) The high stability of some of the deprotonated melamine simulations did seem to confirm that deprotonation could occur at some point. However, as only one deprotonation event was observed at ~560K it seemed a reasonable assumption that these only occurred after annealing.
b) The slight increase in stability of some of the melamine simulations when angled at ~30^{o} to the vertical did suggest some angling of the molecule may occur.
c) The close similarity of energies between the undeprotonated melamine aligned along the [001] direction and that rotated 45^{o} to it suggests that the adlayer could contain more than one orientation.
d) The increase in stability of the adjacent dimer melamine molecules when simulated in the gas phase suggested that dispersion interactions could play a part in the arrangement of these molecules on the Cu surface.
e) The undeprotonated melamine also seemed to be relatively stable in the horizontal position.
f) The lowest energy structures for the undeprotonated melamine are shown in figure 4.11a and 4.11d.

The results of the previous simulations of isolated melamine molecules adsorbed on Cu(110) in various different orientations and tautomers are summarised in table 4.2.

Figure Number	Molecular Orientation*	Energy of Structure (eV)
4.9	Vertical + 0^o	1.759
4.10	Horizontal	1.846
4.11a&d	Vertical + 0^o	1.784
4.11b&e	Vertical + 45^o	1.759
4.11c&f	Vertical + 90^o	1.583
4.12a&d	Vertical + 0^o - 1xH	1.706
4.12b&e	Vertical + 45^o - 1xH	1.994
4.12c&f	Vertical + 90^o - 1xH	1.984
4.13a&d	Vertical + 0^o - 2xH (opposite)	1.171
4.13b&e	Vertical + 45^o - 2xH (opposite)	1.631
4.13c&f	Vertical + 90^o - 2xH (opposite)	1.634
4.14a&d	Vertical + 0^o - 2xH (same)	1.352
4.14b&e	Vertical + 45^o - 2xH (same)	0.142
4.14c&f	Vertical + 90^o - 2xH (same)	0.136
4.15a&c	Tautomer 1 Angle 60^o + 0^o	0.527
4.15b&d	Tautomer 1 Angle 60^o + 90^o	0.206
4.16a&c	Tautomer 2 Angle 60^o + 0^o - 1xH	1.224
4.16b&d	Tautomer 2 Angle 60o + 90o - 1xH	1.915

Table 4.2: This is a summary of all the energies of the previous simulations of various different arrangements and tautomers of melamine on Cu(110).

* - The molecular orientation code corresponds to 'Vertical' being with the cyclic plane perpendicular to the surface, 'Horizontal' being with the cyclic plane parallel to the surface. The additional angle corresponds to the number of degrees of rotation of the molecule's cyclic plane to the [110] direction. The nxH corresponds to the number of protons removed from the melamine. Finally tautomers 1 and 2 are angled at ~60^o to the surface.

4.9. Crystal Structural Arrangements of Melamine on C(6x2)

The next stage in the analysis involved arranging the melamine on the (6x2) unit cell. As the undeprotonated upright melamine aligned with the cyclic plane parallel to the [110] direction of the crystal was the most stable isolated molecule various arrangements based on this structure were tried first. Four bright spots were observed within this unit cell in the STM image (see figure 4.8) which suggested that it contained 4 melamine molecules. This was verified by simulating an STM of an isolated undeprotonated melamine rotated 45^{o} to both the [110] and the [001] directions of the Cu crystal (see figure 4.9) where a bright spot was found to correspond to one melamine molecule. A series of potential structures were investigated. These all initially corresponded to pmg symmetry but in order to be viable structures they must also exhibit this symmetry after the structure had been relaxed. Although no firm evidence of hydrogen bonding had been observed, due to the nature of the molecule (i.e. many N-H and N groups spaced around the molecule) it seemed reasonable to assume that this was a definite possibility. Again, each 6x2 surface unit cell contained 5 layers, two lower fixed and 3 upper were allowed to relax.

4.9.1. Structural Simulation 1

This simulation contained only 2 melamine molecules per unit cell. Although it seemed unlikely, we considered the possibility that the close proximity of adjacent molecules may produce two STM imaged spots per molecule. So, in order to verify this hypothesis, this structural simulation was run. It consisted of the melamine arranged with the cyclic plane of the melamine at right-angles to the Cu surface and rotated 45^{o} to both the [110] and the [001] directions of the Cu crystal (see figure 4.17). Although reasonably stable the simulated STM image did not correspond to the experimental one.

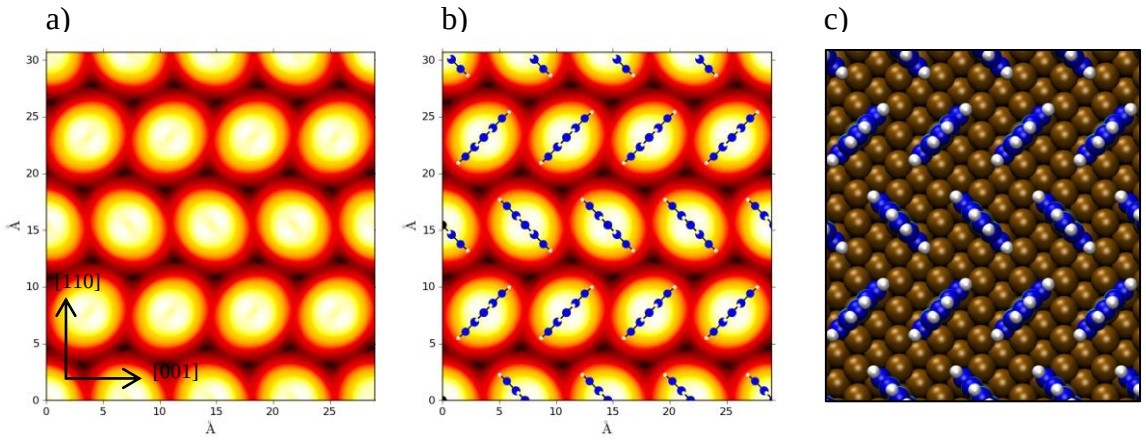

Figure 4.17: Two melamine molecules bonded to Cu(110) surface on the (6x2) unit cell. Here V_t = -0.3 V and ΔE_{Tot} = -1.638eV (calculated).

4.9.2. Structural Simulation 2

This simulation contained four melamine molecules arranged as shown in figure 4.18. The molecular planes of adjacent molecules were initially placed very close together and upon relaxing the melamine molecules moved apart. This was ~80meV more stable than the previous simulation. However, the simulated STM failed to resolve the individual melamine molecules within a pair (see figure 4.18). This suggested that perhaps the melamines must be accommodated further apart in order to produce distinct STM images.

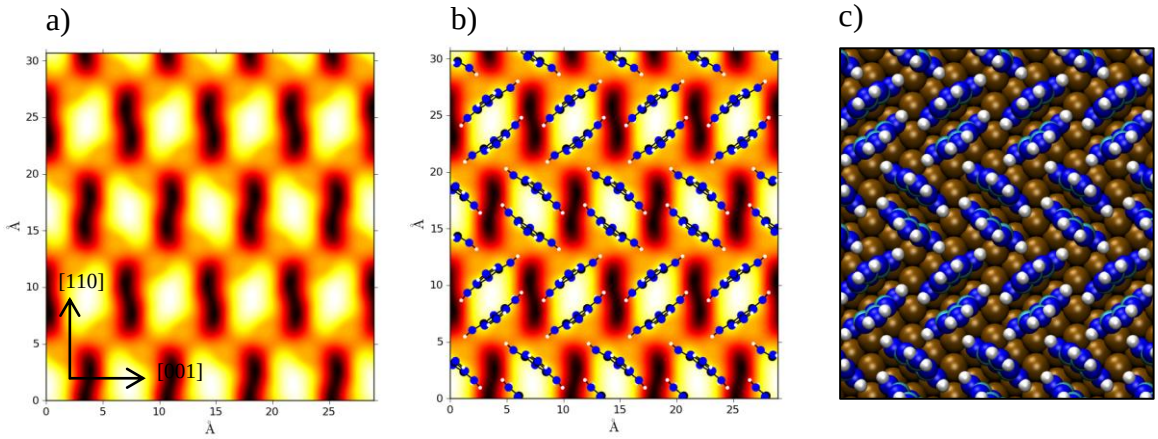

Figure 4.18: Four melamine molecules bonded to Cu(110) surface on the (6x2) unit cell. Here V_t = -0.3 V and ΔE_{Tot} = -1.719eV (calculated).

4.9.3. Structural Simulation 3

As the previous structure had been so energetically favourable a series of variations were made of it. The first one consisted of angling the molecule with the plane of the melamine ~30^{o} to the vertical. This produced a structure that was ~20meV more energetically favourable. It also produced a simulated STM image that was very similar to the experimental one (see figure 4.19). A number of hydrogen atoms were found to be placed relatively close to nitrogen atoms in adjacent molecules (2.4Å – 2.6Å). Although slightly longer than the average hydrogen bond, this may have contributed to the overall stability of this structure.

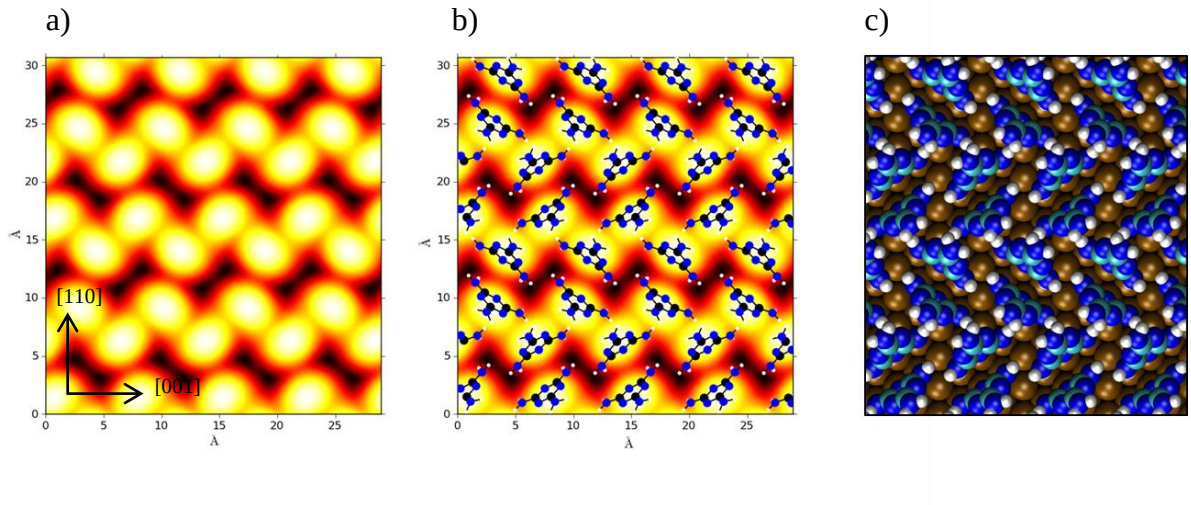

Figure 4.19: Four melamine molecules bonded to Cu(110) surface on the (6x2) unit cell. Here V_t = -0.3 V and ΔE_{Tot} = -1.742eV (calculated).

4.9.4. Structural Simulation 4

This simulation investigated the possibility of further angling of the molecules by placing the cyclic plane of the melamine ~60^{o} to the vertical. However, the final relaxed structure was almost identical to structural simulation 3. This further suggested that there is a strong tendency for melamine to be angled with its cyclic plane ~30^{o} to the vertical.

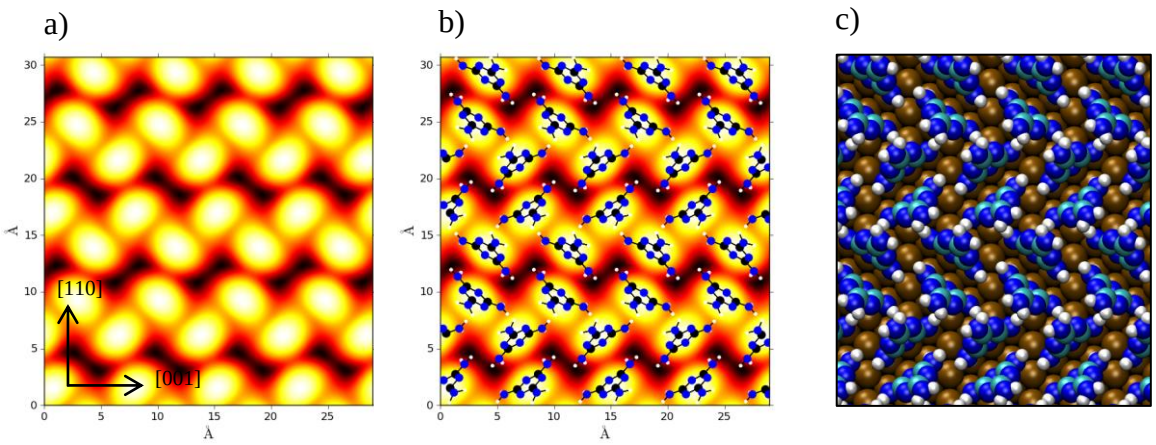

Figure 4.20: Four melamine molecules bonded to Cu(110) surface on the (6x2) unit cell. Here V_t = -0.3 V and ΔE_{Tot} = -1.745eV (calculated).

4.9.5. Structural Simulation 4 – Minus Hydrogen – Tautomer 1

This is a further investigation of this highly stable arrangement. Due to the stability of some single deprotonated melamine structures a single deprotonated arrangement was simulated. Although this simulation was highly stable, the simulated STM image did not correspond well with the experimental one. It is difficult to accurately measure the energy of deprotonation and so, although a plausible structure, it is not as likely to form as structural simulation 4.

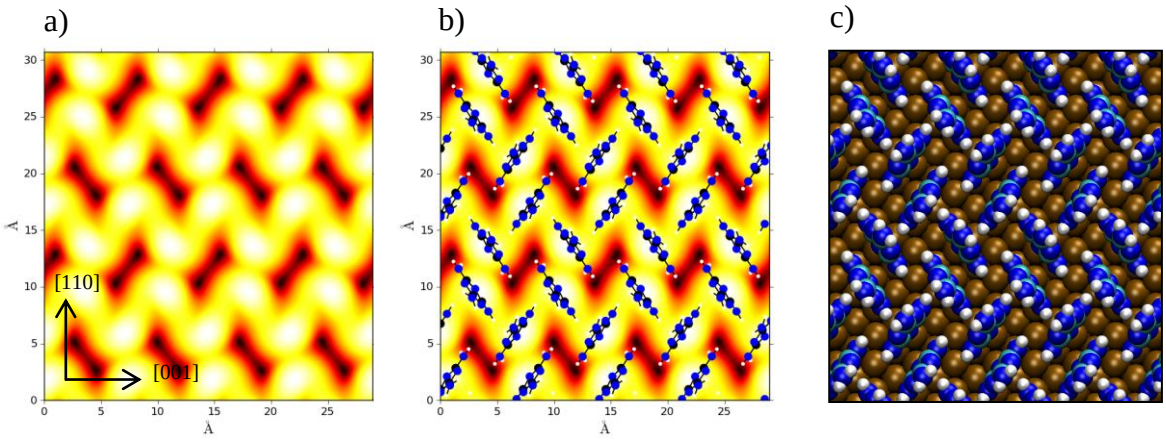

Figure 4.21: Four melamine molecules bonded to Cu(110) surface on the (6x2) unit cell. Here V_t = -0.3 V and ΔE_{Tot} = -1.751eV (calculated).

4.9.6. *Structural Simulation 4 – Minus Hydrogen – Tautomer 2*

Another investigation of this highly stable arrangement involved placing one of the tautomer configurations of melamine in the arrangement of simulation 4. However, not only was this simulation was not very stable (see figure 4.22) but the simulated STM image did not correspond as well with the experimental one.

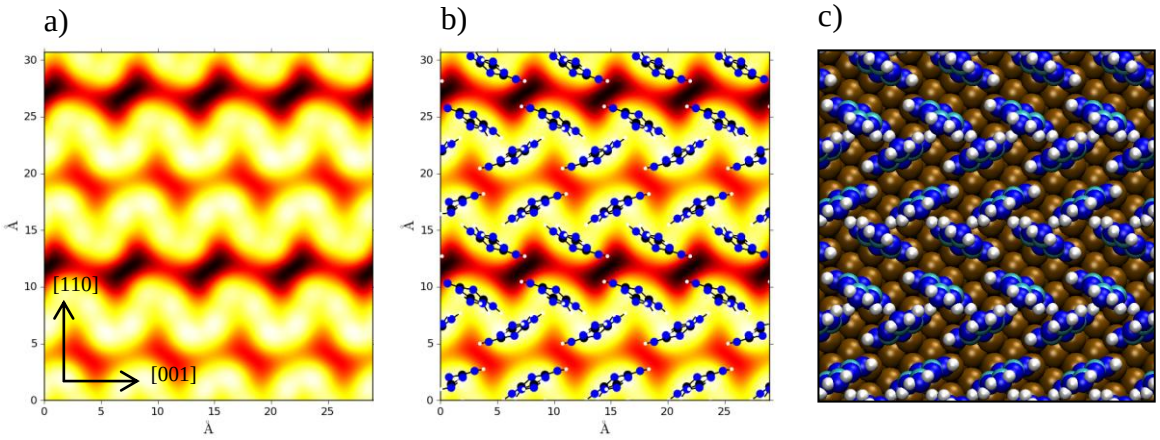

Figure 4.22: Four melamine molecules bonded to Cu(110) surface on the (6x2) unit cell. Here V_t = -0.3 V and ΔE_{Tot} = -1.103eV (calculated).

4.9.7. *Structural Simulation 5*

As simulation 4 was so stable several more variations of this structure were simulated. This structure investigated the possibility that the melamine was more rotated about the z-axis. Two of the rows were rotated ~10^o clockwise and two of the rows rotated ~10^o anti-clockwise (see figure 4.23). However, this produced a slightly less energetically favourable structure. Also, the simulated STM image produced less well defined bright spots.

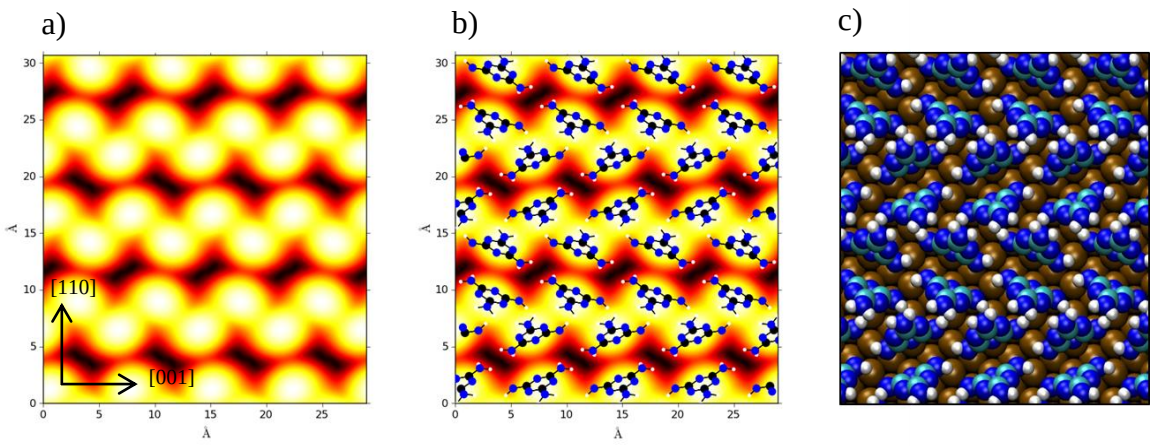

Figure 4.23: Four melamine molecules bonded to Cu(110) surface on the (6x2) unit cell. Here V_t = -0.3 V and ΔE_{Tot} = -1.663eV (calculated).

4.9.8. Structural Simulation 6

This simulation was an attempt to further modify the previous simulation. This involved rotating the melamine molecules around the z-axis in the opposite direction (see figure 4.23). The simulation was also started with the cyclic plane of the melamine at ~60^{o} to the vertical (z-axis). The reason for this was to attempt to investigate if hydrogen bonding occurred between the adjacent melamine rows. The simulation, as expected, relaxed the melamine molecules to a similar angle as in the previous simulation (see figure 4.23). However, this structure now contained some hydrogen bonding in-between some of the melamine on the same row (see 4.24c). This was reflected in the increased stability of this structure. However, the STM simulation contained blurring between the melamine molecules on the same row (see figure 4.24a and 4.24b) and adjacent rows were arranged angled to one another.

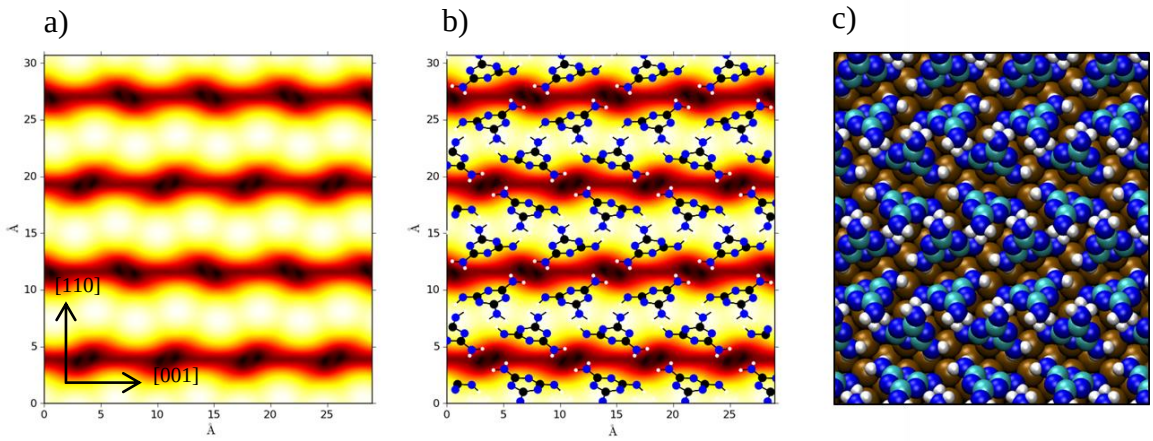

Figure 4.24: Four melamine molecules bonded to Cu(110) surface on the (6x2) unit cell. Here V_t = -0.3 V and ΔE_{Tot} = -1.733eV (calculated).

4.9.9. Structural Simulation 7

This simulation was an attempt to align the bright spots on the simulated STM image (see figure 4.25). This was done by shifting the melamine rows by ±0.25 lattice spacings in the opposite directions. However, the melamine simply relaxed back to almost exactly the same structure as before.

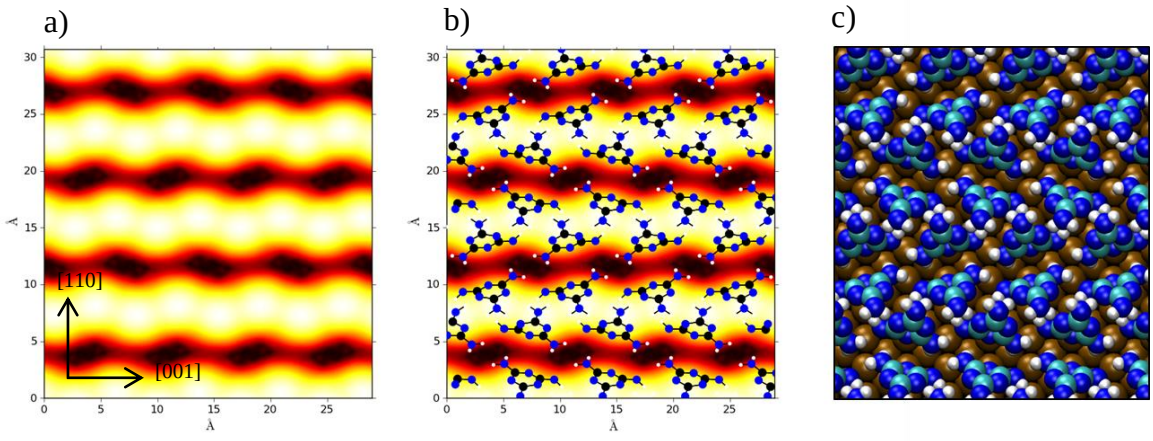

Figure 4.25 Four melamine molecules bonded to Cu(110) surface on the (6x2) unit cell. Here V_t = -0.3 V and ΔE_{Tot} = -1.733eV (calculated).

4.9.10. Structural Simulation 8

This simulation investigated what would happen if the melamine was placed aligned parallel to the [110] direction (see figure 4.26). The melamine was also angled at ~30^{o} to the vertical with each adjacent row angled inward. It was believed that there may be some hydrogen bonding in-between the rows so, if there was, this simulation should relax towards a stable structure containing them. This structure did indeed relax to a structure containing hydrogen bonds. It did this by angling one row by ~45^{o} to the vertical and the other row was almost upright to the surface. Both the melamine rows were rotated by ~10^{o} in the same direction about the z-axis. Although this relaxed to a very stable structure the simulated STM image bore little resemblance to the experimental images.

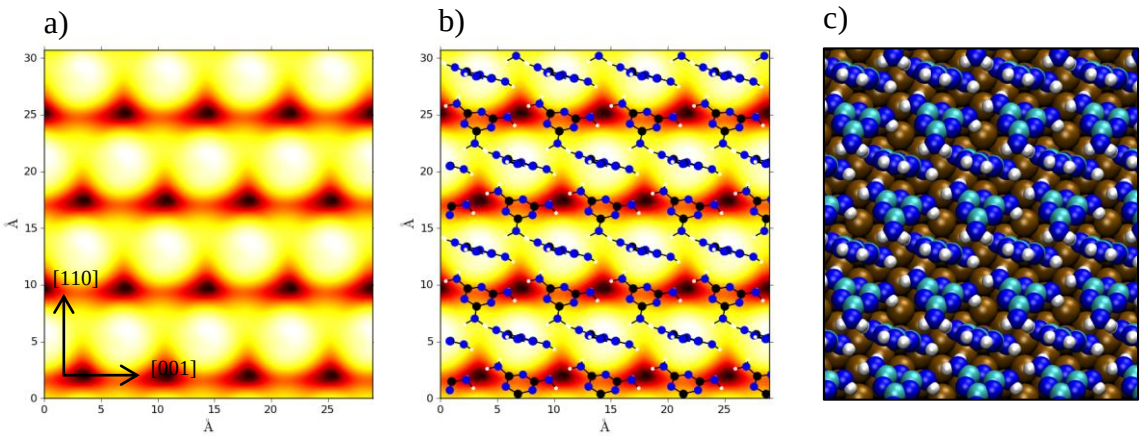

Figure 4.26 Four melamine molecules bonded to Cu(110) surface on the (6x2) unit cell. Here V_t = -0.3 V and ΔE_{Tot} = -1.740eV (calculated).

4.9.11. Structural Simulation 9

This was another potential arrangement. This time the melamine was angled so that the cyclic plane of the molecule was ~20^{o} to the [110] direction of the crystal. However, the stabilisation energy was low and the simulated STM bore little relation to the experimental one (see figure 4.27).

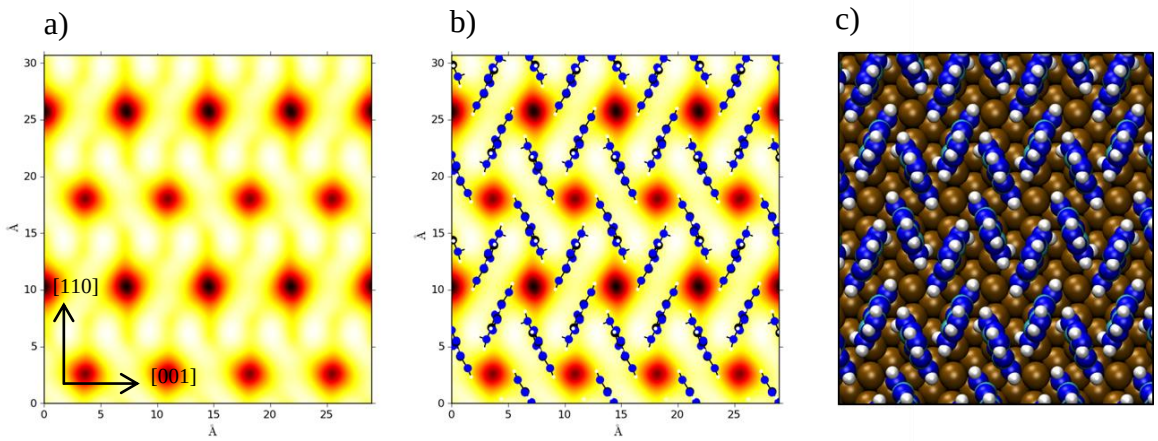

Figure 4.27 Four melamine molecules bonded to Cu(110) surface on the (6x2) unit cell. Here V_t = -0.3 V and ΔE_{Tot} = -1.408eV (calculated).

4.9.12. Structural Simulation 10

This simulation produced a very stable structure and the simulated STM was in reasonably good agreement with the experimental one. On top of this, during relaxation the final configuration changed radically from the original one (see figure 4.28).

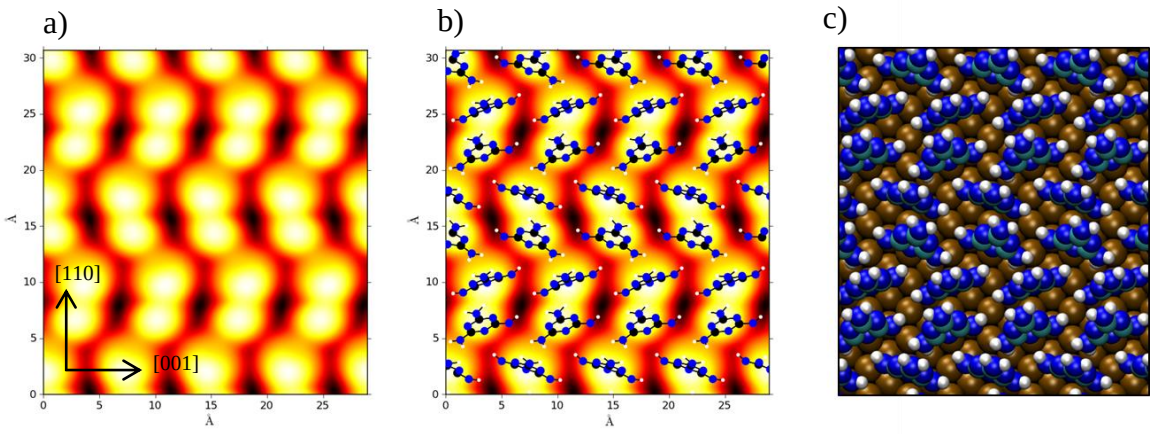

Figure 4.28 Four melamine molecules bonded to Cu(110) surface on the (6x2) unit cell. Here V_t = -0.3 V and ΔE_{Tot} = -1.700eV (calculated).

4.9.13. *Structural Simulation 11*

This simulation was very similar to Simulation 4. Again, it changed radically from the original one and produced a configuration of high stability and an STM that was in good agreement with the experimental one (see figure 4.29). Interestingly, the final configuration of this simulation was almost identical to simulation 10. The only difference was that it was a reflection of it in the x-direction.

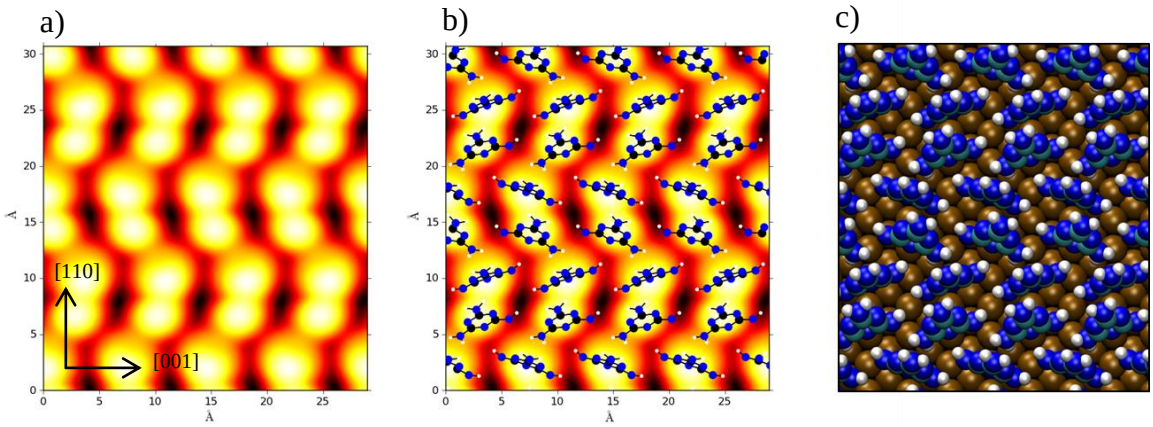

Figure 4.29: Four melamine molecules bonded to Cu(110) surface on the (6x2) unit cell. Here V_t = -0.3 V and ΔE_{Tot} = -1.704eV (calculated).

4.9.14. *Structural Simulation 11 – Minus Hydrogen – Tautomer 1*

Due to the stability of the previous two simulations some variations of it, where some of the NH_2 group hydrogens were removed (i.e. a single deprotonated melamine) from each of the (four) melamine molecules were done. Although the stability of these simulations was high the correspondence to the experimental STM images was low (see figure 4.30). In this version alternating hydrogens were removed from each adjacent row.

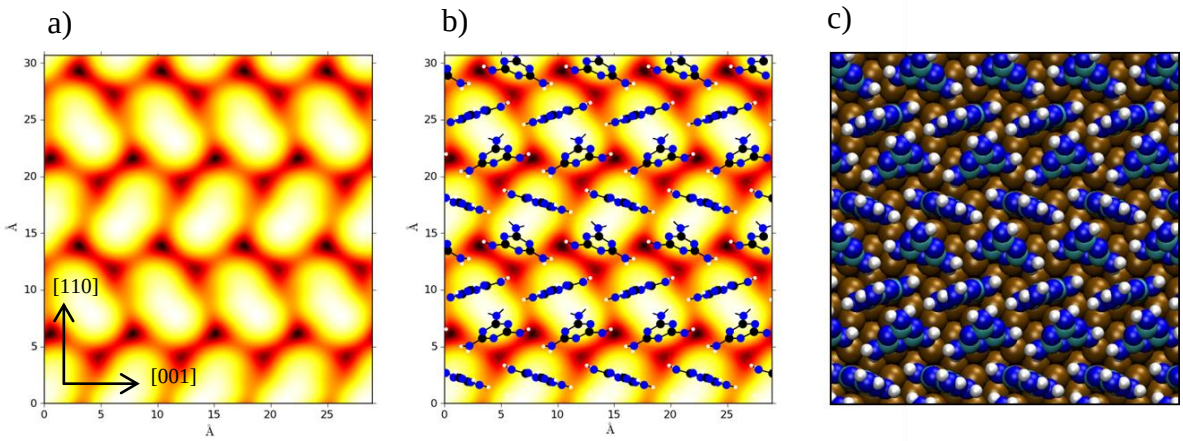

Figure 4.30: Four melamine molecules bonded to Cu(110) surface on the (6x2) unit cell. Here V_t = -0.3 V and ΔE_{Tot} = -1.917eV (calculated).

4.9.15. Structural Simulation 11 – Minus Hydrogen – Tautomer 2

This structure corresponds to the second variation of the single deprotonated melamine. This time the same hydrogen was removed from each adjacent row. On the next two adjacent rows a different NH_2 hydrogen was removed. Again, the stability was high but the correspondence to the experimental STM images was low (see figure 4.31).

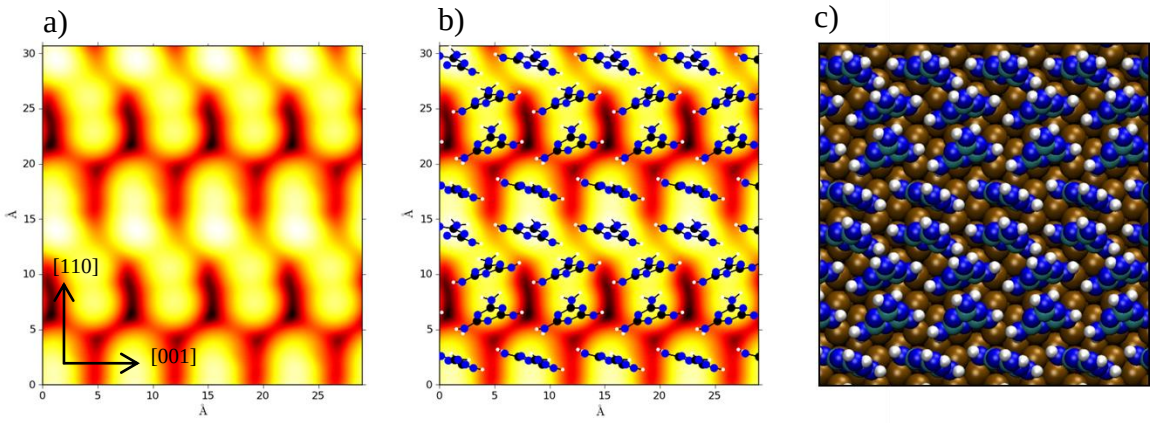

Figure 4.31: Four melamine molecules bonded to Cu(110) surface on the (6x2) unit cell. Here V_t = -0.3 V and ΔE_{Tot} = -1.904eV (calculated).

4.9.16. Structural Simulation 11 – Minus Hydrogen – Tautomer 3

This structure corresponds to the third variation of the single deprotonated melamine. This time the same hydrogen was removed from each adjacent row. Again, the stability was high but the correspondence to the experimental STM images was low (see figure 4.32).

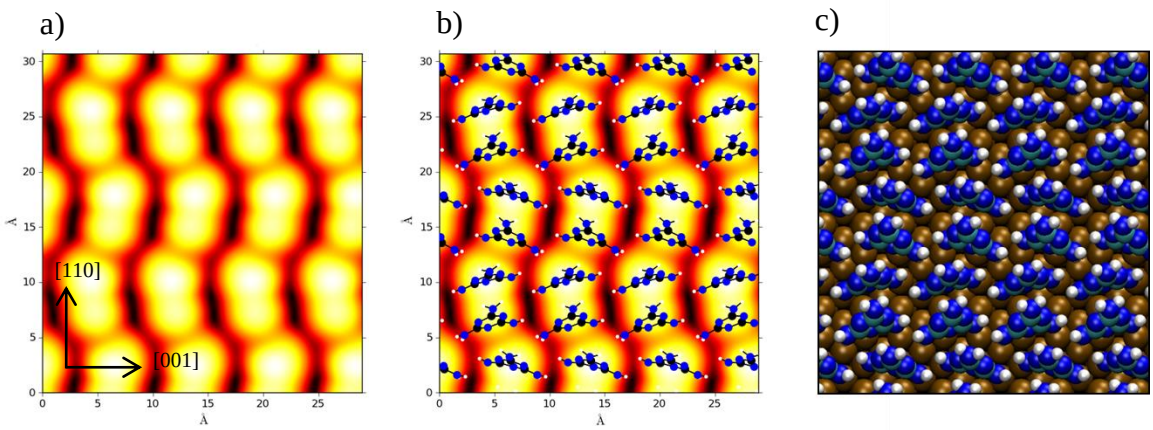

Figure 4.32: Four melamine molecules bonded to Cu(110) surface on the (6x2) unit cell. Here V_t = -0.3 V and ΔE_{Tot} = -1.943eV (calculated).

4.9.17. Structural Simulation 12

This simulation converged to a reasonably stable structure, however, the STM image did not correspond well to experimental data. This simulation seemed to suggest that the melamine rows were angled in the same direction (see figure 4.33).

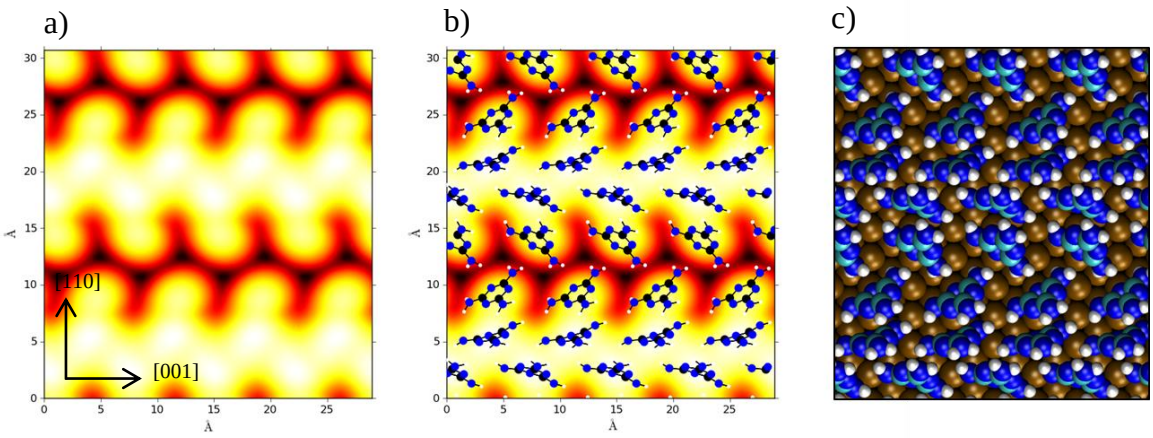

Figure 4.33: Four melamine molecules bonded to Cu(110) surface on the (6x2) unit cell. Here V_t = -0.3 V and ΔE_{Tot} = -1.683eV (calculated).

4.9.18. Structural Simulation 13

This simulation was the most unstable and involved aligning the melamine with the [001] axis of the crystal. The STM simulation bore little resemblance to the experimental one. However, it did serve to further illustrate that the molecule was most likely bonded with a nitrogen directly over (or close to) an upper Cu row atom and angled with the axis of the molecule aligned with the [110] direction of the crystal (see figure 4.34).

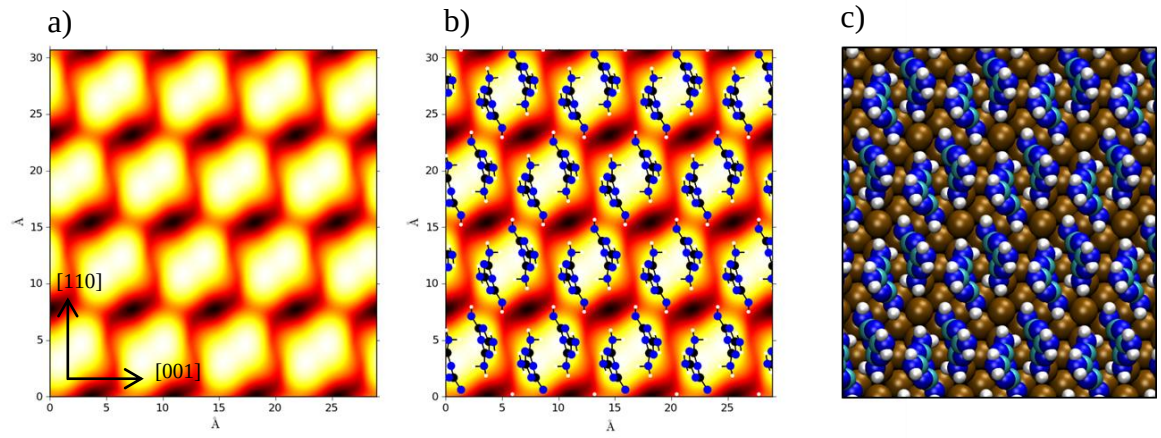

Figure 4.34: Four melamine molecules bonded to Cu(110) surface on the (6x2) unit cell. Here V_t = -0.3 V and ΔE_{Tot} = -1.306eV (calculated).

4.9.19. Structural Simulation 14

This simulation relaxed to a structure where one row of melamine was slightly more upright than the other (see figure 4.35). This resulted in an STM simulation that was very similar to the experimental one except the more upright row of melamine molecules appeared to be much brighter than the other. This was not observed in the experimental data. Also, the stability of this simulation was relatively poor.

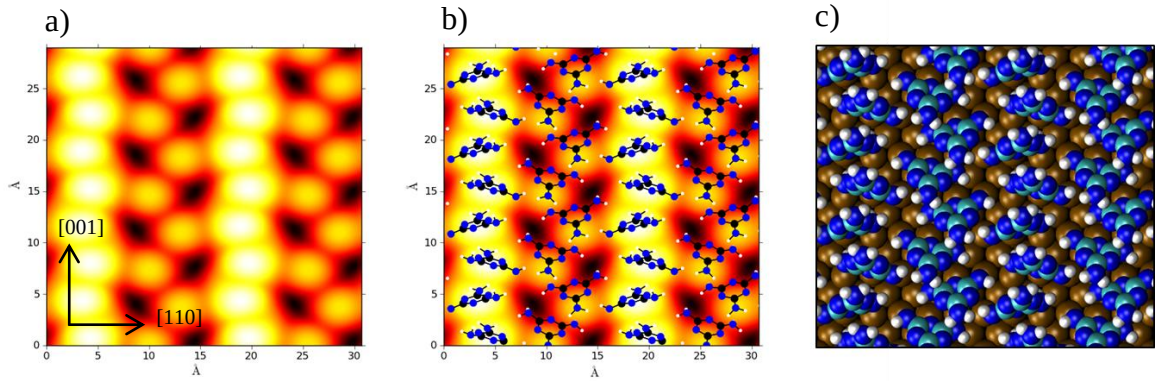

Figure 4.35: Four melamine molecules bonded to Cu(110) surface on the (6x2) unit cell. Here V_t = -0.3 V and ΔE_{Tot} = -1.496eV (calculated).

4.9.20. Structural Simulation 15

This simulation was an attempt to improve on the previous simulation (Simulation 14). As the previous simulation had produced a simulated STM in good agreement with the experimental one some variations of it were simulated. The row which contained the bright spots on the STM was reflected and moved to the other part of the unit cell. However, the structure did not relax to an energetically favourable structure (see figure 4.36). Also, the simulated STM did not particularly resemble the experimental one. However, the bright spots were all well separated and of approximately the same size like the experimental one. This suggested that the angling and spacing of the melamine was correct. However, the overall arrangement was not.

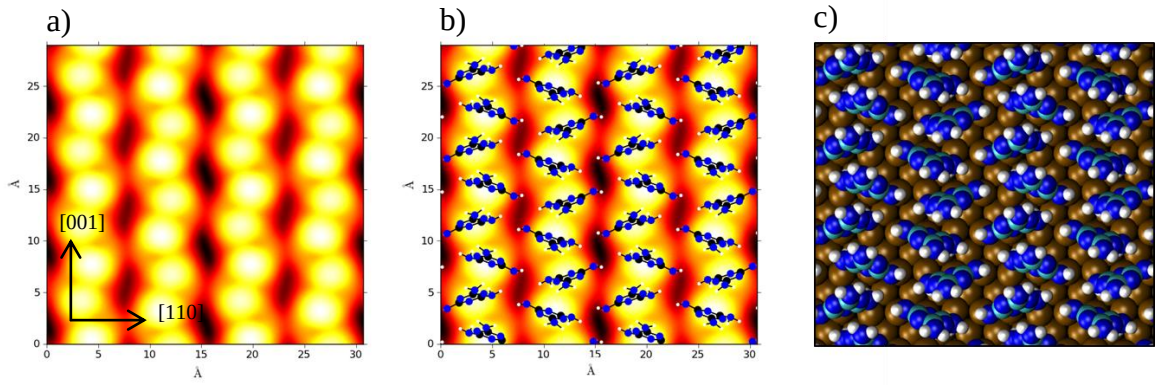

Figure 4.36: Four melamine molecules bonded to Cu(110) surface on the (6x2) unit cell. Here V_t = -0.3 V and ΔE_{Tot} = -1.468eV (calculated).

4.9.21. Structural Simulation 16

The previous structure was rearranged in order to space out the melamine more (see figure 4.37). This simulation did not relax to a particularly energetically favourable structure. This is perhaps surprising as some of the distances of hydrogens from adjacent nitrogens suggested that this structure contained some hydrogen bonding. The simulated STM gave well-spaced bright spots of even intensity but the overall arrangement did not correspond well to the experimental data. This simulation, and the previous two also suggested that the melamine was arranged with the molecules all at approximately the same orientation to the surface as the more the plane of the molecule was aligned with the surface the less the intensity of the image produced when STM simulated.

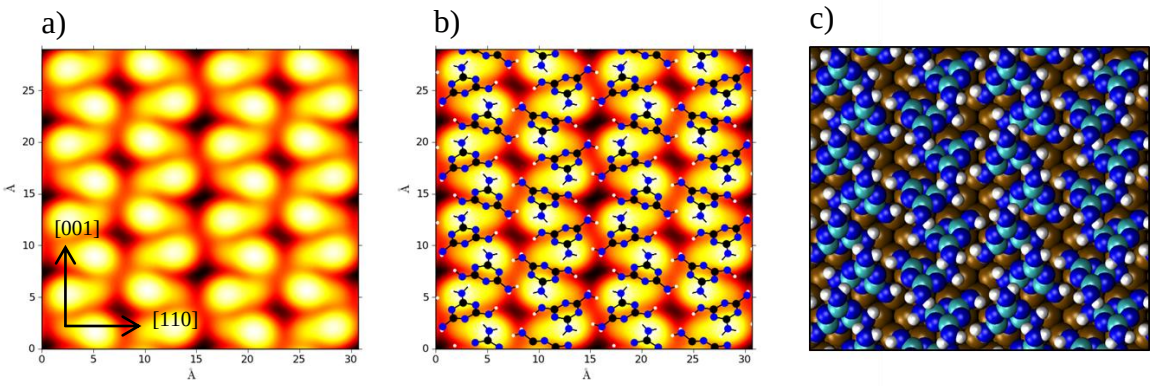

Figure 4.37: Four melamine molecules bonded to Cu(110) surface on the (6x2) unit cell. Here V_t = -0.3 V and ΔE_{Tot} = -1.433eV (calculated).

4.9.22. Structural Simulation 17

This structure was somewhat of a departure from previous models and investigated the possibility that the melamine formed a "bi-layer" on the surface. Bi-layers have been observed previously and so this arrangement was studied for completeness. However, the stability of this structure was very poor (ΔE_{Tot} = -1.417eV) and the simulated STM did not correspond at all well with the experimental one and is not shown here for that reason.

4.10. Conclusions – Part 2

Many different configurations and arrangements of melamine on Cu(110) were tried. It seems clear that, from a purely energetic point of view, that structural simulation 4 is the most likely candidate for the room temperature arrangement. Also, when simulated STM images are produced, a reasonably good match with experimental data is obtained. It therefore seems reasonable to assume that structural simulation 4 (see figure 4.20) is the most likely candidate for the room temperature structure of melamine bonded to Cu(110).

The results of the previous simulations of melamine molecules adsorbed on Cu(110) in various different orientations and tautomers in a C(6x2) unit cell are summarised in table 4.3.

Figure Number	Molecular Simulation *	Energy of Structure (eV)
4.17	1	1.638
4.18	2	1.719
4.19	3	1.742
4.20	4	1.745
4.21	4 - 1xH -Tautomer 1	1.751
4.22	4 - 1xH -Tautomer 2	1.103
4.23	5	1.663
4.24	6	1.733
4.25	7	1.733
4.26	8	1.740
4.27	9	1.408
4.28	10	1.700
4.29	11	1.704
4.30	11 - 1xH -Tautomer 1	1.917
4.31	11 - 1xH -Tautomer 2	1.904
4.32	11 - 1xH -Tautomer 3	1.943
4.33	12	1.683
4.34	13	1.306
4.35	14	1.496
4.36	15	1.468
4.37	16	1.433
NA	17	1.417

Table 4.3: This is a summary of all the energies of the previous simulations of various different arrangements and tautomers of melamine in a C(6x2) unit cell on Cu(110).

* - The molecular orientation code corresponds to the simulation number (see the relevant figure for more information). The nxH corresponds to the number of protons removed from the melamine. Finally tautomers 1, 2 and 3 correspond to various different tautomers.

4.11. Bibliography

[1] J. V. Barth, G. Costantini, K.Kern. *"Engineering Atomic and Molecular Nanostructures at Surfaces."* Nature 2005, **437**(7059), 671-679.

[2] J. V. Barth. *"Molecular Architectonic on Metal Surfaces."* Annu. Rev. Phys. Chem. 2007, **58**, 375-407.

[3] S. M. Barlow, R. Raval. *"Complex Organic Molecules at Metal Surfaces: Bonding, Organisation and Chirality."* Surf. Sci. Rep. 2003, **50**(6-8), 201-341.

[4] L. M. A. Perdigão, E. W. Perkins, J. Ma. *"Bimolecular Networks and Supramolecular Traps on Au(111)."* J. Phys. Chem. B 2006, **110**(25), 12539-12542.

[5] S. Pan, Q. Fu, T. Huang. *"Design and Control of Electron Transport Properties of Single Molecules."* PNAS 2009**, 106**(36), 15259-15263.

[6] S. Jensen, H. Früchtl, C. J. Baddeley. *"Coupling of Triamines with Diisocyanates on Au(111) Leads to the Formation of Polyurea Networks."* J. Am. Chem. Soc. 2009, **131**(46), 16706-16713.

[7] F. Silly, A. Q. Shaw, M. R. Castell. *"Melamine Structures on the Au(111) Surface."* J. Phys. Chem. C 2008**, 112**(30), 11476-11480

[8] M. Sassi, V. Oison, J. Debierre. *"First Principle Study of a Bimolecular Thin Film on Ag(111) Surface."* Surface Science 2008, **602**(17), 2856-2862.

[9] M. Mura, N. Martsinovich, L. Kantorovich. *"Theoretical Study of Melamine Superstructures and their Interactions with the Au(111) Surface."* Nanotechnology 2008, **19**(46), 465704 (14pp).

[10] Hai-Ming Zhang, Zhao-Xiong Xie, La-Sheng Long. *"One-Step Preparation of Large-Scale Self-Assembled Monolayers of Cyanuric Acid and Melamine Supramolecular Species on Au(111) Surfaces."* J. Phys. Chem. C 2008, **112**(11), 4209-4218.

[11] C. H. Schmitz, J. Ikonomov, M. Sokolowski. *"Two Commensurate Hydrogen-Bonded Monolayer Structures of Melamine on Ag(111)."* Surface Science 2011, **605**(1-2), 1-6.

[12] L. M. A. Perdigão, G. N. Fontes, B. L. Rogers. *"Coadsorbed NTCDI-Melamine Mixed Phases on Ag-Si(111)."* Physical Review B 2007, **76**(24), 245402.

[13] C. Bombis, N. Kalashnyk, W. Xu. *"Hydrogen-Bonded Molecular Networks of Melamine and Cyanuric Acid on Thin Films of NaCl On Au(111)."* Small 2009, **5**(19), 2177-2182.

[14] S. Bizzari, K. Yokose. *"Chemical Economics Handbook"* 2008.

[15] C. T. Seto, G. M. Whitesides. *"Self-Assembly Based on the Cyanuric Acid-Melamine Lattice."* Journal of the American Chemical Society 1990, **112**(17), 6409-6411.

[16] G. M. Whitesides, J. P. Mathias, C. T. Seto. *"Molecular Self-Assembly and Nanochemistry: A Chemical Strategy for the Synthesis of Nanostructures."* Science 1991, **254**(5036), 1312-1319.

[17] X. Li, D. N. Chin, G. M. Whitesides. *"Synthesis and Evaluation of Thioether-Based Tris-Melamines as Components of Self-Assembled Aggregates Based on the CA·M Lattice"* Journal of Organic Chemistry 1996, **61**(5), 1779-1786.

[18] M. G. J. Cate ten et al. *"Self-Assembly and Stability of Double Rosette Nanostructures with Biological Functionalities."* Organic & Biomolecular Chemistry 2005, **3**(20), 3727-3733.

[19] A. G. Bielejewska, C. E. Marjo, L. J. Prins. *"Thermodynamic Stabilities of Linear and Crinkled Tapes and Cyclic Rosettes in Melamine-Cyanurate Assemblies: A Model Description."* Journal of the American Chemical Society 2001, **123**(31), 7518-7533.

[20] S. Yagai, Y. Monma, N. Kawauchi. "*Supramolecular Nanoribbons and Nanoropes Generated from Hydrogen-Bonded Supramolecular Polymers Containing Perylene Bisimide Chromophores."* Organic Letters 2007, **9**(6), 1137-1140.

[21] J. Barberá, L. Puig, P. Romero. *"Propeller-Like Hydrogen-Bonded Banana-Melamine Complexes Inducing Helical Supramolecular Organizations."* Journal of the American Chemical Society 2006, **128**(13), 4487-4492.

[22] J. M. Kerckhoffs, M. G. J. Ten Gate, M. A. Mateos-Timoneda. *"Selective Self-Organization of Guest Molecules in Self-Assembled Molecular Boxes."* Journal of the American Chemical Society 2005, **127**, 12697-12708.

[23] R. Thomas, G. U. Kulkarni. *"A Hydrogen-Bonded Channel Structure Formed by a Complex of Uracil and Melamine."* Beilstein Journal of Organic Chemistry 2007, **3**, 17-21.

[24] A. Saha, S. Manna, A.K. Nandi. *"A Mechanistic Approach on the Self-Organization of the Two-Component Thermoreversible Hydrogel of Riboflavin and Melamine."* Langmuir 2007, **23**(26), 13126-13135.

[25] T. Kawasaki, M. Tokuhiro, N. Kimizuka. *"Hierarchical Self-Assembly of Chiral Complementary Hydrogen-Bond Networks In Water: Reconstitution of Supramolecular Membranes."* Journal of the American Chemical Society 2001, **123**(28), 6792-6800.

[26] J. C. MacDonald, G. M. Whitesides. *"Solid-State Structures of Hydrogen-Bonded Tapes Based on Cyclic Secondary Diamides."* Chemical Reviews 1994, **94**(8), 2383-2420.

[27] E. W. Hughes. *"The Crystal Structure of Melamine."* Journal of the American Chemical Society 1941, **63**, 1737-1752.

[28] I. M. Klotz, T. Askounis. *"Absorption Spectra and Tautomerism of Cyanuric Acid, Melamine and Some Related Compounds."* Journal of the American Chemical Society 1947, **69**(4), 801-803.

[29] M. Ito. *"The Raman Spectrum of Cyanuric Acid."* Bulletin of the Chemical Society of Japan 1953, **26**(6), 339-341.

[30] M. Arduin, M. Crego-Calama, P. Timmerman. *"A Novel Type of Hydrogen-Bonded Assemblies Based on the Melamine·Cyanuric Acid Motif."* Journal of Organic Chemistry 2003, **68**, 1097-1106.

[31] C. F. Cullis, M. M. Hirschler. *"Experimental Techniques for the Combustion of Fuels of Low Volatility and High Reactivity."* Symposium (International) on Combustion 1981, **18**(1), 1575-1582.

[32] W. C. Kuryla, A. J. Papa. *"Flame Retardancy of Polymeric Materials."* 1973-1979, **Vol. 1-5**.

[33] H. R. Allcock, F. W. Lampe. *"Contemporary Polymer Chemistry."* 1981, Prentice Hall, New Jersey.

[34] R. B. Seymour, C. E. Carraher. *"Giant Molecules."* 1990, Wiley, New York.

[35] J.K. Sears, J. R. Darby. *"The Technology of Plasticizers."* 1982, Wiley, New York.

[36] W. W. Reynolds. *"Physical Chemistry of Petroleum Solvents."* 1963, Reinhold, New York.

[37] C. G. Roffey. *"Photopolymerization of Surface Coatings."* 1982, Wiley, New York.

[38] J. W. Nicholson. *"The Chemistry of Polymers."* The Royal Society of Chemistry, Cambridge, 1991.

[39] M. Bicher, C. Guran, I. Jitane. *"Contributions to the Coordinative Chemistry of S-Triazines. Part 7. Cu(Ii) Complex-Compounds with Melamine."* Rev. Roum. Chim. 1994, **39**(10), 1203-1207.

[40] J. P. Mathias, C. T. Seto, E. E. Simmanek, G. M. Whitesides. *"Self-Assembly Through Hydrogen Bonding: Preparation and Characterization of Three New Types of Supramolecular Aggregates Based on Parallel Cyclic CA3·-M3""* J. Am. Chem. Soc. 1994, **116**(5), 1725.

[41] J. A. Zerkowski, J. C. MacDonald, G. M. Whitesides. *"Investigations into the Robustness of Secondary and Tertiary Architecture of Hydrogen-Bonded Crystalline Tapes."* Chem. Mater. 1994, **6**(8), 1250.

[42] M. M. Chowdhry, D. Mingos, A. White, D. J. Williams. *"Novel Supramolecular Self-Assembly of a Transition-Metal Organo Network Based on Simultaneous Coordinate- and Hydrogen-Bond Interactions."* Chem. Commun. 1996, **8**, 899-900.

[43] W. J. Jones, W. Orville-Thomas. *"The Infra-Red Spectrum and Structure of Melamine."* Transac. Far. Soc. 1959, **55**, 203-210.

[44] E. G. Cox, G. A. Jeffrey. *"Order Length Relationships for Pi-Bonds in Heteronuclear Molecules."* Proc. Roy. Soc. A 1951, **207**(1088), 110-121.

[45] H. O. Jenkins *"Bond Order - Length Relationships."* J. Am. Chem. Soc. 1955, **77**(11), 3168-3169.

[46] T. H. Goodwin, A. L. Porte. *"Calculated Bond Lengths in Some Cyclic Compounds. Part 4. Pteridine and Melamine and a Correlation Curve for C-N Bonds."* J. Chem. Soc, 1956, 3595.

[47] Y. L Wang, A. M. Mebel, C. J. Wu. *"IR Spectroscopy and Theoretical Vibrational Calculation of the Melamine Molecule."* J. Chem. Soc. 1997, Faraday Trans., **93**(19), 3445-3451.

[48] W. Sawodny, K. Niedenzu, J. W. Dawson. *"Vibrational Spectrum and Assignment of Normal Vibrations of Melamine."* J. Chem. Phys. 1966, **45**(8), 3155.

[49] D. Goodgame, I. Hussain, A. White. *"Synthesis and Structure of a Copper(II) Melamine Complex, [Cu(C3H6N6)(Mu-OCH3)(ONO2)(HOCH3)](2), with Direct Cu-Melamine Coordination ."* J. Chem. Soc. 1999, **17**, 2899-2900.

[50] A. McNutt. *"Structural Studies of the Adsorption of the Nucleic Acid Bases on Cu(110)."* PhD thesis, University of Liverpool, 2002.

5. Chapter Five – Summary and Conclusions

The simulations presented in this thesis were carried out in order to gain an understanding of the organisation of thymine and melamine on a Cu(110) surface. The TPD data resulted in knowledge about whether or not either of the molecules deprotonated and, if so, at what temperature. The RAIRS data resulted in knowledge about what orientations were and weren't possible for either molecule. The LEED data resulted in knowledge about what long−range repeating structures occurred as well as their nature. The XPS data for the thymine resulted in a detailed image of how the thymine molecules orientated on the Cu(110) surface. The DFT produced accurate information on the stability of each of the systems modelled as well as information on how the molecules bond to the surface. This powerful range of surface science techniques has provided complimentary information in order to construct a detailed understanding of the system. However, as useful as these techniques were, it was the combination of simulated and experimental STM images which finally resulted in confirmation of the accuracy of our proposed models. This knowledge has resulted in a reliable description of the chemical form, geometry, bonding points to the surface for each molecule in addition to the intermolecular forces that stabilise organisation.

Chapter 3 focuses exclusively upon how thymine bonds to Cu(110). The two phases that were observed display different characteristics. The room temperature phase does not seem to demonstrate any chirality. It seems to form due to delocalised π−electrons from the cyclic ring structure in the thymine molecules. These delocalised electrons overlap and form a structure that is more stable and thus the bonding of adjacent thymine molecules along the same row is most likely a combination of π−stacking and van der Waals interactions. The question as to why these rows form at the separation they do is less clear. However, the spacing of two Cu rows between each adjacent row does seem to suggest that the surface plays an integral role in this. Analysis of the cell size versus adsorption energy shown in figure 3.14 seemed to suggest that there was a kinetic barrier in-between the rows and the only thing that could have reasonably caused this was the surface as the rows are too far from each other to feel any electrostatic repulsion. The spots observed in-between these rows that seem to repeat every 4 rows are still unexplained. Investigations into variations in the bias

voltage and tunnelling current (see figures 3.20 to 3.28) seemed to suggest that these were caused by the methyl group. However, they did not explain why they occurred with the periodicity that they did.

Chapter 3 then goes on to describe the higher temperature phase that then occurs. As to why the high temperature phase forms in the way that it does is less clear. It demonstrates a distinct chiral behaviour with double strands occurring at approximately the same orientation to the surface with no preference for location. Although the method of formation cannot be deduced from our methodology it is possible to speculate that the angled nature of our structures allows the Cu surface to maintain a stable form that it could not do in the lower temperature structure. It is obvious that an activation barrier of some sort must be surmounted and that it is only more stable than the lower temperature structure in this double stranded form. Although a more stable high temperature structure than the lower temperature phase was found it is still not clear exactly why the structure angles relative to the surface in the way it does nor why it forms a double strand. DFT calculations do confirm that isolated double strands are the most stable (see figures 3.42-3.43) but they do not explain the exact nature of why. However, the simulated STM images of these two structures does match very well the experimental ones with one of the rows being of a slightly more zig-zag nature than the other.

Chapter 4 goes on to use similar techniques to analyse a completely different molecule, namely melamine. Only a room temperature structure was discussed and this time the structure was 2D in nature. Before the DFT analysis was carried out as much experimental data as possible was gathered. RAIRS, LEED, TPD and STM experimental data was carefully scrutinised and analysed. Although this data did seem to suggest a predominantly upright structure it was still not clear exactly how it bonded to the Cu surface. Nor was it impossible that the melamine either deprotonated or tautomerised. Many different potential structures were modelled using our methodology of combining both a stable structure as well as a simulated STM image similar to our experimental one. The Tersoff-Haman technique, although relatively simple in nature, has proven to be highly reliable in previous studies. Many different simulations were conducted; however, only two (almost identical) structures produced both a stable structure as well as a similar simulated STM to the experimental one (see figures 3.19-3.20). Various tautomers were also considered but none produced a simulated STM image that resembled the experimental one.

To conclude, the work presented in this thesis clearly demonstrates the role of surfaces in directing unusual molecular arrangements. Although it is impossible to predict how different molecules will arrange on the surface it is now possible, utilising the very latest developments in experimental and theoretical techniques to formulate a cohesive argument as to how and why different molecules may arrange themselves into the structures that they do on different surfaces. The random motions exhibited by these molecules at various different temperatures allow them to interact and to then find a stable kinetic structure. It is also possible to control this temperature to decide which structure will form.

Finally, this thesis has clearly demonstrated the importance that van der Waals interactions play in self-assembled structures on surfaces. Only recently has it become possible to accurately model these, relatively weak, intermolecular interactions. Although it was suspected that these interactions may play a role in self-assembled structures on surfaces it was thought that hydrogen bonds as well as π−stacking were the primary forces responsible for deciding how these, relatively small, molecules would bond together on a surface. The result is all the more surprising in the fact that both the molecules in question contain atomic groups in positions that could quite readily form hydrogen bonds and, in the case of thymine, do so in every living thing on our planet.